



**HAL**  
open science

# Symmetry effects in optical properties of single semiconductor quantum dots

Katarzyna Kowalik

► **To cite this version:**

Katarzyna Kowalik. Symmetry effects in optical properties of single semiconductor quantum dots. Condensed Matter [cond-mat]. Université Pierre et Marie Curie - Paris VI, 2007. English. NNT : . tel-00288343

**HAL Id: tel-00288343**

**<https://theses.hal.science/tel-00288343>**

Submitted on 16 Jun 2008

**HAL** is a multi-disciplinary open access archive for the deposit and dissemination of scientific research documents, whether they are published or not. The documents may come from teaching and research institutions in France or abroad, or from public or private research centers.

L'archive ouverte pluridisciplinaire **HAL**, est destinée au dépôt et à la diffusion de documents scientifiques de niveau recherche, publiés ou non, émanant des établissements d'enseignement et de recherche français ou étrangers, des laboratoires publics ou privés.

Uniwersytet Warszawski  
*Instytut Fizyki Doświadczalnej*

Université Pierre et Marie Curie – Paris VI  
*ED 107 Physique de la Région Parisienne*

# THESIS

*presented for the degree of*

DOCTOR OF PHYSICS OF  
WARSAW UNIVERSITY  
and UNIVERSITÉ PARIS VI

*by*

**Katarzyna KOWALIK**

---

## Symmetry effects in optical properties of single semiconductor quantum dots

---

*Jury:*

<i>Examiner:</i>	Maria CHAMARRO	Professor - University Paris 6
<i>Supervisor:</i>	Jan GAJ	Professor - Warsaw University
<i>Referee:</i>	Marek GODLEWSKI	Professor - Polish Academy of Sciences
<i>Invited member:</i>	Olivier KREBS	Chargé de recherche - CNRS
<i>Referee:</i>	Henri MARIETTE	Directeur de recherche - CNRS
<i>Supervisor:</i>	Paul VOISIN	Directeur de recherche - CNRS
<i>Examiner:</i>	Dariusz WASIK	Doctor hab. - Warsaw University

September, 2007



Université de Varsovie  
*Institut de Physique Expérimentale*

Université Pierre et Marie Curie – Paris VI  
*ED 107 Physique de la Région Parisienne*

# THÈSE DE DOCTORAT

*pour obtenir le grade de*

DOCTEUR DE L'UNIVERSITÉ DE VARSOVIE et  
DE L'UNIVERSITÉ PARIS VI

Discipline : Physique de la Matière Condensée

*présentée par*

**Katarzyna KOWALIK**

---

## Effets de symétrie sur les propriétés optiques de boîtes quantiques uniques de semiconducteur

---

*Soutenue publiquement le 5 Septembre 2007 devant le jury composé de :*

<i>Examineur</i>	Maria CHAMARRO	Professeur - Université Paris VI
<i>Directeur de thèse</i>	Jan GAJ	Professeur - Université de Varsovie
<i>Rapporteur</i>	Marek GODLEWSKI	Professeur - Académie Polonaise des Sciences
<i>Invité</i>	Olivier KREBS	Chargé de recherche - CNRS
<i>Rapporteur</i>	Henri MARIETTE	Directeur de recherche - CNRS
<i>Directeur de thèse</i>	Paul VOISIN	Directeur de recherche - CNRS
<i>Examineur</i>	Dariusz WASIK	Dr. hab. - Université de Varsovie

---

Laboratoire de Photonique et de Nanostructures - CNRS UPR 20 - Marcoussis



*"The difficult is what takes a little time; the impossible is what takes a little longer."*

Fridtjof Nansen



---

# Preface

*"Writing is a way of thinking. Writing actually creates thought, and generates your ability to think: you discover thoughts you hardly knew you had, and to know what you know. You learn as you write."*

Sheridan Baker, "The Practical Stylist"

There are numerous paths leading to knowledge. Some of them may be through deduction, some — through observation. All of them have one thing in common. Whichever we take we can ultimately proceed further in only one way — share the knowledge. Thanks to written words we can base on the experience of previous generations, exchange our thoughts and ideas with people miles away; pass our achievements to our children. Therefore especially for scientists it is important to systematize, to describe, to summarize, and to present their work in a book form.

Obviously the writer and the Readers have to use the same code for communication. I hope that small mistakes will not cause misunderstanding of all information contained in my thesis. English is not my mother's tongue. I have tried to do my best, but I know it is still very far from the ideal. I have this rare luck that the most crucial information I would like to show to the Readers is presented in a form of equations or figures. They cannot be misleading so much.

While writing this dissertation I did not only realized how much I had learned during my PhD, and how much I still had to learn. These few years taught me also how to pose questions and which of them are important, how to solve problems, and how to implement some theoretical ideas into reality and *vice versa* — condense reality into mathematical models. I hope that following my *work* the Reader will find in it the same *leitmotiv* that I followed conducting experiments, building models, and conjuring interpretations.

I start my dissertation with *Acknowledgments*, to express my appreciation to some special persons, to thank people who supported me, who were involved in my work, and who shaped my growing up as a physicist. In the physics universe often the information code is "zipped" to the *Symbols and Acronyms*. So in the next pages I list the most important ones. The notation I use is consistent with one usually met in quantum mechanics books and articles about solid state physics, which I refer to at the end of this thesis. Next several pages contain a short summary of the presented dissertation in French, Polish, and English. I devote *Chapter 1* to the motivation of my research. I include there a short summary of the well established results regarding the thesis subject and I give some more details on key features of semiconductor heterostructures, which are essential for the topic.



---

I discuss the consequences of zero-dimensionality of the structures and their general symmetry description. The point group symmetry considerations are helpful in order to better understand the role of external perturbations, which were used to influence the quantum states degeneracies. Before showing the main results I obtained I need to say a few words about my experiments. *Chapter 2* describes the samples and experimental techniques. All the characterization details of investigated structures, precise look into experimental setup are shown in order to determine our capabilities and limitations. Next *Chapters* present results of my experimental work, its theoretical description, and interpretation within the existing models. I organize them in a following way: *Chapter 3* — influence of electric field on the emission from quantum dots, *Chapter 4* — influence of magnetic field on quantum dots, *Chapter 5* — optical orientation of spin in a quantum dot. Each of these *Chapters* consists of theoretical considerations and the comparison with measured data. The emphasis is put on elimination of unwelcome effects and complex analysis of observations. The main conclusions and future prospects are presented in *Chapter 6*. It summarizes the whole *work*. At the end I place the *References* and the *Publication List*, where the published works (by other authors and myself) on the topics related to the dissertation can be found.

*Paris–Warsaw, 2006/2007*

Katarzyna Kowalik

A handwritten signature in black ink, appearing to read 'Kowalik', with a stylized, overlapping flourish on the left side.

---

# Acknowledgments

I thank all the people who helped me in preparing my PhD thesis. It would be difficult to list all of them, so I mention by name only those who contributed most directly to the work reported here and whose support was very important for me.

This dissertation was written under joined supervision of two universities: Warsaw University (Warsaw, Poland) and Pierre-Marie Curie University (Paris, France). During my *”co-tutelle”* PhD I have interacted with members of two research groups, the group of Prof. Jan Gaj at the Institute of Experimental Physics (Warsaw University) and of Dr. Paul Voisin at the Laboratories for Photonics and Nanostructures (CNRS). I would like to acknowledge all members of both groups.

I wish to thank:

My PhD supervisors — **Prof. Jan Gaj** (Warsaw University) and **Dr. Paul Voisin** (Laboratoire de Photonique et de Nanostructure-CNRS), for their support and care during preparing this thesis, for discussions, advice, and help in understanding physics. Thank you Paul for encouraging me to do theoretical calculations!

**Dr. Olivier Krebs** — for huge help in experiments, his guidance into density matrix formalism, long discussions about results and infinite patience. Hearty thanks for checking the manuscript. I would like to acknowledge his *”emigration”* support (his help to pass through the administration and to reduce the language barriers).

Current and former headmasters of the laboratories: **Prof. Marian Grynberg** (WU), **Prof. Michał Baj** (WU), **Prof. Roman Stępniewski** (WU), and Prof. **Jean-Yves Marzin** (LPN-CNRS), for enabling me research in their laboratories.

**Prof. Maria Chamarro** and **Dr. hab. Dariusz Wasik** — for the acceptance to participate in my jury, and **Prof. Marek Godlewski** and **Prof. Henri Mariette** — for agreement to be the referees of my manuscript.

**Dr. hab. Andrzej Golnik** — for help with experimental setup and productive discussions about experiments.

**Dr. Pascale Senellart** — for introduction into the *”clean room”* world and working out the technology for in-plane field-effect devices.

---

**Dr. Aristide Lemaître** — for III-V samples. I would like to thank him as the local contact of Sandie Network of excellence which provided most of my financial support during my stay in France.

I am grateful to all my colleagues from the Polish group: **Dr. Arkadiusz Kudelski**, **Dr. Paulina Płochocka**, **Dr. Wiktor Maślana**, **MSc. Jan Suffczyński**, **MSc. Bernard Piechal**, and the French group: **Dr. Benoît Eble**, **Dr. Emmanuelle Peter**, **Dr. Sabine Laurent** — for technical assistance and warm atmosphere in the laboratory; and to **MSc. Piotr Wojnar** from Polish Academy of Sciences — for the samples and discussions about II-VI materials.

All the people from the **”clean room” staff** in LPN and from **the Helium liquifier staff** at WU — for teaching me about technology and cryogenics.

**Dr. Stefan Seidl** — for discussions about optical orientation of excitons.

**Dr. Michał Jakubczyk** — for ”on-line” help with  $\text{\LaTeX}$  and fruitful discussions about the philosophy of science.

I would like to express my deepest gratitude to **my Dad** and **my Sister**, for supporting me all the time.

**Dziękuję bardzo! Merci beaucoup! Thank you very much!**

---

# Notation

In this *work* the notation is consistent with that commonly used in books devoted to the quantum mechanics and articles about solid stated physics. Below there is a short list of symbols, acronyms, constants, and material parameters, which are of the most importance for the presented subject.

## Acronyms and Symbols

- PL – photoluminescence,  $\mu$ -PL - micro-photoluminescence (PL with the spatial resolution of the order of single microns)
- PLE – photoluminescence excitation
- QD – quantum dot
- WL – wetting layer
- FSS ( $\delta_1$ ) – fine structure splitting (splitting of excitonic line due to the anisotropic electron-hole interaction)
- $\delta_0$  – splitting between the excitonic states with angular momentum  $\pm 1$  and  $\pm 2$  (called "bright-dark" splitting)
- $\delta_2$  – splitting of the excitonic states with angular momentum  $\pm 2$
- $\Delta_{l-h}$  – splitting between heavy- and light-hole excitons
- X – neutral exciton (a correlated electron-hole pair), also a line in PL spectra related to the transition from excitonic state  $|X\rangle$  to the empty crystal
- XX – two-exciton complex, also a line in PL spectra related to the transition from biexcitonic state  $|XX\rangle$  to the excitonic state
- X+ – positively charged exciton, also a line in PL spectra related to the transition from positively charged excitonic state  $|X+\rangle$  to the single hole state
- X- – negatively charged exciton, also a line in PL spectra related to the transition from negatively charged excitonic state  $|X-\rangle$  to the single electron state

---

## Fundamental physical constants

- Planck's constant  $h = 6.62618 \cdot 10^{-34} JS$ ,  $\hbar = h/2\pi$
- Charge of electron  $e = 1.602189 \cdot 10^{-19} C$
- Free electron mass  $m_e = 9.10953 \cdot 10^{-31} kg$
- Bohr magneton  $\mu_B = 5.78838263 \cdot 10^{-2} meV/T$
- Boltzmann constant  $k_B = 1.3806505 \cdot 10^{23} J/K$  ( $86.173432 \mu eV/K$ )

## Material parameters (in helium temperatures)

For III-V quantum dots <sup>1</sup>:

- Energy gap InAs:  $0.418 eV$
- Energy gap GaAs:  $1.51 eV$
- Effective mass of electron:  $m_e = 0.067 m_e$
- Effective mass of heavy-hole (InAs, in-plane):  $m_{h,\perp} = 0.11 m_e$
- Effective mass of heavy-hole (InAs, vertical):  $m_{h,\parallel} = 0.34 m_e$

For II-VI quantum dots <sup>2</sup>:

- Energy gap CdTe:  $1.606 eV$
- Energy gap ZnTe:  $2.391 eV$
- Effective mass of electron (CdTe):  $m_e = 0.099 m_e$
- Effective mass of heavy-hole (CdTe, in-plane):  $m_{h,\perp} = 0.512 m_e$
- Effective mass of heavy-hole (CdTe, vertical):  $m_{h,\parallel} = 0.193 m_e$

---

<sup>1</sup>after S. Laurent, *PhD thesis*, and references therein

<sup>2</sup>after A. Lemaître *et al.*, PRB57, 1988, and references therein

---

# Resumé /Streszczenie /Abstract

**R**ÉSUMÉ. Cette thèse porte sur l'étude des relations entre la symétrie des boîtes quantiques de semiconducteur auto-assemblées III-V et II-VI (QDs, anglais *quantum dots*) et leurs propriétés optiques. L'intrication de polarisation d'une paire de photon émise dans la cascade biexciton-exciton d'une boîte quantique d'InGaAs a été récemment démontrée par deux groupes [1, 2]. En principe, l'éclatement de structure fine (FSS, anglais *fine structure splitting*) du niveau fondamental d'un exciton neutre, qui caractérise l'anisotropie native des boîtes quantiques, doit être inférieur à la largeur des raies radiatives. Dans le cas contraire, la collection de photons intriqués nécessite une *post-sélection* draconienne, qui réduit fortement l'efficacité d'une telle source [2]. Une technique fiable permettant un tel contrôle de la structure fine est fortement souhaitable afin d'envisager de futures applications des boîtes quantiques comme source des photons intriqués en polarisation. Dans ce but, l'application d'une perturbation externe semble être une technique très prometteuse. Différentes stratégies pour lutter contre cette levée de dégénérescence ont été abordées par divers groupes de recherche ces dernières années : (i) effectuer un traitement post-croissance tel qu'un recuit pour modifier les propriétés structurales des boîtes [3, 4]), (ii) appliquer une perturbation externe comme par exemple une contrainte uni-axiale [5], en vue de compenser l'anisotropie, (iii) chercher à produire une dégénérescence fortuite en appliquant un champ magnétique transverse [6]. C'est cette dernière méthode qui en 2006 a donné les résultats les plus probants, en démontrant le contrôle du degré d'intrication des photons émis par une boîte quantique unique. C'est donc dans un contexte d'intense compétition internationale que nos propres travaux ont été menés. Nous nous sommes concentrés sur l'exploration de deux effets : (i) la déformation par un champ électrique externe de la fonction d'onde des excitons de boîtes quantique [7], (ii) le déplacement Zeeman des niveaux excitoniques par un champ magnétique transverse pouvant conduire à une dégénérescence accidentelle des deux niveaux d'exciton [8].

Le premier **Chapitre 1** (*Introduction: quantum dots for entangled photons emission*) sert à introduire brièvement les propriétés fondamentales des boîtes quantiques de semiconducteur. Nous donnerons une description simple de leurs états électroniques, suffisantes pour discuter les propriétés optiques de ces objets et bien comprendre le rôle que joue l'anisotropie des boîtes. En particulier la levée de dégénérescence des niveaux excitoniques sera décrite ainsi que ses conséquences pour l'émission de photons intriqués en polarisation.

---

Dans le **Chapitre 2** (*Samples and Experimental setups*) nous décrivons les échantillons de boîtes quantiques étudiés au cours de cette thèse, à savoir des boîtes InAs/GaAs et CdTe/ZnTe. Nous présenterons les procédés technologiques utilisés pour réaliser des structures à effet de champ en vue de l'application d'un champ électrique. Enfin les différents montages expérimentaux de micro-photoluminescence seront détaillés.

Dans la partie suivante (**Chapitre 3**, *Influence of electric field on quantum dots*) nous présenterons des résultats de spectroscopie de boîtes quantiques individuelles dans un champ électrique. La levée de dégénérescence des excitons est reliée à l'interaction anisotrope d'échange entre électron et trou laquelle dépend sensiblement de la forme de la fonction d'onde excitonique. Un champ électrique semble être un bon moyen pour modifier cette dégénérescence et donc éventuellement l'annuler. Le champ est d'abord appliqué dans le plan des boîtes, géométrie qui semble la plus propice à changer la symétrie des fonction d'ondes. Selon la direction du champ par rapport aux axes principaux des boîtes il devrait être possible d'augmenter ou diminuer le FSS. Par la technologie de contacts sur des matériaux d'III-V (structures de diode n-Schottky et Schottky-Schottky) il nous a été possible d'appliquer le champ électrique avec succès sur des boîtes quantiques. Des changements systématiques de l'anisotropie optique de la luminescence étaient obtenus [7]. Ceux-ci sont le fruit de deux effets concurrents : la modification prévue de la symétrie des fonction d'ondes et la modification du recouvrement des fonctions d'onde d'électron et trou. Le dernier effet devrait toujours mener à la réduction de l'interaction d'échange. Afin d'estimer sa valeur nous avons exécuté des expériences dans une configuration de champ électrique parallèle à la direction de croissance des QDs. Dans cette configuration le champ ne semble pas devoir modifier significativement la symétrie des fonctions d'ondes pour un électron et un trou. Les changements de structure fine devraient être provoqués principalement par la séparation spatiale des porteurs. Les variations observées dans le champ vertical étaient plus petites que pour la configuration dans le plan, ce qui confirme notre hypothèse. Mais pour autant, l'asymétrie observée en renversant le sens du champ électrique indique aussi que le champ vertical produit un effet sur la symétrie des excitons [9]. Ceci se comprend assez bien car le champ électrique vertical déplace les porteurs par rapport aux régions de forte anisotropie des boîtes quantiques situées au dessus et au dessous du coeur de la boîte.

Les changements de FSS dans le champ horizontal qui ont été obtenus, sont relativement grands (comparable au décalage Stark), mais l'utilité de cette méthode reste limitée par la diminution d'intensité (due à la séparation spatiale des porteurs, et à leur ionisation hors des boîtes par échappement tunnel). Toutefois, l'annulation complète de la structure fine a été observée sur quelques boîtes quantiques possédant une anisotropie initiale faible.

D'autres mesures sur les complexes excitoniques tels que biexciton et trions nous ont permis de déterminer la position spatiale relative d'un électron et d'un trou à l'intérieur d'une boîte [9]. Les études de l'influence du champ électrique sur les propriétés optiques de boîtes II-VI ont été limitées à des observations liées aux fluctuations de champs électriques locaux, responsables de variations non-contrôlées de la structure fine excitonique [10].

---

Le **Chapitre 4** (*Influence of magnetic field on quantum dots*) est consacré à la description de l'influence du champ magnétique externe sur l'émission des boîtes. Pour des boîtes II-VI, la technologie de fabrication d'électrodes n'étant pas disponible, l'application d'un champ magnétique mérite vraiment d'être exploré. Nous avons expérimentalement observé que pour des boîtes CdTe/ZnTe les changements de FSS dépendent de l'amplitude et de la direction du champ magnétique appliqué. Pour le champ appliqué oblique aux axes principaux d'une boîte nous avons noté une rotation de la polarisation d'émission. L'explication de ces résultats repose sur le couplage très particulier entre les états "brillants" et les états "noirs" dans la configuration de champ transverse, comme le montre un modèle théorique de l'interaction Zeeman dans cette configuration. Il faut pour cela introduire un facteur de Landé transverse non nul pour les trous, ce qui suggère d'inclure le mélange de bande entre trous lourds et trous légers. Nous avons obtenu une bonne concordance entre les résultats expérimentaux et la théorie [8] : qualitative en ce qui concerne la rotation de la polarisation et de l'intensité des raies de luminescence, et quantitative pour l'évolution des niveaux d'énergie et de la structure fine. Très important d'un point de vue théorique, ont été prises en considération non seulement la direction du champ par rapport aux axes des boîtes, mais également par rapport aux axes du cristal. Le formalisme théorique était nécessaire pour comprendre comment le champ magnétique peut modifier la dégénérescence du spin dans certains cas seulement, et pour expliquer le rôle de l'anisotropie du facteur  $g$  transverse des états de trou. Les mesures dans le champ longitudinal ont quant-à elles fourni des informations sur le facteur  $g$  longitudinal des excitons. Elles montrent la gamme de champ pour laquelle l'anisotropie de QD devient négligeable par rapport à l'énergie Zeeman, conditions dans lesquelles on obtient l'émission des états propres bien polarisés circulairement.

Les études de la rotation du spin de l'exciton considéré comme un système à deux niveaux sont présentées dans le **Chapitre 5** (*Towards entanglement*) dans l'optique principale d'étudier sa cohérence quantique. En premier lieu, nous montrons la disparition de cette précession quand l'éclatement de structure fine est annulée grâce à un champ électrique : cela se manifeste par une résonance de l'orientation optique du spin de l'exciton sous excitation quasi-résonnante. La largeur de cette résonance permet de remonter de manière très originale à la largeur de raie homogène de la boîte quantique. Réciproquement, on observe que pour des boîtes quantiques avec une forte levée de dégénérescence, on peut réaliser l'alignement optique des excitons par une excitation résonnante (assistée par un phonon LO) polarisée linéairement et parallèlement aux axes de la boîte quantique. De manière plus générale, en fixant la polarisation de l'excitation et en variant la base de détection de la polarisation de la luminescence, nous mettons en évidence de forts effets de conversion de la polarisation (circulaire en linéaire et réciproquement) provoqués par la précession du spin de l'exciton dans le champ magnétique effectif (champ externe + interaction d'échange anisotrope). Ces effets sont la preuve que l'exciton garde parfaitement sa cohérence quantique aux échelles de temps de la luminescence. Tous les résultats présentés sont en bon accord avec une description théorique basée sur le formalisme de la matrice densité.



---

Le dernier **Chapitre 6** (*Conclusions*) présente un sommaire des résultats obtenus. Les études expérimentales et modélisations théoriques confirment que les perturbations externes, comme le champ électrique et magnétique, peuvent être utilisées pour modifier la structure des niveaux excitoniques des boîtes afin de contrôler leurs propriétés optiques. Les études détaillées de la direction de perturbation par rapport aux axes de l'anisotropie nous ont permis de comprendre les mécanismes de l'influence de ces champs sur les niveaux excitoniques. Le contrôle de la structure fine donne une chance d'augmenter la symétrie pour améliorer le degré d'intrication des paires de photons corrélés émis par un biexciton.

---

**S**TRESZCZENIE. Celem pracy było zbadanie wpływu symetrii układu na własności emisji pojedynczych fotonów z półprzewodnikowych kropek kwantowych. Głównym zadaniem było znalezienie odpowiednich technik umożliwiających kontrolowane zmiany własności optycznych kropek. Szczególnie ważne było przetestowanie różnych zaburzeń zewnętrznych, które mogły zmienić stopień degeneracji spinowej a przez to umożliwić emisję par splątanych fotonów. Jakkolwiek splątanie w kaskadzie bieksyton-ekscyton zostało już zaobserwowane [1, 2], ale opracowanie specjalnych technik umożliwiających zmiany anizotropii kropek jest ciągle pożądane. Jeśli anizotropia kropki (mierzona rozszczepieniem ekscytonowym w luminescencji – FSS, z angielskiego *fine structure splitting*) jest większa niż naturalna szerokość linii, wtedy efektywność rejestrowanych par splątanych fotonów jest bardzo mała i dramatycznie spada wraz z przekryciem się poziomów ekscytonowych [2]. Stosując różne metody starano się zmniejszyć rozszczepienie ekscytonowe: albo ingerując w proces wzrostu (wygrzewanie, relaksacja naprężenia [3, 4]) lub przykładając zewnętrzne zaburzenie o określonej symetrii: pole elektryczne [7], naprężenie jednoosiowe [5], pole magnetyczne [6, 8]. Ostatnia metoda została wykorzystana do uzyskania splątania na kropkach z materiałów III-V [6].

Skupiliśmy się na wykorzystaniu dwóch rodzajów pól: elektrycznego i magnetycznego, które mogą modyfikować przejścia ekscytonowe z pojedynczej kropki kwantowej. W obu przypadkach uzyskane wyniki doświadczalne potwierdzają, że rozszczepienie ekscytonowe może być zmieniane w kontrolowany sposób a nawet zlikwidowane całkowicie.

**Rozdział 1** (*Introduction: quantum dots for entangled photons emission*) zawiera krótkie wprowadzenie do tematu – opis atomowej budowy kropek kwantowych i dyskusję relacji między symetrią kropki a własnościami fotonów przez nią emitowanych. Szczególnie skupiliśmy się na wytłumaczeniu zjawiska rozszczepienia ekscytonowego w widmie luminescencji.

Kolejny **Rozdział 2** (*Samples and Experimental setups*) prezentuje przygotowanie do eksperymentu – od opisu badanych próbek, poprzez ich technologiczne przygotowanie (wykonanie kontaktów elektrycznych umożliwiających przykładanie pola elektrycznego) aż po przedstawienie technik pomiarowych i układu umożliwiającego badanie pojedynczych kropek kwantowych.

**Rozdział 3** (*Influence of electric field on quantum dots*) zawiera wyniki eksperymentalne i dyskusję wpływu pola elektrycznego na własności optyczne kropek kwantowych. Rozszczepienie w widmie jest związane z anizotropowym oddziaływaniem wymiennym między elektronem a dziurą formującym ekscyton. Ze względu na charakter tego oddziaływania potencjalnie najlepszym kandydatem na zaburzenie mogące wpłynąć na degenerację stanów jest właśnie pole elektryczne. Przyłożone w płaszczyźnie kropki powinno zmienić symetrię funkcji falowych dla elektronu i dziury i zależnie od kierunku względem osi głównych kropki albo zwiększyć albo zmniejszyć rozszczepienie w widmie. Dzięki opracowaniu technologii kontaktów na materiałach III-V (struktury n-Schottky i Schottky-Schottky) możliwe było przyłożenie pola elektrycznego w płaszczyźnie kropek kwantowych. Uzyskano systematyczne zmiany optycznej anizotropii luminescencji pojedynczych kropek kwantowych wraz z przykładanym polem [7]. Mierzone zmiany są wynikiem współ-

---

zawodnictwa dwóch efektów: oczekiwanej zmiany symetrii jedno-cząstkowych funkcji falowych oraz zmiany ich przekrycia. Ten ostatni zawsze powinien prowadzić do zmniejszenia oddziaływania wymiennego. Aby oszacować jego wartość przeprowadziliśmy pomiary dla struktur z polem elektrycznym prostopadłym do płaszczyzny kropek. W tej konfiguracji pole nie powinno silnie modyfikować symetrii funkcji elektronu i dziury, a zmiany w widmie powinny być wywołane głównie przestrzennym rozseparowaniem nośników. Obserwowane zmiany FSS w polu pionowym były kilka razy słabsze niż w polu w płaszczyźnie, co potwierdza tą hipotezę [9]. Dodatkowe badania kompleksów ekscytonowych umożliwiły dokładniejsze określenie przestrzennego ułożenia elektronu i dziury oraz wyznaczenie dipola w kierunku wzrostu struktury [9]. Badania wpływu pola elektrycznego na własności optyczne kropek z materiałów II-VI ograniczały się do pomiarów w funkcji pól lokalnych. Badania te stanowiły podstawę do identyfikacji linii ekscytonowych pochodzących z tej samej kropki kwantowej [11]. Fluktuacje ładunku w otoczeniu kropki mogą również prowadzić do niekontrolowanych zmian rozszczepienia [10], dlatego ważne jest określenie czynników wywołujących fluktuacje i parametrów zmniejszających ich statystyczne występowanie. Aczkolwiek uzyskane zmiany FSS w polu elektrycznym w płaszczyźnie dla kropek kwantowych InAs/GaAs są znaczne (porównywalne z przesunięciem Starka dla linii), lecz możliwość zastosowania tej metody jest ograniczona przez zmniejszenie intensywności luminescencji (skutek separacji nośników i tunelowania poza kropkę) oraz silne poszerzenie (spektralne przesunięcia linii związane z fluktuacją ładunku). Dlatego obserwacja całkowitego przywrócenia degeneracji poziomów ekscytonowych była możliwa tylko dla kropek z naturalnie małą anizotropią.

Drugim zaburzeniem wykorzystanym do zmiany rozszczepienia w widmie było pole magnetyczne przyłożone w płaszczyźnie kropek kwantowych. Wyniki doświadczalne i model teoretyczny przedstawia **Rozdział 4** (*Influence of magnetic field on quantum dots*). W związku z problemami w otrzymaniu dobrej jakości kontaktów elektrycznych na materiałach II-VI, ta metoda wydaje się najbardziej obiecująca dla tego typu struktur. Zaobserwowano zmiany FSS dla kropek kwantowych CdTe/ZnTe zależne od amplitudy i kierunku przykładanego pola. W przypadku pola nierównoległego do głównych osi kropki kwantowej dodatkowo zarejestrowano skrócenie płaszczyzny polaryzacji emisji. Zaobserwowano silne sprzężenie ze stanami "ciemnymi", które w obecności pola zostały udozwolone optycznie i pojawiały się w widmie (około  $1\text{meV}$  poniżej stanów "jasnych"). Wyniki eksperymentalne zostały przedyskutowane w modelu spinowego oddziaływania Zeemana i dzięki szerokiemu rozbudowaniu bazy dyskutowanych stanów (stany nieaktywne optycznie i dziury lekkie) możliwe było wyjaśnienie doświadczalnych wyników i pełna dyskusja zjawiska [8]. Otrzymano jakościową (skrócenie płaszczyzny polaryzacji, anizotropia intensywności dla stanów ciemnych) i ilościową (przesunięcie poziomów, zmiany rozszczepienia) zgodność między danymi doświadczalnymi a teorią. Szczególnie ważne w rozważaniach teoretycznych okazało się uwzględnienie kierunku zaburzenia nie tylko względem osi głównych kropki kwantowej, ale także osi kryształu. Badanie te pozwoliły określić przydatność pola magnetycznego jako zaburzenia zmieniającego strukturę przejść optycznych z pojedynczej kropki kwantowej, na dodatek zaowocowały wyznaczeniem  $g$ -czynnika Landego dla elek-

---

tronu i dziury w płaszczyźnie. Pomiary w polu magnetycznym w kierunku wzrostu struktury pozwoliły określić efektywny  $g$ -czynnik ekscytonowy oraz wyznaczyć zakres pól przy których rozszczepienie Zeemanowskie determinuje własności emisji i możliwa jest obserwacja czystych stanów spinowych.

Badania koherencji spinowej w układzie dwupoziomowym stanu ekscytonowego są prezentowane w **Rozdziale 5** (*Towards entanglement*). Przejście przez zero z rozszczepieniem zostało zmierzone bezpośrednio oraz przy wykorzystaniu zjawiska pompowania optycznego. Przy silnym, rezonansowym pobudzeniu polaryzacja ekscytacji wywołuje nierównowagową populację ekscytonów o określonym momencie elektrycznym. Dla anizotropowej kropki objawia się to w doświadczeniu jako wzrost stopnia polaryzacji liniowej przy pobudzeniu zgodnym z kierunkami anizotropii kropki. Zmniejszając rozszczepienie do zera stany stają się czyste spinowo i polaryzacja liniowa luminescencji znika, natomiast wzrasta stopień polaryzacji kołowej. Z pomiarów przy pobudzeniu kołowym obserwujemy silny wzrost stopnia polaryzacji kołowej, gdy  $FSS = 0$ . Szerokość tego rezonansu pozwala wyznaczyć szerokość naturalną linii oraz sprawdzić możliwość splątania stanów. Dodatkowym zjawiskiem pojawiającym się przy silnym pobudzeniu jest konwersja polaryzacji (wzrost stopnia polaryzacji liniowej przy pobudzeniu kołowym i *vice versa*), która została także zbadana na kropkach kwantowym InAs. Obserwacje doświadczalne zostały opisane przy użyciu formalizmu macierzy gęstości.

Ostatni **Rozdział 6** (*Conclusions*) przedstawia podsumowanie uzyskanych wyników badań. Przeprowadzone doświadczenia potwierdzają, że zewnętrzne zaburzenia takie jak pole elektryczne i pole magnetyczne mogą być używane do zmian własności optycznych półprzewodnikowych kropek kwantowych w kontrolowany sposób. Szczegółowe badania wpływu kierunku zaburzenia względem osi anizotropii pozwoliły zrozumieć mechanizmy wpływu tych pól na strukturę przejścia ekscytonowego z pojedynczej kropki. Kontrola rozszczepienia wymiennego w ten sposób daje możliwość podwyższenia symetrii systemu a przez to potencjalnie ułatwia uzyskanie emisji splątanych fotonów z pojedynczej kropki. Wyniki eksperymentalne i teoretyczny opis zjawiska precesji spinu są niezbędne do pełnego zrozumienia procesów emisji z poziomów ekscytonowych w kropkach kwantowych.

---

**A**BSTRACT. The aim of this *work* was to investigate the symmetry effects in optical properties of single semiconductor quantum dots (QDs). The main goal was to find new technologies which would allow us to modify those properties in a controllable way. Especially it was important to test different external perturbations restoring the spin degeneracy of the system what is a prerequisite for the achievement of photon entanglement in a QD emission. Although the polarization-entanglement in biexciton-exciton cascade have been recently demonstrated [1, 2], a reliable technique enabling such a control over QD anisotropy remains highly demanded. If QD anisotropy (measured as fine structure splitting of an excitonic line in photoluminescence – FSS) is larger than the natural linewidth, the rate of entangled photon pairs collected after post-selection gets dramatically reduced [2]. Different strategies for restoring higher symmetry were tested, either by influencing material properties of heterostructures (annealing or strain engineering [3, 4]) or by applying external perturbations compensating the native asymmetry: in-plane electric field [7], uniaxial strain [5], and in-plane magnetic field [6, 8] were tried. The last-mentioned method has given the most satisfactory results so far in GaAs-based self-assembled QDs [6].

We have examined two different pathways consisting in applying external perturbations of specific symmetry, namely an electric field applied parallel to one of the symmetry axes of the QD, and an in-plane magnetic field. In both cases, our experimental results indicate that the FSS in a single QD can be tuned significantly and canceled.

**Chapter 1** (*Introduction: quantum dots for entangled photon emission*) contains short introduction into the subject – description of structural properties of quantum dots and discussion about the relations between the symmetry of dots and the properties of emitted photons. We put emphasis on the explanation of the origin of fine structure splitting in the excitonic spectra.

Next **Chapter 2** (*Samples and Experimental setups*) presents the preparation of experiments – from the description of investigated samples, through technological processing (preparation of field-effect structures), and it ends up with showing the experimental techniques enabling studies on single quantum dots.

**Chapter 3** (*Influence of electric field on quantum dots*) reports the experimental results and the discussion of the influence of electric field on the optical properties of quantum dots. The splitting in the spectra is related with anisotropic exchange interaction between electron and hole, which form an exciton. Because of the character of this interaction, the electric field seems to be a very good candidate as a perturbation to modify it. If applied in the QD plane it should affect the symmetry of the wavefunctions for single carriers and depending on the direction (with respect to QD anisotropy) it should either increase or decrease the splitting in spectra. Thanks to the preparation of field-effective structures on III-V materials (n-Schottky, Schottky-Schottky) it was possible to apply an in-plane electric field. We obtained systematical changes of FSS for individual quantum dots with applied field [7]. The observed FSS changes with the applied voltage result always from both effects: the expected symmetry modification of the wavefunctions and the diminution of the overlap of single carriers wavefunctions. The latter effect

---

always leads to the reduction of the exchange interaction. In order to estimate this contribution from the separation of the interacting carriers, we performed measurements for structures with the field applied in the growth direction. In this vertical configuration the field should not modify strongly the symmetry of the wavefunctions, and the changes in the FSS should be influenced mostly by the spatial separation of an electron and a hole. Observed changes in FSS for vertical field were a few times weaker than those for in-plane configuration, what confirm our explanation how the electric field acts on QDs [9]. From additional tests on the excitonic complexes we gained the knowledge about precise spatial alignment of electrons and holes in a QD, we were thus able to estimate the permanent vertical dipole [9]. The studies of the influence of electric field on QDs made of II-VI materials were limited to the studies of local electric fields. These investigations were used to identify different transitions from the same QD [11]. Charge fluctuations in the QD vicinity may produce non-controlled changes in the excitonic splitting [10]. Therefore it is important to study the mechanisms which produce the fluctuations in order to find the conditions under which they are statistically negligible. Nevertheless the FSS changes in electric field are significant, and for samples with electro-optical devices embedding InAs/GaAs QDs in their intrinsic region they were comparable with Stark shift, but the application of this method is limited by the intensity reduction (due to electron-hole separation and carriers escape out of a dot) and strong line broadening (spectral diffusion of the lines induced by local field fluctuations). Thus electric field enabled us to cancel FSS only for QDs with small native splitting.

Second investigated perturbation used to influence the spin degeneracy, was in-plane magnetic field. Experimental results and theoretical model are presented in **Chapter 4** (*Influence of magnetic field on quantum dots*). This method of FSS control seems to be very promising especially for II-VI QDs, since the technology of electric field-effect structure for these materials is not well established. We observed that an in-plane magnetic field modifies the fine-structure splitting of the excitonic emission of CdTe/ZnTe quantum dots depending on the field direction and amplitude. For the field applied obliquely to the QD anisotropy we noticed rotation of emission polarization. We observed strong coupling between "bright" and "dark" states, that became optically active due to field-induced mixing in this configuration and they appeared in the spectra at  $\sim 1\text{meV}$  below the excitonic doublet. The results were discussed in terms of an effective spin Hamiltonian derived for the exciton ground state. Full hole basis (including light-hole states) was taken into account in the calculations in order to explain all observations [8]. The presented experimental results are in qualitative (polarization rotation) and rough quantitative (splitting variation) agreement with the model based on a Zeeman spin Hamiltonian. It turned out that it is important to take into account not only the direction of the field with respect to QD anisotropy axes, but also with respect to the main crystallographic direction of the host lattice. These studies showed how magnetic field can be used to cancel FSS, and additionally they revealed such information about quantum dots as  $g$ -factors for electrons and holes. Additional studies of the perpendicular configuration of the field allowed to get effective excitonic  $g$ -factors and to estimate the field range for which Zeeman

---

splitting determines the optical properties of the emission.

The studies of spin coherence in the excitonic state are summarized in **Chapter 5** (*Towards entanglement*). Cancellation of FSS in electrically-driven structures was measured in optical pumping experiment. A circularly polarized and quasi-resonant ( $\sim 2LO$ -phonons above the excitonic transition) excitation induces an optical orientation of exciton spin. For an anisotropic QD it manifests itself in the experiment as an increase of the linear polarization degree under corresponding linear excitation, while for an isotropic dot circular  $\sigma^+$  or  $\sigma^-$  excitation amounts to optical preparation of the exciton in one of the spin states  $|\pm 1\rangle$ . As a result, measuring the PL circular polarization provides a very sensitive probe of the excitonic system in the perspective of entangled photon emission. By electrically driving FSS across zero, we have been able to strongly increase the circular polarization to 70%. Remarkably, from the width of this circular polarization resonance we could also deduce the homogeneous linewidth of the excitonic transition. This technique may be used to test the preparation of the excitonic states for entangled emission. An accompanying effect under resonant excitation is conversion of polarization (enhancement of circular polarization under linear polarization and *vice versa*). These phenomena were investigated under  $1LO$ -phonon excitation. Both, linear-to-circular and circular-to-linear conversion was observed. The results were described using density matrix formalism.

Last **Chapter 6** (*Conclusions*) shows the summary of the work. The obtained experimental results confirm that the external perturbations like electric and magnetic fields can be used to modify the optical properties of semiconductor quantum dots in a controllable way. Detailed studies of perturbation direction with respect to QDs eigenaxes allowed to understand how these fields act on the excitonic transitions from single quantum dots. Control of exchange interaction in QDs gives the possibility to restore high symmetry of the system and to obtain entangled photon emission. The studies of FSS strength and spin coherence are prerequisites for full understanding of excitonic emission from quantum dots.





---

# Contents

<b>1</b>	<b>Introduction</b>	<b>1</b>
1.1	Historical background . . . . .	1
1.2	Semiconductor quantum dots . . . . .	3
1.3	Quantum dot structural properties . . . . .	3
1.4	QD electronic states: a simplified description . . . . .	6
1.5	Exciton fine structure of actual quantum dots . . . . .	7
1.6	Polarization correlation in the “biexciton cascade” . . . . .	10
1.7	QD-based source of entangled photons . . . . .	12
1.8	Expression of the anisotropic exchange term . . . . .	16
1.9	Aim of this work . . . . .	18
<b>2</b>	<b>Samples and Experimental setups</b>	<b>21</b>
2.1	Samples . . . . .	22
2.1.1	II-VI samples . . . . .	23
2.1.2	III-V samples . . . . .	25
2.2	Technology . . . . .	27
2.2.1	Devices for in-plane electric field . . . . .	28
2.2.2	Devices for vertical electric field . . . . .	32
2.3	Experimental setups . . . . .	35
2.3.1	Setup for measurements of II-VI materials . . . . .	35
2.3.2	Setup for measurements of III-V materials . . . . .	38
<b>3</b>	<b>Influence of electric field on quantum dots</b>	<b>43</b>
3.1	In-plane electric field . . . . .	45
3.1.1	PL intensity and linewidth . . . . .	47
3.1.2	Fine structure splitting vs. in-plane field . . . . .	50
3.2	Vertical electric field . . . . .	52
3.2.1	Permanent vertical dipole . . . . .	54
3.2.2	Direct Coulomb integrals . . . . .	55
3.2.3	Fine structure splitting vs. vertical field . . . . .	57
3.3	Local electric field . . . . .	57
3.3.1	Transition identification . . . . .	57
3.3.2	Fine structure vs. local field . . . . .	61
3.4	Conclusion – FSS tuning . . . . .	63

<b>4</b>	<b>Influence of magnetic field on quantum dots</b>	<b>65</b>
4.1	Exciton Zeeman Hamiltonian . . . . .	67
4.2	Faraday configuration . . . . .	68
4.3	Voigt configuration . . . . .	71
4.3.1	Theoretical model . . . . .	72
4.3.2	Isotropic hole $g$ factor ( $\beta = 0$ ) . . . . .	74
4.3.3	Anisotropic $g$ factor ( $\beta \neq 0$ ) . . . . .	76
4.4	Experimental results . . . . .	79
4.5	Orbital effects . . . . .	81
4.6	Conclusions - FSS manipulation . . . . .	84
4.7	Nuclear field . . . . .	85
<b>5</b>	<b>Toward Entanglement</b>	<b>89</b>
5.1	Exciton spin dynamics in density matrix formalism . . . . .	92
5.1.1	Time evolution of the exciton density matrix . . . . .	92
5.1.2	Geometrical representation of spin precession . . . . .	96
5.1.3	Polarization relaxation and conversion in cw experiments . . . . .	98
5.2	Optical orientation/alignment of exciton . . . . .	101
5.2.1	Optical orientation in QDs with tunable FSS . . . . .	101
5.2.2	Optical orientation for different excitations . . . . .	104
5.3	Measurements of polarization conversion . . . . .	107
5.3.1	Circular-to-linear conversion . . . . .	107
5.3.2	Linear-to-circular conversion . . . . .	110
5.3.3	Conversion of polarization for trions . . . . .	112
5.4	Conclusion . . . . .	114
<b>6</b>	<b>Conclusions</b>	<b>117</b>

---

# List of Figures

1.1	Topographical image of quantum dots. . . . .	4
1.2	Cross-section image of a single quantum dot. . . . .	4
1.3	Piezoelectric potentials around quantum dot – calculations. . . . .	5
1.4	Scheme of the level splitting of the excitonic state in a quantum dot. . . . .	9
1.5	FSS - observation in PL. . . . .	9
1.6	Scheme of emission cascade from a single neutral quantum dot. . . . .	11
1.7	Density matrices for the XX–X photon cascade. . . . .	14
1.8	Dynamics in a quantum dot – PL decay and absorption. . . . .	15
2.1	Scheme of II-VI samples – layers ordering. . . . .	23
2.2	Typical $\mu$ -photoluminescence spectrum of the sample $A_{26}$ . . . . .	24
2.3	Typical $\mu$ -PL spectrum of the sample $B_{26}$ . . . . .	25
2.4	Scheme of III-V sample wafer with examples of macro-PL. . . . .	26
2.5	Scheme of III-V sample – layers ordering. . . . .	27
2.6	Scheme of of Schottky-Schottky device on the sample surface. . . . .	28
2.7	Scheme of Schottky-Schottky device on the border of etched mesas. . . . .	29
2.8	Scheme of n-Schottky device. . . . .	30
2.9	Voltage-current characteristics of the in-plane Schottky-Schottky device. . . . .	31
2.10	Scheme of device for vertical electric field. . . . .	33
2.11	Scheme of sample mounting. . . . .	33
2.12	Voltage-current characteristics of the vertical n-Schottky device. . . . .	34
2.13	Scheme of experimental setup for $\mu$ -PL measurements of II-VI materials. . . . .	37
2.14	Scheme of experimental setup for $\mu$ -PL measurements of III-V materials (version 1). . . . .	39
2.15	Scheme of experimental setup for $\mu$ -PL measurements of III-V materials (version 2). . . . .	40
3.1	PL evolution under in-plane electric field. Stark effect. . . . .	46
3.2	PL evolution under in-plane field for non- and quasi-resonant excitation. . . . .	48
3.3	Linewidth and intensity of the excitonic lines vs. applied voltage. Tunneling model. . . . .	49
3.4	FSS changes with in-plane electric field. . . . .	51
3.5	Example of FSS cancelation with in-plane electric field. . . . .	51

3.6	PL evolution under vertical electric field – charging effects. . . . .	52
3.7	Stark shift of different excitonic complexes from a single quantum dot (non- and quasi-resonant excitation). . . . .	53
3.8	FSS changes vs. vertical electric field. . . . .	55
3.9	Binding energies of charged excitons in a quantum dot. . . . .	56
3.10	Time evolution of the spectra from a single quantum dot in a fluctuating electric field. . . . .	58
3.11	Temporal evolution of the spectrum for different excitation power – time scale of the electric field fluctuations. . . . .	59
3.12	Correlation between the energy positions of the biexciton and trion lines with neutral exciton. . . . .	60
3.13	Correlation between the intensities of the charged exciton and biexciton lines. . . . .	62
3.14	Correlations between line position (Stark effect) and FSS for excitonic and biexcitonic lines. . . . .	62
4.1	Calculation and experimental measurements of energy of heavy-hole excitonic levels as a function of longitudinal magnetic field. . . . .	69
4.2	Evolution of spectrum from a single quantum dot under longitudinal magnetic field. $g$ factors for different excitonic complexes. . . . .	69
4.3	Statistics of $g$ factors for II-VI samples. . . . .	70
4.4	Linear polarization degree vs. magnetic field (model and experimental results). . . . .	72
4.5	Scheme of experimental configuration in Voigt experiment. . . . .	73
4.6	Evolution of heavy-hole excitonic levels as a function of in-plane field for two perpendicular directions of the field. . . . .	75
4.7	FSS absolute value vs in-plane field direction. . . . .	75
4.8	FSS absolute value on a color scale vs in-plane field direction for a strong $g$ factor anisotropy. . . . .	77
4.9	Schematics of the crystallographic axis configuration with respect to the QD principal axes. . . . .	78
4.10	Rotation angle of the PL polarization orientation vs in-plane magnetic field. . . . .	78
4.11	Experimental results showing PL evolution with in-plane magnetic field. . . . .	80
4.12	Experimental results showing FSS changes with in-plane magnetic field. . . . .	80
4.13	FSS and PL polarization rotation under in-plane magnetic field. . . . .	81
4.14	Model of the wavefunction suppression in magnetic field – canceling field vs. wavefunction size and dot ellipticity. . . . .	83
4.15	Overhauser shift for $X^+$ vs. excitation power. . . . .	86
4.16	Circular polarization of excitonic line induced by dynamic nuclear polarization. . . . .	87
5.1	Raman scattering of the laser line in the GaAs barrier. . . . .	91
5.2	Scheme of the Poincaré’s sphere and examples illustrating spin precession in magnetic field. . . . .	97

---

5.3	Optical pumping - FSS tuning. . . . .	102
5.4	Optical pumping - test of spin degeneracy. . . . .	103
5.5	Zoom of PL spectra for two chosen excitons $B$ and $C$ . . . . .	104
5.6	Optical pumping effect on excitons $B$ and $C$ . . . . .	105
5.7	Conversion of circular-to-linear polarization on excitons $B$ and $C$ . . . . .	108
5.8	Conversion of circular-to-linear polarization - theory. . . . .	109
5.9	Conversion of circular-to-linear polarization - theory. . . . .	109
5.10	Conversion of linear-to-circular polarization on excitons $B$ and $C$ . . . . .	111
5.11	Effect of optical pumping and conversion for $X^-$ . . . . .	113

---

---

# CHAPTER 1

---

## Introduction: semiconductor quantum dots for emission of entangled photons

### Contents

---

1.1	Historical background . . . . .	1
1.2	Semiconductor quantum dots . . . . .	3
1.3	Quantum dot structural properties . . . . .	3
1.4	QD electronic states: a simplified description . . . . .	6
1.5	Exciton fine structure of actual quantum dots . . . . .	7
1.6	Polarization correlation in the “biexciton cascade” . . . . .	10
1.7	QD-based source of entangled photons . . . . .	12
1.8	Expression of the anisotropic exchange term . . . . .	16
1.9	Aim of this work . . . . .	18

---

*“If quantum mechanics hasn’t profoundly shocked you, you haven’t understood it yet.”*

Niels Bohr

## 1.1 Historical background

SINCE THE FIRST TRANSISTOR PATENT in 1928 by J. E. Lilienfeld [12] and the construction of the first transistor in 1947 by W. Shockley, J. Bardeen and W. Brattain [13] at Bell Laboratories, the semiconductor materials have been attracting a lot of attention in Sciences. The growing interest in this field of solid state physics was related not only with new opened prospects in quantum mechanics studies, but also with possible industrial applications. The physicists’ curiosity

and the market demand have been the driving forces of a fast technology development. The progress was so intense that in only fifty years the biggest advantage of semiconductor devices, their constant size reduction to micrometer scale, has reached its fundamental limit. The end of XX<sup>th</sup> century revealed a question if the atom size limitation will cause the end of semiconductor technology development? The answer to this question was building up at the same time. The future of semiconductor science relies on quantum bits or "qubits", based on a quantum system containing a logical "bit" [14]. The history of quantum computation starts even before the computer science. The roots of this discipline are in K. Gödel theory of computational and non-computational functions [15], then it grew up with research on Church-Turing machines [16, 17], and for a long time existed only as a branch of mathematics. At the beginning of 80's, physicists started to combine it with the famous Einstein-Podolski-Rosen paradox [18] of quantum mechanics, which thanks to Bell theorem [19] can be experimentally tested in a now well-established formal framework. The success of such experiments naturally lead to the idea of quantum computing with physical systems. This "quantum" way of operating the information gives us a unique possibility to transfer it securely, as one cannot clone a unknown quantum state, otherwise EPR paradox would guarantee existence of information transfer faster than light! Quantum cryptography (see e.g. [20]) opened a new branch of investigations extensively exploring quantum entanglement as the computational ground. Although the theoretical basis of quantum computer operations is clear, the challenge remains to find the right system, probably a semiconductor one, which could be easily integrated with standard micro-electronic devices. Pioneering experiments [21] first demonstrated that qubits can be stored in the polarization state of photons. The next step was then to find a (semiconductor) non-classical light source emitting pulses containing exactly one photon. One of the proposals was to use quantum dots as a source of single photons on demand [22], which has been experimentally achieved in different groups, even though improvement of such sources (operating temperature, emission rate, etc.) is required to compete with optical parametric sources already available as commercial products [23]. Time will tell whether quantum dots can answer to this challenge.

In the next *Sections* of this introduction, the ground physical properties of quantum dots will be reviewed. We will start first with the information about characteristic quantities regarding the atomistic structure. Next, the structure of electron/hole confined levels will be described, before the interaction between confined carriers will be considered. In particular, the direct and exchange Coulomb interactions will be discussed in more detail, as they are related to the selection rules of optical emission from quantum dots. In particular the role of the symmetry of the system will be highlighted in this context. Briefly the characteristics of single photon emission from quantum dots will be described, whereas the last *Section* will present to the aim of the works shown in this thesis.

## 1.2 Semiconductor quantum dots

**Quantum dots (QDs)** are nanometer size structures in which the motion of carriers is restricted in all spatial directions. This 3D confinement makes the energy spectrum of a single carrier quantized in shells of discrete levels. Due to this analogy with the energy spectrum of atoms, quantum dots are often called "artificial atoms". In semiconductor QDs, the potential walls produced by a material barrier surrounding the QD plays the role of the nucleus Coulomb potential in atoms. Electrons occupy discrete energy levels and, analogically to atoms, excited and ionized states can be formed. Although there are many similarities between an isolated atom and a quantum dot, one should not forget about important differences, which come from the specific properties of solid state. Also, one has to be careful with "expanding" our intuitions from other low-dimensional structures. For example, when under excitation with light an electron is promoted from the valence band to the conduction band, the Coulomb interaction between this promoted electron and the hole left in the valence band plays a significative correction to the single particle energy. Such a correlated electron-hole pair in a QD will be named an **exciton** in analogy to the case of bulk materials. The symbol  $X$  will be used to denote the exciton state. In the case of QDs, the name "exciton" has become quite conventional though not very meaningful, since in forming an excitonic state the electrostatic Coulomb interaction between carriers should be the leading term. This is definitely not the case in QDs where electron-hole correlation is still dominated by the barrier confinement.

The most intensely studied QDs are made from III-V binary compounds: arsenides (e.g. InAs/GaAs), nitrides (e.g. GaN/GaN), phosphides (e.g. InP/GaP). More recently, II-VI materials gained a large interest thanks to their light emission at higher temperature (compared to III-V materials). Telluride (e.g. CdTe/ZnTe) and selenide (e.g. CdSe/ZnSe) compounds have been among the most intensively investigated II-VI QDs.

## 1.3 Quantum dot structural properties

In this *work* we focus only on properties of self-assembled semiconductor quantum dots. A detailed description of the samples with QDs studied in our experiments will be given in *Chapter 2*. Here general properties of QD structure and growth are recalled. The growth method is based on self-induced rearrangement of the semiconducting epitaxial layers generally due to a strong lattice mismatch. For this reason, one cannot have full control over the QD ordering and geometry. Even though growth conditions have obvious strong influence on QD sample properties, a post-growth treatment is often required to improve these properties. Recently such techniques have been strongly developed by different research groups <sup>1</sup>. One of the most important parameters of QD heterostructures is the QD density. Typically it varies from  $10^7 cm^{-2}$  to  $10^{12} cm^{-2}$ . One can see in the

<sup>1</sup>For example: rapid thermal annealing [24], focused laser beam heating [25], or strain engineering [4].



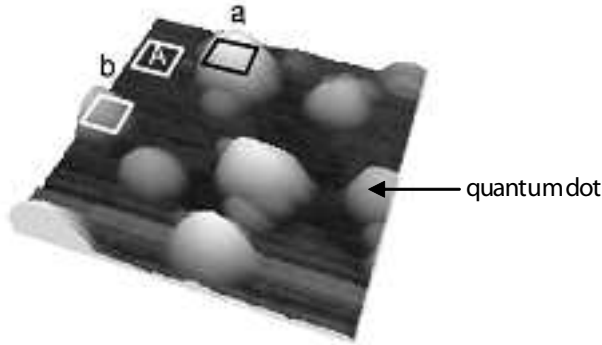


**Figure 1.1.** Topographical image of InAs QDs on GaAs (001) surface with a scan range of  $95\text{nm}$  and height range of  $8.1\text{nm}$ . (from Ref. [26]).

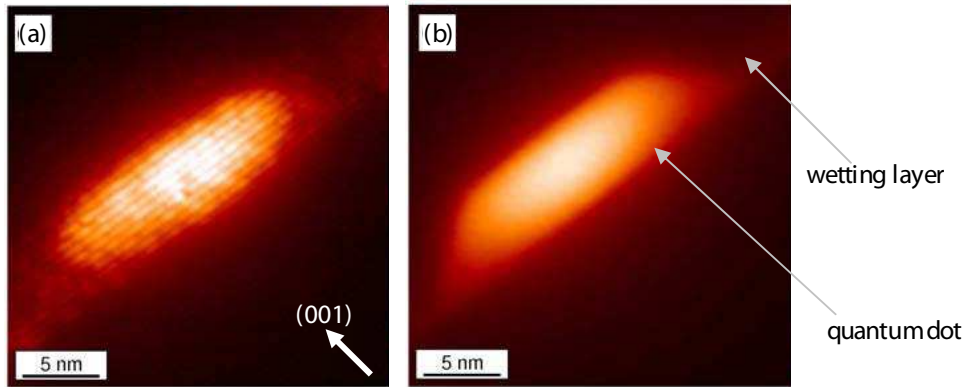


**Figure 1.2.** (a)  $40 \times 40\text{nm}^2$  cross-sectional scanning tunneling microscopy image of a InAs/GaAs quantum dot. (b) Outward relaxation on the surface (after cleaving) - calculations based on the elastic theory (from Ref. [27]).

Scanning Tunnelling Microscope (STM) view presented in Fig. 1.1 that dots can be spatially placed very close one to another, (at the  $10\text{ nm}$  scale). Convenient optical investigation of an individual QD requires thus samples with a low QD density (below  $10^9\text{cm}^{-2}$ ). In *Chapter 2* we will describe some experimental tools, which allow us to have an access to the micro-world and to perform measurements on individual zero-dimensional objects.

A self-assembled QD consists of  $\sim 10^3 - 10^5$  atoms of one material embedded in a host barrier material. The detailed information about QD atomistic structure like shape, size and composition can be determined from the scanning tunneling microscopy (STM) or Transmission Electron Microscopy (TEM) [28, 29]. STM analysis has been extensively carried out by P. M. Koenraad *et al.* [30] and revealed very interesting details of QD atomic structure. The (110) plane containing the growth direction [001] is a natural cleaving plane of the crystal offering access to the cross-section of QDs. Such images realized with atomic resolution clearly indicate the QD size of the order of a few nm ( $2 - 5\text{nm}$  in height and  $10 - 30\text{nm}$  in

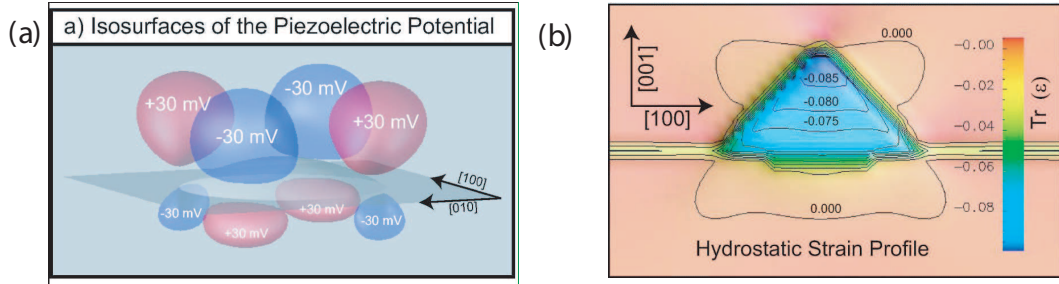


**Figure 1.3.** (a) Piezoelectric potential for a lens-shaped InAs/GaAs quantum dot (base  $25.2 \text{ nm}$ , height  $5 \text{ nm}$ ). The isosurfaces represent potential values of  $30$  and  $-30 \text{ mV}$ . The dot and the wetting layer are represented as a gray surface. (b) Contour plot of the hydrostatic strain for a square-based pyramid with  $11.3 \text{ nm}$  base and  $5.6 \text{ nm}$  height (from Ref. [34]).

diameter) and additionally evidence the lattice relaxation (see Fig. 1.2) around the dot. The latter can be directly related to the chemical composition of a dot. It turns out that during the growth process the barrier material interdiffuses into QDs. For InAs QDs grown on GaAs the Indium profile is strongly asymmetric (the In content varies linearly from 60% at the bottom to 100% at the top [31]). The chemical composition in real space corresponds to the confinement potential profile experienced by carriers. Strong intermixing of materials has thus very important consequences in electronic structure of the system and on spatial localization of electrons and holes [32]. Those effects will be discussed later in *Chapter 3*. QDs made from different compounds and grown at different conditions differ from each other, but there is a common feature: the lateral size is a few times larger than the vertical one. The second important characteristics coming out from morphology studies by STM is the presence of regular monoatomic layers below QDs (see Fig. 1.2). This builds up an ultra-thin quantum well which is called a **wetting layer (WL)**, and whose two-dimensional density of states can strongly influence QD electronic and optical properties. First, QD states can couple to this 2D-continuum [33] leading to a dramatic change of the expected 0D absorption spectrum. Second, optical excitation above WL band edge produces excitons or uncorrelated electrons and holes not directly in QDs. This can be useful to investigate the saturation regime of QD population, but may appear as a major drawback in experiments on single QDs where generally the charge state or population has to be kept under precise control. For such studies, QDs with discrete excited levels well separated from the 2D continuum must be privileged.

The clear vertical asymmetry of QDs has been first considered theoretically by M. Grundmann *et al.* (Ref. [35]) for band structure calculations in the framework of  $\mathbf{k}\cdot\mathbf{p}$  formalism. More recently, an atomistic approach based on pseudo-potentials method has been also applied by G. Bester and A. Zunger [34] to take into account the exact symmetry (in particular at atomic scale) of QDs. Detailed calculations allowed them to compare contributions of different effects into the level structure of electrons and holes, as they naturally take into account the shape of potential barriers as well as the role of atomistic interfaces (of lower symmetry) or of strain

and piezo-induced effects. It turns out that the piezoelectricity of the strained materials must be taken into account in order to explain some optical properties of self-assembled QDs. An example of calculations is shown in Fig. 1.3. The effective potential due to the strain varies from the bottom to the top of a QD and a quadrupolar potential of piezo-charge clearly influences the preferential alignment of the carriers along crystallographic axes of the lattice. Note that this contributes also as a perturbation of  $C_{2v}$  symmetry (meaning that directions  $[110]$  and  $[-110]$  are not equivalent) even in the case of a square based pyramid-like QD, since the quadrupolar potential has different strength on top and bottom of the QD. Although in experiments all listed effects contribute together and only a combined effect is observed, theoretical predictions about the signs and the magnitude of the shape-, interface-, strain-, and piezo-electric -effects are obviously useful to chose an external perturbation to modify the optical properties of QDs.

More detailed description of the properties of quantum dots requires the discussion of their symmetry. We put emphasis on this aspect in the next *Section*, because it is essential for this *work*.

## 1.4 QD electronic states: a simplified description

In order to understand how the actual symmetry of a QD impacts on its optical properties, we first need to describe in more detail the electronic states. The single particle Hamiltonian for an electron or a hole is composed of two terms: kinetic energy and the potential energy (including spin-orbit interaction). The first one is invariant under all unitary operations acting on spatial coordinates, while the second reflects the actual symmetry of the QD system and thus determines the point group symmetry of the total Hamiltonian (see e.g. Ref. [36]). The investigated III-V and II-VI compounds crystallize in zinc-blend structure with symmetry  $T_d$ , but as soon as a nanostructure is grown with an anisotropy between the growth direction (say parallel to  $[001]$  axis) and the lateral directions, the symmetry point group reduces to  $D_{2d}$ . This would be the case for a square based parallelepipedic QD (neglecting the presence of the WL). In such a case the in-plane directions  $[110]$  and  $[-110]$  transform into each other by the fourfold roto-inversion<sup>2</sup>. Actually, this is never the case, as in addition to the vertical/horizontal anisotropy, the obvious lack of symmetry along the growth axis leads to the lower symmetry point group  $C_{2v}$ . Due to this reduced symmetry, the projection of the total angular momentum operator  $\hat{J}_z$  along  $z$  is no longer a good quantum number for the QD eigenstates. As will be discussed further, the optical properties get thus anisotropic for a light propagating along  $z$ . Nevertheless, it remains very useful to use a basis of  $\hat{J}_z$  eigenstates while treating as a perturbation the terms of the QD potential leading to  $C_{2v}$ . This is the general framework which will be generally used in this thesis. Let us write more explicitly the electron (hole) wavefunctions  $\Psi_{n,l_z,j_z}^{e(h)}$  forming this

---

<sup>2</sup>This symmetry operation consists of a  $\pi/2$  rotation around  $z$  followed by an inversion of  $z$  coordinate.

basis in the effective mass approximation (EFA):

$$\Psi_{n,l_z,j_z}^{e(h)} = F_{n,l_z}^{e(h)}(\vec{r})u_{n,j_z}^{e(h)}(\vec{r}) \quad (1.1)$$

The indexes  $l_z$  and  $j_z$  refer respectively to the angular momentum projection on  $z$  of the envelope function  $F_{l_z}^{e(h)}(\vec{r})$  and of the crystal Bloch function  $u_{j_z}^{e(h)}(\vec{r})$ , the latter assumed to be the same for barrier and QD materials, while  $n$  is a subband index required to describe the valence band components originating from the three degenerate  $X, Y, Z$ -like atomic orbitals. The envelope functions  $F_{n,l_z}^{e(h)}$  are the solutions of the single band EFA Hamiltonian respectively for the electron (e) band and the three hole (h) bands indexed by  $n$ . In analogy to atoms they correspond to wave functions of symmetry  $S, P, D, \dots$ . In this basis, the QD potential of  $D_{2d}$  symmetry couples states with constant total angular momentum  $l_z + j_z$ . As in interband optical transitions the oscillator strength is weighted by the envelope function overlap  $|\int F_{l_z}^e(\vec{r})F_{l_z}^h(\vec{r})|^2 = \delta_{l_z,l_z}$  this coupling turns out to be of rather weak importance. In contrast, even though the coupling of  $C_{2v}$  symmetry has a smaller magnitude it will reveal more crucial because of a drastic change of optical selection rules. In most of the situations discussed further, it is thus enough to focus on the Bloch part of the eigenstates associated with the envelope of  $S$  ( $l_z = 0$ ) character. Under this assumption, the final basis of convenient use may be reduced to the spin state basis for electrons (i.e.  $u_{+1/2}^e \equiv |+\frac{1}{2}\rangle = |\uparrow\rangle$ ,  $u_{-1/2}^e \equiv |-\frac{1}{2}\rangle = |\downarrow\rangle$ ), while for holes only the Bloch states of heavy-hole band ( $j_z = \pm 3/2$ ) and light-hole band ( $j_z = \pm 1/2$ ) can be retained<sup>3</sup>. The corresponding basis is recalled below, with a double arrow  $\uparrow\uparrow$  to represent the hole spin degree of freedom.

$$\begin{aligned} |+\frac{3}{2}\rangle &= \frac{1}{\sqrt{2}}|X + iY\rangle \uparrow\uparrow \\ |+\frac{1}{2}\rangle &= \frac{1}{\sqrt{6}}|X + iY\rangle \downarrow\downarrow - \sqrt{\frac{2}{3}}|Z\rangle \uparrow\uparrow \\ |-\frac{1}{2}\rangle &= -\frac{1}{\sqrt{6}}|X - iY\rangle \uparrow\uparrow - \sqrt{\frac{2}{3}}|Z\rangle \downarrow\downarrow \\ |-\frac{3}{2}\rangle &= -\frac{1}{\sqrt{2}}|X - iY\rangle \downarrow\downarrow \end{aligned} \quad (1.2)$$

## 1.5 Exciton fine structure of actual quantum dots

When an electron-hole pair is photocreated or captured from the wetting layer in the QD, it forms a strongly correlated two-particle state. This complex named in the following exciton is described by an Hamiltonian which is the sum of both single particle Hamiltonians plus the Coulomb interaction between the particles. The latter decomposes into a direct term which amounts to a few tens of  $meV$ , and an exchange term due to Pauli principle and indiscernibility between conduction and valence electron (although they belong to different bands). The exchange term is much smaller in magnitude, but as it acts like a spin-dependent interaction; it

<sup>3</sup>Here we do not include the valence split-off band corresponding to  $|J| = 1/2$  which is assumed to be well separated in energy from the  $|J| = 3/2$  subband.

influences dramatically the structure of the exciton ground state.

In lens- or pyramid-shaped self assembled quantum dots, the hole ground state has a pronounced heavy-hole character (above 90% according to Ref. [37]). As a result, to the first order the four possible spin configurations of a ground state exciton read:

$$\begin{aligned}
|+1\rangle &= \left| +\frac{3}{2}, -\frac{1}{2} \right\rangle \equiv |\uparrow, \downarrow\rangle \\
|-1\rangle &= \left| -\frac{3}{2}, +\frac{1}{2} \right\rangle \equiv |\downarrow, \uparrow\rangle \\
|+2\rangle &= \left| +\frac{3}{2}, +\frac{1}{2} \right\rangle \equiv |\uparrow, \uparrow\rangle \\
|-2\rangle &= \left| -\frac{3}{2}, -\frac{1}{2} \right\rangle \equiv |\downarrow, \downarrow\rangle
\end{aligned} \tag{1.3}$$

The two states  $|\pm 1\rangle$  are dipole-active (they can couple to light), and for this reason are called "bright" states. In experiments these states recombine radiatively giving rise to photoluminescence. The second pair  $|\pm 2\rangle$  is optically non-active, therefore these states are called – "dark" states. However, these electron-hole states are not in general eigenstates of the total Hamiltonian because of the electron-hole exchange.

This gives rise to the **exciton fine structure splitting (FSS)** which is of central importance for this *work*. Formally, the corresponding Hamiltonian can be represented by the following expression [38]:

$$\hat{H}_{ex} = \frac{\delta_0}{2} \hat{\sigma}_z^e \hat{\sigma}_z^h + \frac{\delta_1}{4} (\hat{\sigma}_x^e \hat{\sigma}_x^h - \hat{\sigma}_y^e \hat{\sigma}_y^h) + \frac{\delta_2}{4} (\hat{\sigma}_x^e \hat{\sigma}_x^h + \hat{\sigma}_y^e \hat{\sigma}_y^h) \tag{1.4}$$

where the Pauli matrices  $\sigma_i^{e,h}$  act on the spin components of the electron (e) or hole (h) respectively. Here, we used a  $\pm 1/2$  pseudo-spin to describe the QD hole ground states with angular momentum  $j_z = \mp 3/2$ . The quantities  $\delta_0$ ,  $\delta_1$ , and  $\delta_2$  describe the exciton quartet fine structure as follows:  $\delta_0$  - between states of angular momentum  $|M| = 1$  and  $|M| = 2$  (or  $\sigma_z^e + \sigma_z^h = 0$ ),  $|\delta_1|$  (i.e. FSS) - between the components of the optically active doublet ( $M = \pm 1$ ), and  $|\delta_2|$  - between the dark states ( $M = \pm 2$ ). These parameters are determined by the quantum dot properties (size, shape, composition, strain field, etc). The arbitrary directions  $x$ ,  $y$  of the Pauli matrices correspond here to the eigenaxes of the QD. We use the following definitions of the matrix representations of the angular momentum operators:

$$\hat{\sigma}_x = \begin{pmatrix} 0 & 1 \\ 1 & 0 \end{pmatrix} \quad \hat{\sigma}_y = \begin{pmatrix} 0 & -i \\ i & 0 \end{pmatrix} \quad \hat{\sigma}_z = \begin{pmatrix} 1 & 0 \\ 0 & -1 \end{pmatrix} \tag{1.5}$$

Figure 1.4 shows schematically how the reduction of the symmetry influences the degeneracy of exciton levels and in consequence gives rise to the fine structure

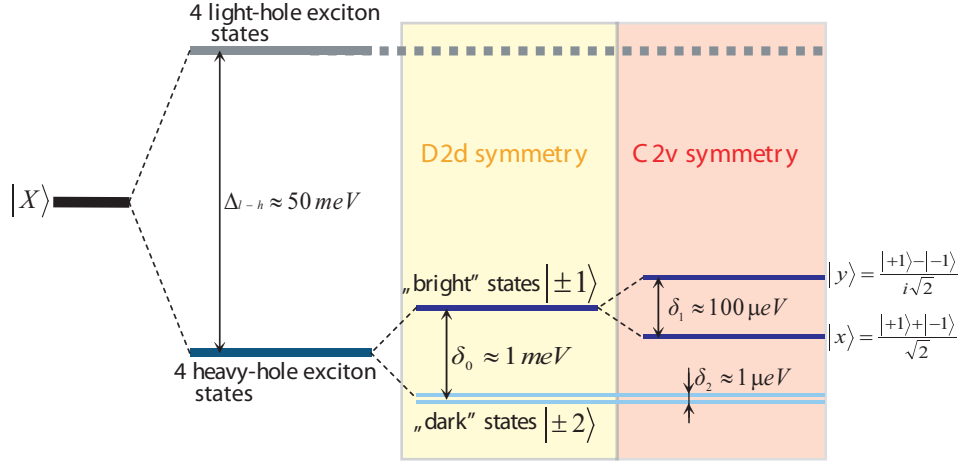


**Figure 1.4.** Scheme of the level splitting of the exciton state. From left to the right: evolution of level splitting after including different terms: first – splitting between light- and heavy-hole excitons, next (yellow shaded area) – splitting induced by lowering the symmetry to  $D_{2d}$  symmetry (case of an isotropic QD), and last (red shaded area) – lowering to the  $C_{2v}$  symmetry (case of an anisotropic QD)

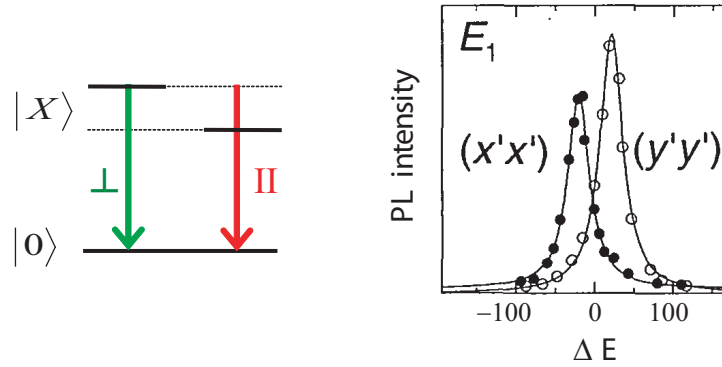


**Figure 1.5.** On the left: scheme of emission from an excitonic level. On the right: excitonic doublet in PL measured in two linear orthogonal polarization (from Ref. [39]).

of excitonic transitions. In the system of  $D_{2d}$  symmetry bright states should not be split, whereas for dark states the degeneracy is already lifted. Note the characteristic relative energy scale: splitting between heavy- and light-holes  $\Delta_{l-h}$  is around few tens of  $meV$ , between dark and bright states  $\delta_0 \sim 1 meV$ , between two bright states  $\delta_1$  – from zero up to hundreds of  $\mu eV$ , and between two dark states  $\delta_2 \sim 1 \mu eV$ . We will concentrate mostly on the heavy-hole bright states. The other states will be considered only if they may mix with those states and in this way influence optical properties of the system.

The origin of the symmetry breakdown governing this fine structure splitting is not fully established. FSS can result from any combination of in-plane shape anisotropy of a dot (elongation of the dot due to preferential growth direction),

piezoelectric potential in the dot vicinity (due to the vertically asymmetric strain field [40]), and local symmetry breakdown due to chemical bond alignment at the dot interfaces [34]. Typically the interaction is of the order of several tens of  $\mu\text{eV}$ , which is a small correction. The first experiments showing the fine structure for excitons in an individual quantum dot was presented by D. Gammon *et al.* [39]. As theoretically predicted the splitting is revealed in photoluminescence experiments of individual QD as doublet structure of excitonic emission (see Fig. 1.5). This doublet is also characterized by orthogonal linear polarizations due to the coupling between the exciton states  $|+1\rangle$  and  $|-1\rangle$  (term proportional to  $\delta_1$  in 1.4).

## 1.6 Polarization correlation in the “biexciton cascade”

Because of the strong localization of carriers in QD’s one may observe a rich variety of different excitonic complexes depending on the excitation conditions. For example, by electrical injection of carriers we can fill or make empty a given dot with electrons and/or holes, which yields specific signatures in PL or electro-PL spectra. The corresponding excitonic complexes can thus be divided into two groups: **neutral complexes** and **charged complexes**. The first of these groups contains **excitons** and **biexcitons** which are obviously correlated because the biexciton creates an exciton when recombining radiatively. For this reason, the optical recombination of a biexciton to the “empty” QD state represents a cascade of 2 photons emitted successively. This photonic cascade which obeys the dipolar optical selection rules of the QD exhibits very remarkable polarization properties, which in principle may lead to photon entanglement if some specific criteria are fulfilled (see next *Section*). In this *Section*, we review briefly the signature of polarization correlations in classical experiments.

The biexciton state has no fine structure since it is built from two excitons of opposite spins. For the same reason, it has zero angular momentum like the “empty” QD state  $|0\rangle$ . However, the optical transition from this state goes to the split excitonic levels. In consequence, the exciton (X) and biexciton (XX) lines appear both in PL spectra as two linearly polarized doublets (see Fig. 1.6). The above described fine structure splitting of X is thus transferred to the XX lines, with an opposite sign. This mirrored sequence of linear polarization is remarkable because it reveals the optical selection rules which govern the biexciton cascade: both transitions from (X) or to (XX) one of the exciton eigenstates have the same linear polarization, say  $x$  or  $y$  (see Fig. 1.6). This non-intuitive property results from the fermion nature of the electrons <sup>4</sup>. If the splitting is zero, it is in contrast obvious that a first photon which would be circularly polarized  $\sigma^+$  must be followed

---

<sup>4</sup>By introducing the creation operators (promotion of a valence electron to the conduction band)  $a_{\pm 1}^+ = c_{\mp 1/2}^+ c_{\mp 3/2}$  of the  $|\pm 1\rangle$  ground excitons, the Pauli exclusion principle simply reads  $(a_{\pm 1}^+)^2 = 0$ , while  $a_{-1}^+ a_{+1}^+ \neq 0$ . It follows that the creation operator  $a_{\theta}^+ = (a_{+1}^+ + e^{-i2\theta} a_{-1}^+)/\sqrt{2}$  of a linearly polarized exciton satisfies  $a_{\theta}^+ a_{\theta+\pi/2}^+ = 0$ , which forbids the biexciton creation with 2 photons of orthogonal linear polarizations.

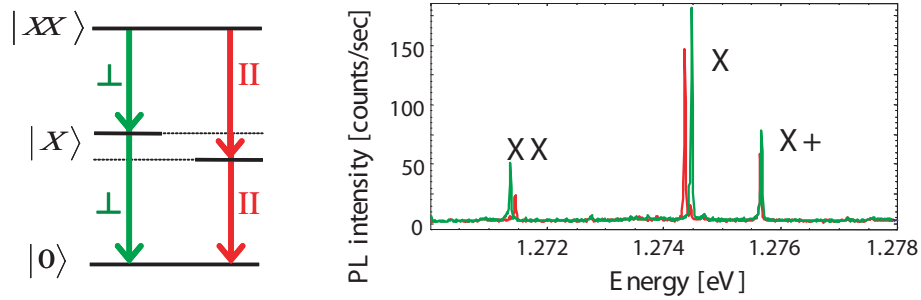


**Figure 1.6.** (on the left) Scheme of photon emission in biexciton-exciton cascade. Example of photoluminescence spectra from single InAs/GaAs QD. Three different transitions can be identified: X – excitonic line, XX – biexcitonic line, X+ – positively charge excitonic line. For neutral excitons also fine structure can be resolved. Color (red and green) correspond to two orthogonal linear polarizations.

by a second photon  $\sigma^-$  to obey the conservation of angular momentum.

The spectral correlation of linear polarizations provides actually a very selective criterion to identify the exciton and biexciton lines from the same QD. Generally, charged excitons are also observed either due to residual (or intentional) doping of the host materials or generated in a controllable way by a vertical electric field. Different complexes have been studied both experimentally (charge state from +6 up to  $-8$  in [41]) and theoretically [42]. The process of filling the dot with electrons reveals strong configuration interaction and follows the Hund’s rule and “Aufbau principle” essentially like in atom shells. However for holes the filling sequence is much more complicated. Strong spin-orbit interaction for holes breaks the Hund’s rule and shell filling does not follow the “Aufbau principle”. It results in very interesting phenomena like for example filling a  $d$ -shell before closing a  $p$ -shell. Additionally, from studies of charged excitons one gets details about Coulomb interactions between carriers, which are complementary to exchange interaction studies. The singly charged excitons (or trions) were usually observed in our experiments. Their spectral lines are characterized by the absence of fine structure splitting due the vanishing exchange when two electrons (or holes) are in a singlet configuration. Although mostly neutral excitons and sometimes singly charged excitons have been studied in this *work*, it is useful to keep in mind those effects. They clearly show important features of semiconductor zero-dimensional structures, helpful for a global understanding of a system, like for example the fine structure of doubly and triply charged excitons and singly and doubly charged biexcitons (see e.g. B. Urbaszek *et al.* [43]).



## 1.7 Requirements for a QD-based source of polarization entangled photons

For typical semiconductor light sources, like laser or diodes, the statistics of photon emission has a Poisson (or super-Poisson) distribution. Even after strong attenuation, the deterministic triggering of single photons is not possible because when the pulses contain a single photon with a probability  $p$ , they contain two photons with a probability  $p^2$  <sup>(5)</sup>. The basic requirement for a true non-classical photon statistics is that emission be produced by a discrete system. For such a system excited optically or electrically in a controllable way, triggered emission of single photons can then be obtained. Nowadays, there are many kinds of single photon sources which have been already tested: single molecules [44], colored centers in diamond [45], mesoscopic quantum wells [46], and quantum dots [22, 47]. The latter two examples can be easily operated and integrated in other semiconductor devices. Therefore they look very promising for future applications in quantum cryptography. In addition to this single photon emission property, semiconductor quantum dots offer the possibility to generate pairs of polarization-entangled photons as originally proposed by O. Benson *et al.* [48] thanks to the biexciton radiative cascade.

If a biexciton state is formed after a short pulsed excitation, then the QD system will relax its energy through a radiative cascade which consists of *two* photons of slightly different energies, which are correlated in polarization (as discussed in the previous *Section*) as well as in time (the X photon comes after the XX photon). These correlations may lead to the formation of a polarization-entangled 2-photon state which reads  $(|+-\rangle + |-+\rangle)/\sqrt{2} \equiv (|HH\rangle + |VV\rangle)/\sqrt{2}$  in the basis of circularly polarized photons  $|\pm\rangle$ , or linearly polarized photons  $|H\rangle$  (Horizontal) and  $|V\rangle$  (Vertical). Yet to obtain such a maximally entangled quantum state of light [49], several conditions must be fulfilled by the QD system. One of the most restrictive requirement concerns the evolution of the solid state quantum emitter during the typical time of the 2-photon emissions. As in general, the exciton level which is the intermediate level of the cascade is split by the FSS  $\delta_1$ , it opens two distinguishable recombination paths that we can assume to be the  $H$  and  $V$  paths. The 2-photon state cannot be described by its sole polarization components because the 2-photon wavepacket including the spectral information cannot be factorized with respect to the polarization states  $|HH\rangle$  and  $|VV\rangle$ . The non-maximally entangled state reads now [2]:

$$|2ph\rangle = \alpha|2ph_H\rangle|HH\rangle + \beta|2ph_V\rangle|VV\rangle \quad (1.6)$$

where  $\alpha$  and  $\beta$  correspond to the probability of emission along the  $H$  or  $V$  path respectively ( $|\alpha|^2 + |\beta|^2 = 1$ ), and the kets  $|2ph_{H(V)}\rangle$  describe the 2-photon wavefunctions. Note this state has still perfect correlation in the basis of QD eigenstate polarization as we did not introduce here exciton spin relaxation. The degree of

---

<sup>5</sup>Therefore, attenuated sources of single photons which rely on a probability  $p \ll 1$  are not very efficient in terms of emission rate, and definitely not deterministic.

entanglement of the state Eq. 1.6 is then given by  $\gamma = \alpha^*\beta\langle 2ph_H|2ph_V\rangle$ . The second-order perturbation theory approximation applied to the dipolar spontaneous emission enables to give simple expressions for the wavefunctions  $|2ph_{V(H)}\rangle$  with Lorentzian functions. It is thus possible to derive a more explicit form for the entanglement parameter:

$$\gamma = \frac{\alpha^*\beta}{1 + \delta_1^2/2\Gamma^2} \quad (1.7)$$

where  $\Gamma$  is the homogeneous linewidth of the excitonic lines. The FSS plays thus a dramatic role on the degree of entanglement: as soon as the exciton splitting is larger than the level width  $\Gamma$  the two  $H$  or  $V$  paths become distinguishable and the entanglement vanishes. The numerator  $\alpha^*\beta$  in Eq. 1.7 is related to the “branching ratio” between the two paths. It is maximum when both decay paths have the same probability. As we will see in next *Chapters* the heavy- to light-hole mixing is susceptible to affect this equilibrium since it gives rise to anisotropy of the dipolar oscillator strength [50, 51]. Like the FSS such a mixing is allowed in  $C_{2v}$  symmetry. Finally, any spin relaxation mechanism which directly affects the polarization of the intermediate exciton level would lead to a drastic reduction of the entanglement. Obviously, it can be neglected if the associated relaxation time  $\tau_s$  is much longer than the radiative lifetime  $\tau_r = \hbar/\Gamma$ . This issue will be addressed more specifically in *Chapter 5*.

In practice, the biexciton-exciton cascade can be studied in correlation experiments. The two steps of the cascade can be treated as two coherent beams and correlations between them can be investigated using a Hanbury–Brown and Twiss interferometer [52]. The idea of such measurements relies on the splitting of the photoluminescence into two beams, whose polarization properties are analyzed separately, with synchronized collecting photodiodes. As output one gets the joint probability of detecting one photon at time  $t$  and another photon at time  $t + \Delta t$  in a specific set of detection polarizations and detection energy. For example, the autocorrelation function of an excitonic line emitted by a single QD shows a clear antibunching phenomenon at  $\Delta t = 0$ , which is a signature of the emission of photons one by one. One can imagine a big variety of auto- and cross-correlation studies for excitonic complexes. From such measurements we may gain a better knowledge about spin memory effects ([53, 54]), about the process of carrier capture ([54]), and the most important for this *work* – about properties of the cascade emission. The photon correlation measurements turn out to be the standard method for proving entanglement <sup>6</sup>.

The cross-correlation function between  $\mathbf{XX}$  and  $\mathbf{X}$  depends on the chosen basis of detection, circular or linear. If a quantum dot has exactly degenerate excitonic state then the polarization correlation is maximum for all choices of basis according to the selection rules discussed in the previous *Section*. This corresponds to

---

<sup>6</sup>The aim of this *work* is the preparation of a quantum system for entanglement. Since our experiments did not require any single photon counting studies, we will not describe the technique of correlation measurements in detail. We focused on the optical features of QD PL emission, which are related to the underlying symmetry of the system.

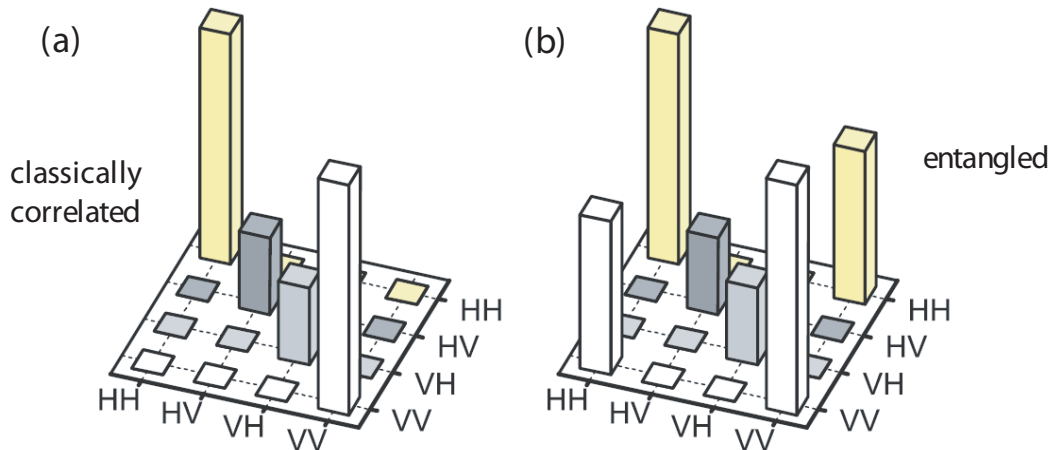


**Figure 1.7.** (a) Density matrices representing the predicted state for ideal classically correlated (a) and entangled (b) photon pairs including an uncorrelated background of 50% (from Ref. [55]).

the situation of maximal entanglement for which the polarization of the photons remains undetermined until one of them is measured. If in contrast  $\delta_1 \gg \Gamma$  then the polarization correlation survives only in the basis of polarization associated to the exciton eigenstates; there is no entanglement. Such measurements can be performed systematically with 16 configurations of analyzers to construct the density matrix of the 2-photon states [49]. The diagonal terms represent classical correlation between different 2-photon states of a chosen basis (e.g. vertical and horizontal polarization of photons) and the off-diagonal terms – “coherence” between different states. The entanglement quantity  $\gamma$  requires non-zero off-diagonal terms in the density matrix (see Fig. 1.7 (b)). Recently polarization-entangled emission from semiconductor QDs has been reported by two research groups [1, 2]. In the work of R. M. Stevenson *et al.* [55, 1] the fine structure splitting was reduced by combining methods of annealing and tuning by in-plane magnetic field, whereas in the work of N. Akopian *et al.* [2] a spectral filtering technique was used to achieve a post-selection of the 2-photons. The latter consists in the rejection of almost all events, but those which have a non-negligible probability to be entangled, i.e. within the narrow energy windows corresponding to the overlap of the Lorentzian excitonic lines.

It is obvious from Eq. 1.7 that the key parameter of a QD for entangled photons emission is the ratio  $\delta_1/\Gamma$ . Since most of this *work* is devoted to the measurement and possible control of  $\delta_1$ , we will first review briefly the current knowledge on  $\Gamma$ . The natural linewidth  $\Gamma$  of an excitonic line, which reflects the coupling of the QD emitter to the photonic modes, can be measured in many different ways. For examples, it was successfully determined i) from measurement of PL radiative decay <sup>7</sup> (see e.g. results of J. M. Smith *et al.* [56], Fig. 1.8), ii) from high-resolution

<sup>7</sup>Under the assumption that the PL decay is dominated by radiative recombination processes  $\Gamma = \hbar/\tau_r$ . If non-radiative recombination mechanisms are dominant the actual

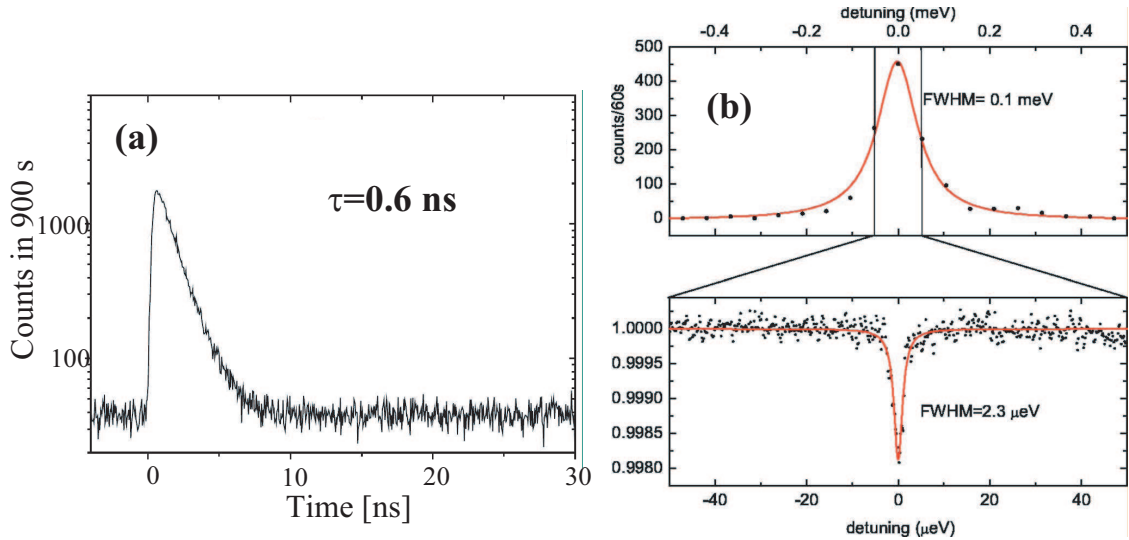


**Figure 1.8.** (a) PL decay curve measured for an exciton in InAs/GaAs quantum dot (from Ref. [56]). (b) PL (top) and absorption (bottom) spectrum of X- in InAs/GaAs QD (from Ref. [57]).

transmission spectroscopy (see e.g. results of A. Högele *et al.* [58], or of S. Seidl *et al.* – Fig. 1.8), iii) from measurement of the PL coherence time [59], iv) from temporal autocorrelation of PL photon counts [60, 2, 54], and v) in this *work*, from the resonance of PL optical orientation in an electric field (see *Chapter 5, Section 5.2.1*). It generally amounts to  $\approx 1 \mu\text{eV}$  (i.e.  $\sim 1 \text{ GHz}$ ). Time-resolved studies of the photoluminescence in charged-tunable QDs could demonstrate that the dynamics of excitonic complexes depends significantly on their structure [56]: i) the PL decay for XX is about twice faster than for X, ii) PL decay of X contains fast (several hundreds of picoseconds) and slow (few nanoseconds) components, due to, e.g. the repopulation process between dark and bright states. This effect demonstrates the limits of measurements performed in the time domain. On the other side, direct measurements in the energy domain suffer from possible spectral diffusion, in particular when Stark-modulation techniques are used. Finally, the methods based on quantum interference seem thus more reliable as they enable to get rid of the inhomogeneous contributions to  $\Gamma$ , but the acquisition time which is usually required does not make them very appropriate for fast characterization.

To improve the maximum theoretical entanglement predicted by Eq. 1.7 we could first consider the possibility to increase  $\Gamma$ . In other words, is it possible to modify significantly the coupling to light of the QD emitter? The demonstration of Purcell effect has proven that it can be achieved by using micro-cavity effects [61], when the QD excitonic line falls in resonance with a narrow optical mode of the cavity. In such a case it also favors the emission in a specific spatial direction which can be very useful to improve the effective brightness of a single QD. Recent promising results of cavity implementation have been obtained with photonic

---

$\Gamma$  could be much smaller. For this reason, there has been in the last decade strong efforts to develop other experimental techniques to confirm this result.

crystals (see e.g. T. Yoshie *et al.* [62] and A. Badolato *et al.* [63, 64]), as well as with more usual semiconductor cavities, like micro-pillars (J. P. Reithmaier *et al.* [65]) and micro-disks (E. Peter *et al.* [66]). However, structuring the space of electrodynamic modes brings in new difficulties because of the polarization splitting of the optical modes due to the imperfect symmetry of actual cavities. This gives rise to a very asymmetric branching ratio (i.e.  $\alpha^*\beta \rightarrow 0$  in Eq. 1.7). Even though cavity effects could help for the overall efficiency of a QD-based entangled photon emitter, it turns out to be rather necessary to develop techniques for controlling the QD FSS ( $\delta_1$ ), either by a post-growth treatment or dynamically by an external field. Before presenting the strategy we have chosen, we review in the next *Section* the theoretical parametric dependence of  $\delta_1$ .

## 1.8 Expression of the anisotropic exchange term

A consistent theory of the electron-hole exchange in semiconductors has been developed in the  $\mathbf{k} \cdot \mathbf{p}$  formalism by G. E. Pikus and G. L. Bir [67, 68, 36]. In the limit of vanishing exciton wave-vector ( $\vec{K} \rightarrow 0$ ) two contributions are identified: an analytical (or short-range) term and a non-analytical term (in the wave-vector-space representation) which is often called the long-range exchange contribution. In the case of an exciton confined in a lens-shaped quantum dot, characterized by a much stronger confinement along  $z$  than along in-plane directions, the long-range part is the dominant contribution [69, 70] and reads:

$$\delta_1 = \frac{4\pi}{(2\pi)^3} \frac{1}{4\pi\epsilon_0\epsilon_r} \left( \frac{e\hbar P_{cv}}{m_0 E_g} \right)^2 \int d\mathbf{q} \frac{q_x^2 - q_y^2}{q^2} \left| \int d\mathbf{r} \Psi_{exc}(\mathbf{r}, \mathbf{r}) e^{i\mathbf{q}\cdot\mathbf{r}} \right|^2 \quad (1.8)$$

where  $\Psi_{exc}(\mathbf{r}_e, \mathbf{r}_h)$  is the envelope function of the ground state exciton,  $P_{cv}$  is the interband dipolar matrix element,  $m_0$  is the electron mass,  $E_g$  is the semiconductor forbidden gap and  $\epsilon_0\epsilon_r$  is the permittivity at excitonic transition frequency. This expression shows how the exciton wavefunction  $\Psi_{exc}(\mathbf{r}_e, \mathbf{r}_h)$ , and more precisely its anisotropy revealed by the term  $\frac{q_x^2 - q_y^2}{q^2}$  determines the strength of the anisotropic exchange. The appearance of  $\Psi_{exc}(\mathbf{r}, \mathbf{r})$  expresses contact character of the electron-hole exchange.

In the center of mass approximation of separable dependencies along  $x$  and  $y$  of the exciton wave function  $\Psi_{exc}(\mathbf{r}_e, \mathbf{r}_h) = F_x(x)F_y(y)f(\boldsymbol{\rho})\phi_e(z_e)\phi_h(z_h)$ , Equation 1.8 can be cast into:

$$\delta_1 = \frac{1}{2\pi} \frac{1}{4\pi\epsilon_0\epsilon_r} \left( \frac{e\hbar P_{cv}}{m_0 E_g} \right)^2 \iint_{q_x, q_y} \frac{q_x^2 - q_y^2}{q} \tilde{F}_x^2(q_x) \tilde{F}_y^2(q_y) P(q) f^2(0) \quad (1.9)$$

where:

$$\begin{aligned}
P(q) &= \int dz' \int dz \phi_e(z') \phi_h(z') \phi_e(z) \phi_h(z) \times \exp(-q|z - z'|) \\
\tilde{F}_x(q) &= \int dx F_x(x) e^{-iqx} \\
\tilde{F}_y(q) &= \int dy F_y(y) e^{-iqy}
\end{aligned}$$

This expression shows more explicitly the dependence of the FSS on the exciton wave function symmetry. If both functions  $F_x$  and  $F_y$  which describe the in-plane correlated<sup>8</sup> motion of the electron and hole are identical then the FSS vanishes since the sum in Eq. 1.9 separates into two terms which are exactly opposite to each other. In contrast, if the exciton wave function has different extensions  $L_x$  and  $L_y$  along  $x$  and  $y$  directions, due e.g. to the potential of an elongated quantum dot, it results in a finite FSS. Equation 1.9 shows besides that the strength of FSS depends on the function  $P(q)$  which roughly speaking corresponds to the overlap along  $z$  of the electron and hole wavefunctions.

If we consider that the Fourier transforms  $\tilde{F}_x$  and  $\tilde{F}_y$  are Gaussian-like for the exciton ground state, we can estimate  $\delta_1$  by assuming that these functions are constant in the interval defined by  $|q| < 2/L_{x(y)}$  and zero outside. To obey normalization condition, we find that  $\tilde{F}_{x(y)}^2(q) \sim \pi L_{x(y)}/2$ . If we introduce a parameter  $\xi$  to describe the exciton wavefunction anisotropy in the form  $L_x = L(1 + \xi)$  and  $L_y = L(1 - \xi)$  where  $L$  is the average in-plane exciton diameter, we eventually get the following approached expression for  $\delta_1$ :

$$\delta_1 \approx \frac{\alpha}{4\pi\epsilon_0\epsilon_r} \left( \frac{e\hbar P_{cv}}{m_0 E_g} \right)^2 \frac{\xi}{L^3} \quad (1.10)$$

where  $\alpha$  is a numerical constant<sup>9</sup>. We have assumed that  $P(q) \sim 1$  because  $|q| < 2/L_{x(y)} \ll 2/L_z$  and we used for the relative in-plane movement  $f(\rho)$  a gaussian function such that normalization condition yields  $f^2(0) = 4/\pi L^2$ . The dependence of FSS appears linear in the anisotropy parameter  $\xi$ , and cubic with the reciprocal QD diameter  $1/L$ . An order of magnitude for an InGaAs quantum dot of diameter  $L = 20 \text{ nm}$  with material parameters  $E_g = 1.2 \text{ eV}$  and  $\epsilon_r = 12$  reads:

$$\delta_1 \approx -\xi 178 \mu\text{eV} \quad (1.11)$$

For a QD in-plane anisotropy  $\xi = 0.1$  we thus get a FSS of about  $20 \mu\text{eV}$  which is of the order of magnitude of the average value usually measured for InGaAs QDs ( $30 \mu\text{eV}$ ). This long-range contribution is therefore very likely the leading term which determines  $\delta_1$  in this case. It is yet noteworthy that the parametrical

---

<sup>8</sup>by correlated motion we understand here a common motion of electron and hole occupying the same position  $\mathbf{r}$ , as imposed by the contact character of the exchange interaction.

<sup>9</sup> $\alpha = 16(\sqrt{2} - 3\ln(1 + \sqrt{2})) \approx -19.7$

dependence of Eq. 1.10 involves the energy gap  $E_g$  experienced by the exciton, which is not uniform in a QD and strongly depends on actual composition and strain. This parameter is thus not known with high certainty. The expressions given above for  $\delta_1$  are thus mainly useful to understand how it will be possible to act on the FSS by an external perturbation as discussed briefly below.

## 1.9 Aim of this work: changing the FSS by an external perturbation

As discussed above, the excitonic fine structure splitting is the key parameter which determines the suitability of a specific semiconductor QD for the generation of polarization entangled photon pairs. Since it may be seen as a manifestation of the actual QD symmetry, the general idea to tackle the FSS reduction is to find some appropriate perturbations which in combination with the QD native properties may compensate the effects of the low symmetry, and possibly restore a higher symmetry. This *work* reports on experimental results and theoretical interpretation of FSS modification induced by external electric or magnetic fields.

Let us first discuss the symmetry modifications achievable by applying an electric field perpendicular to the growth axis. With respect to a cylindrical QD of circular basis, an in-plane elongation is a perturbation with  $D$ -type symmetry<sup>10</sup> while an **in-plane electric field** corresponds to a perturbation with  $P$ -type symmetry: when developing the corresponding perturbations on the single particle wave functions up to second order, it appears that an electric field applied along the long axis of the dot can compensate the  $D$  component at the expense of introducing a  $P$  component. Nevertheless, as seen in the previous *Section*, the FSS is determined by the symmetry of the *exciton* wavefunction. The effect of an in-plane electric field is not that intuitive. For instance, calculations show that the field-induced spatial separation between electron and hole wave-functions having (each of them) a cylindrical symmetry does not give rise to any FSS<sup>11</sup>. This is actually the combination of the QD potential delimited by “hard wall” barriers with the electric-field induced shift which may lead to an efficient change of the exciton symmetry, and thus of the FSS. Indeed, because of the barriers, the single particle wave-functions get compressed in the direction of the applied field, which then leads to a reduction of the exciton extension in the field direction<sup>12</sup>. This is this simple proposal of FSS tuning, that we have tried to implement with QD samples and which will be the heart of the studies presented in *Chapter 3*. We will see also that applying an electric field parallel to the QD growth axis offers an alternative method, which in terms of symmetry could seem even more natural, but still lacks for a quantitative theory.

<sup>10</sup>The difference of  $2D$ -potential between a circular-based and an elliptical-based QD (say, elongated along  $x$ ) transforms as  $x^2 - y^2$ .

<sup>11</sup>Detailed calculations can be found in PhD thesis of A. Jankovic [71], where e.g. a comparison between perturbation and variational methods for this problem is discussed.

<sup>12</sup>Even though electron and hole get slightly separated by the field.

Regarding the influence of an **in-plane magnetic field** on FSS, two types of effects are expected : i) the Zeeman spin interaction in Voigt configuration which may shift in energy both linearly polarized excitons differently, and ii) the anisotropic orbital compression of the excitonic wavefunction in one direction which may compensate its native anisotropy. In *Chapter 4* we will develop the model of Zeeman spin interaction to describe the FSS change observed experimentally. The key point will rely on a consistent theory of the effective  $g$  factor for the hole ground states. It is noteworthy that this method was used successfully to demonstrate the emission of polarization entangled photons from an InGaAs QD [55], although it contains some intrinsic drawbacks to produce maximally entangled states. Following the model derived by M. Glazov and E. L. Ivchenko [72] we will discuss numerical evaluations of the orbital effect which in some specific case becomes non-negligible.

Although in-plane electric field and in-plane orbital effect of magnetic field may look similar (they both consist in a compression of the exciton in one direction) one should remember that in the first case we need to go up to the second order of perturbation, whereas in second case first order is sufficient to get symmetry change. In case of electric field one has to take into account the specific symmetry of the QD with the perturbation, which in practice means that one must apply the electric field along a QD principal axis.

**SUMMARY.** *Chapter 1* reviews the most relevant features of self-assembled quantum dots in the perspective of entangled photon pair emission. The exciton fine structure splitting is shown to be responsible of the main defect of actual QD to be overcome. The analysis of the symmetry reduction responsible for the FSS lays the basis of a strategy for influencing the native optical properties of QD by applying an external perturbation: an electric or a magnetic field.





---

---

## CHAPTER 2

---

# Samples and Experimental setups

### Contents

---

<b>2.1</b>	<b>Samples</b> . . . . .	<b>22</b>
2.1.1	II-VI samples . . . . .	23
2.1.2	III-V samples . . . . .	25
<b>2.2</b>	<b>Technology</b> . . . . .	<b>27</b>
2.2.1	Devices for in-plane electric field . . . . .	28
2.2.2	Devices for vertical electric field . . . . .	32
<b>2.3</b>	<b>Experimental setups</b> . . . . .	<b>35</b>
2.3.1	Setup for measurements of II-VI materials . . . . .	35
2.3.2	Setup for measurements of III-V materials . . . . .	38

---

*"Whenever new semiconducting materials become available, whether these new materials are purer or belong to a new family or have an artificial structure, they have often led to the discovery of new phenomena and also novel applications."*

P. Y. Yu, M. Cardona, "Fundamentals of Semiconductors"

AS DISCUSSED IN *Chapter 1* the main objective of this *work* is related to the study of fine symmetry effects in single quantum objects. It requires a special experimental equipment, which will be described in this *Chapter*. Generally, three conditions have to be fulfilled to enable measurements of individual quantum dots. First, a good quality **sample** with quantum dots is needed, preferably with a structure specially designed for optical measurements. Second, experiments on single quantum objects often rely on post-growth processing. Therefore the next requirement is an access to **technology** facilities, in our case for fabricating electro-optic devices. Third, in order to have an insight into the micro-world, measurements have to be carried out in a **experimental setup** designed for micro-photoluminescence, i.e. an optical setup with high spatial resolution and great mechanical stability.

In *Section 2.1* the investigated samples will be described. Their structure and basic optical characteristics will be presented together. The technology of field-effect device will be introduced in the next *Section 2.2*. All steps of the sample processing will be schematically explained, and the device quality will be briefly discussed on the basis of their electrical characteristic. This *Chapter* will be completed by the description of the experimental setups in *Section 2.3*. We will put emphasis on the elimination of experimental artefacts, which could produce systematic errors in polarization-resolved measurements.

Experiments have been done on two types of materials and in different experimental configurations. The part of the work regarding II-VI materials was performed in Institute of Experimental Physics at *Warsaw University*, whereas the investigations of III-V materials were done in the Laboratory for Photonics and Nanostructures of the *Centre National de la Recherche Scientifique* in Marcoussis.

## 2.1 Samples

In this *Section* the basic characteristics of investigated samples will be presented. All the samples (II-VI's and III-V's) were grown by molecular beam epitaxy (MBE) technique on (001)-oriented GaAs substrate. The MBE growth<sup>1</sup> is a method of thin film deposition, which allows the production of pure high quality crystals. In ultra-high vacuum atoms of different species are evaporated from heated effusion cells. They condensate on the wafer kept at an appropriate temperature, where they form atomic layers one at a time. The surface quality can be *in situ* monitored during this process thanks to the reflection high energy electron diffraction (RHEED). Shutters in front of effusion cells are used in order to control the composition and the thickness of the layers.

The remarkable progresses of this growth method allowed in the last decades the development of low-dimensional structures like quantum wells, quantum wires, and quantum dots. The first low-dimensional semiconductor structures that could be achieved are quantum wells. Already at that time people predicted that at non-ideal interfaces between different alloys specific quantum states should form. An actual sharp interface may exhibit small deviations from its perfect position with respect to the crystal lattice, introducing some interface roughness. The latter modifies locally the potential seen by electrons or holes, which may result in strong modification of the optical properties of the structure (see e.g. [73]). The interface roughness contributes to the inhomogenous broadening of the spectral linewidth and may even cause a splitting in PL spectra (see e.g. [74]) depending on the specific spatial fluctuations. In particular, isolated fluctuations of the well thickness produce a new kind of states, which have zero-dimensional features (discrete quantum levels) thus are named quantum dots. Another way of spontaneous QD formation during the growth relies on the strain relaxation. If a few mono-atomic layers of a material are deposited on another material to which

---

<sup>1</sup>MBE growth method was invented in 1968 at Bell Telephone Laboratories by J. R. Arthur and A. Y. Cho. The description of the main idea of this technique can be found in every introduction to solid state physics.

Samples	A <sub>26</sub>	B <sub>26</sub>
Cap layer (ZnTe)	0.05 $\mu\text{m}$	0.1 14 $\mu\text{m}$
QD layer (CdTe)	2 ML*	6 ML*
First barrier (ZnTe)	0.1 $\mu\text{m}$	0.35 $\mu\text{m}$
Buffer (CdTe)	4.5 $\mu\text{m}$	4.3 $\mu\text{m}$
Substrate (GaAs)	(001)-oriented	

\* ML = 1 monolayer

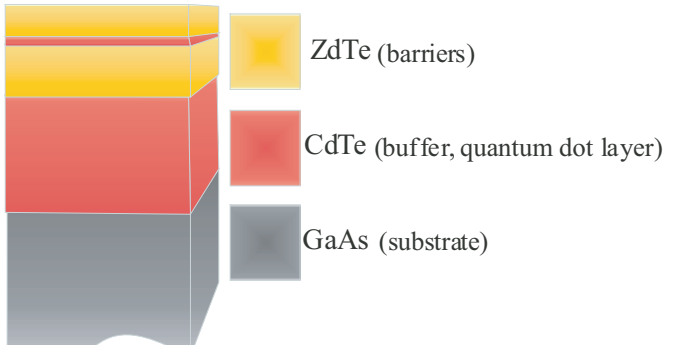


**Figure 2.1.** Structure of II-VI samples: materials and thicknesses of layers for samples  $A_{26}$  and  $B_{26}$  collected in the table (on the left side) and schema of the sample structure (on the right).

they are not lattice-matched, then the resultant strain causes a transition to a 3-dimensional growth leading to the formation of “quantum islands”. The unbroken, strained layer below the islands is called “the wetting layer” (WL) and still exhibits quantum well-like properties although very inhomogeneous. This growth mode is usually called Stranski-Krastanov mode [75] and is mostly used for III-V compounds. Obviously semiconductor heterostructures formed from different binary compounds possess different properties (e.g. different spectral range of photoluminescence). This one and the next two *Sections* do not aim to describe all differences between the samples, but only those regarding sample preparation (growth and processing) and in experimental setup requirements (different wavelength operation range).

### 2.1.1 II-VI samples

The II-VI samples were grown in Institute of Physics, Polish Academy of Sciences in Warsaw (by Grzegorz Karczewski and Piotr Wojnar). Two semiconductor heterostructures from zinc telluride/cadmium telluride (ZnTe/CdTe) were studied. They will be further named  $A_{26}$  and  $B_{26}$ , with an index denoting the kind of material.

The scheme and the table in Fig. 2.1 show the chemical compositions, alignment, and thickness of the layers. Each sample contains a single layer of CdTe QDs sandwiched between ZnTe barriers. Due to strong lattice mismatch between the substrate and the barrier material, the growth process was initiated with a thick CdTe buffer deposition [76]. It prevents formation of dislocations and guarantees high quality surface for barrier growth. It is known that for II-VI materials the surface may act as an effective carrier source [77], therefore the thickness of the cap layer has to be chosen carefully. It should be thick enough to prevent charging of QDs layer. On the other hand, high refractive index of the semiconductor layers causes interferences which may drastically reduce the PL extraction from the sample. It has been shown for quantum wells that the cap width providing optimal emission efficiency is equal to  $\lambda/4$  (with  $\lambda$  the photon wavelength) [78]. Taking

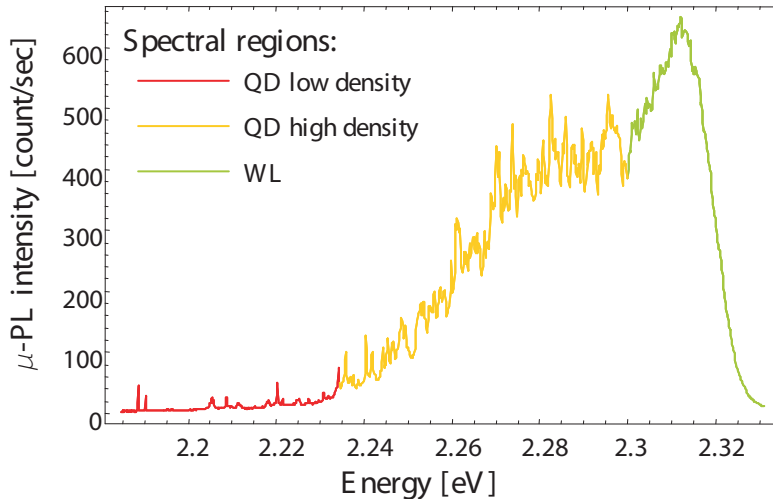


**Figure 2.2.** Typical  $\mu$ -photoluminescence spectrum of the sample  $A_{26}$ . Three different colors of the spectra encode the optical properties of different energy regions: green – dominant signal from wetting layer (WL), yellow – high QD density region, red – low QD density region (single lines from individual QD can be resolved and identified).

into account both effects the cap layer width was chosen to  $0.05 - 0.1\mu m$  [79].

Actually in II-VI materials pure Stranski-Krastanov growth mode cannot be obtained. Although the lattice mismatch between CdTe and ZnTe (6.2% – see [80] and references therein) is comparable with the mismatch for III-V materials, the growth does not occur exactly in the same mode. We investigated two kinds of CdTe/ZnTe quantum dots: i) **fluctuation-type quantum dots** grown by method proposed by G. Karczewski *et al.* [81], and ii) **quantum dots growth induced by Tellurium desorption** – method proposed by F. Tinjod *et al.* [82]. A detailed discussion of different growth methods for II-VI materials can be found e.g. in the work of H. Mariette *et al.* [80].

The **sample  $A_{26}$**  contains fluctuation-type quantum dots made from 2 monolayers of CdTe. The dot size and density were estimated from transmission electron microscopy (TEM) measurements. The typical lateral size is about  $3nm$  and the density is of the order of  $10^{12} cm^{-2}$  [81]. The PL spectrum of QDs ranges from WL energy (around  $2.31eV$ ) down to  $2.2eV$ , where well-resolved lines from individual QDs can be studied (see Fig. 2.2). It has to be stressed here that the QD distribution is strongly asymmetrical, and single photoluminescence lines can be investigated only in the low energy tail of the spectra for the statistically untypical dots. This situation can be described as a few “large”(or “thick”) quantum dots within a dense array of smaller dots.

The formation of QDs in **sample  $B_{26}$**  was induced by desorption of amorphous Tellurium deposited on six monolayers of CdTe [82]. Before the cap deposition, the dot layer was annealed at  $480^{\circ}C$  for 25 minutes. The sample exhibits a broad spectrum, from WL edge down to far red ( $1.8 eV$ ) (see Fig. 2.3). The expansion of QD lines toward the red results likely from annealing process. Besides, the increase of the wafer temperature during island formation leads to: i) formation of larger

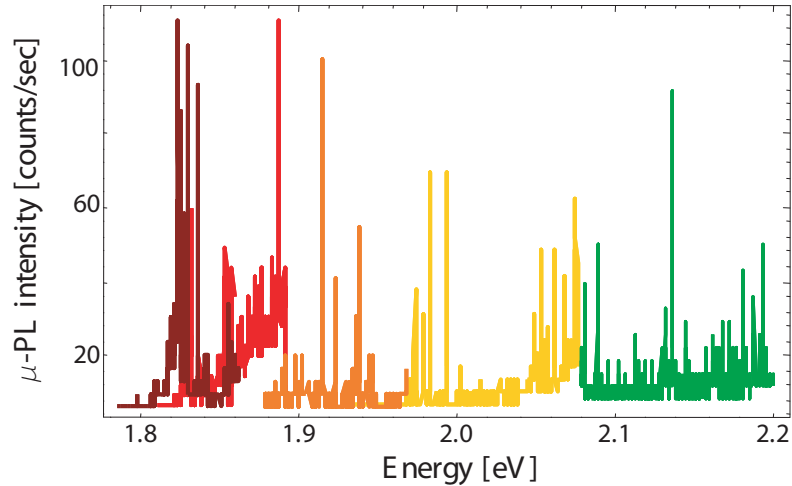


**Figure 2.3.** Typical  $\mu$ -photoluminescence spectrum of the sample  $B_{26}$  (taken at few different positions of the spectrometer).

dots, ii) stronger intermixing of the barrier material into the dots. Both results in a change of the transition energy distribution of the QD spectrum. With an excitation below the barrier energy gap it was possible to observe well-resolved lines in the whole range of QD PL energy. The QD density was not homogenous in the whole wafer  $B_{26}$ , with an inhomogeneity scale of a few tens of  $\mu m$ . This feature was evidenced in  $\mu$ -PL experiments by moving the excitation laser spot position.

Although II-VI systems have promising features (e.g. as single photon sources) due to their more robust excitonic states allowing to study non-classical light emission at higher temperatures [83], the technology of these materials is not as well developed as for III-V materials.

### 2.1.2 III-V samples

The growth of III-V samples was done by Aristide Lemaître in Laboratory for Photonics and Nanostructures-CNRS (LPN-CNRS) in Marcoussis. Two different types of structures (labelled  $A_{35}$  and  $B_{35}$ ) were realized for our investigations in order to apply an electric field parallel to the QD layer ( $A_{35}$ ) or parallel to the growth axis ( $B_{35}$ ). The QD growth occurred in Stranski-Krastanov mode, resulting in formation of islands on a strained wetting layer. During the growth the wafer position was fixed with respect to the Indium (In) and Arsenide (As) effusion cells in order to obtain a strong gradient of QD density along a specific axis (Fig. 2.4). The typical height of the QDs is 3 nm and the lateral size around 20 nm. Macro-photoluminescence measurements at room temperature were used as a test of the density gradient. One can see in Fig. 2.4 that for the upper part of the wafer the QD PL signal is comparable to the WL luminescence, whereas for the lower part the corresponding ratio vanishes. The samples were cleaved into small 5 mm x 10 mm squares, and the pieces of interest were chosen in the region of QD-to-WL PL ratio lower than 1/4, which guarantees a (non-zero) small QD density.

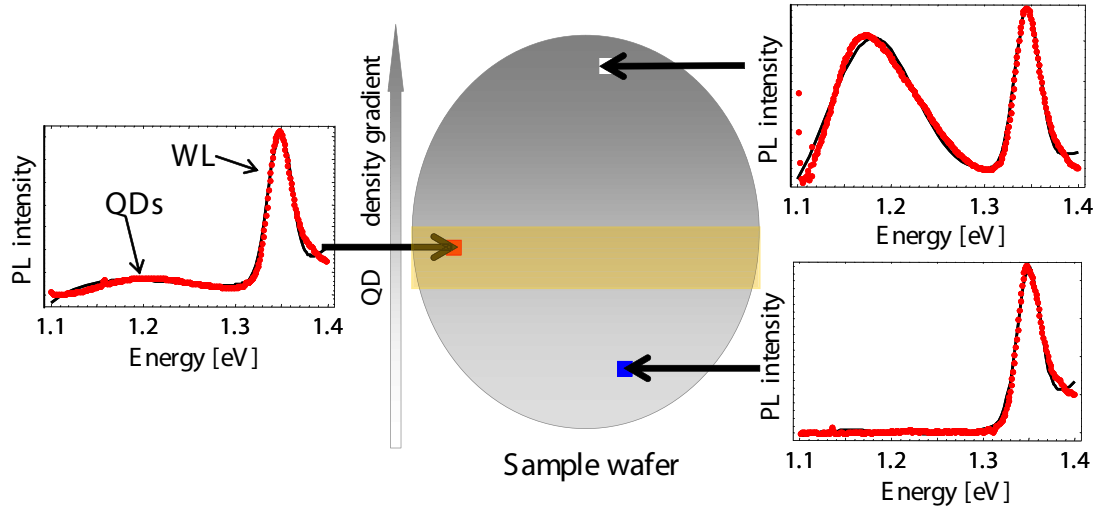


**Figure 2.4.** Scheme of wafer QD density gradient with three examples of macro-photoluminescence spectra for the sample  $A_{35}$  (on sides). Black arrows mark the spots from which the PL signal was collected. Yellow box marks the wafer region from which the samples for further investigations were cleaved.

Both types of III-V samples differ significantly in barrier composition and doping level (see Fig. 2.5). The QD layers are surrounded by GaAs barriers. In order to limit the diffusion of photo-created carriers, additional  $\text{Al}_x\text{Ga}_{1-x}\text{As}$  barriers were used (Aluminium content around 0.2 – 0.3, see the table in Fig. 2.5). In both cases growth conditions were quite similar, hence we assume there is no major difference in QD geometry, shape or composition between the samples. Macro-PL studies revealed very similar energy position of QDs and WL maximum. In  $\mu$ -PL of individual QDs we did not notice more differences between samples than those observed between different QDs from the same wafer <sup>2</sup>.

The **sample  $A_{35}$**  was designed for in-plane electric field devices [7]. The additional barriers with Aluminium were placed symmetrically at the bottom and at the top of the structure to stop carrier diffusion to the substrate and the surface, respectively. The GaAs cap layer is necessary to avoid oxidation of the AlGaAs layer, which could make inefficient any further technological process of the sample. This structure was not intentionally doped.

The **sample  $B_{35}$**  was designed for realizing a charge-tunable QD sample [84] following the same parameters as reported in [85], but enabled us as well to vary significantly the electric field in the regime of neutral exciton PL. It has actually a single  $\text{Al}_x\text{Ga}_{1-x}\text{As}$  blocking barrier at the top side of the sample to limit electrical injection from the electrodes. The back electrode was defined during the growth as a doped GaAs layer, which is separated by 25 nm of intrinsic GaAs from the QD layer. To study the response of QDs to both directions of a vertical electric field two kinds of doping were used: n-type (Silicon, Si:  $2 \times 10^{18} \text{cm}^{-3}$ ) and p-type

<sup>2</sup>One has to compare  $A_{35}$ - and  $B_{35}$ -type heterostructures under the same QD charge state. It means that in n(p)-Schottky device a small voltage is required to observe the emission from neutral state of a QD.

Samples	A <sub>35</sub>	B <sub>35</sub>	
Cap layer (GaAs)	5 nm	20 nm	
High barrier (GaAlAs) Al content (x)	20 nm x=0.2	100 nm x=0.3	
Barrier (GaAs)	200 nm	30 nm	
QD layer (InAs)	2 nm	2 nm	
Barrier (GaAs)	200 nm	25 nm	
High barrier (GaAlAs) Al content (x)	20 nm x=0.2		
Doped layer (n/p-GaAs)		200 nm	
Substrate (GaAs)	(001)-oriented		GaAs (substrate)

**Figure 2.5.** Structure of III-V samples: materials and thicknesses of layers for samples  $A_{35}$  and  $B_{35}$  collected in the table (on the left side) and scheme of the sample structure (on the right).

(Beryllium,  $\text{Be}: 2 \times 10^{19} \text{cm}^{-3}$ ). This will be indicated as a superscript in the sample labels (e.g.  $B_{35}^n$  for n-type back contact).

## 2.2 Fabrication technology of electric field effect devices

The technology of micron-size electro-optical devices is much better established for III-V materials than for II-VI's. Hence only samples  $A_{35}$  and  $B_{35}$  could be processed in the perspective of controlling the internal electric field in the QD region. Two different geometries were designed: vertical and in-plane (with respect to the QDs layer). We will not describe all details of the procedure, but only present schematically the different steps of processing. The technology of vertical field-effect QD devices was recently developed in LPN by Sabine Laurent and Benoît Eble under the supervision of A. Lemaître and O. Krebs. Based on this experience we could develop the technology for in-plane field-effect devices in collaboration with Pascale Senellart (LPN).

We should stress here that in all devices we used a metal-semiconductor heterojunction forming a Schottky contact, which acts either as a control gate (with no leak) when the semiconductor is intrinsic, or as an injection electrode when the semiconductor is heavily doped. The properties of the gold Schottky barrier enable us to estimate with high accuracy the electric field across the biased junction from the knowledge of the distance between the electrodes, and the material residual doping.



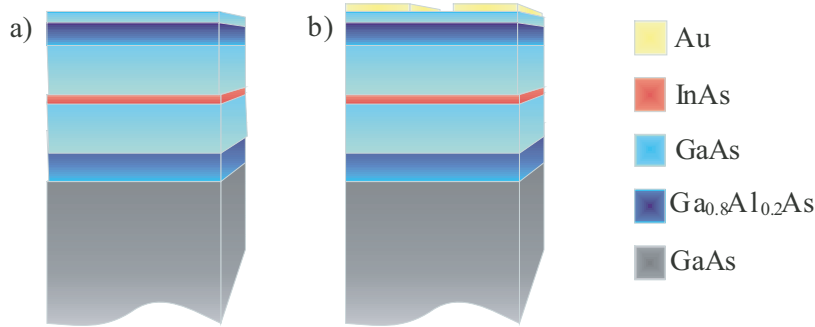


**Figure 2.6.** Scheme of Schottky-Schottky device on the sample surface ( $A_{35}^{SSsurf}$ ). Only one step of the technology is required. a) sample structure, b) metallization of the lithographically defined patterns.

### 2.2.1 Devices for in-plane electric field

First we will focus on the **in-plane device** engineering. Three different configurations have been considered: (i) two Schottky gates evaporated on the sample surface, (ii) two Schottky gates evaporated on the edges of a chemically etched mesa, and (iii) one n-Ohmic diffused contact and one Schottky gate deposited on the sample surface. The gates on the samples worked also as an optical mask allowing us to measure the luminescence from individual QDs. The type of fabricated structure will be indicated as a superscript in the sample name,  $A_{35}^{SSsurf}$  for Schottky-Schottky on the surface,  $A_{35}^{SSetch}$  for Schottky-Schottky at mesa edges, and  $A_{35}^{nS}$  for n-Schottky.

#### Schottky-Schottky device on sample surface

The technology of Schottky gates evaporated on the surface is the simplest, and the quickest one. Since both contacts are identical, this requires only one step of lithography (see Fig. 2.6):

- **Patterning of the surface by electron beam lithography** – The mask used for defining the contacts consists of pairs of rectangular shapes ( $300 \mu m \times 300 \mu m$ ), separated by a narrow gap of  $2 \mu m$ . This channel was parallel to one of the sample edges. Such a configuration was chosen to apply an electric field along one of the main  $[110]$  crystallographic axis of the crystal which usually corresponds to one of the optical eigenaxes of InAs QDs.
- **Metallization** – A gold layer was deposited to form the Schottky barrier. To provide a good adhesion to the surface and prevent diffusion into the heterostructure a thin ( $300 \text{ \AA}$ ) Titanium layer was first deposited. The gold layer ( $2000 \text{ \AA}$ ) was thick enough to achieve successful electrical bonding.

The advantage of this kind of devices relies on the simplicity of its processing. However it does not completely guarantee the desired in-plane geometry of electric field, since the gates are  $\sim 225 \text{ nm}$  above the QD layer. Approximately, considering

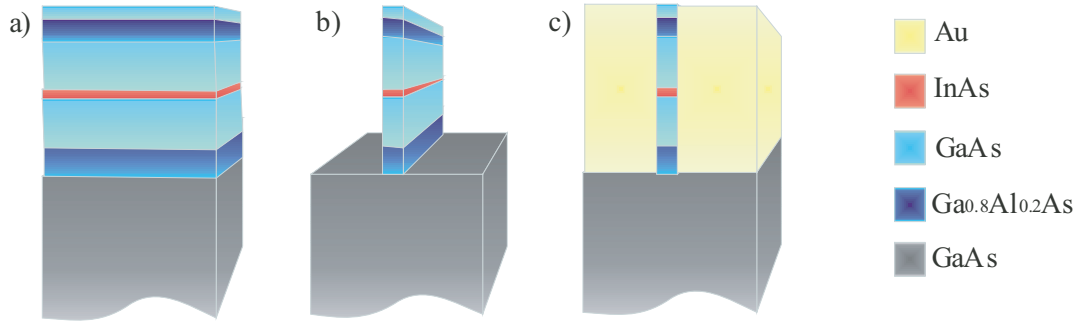


**Figure 2.7.** Scheme of Schottky-Schottky contacts on the border of etched mesas ( $A_{35}^{SSetch}$ ). From left to right successive processes are illustrated: a) sample structure, b) dry Cl etching of lithographically designed structure, c) metallization contacts on mesa edges.

the relative distances gate-to-gate and gate-to-QDs, the field lines should be well parallel to the QD layer, but not close to the edges of the contacts where a vertical field component likely appears.

### Schottky-Schottky device on etched structures

In order to avoid the possible problems with the vertical field component occurring with top contacts on the sample surface, another type of Schottky device was prepared. The processing (schematically shown in Fig. 2.7) is the following:

- **Lithography pattern** – We used in this case **UV optical lithography** due to the optical resin properties. In contrast to the poly-methyl methacrylate (PMMA) resin used in electron lithography, a large optical resin thickness can be easily achieved. The resin after annealing offers a better resistance to etching. The optical mask contained a series of  $2\ \mu\text{m}$ -wide lines, forming a square net with a period of  $500\ \mu\text{m}$ ;
- **Dry chloride etching** – This process acting on the lattice pattern produced the desired mesas. We etched the structure down to the lowest AlGaAs barrier. Cl-ions react selectively with semiconductor material and erode the material in a controllable way. The obtained mesas were broader (by about  $1\ \mu\text{m}$ ) than the lithography pattern. This effect could have been induced during etching by chemical reactions between Cl, resin and sample material;
- Ti/Au ( $300/\sim 4500\text{\AA}$ ) metallization completed the process <sup>3</sup>.

The larger size of mesa (than intended,  $2\ \mu\text{m}$ ) already revealed problems of this process. Although the desired in-plane geometry should be better achieved here, the structure did not present ideal electrical properties. The products of chemical

<sup>3</sup>In order to check the required thickness of the metallic layer the sample was cleaved after etching. From one part the resin was removed and the height of mesas was measured by scanning the structure shape with a surface profiler.

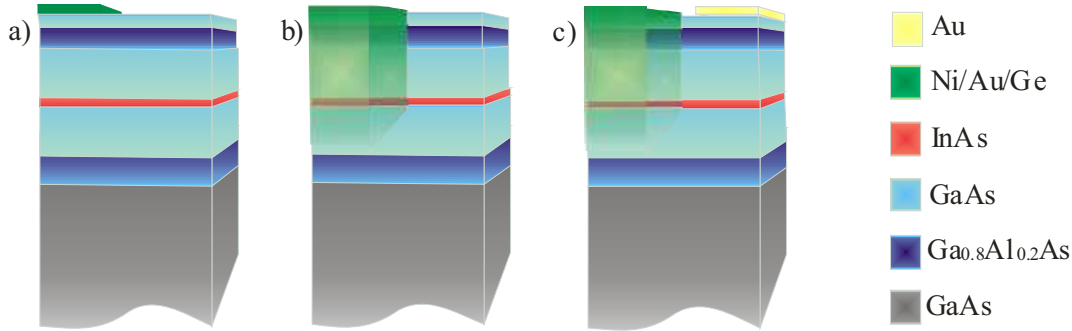


**Figure 2.8.** Scheme of n-Schottky device ( $A_{33}^nS$ ). From left to right: metal deposition of Ohmic contact, diffusion by annealing, Schottky barrier deposition.

reactions during the etching process, staying on the mesa borders, likely caused imperfect junction with the lateral Schottky electrodes and could be a source of uncontrolled charges.

### n-Schottky device

To avoid the difficulties with previously described processes a n-Schottky device was fabricated. This hybrid diode-type structure should ensure a good field geometry without the problems due to chemical etching. It turned out to be a bit more complicated in realization. Figure 2.8 illustrates the following technological steps:

- Definition of the Ohmic contacts by optical lithography. The pattern consists of a lattice of  $100 \mu m \times 100 \mu m$  squares;
- Ni/Au/Ge multilayer deposition (Ni  $100\text{\AA}$ , Ge  $600\text{\AA}$ , Au  $1200\text{\AA}$ , Ni  $200\text{\AA}$ , Au  $2000\text{\AA}$ ) to form the n-type contact;
- **Rapid thermal annealing** for 10 seconds at about  $410^\circ\text{C}$  in nitrogen atmosphere to induce merging of metals and diffusion inside the sample structure. This creates a good Ohmic contact;
- Optical lithography defining the Schottky gates of geometrical shape and size identical to the ohmic ones. The crucial point of this second lithography is to align the mask with respect to the first pattern, as this will determine the distance between electrodes. We could achieve devices with a distance between the contacts of  $2\mu m$ .
- Ti/Au ( $300/2000\text{\AA}$ ) metal deposition finalized the procedure of the n-Schottky device.

For all of these structures, a hidden source of problems comes from the residual doping of the materials and from the dielectric-like barriers possibly formed at the interfaces which gives rise to accumulation of photocreated carriers and thus to a field screening effect. This is the reason to reduce as much as possible the width

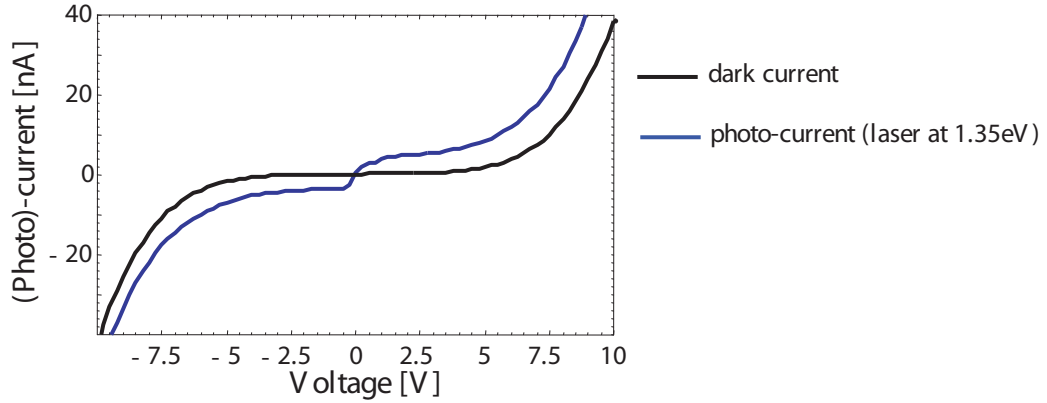


**Figure 2.9.** Voltage-current characteristics of the in-plane Schottky-Schottky device measured at 4K in two different conditions. Curves: black – without sample illumination, blue – illumination of the working channel with the laser beam (laser energy 1.35 eV).

between the contacts as compared to the depletion length of the materials (of the order of  $1\mu m$ , see page 34).

### Electrical characteristics

The current-voltage characteristics (the current through the device as a function of the voltage between the gates) is a simple and fast measurement to estimate the quality of the devices. Figure 2.9 displays two typical I-V curves obtained with a Schottky-Schottky on surface device. The measurement was carried out at 4 K with (blue) and without (black) illumination of the active channel. The characteristics is anti-symmetrical with respect to voltage directions and non-linear for absolute voltages above 5 V, indicating an increase of leaky currents through one of the Schottky barriers. For etched Schottky-Schottky devices the I-V characteristics looked quite similar. Only for the n-Schottky devices the current-voltage dependence was asymmetrical as expected for a diode structure. The effective breakdown voltage strongly depends on the temperature and duration of the annealing used for contact formation. Under illumination some photo-current adds to the dark-current as illustrated in Fig. 2.9. Its sign may reveal the presence of a built-in electric field and actually may depend on the specific position of the laser spot with respect to the device edges.

For in-plane devices it is not easy to estimate precisely the electric field acting on the dots for several reasons: (i) the electrodes deposited on the sample surfaces possess some roughness on the borders, so the distance between the gates varies slightly along the channel (it also can cause problems with the precise determination of the field direction), (ii) in case of diffused electrodes (n-Schottky) the junction position is not well known, (iii) due to the gate geometry and to residual doping the field is not homogenous in the QD plane. Besides, the Schottky-Schottky device on etched structure likely experiences charge accumulation on the mesa's edge. In this case, the effective field seen by the dots may strongly differ from the nominal value.

## 2.2.2 Devices for vertical electric field

The **vertical device** processing was done in a very similar way for n- and p-type structures [86, 84, 87]. Below the preparation of n-Schottky diode is described, while the specificities of p-Schottky samples will be discussed further. The successive steps of processing are schematically shown in Fig. 2.10.

- The net-shaped optical lithography pattern for defining the electrodes to the back contact is defined;
- at least half of the distance between the surface and doping layer is etched by wet chemical process <sup>4</sup>;
- in order to realize an Ohmic contact Ni/Au/Ge multilayers are deposited on the surface;
- the metallic multi-layer is diffused down to the doped layer using rapid (10 sec.) thermal annealing at 380°C. This back contact is characterized by a very low resistivity (confirmed by its Ohmic character);
- the second lithography defines the square patterns for top Schottky electrodes;
- a thin metallic layer (50Å) of Ni and Cr forms the base of the top contact;
- the Ni/Cr layer is semitransparent to make possible optical measurements of the QDs underneath, hence the Schottky barrier has to be completed by an additional metal layer, to enable the electrical connection. A third lithography designs squares which partially overlap with Ni/Cr Schottky electrode;
- Ti/Au (300/2000Å) deposition finalizes the vertical device structure. The thin Ni/Cr layer cannot work as an optical mask for high QDs density region, therefore before last metallization we deposited polystyrene micro-spheres (0.989 $\mu m$  and 2.182 $\mu m$ ) on the sample surface. They are poured in an isopropanol solution. Short immersion of the sample in this bath results in a random distribution of spheres on its surface. To prevent the resin degradation during the bath in isopropanol we must anneal it longer than usually. After the metallization and the lift-off we obtain the metallic mask with holes of 1 – 2 $\mu m$  diameters, after the spheres are dissolved in acetone.

The only difference for p-Schottky device regards the Ohmic contact preparation. After the first lithography, a wet chemical etching process was used to get a direct access to the p-doped layer in the sample structure. Then instead of diffusing Ni/Au/Ge contact just a Ti/Au (200/2000Å) metallization was deposited. It makes a Schottky contact of very narrow depletion length (because of the strong underneath p-doping). The latter acts as an Ohmic contact because the carriers can easily tunnel through the very thin Schottky barrier.

<sup>4</sup>The recipe of the etching solution is  $H_3PO_4/H_2O_2/H_2O$  in proportions: 3/1/40. It etches around 1000 Å/ minute.

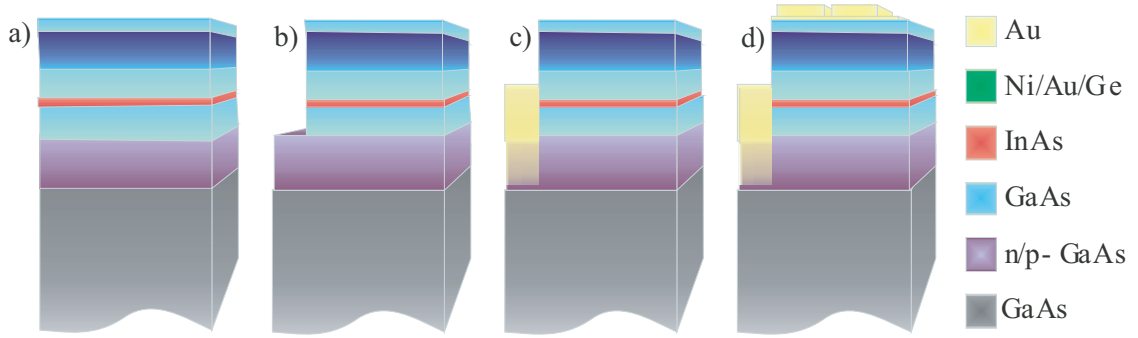


**Figure 2.10.** Device for vertical electric field (samples  $B_{35}$ ). Sequentially from the left to the right the device processing is shown. a) structure of the sample, b) wet chemical etching down to the doped layer, c) Ohmic contact deposition, d) Schottky gate forming from semi-transparent layer and gold mask with micro-holes.

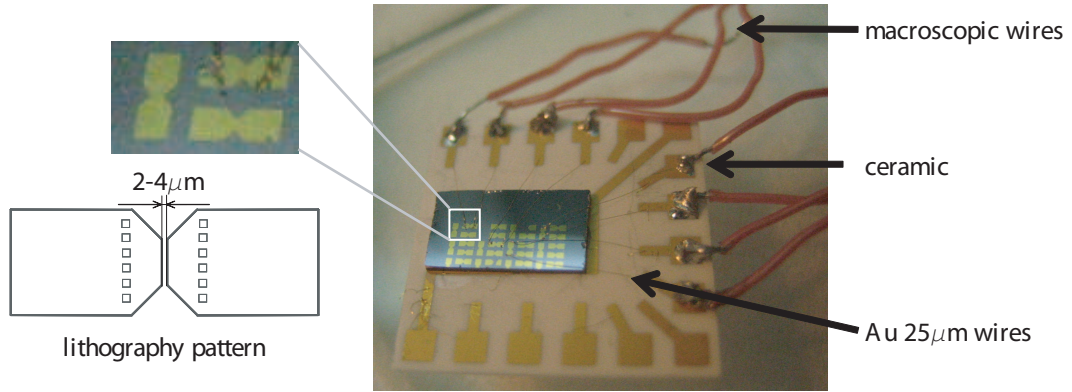


**Figure 2.11.** Device for in-plane electric field (samples  $A_{35}^{SSsurf}$ ). Photograph (by *O. Krebs*) of the sample mounted on the ceramic. On the left – zoom of the sample surface showing the shape and the directions of the metallic gates (on one of them a pair of contacts and a pair of bonding wires are visible), below – photolithography pattern.

Further device fabrication process was common for all samples. In order to make the required electrical bondings, the sample was glued on a ceramic holder (with optical resin or silver paste) which in turn was attached to the cold finger of a cryostat for optical measurements. The sample electrodes were connected to the gold pads on the ceramic holder using  $25\mu\text{m}$  gold wires. The electrical connections to the apparatus of the lab was completed by soldering macroscopic wires to the gold pads. The final processed and connected sample is displayed in Fig. 2.11. One can see that the patterned ceramic holders enable connections of several devices from the same piece of sample. For instant it was possible to connect devices of different field directions in the case of in-plane field structures.

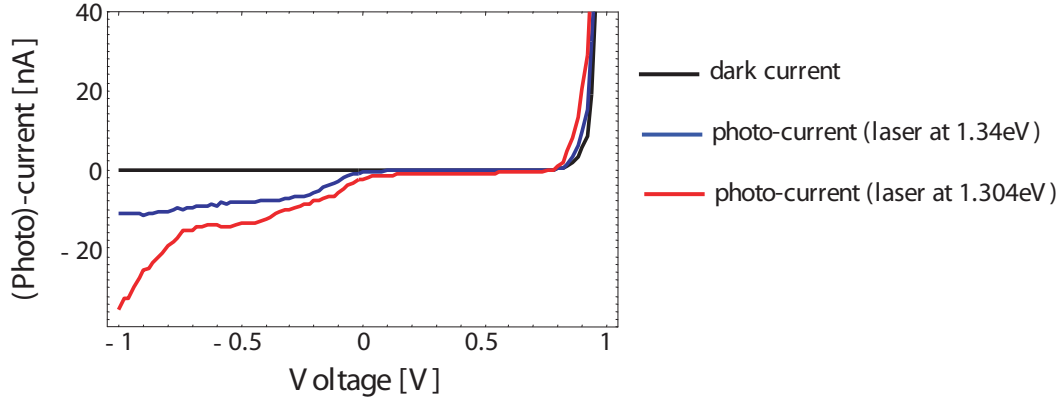


**Figure 2.12.** Voltage-current characteristics of the vertical n-Schottky device measured at 4 K in three different conditions. Black curve – without sample illumination, blue curve – illumination the working semitransparent gate with the laser beam (laser energy 1.34 eV), red curve – illumination the working semitransparent gate with the laser beam (laser energy 1.304 eV).

## Device for vertical field - electrical characteristic

Devices intended for vertical field should work as n(p)-Schottky diodes. Typical I-V characteristics of a processed diode are shown in Fig. 2.12. This measurement was performed at 4 K. The black curve corresponds to the dark current. The diode character of the device is clearly evidenced – in reverse bias the current is very small (a few tens pA), whereas in forward bias the current increases exponentially with applied voltage. When illuminating the Schottky gate (semitransparent part) we observe photo-current, which dominates the electric properties of the device in the reversed bias region. Obviously the effect depends on the excitation power, since it is related with the number of photo-created carriers (hence the negative sign of the photo-current for n-Schottky device). Also excitation energy influences the characteristics – comparing two (blue and red) curves in Fig. 2.12 we see that the corresponding voltage ranges with the plateau (small current) are different.

Knowing the distance between the gates ( $d = 175$  nm), and the Schottky barrier height ( $\approx -0.8$  eV for n-type,  $\approx +0.8$  eV for p-type) we can estimate the applied electric field with a high precision with respect to in-plane electric field structures. Some uncertainty could come from the residual doping of the layers grown above the doped one. However, for a residual doping of  $10^{15}$  cm<sup>-3</sup> and a 1 V barrier, the depletion length  $W$ <sup>5</sup> would amount to  $\sim 1\mu\text{m}$  which is much longer than the distance  $d$  between the electrodes. This should produce a negligible perturbation of the nominal field. Note that using n- and p-Schottky devices enabled us to apply a field in opposite directions with respect to the growth axis, i.e. with respect to the top and bottom of the pyramid-like or lens-like QDs.

<sup>5</sup> $W = \sqrt{2\varepsilon_r\varepsilon_0 V_b / e\rho}$  where  $V_b$  is the barrier height,  $\rho$  the free carrier density, and  $\varepsilon_r\varepsilon_0$  the dielectric constant of the material.

## 2.3 Experimental setups

Ideally for the investigation of symmetry-related effects, we would like to have a controllable means to break or restore continuously some symmetry elements of the system. Thus the experimental setup should provide the possibility to apply an external perturbation to the system in addition to the access to the quantity we want to measure. In this *Section* we describe the setup developed for photoluminescence (PL) measurements of individual QD in magnetic and/or electric fields. In principle, the lack of inhomogeneous broadening for individual QDs gives unique possibilities to observe interactions of order of a few  $\mu\text{eV}$ 's in solid state matter. However, for this purpose the resonant absorption or reflectivity experiments are definitely preferable, because they offer much higher resolution limited by the laser line-width. However, the latter present also a number of drawbacks:

- very low oscillator strength of quantum dots makes the absorption measurement technically sophisticated (namely, a modulation technique is needed) [88];
- the micro-absorption setups are based generally on optical fibers, hence the important information about light polarization can be easily lost;
- the line broadening in high voltages for in-plane electric field device, gets to some extent intrinsically incompatible with the standard modulation technique [89];

For these reasons no absorption signal on single II-VI QD was reported so far. In this situation PL was chosen as the main experimental technique.

Spectroscopic studies were carried partly in LPN (III-V quantum dots) and partly at Warsaw University (II-VI quantum dots), where specific equipments have been developed.

### 2.3.1 Setup for measurements of II-VI materials

The schematic picture of the setup is shown in Fig 2.13, where one can find the most important information about arrangement of the optical elements. For  $\mu$ -PL measurements a specially designed **mirror objective** with a magnification  $\times 100$  and numerical aperture 0.7 was used [90]. Originally it was invented for chemical and biological specimens. A special holder for the semiconductor sample was added by A. Kudelski [91] to adapt the system for measurements of semiconductor materials. The focal plane is exactly at the back side of the quartz objective where the sample is attached. Such construction guarantees excellent mechanical stability and prevents sample displacement with respect to the microscope during measurements in magnetic field. The body of the objective is made of suprasil, enabling immersion into liquid helium bath and measurements for **temperatures 1.5 – 300K**. The cryogenic part of the setup consisted of an optical cryostat (*Spectromag 4000, Oxford Instruments*) with a superconducting coil. The applied **magnetic field** ranged from **-7T** up to **+7T** and two pairs of optical windows allowed experiments both **in Faraday** and **in Voigt geometry**. The



QDs luminescence was excited by the beam of a **CW doubled YAG** (532nm) or **Ar+** (488nm or multi-UV lines) **laser**. It was sent to the sample after reflection on a dichroic mirror (or just a thin glass plate) placed at a small angle with respect to the main optical axis of the setup (objective – monochromator entrance slit), as the polarization anisotropy induced by this elements should remain as low as possible. The mirror position could be changed during the experiments, in order to move the laser spot position on the sample. The laser beam was expanded to fit the objective aperture when necessary. This point is important because the central part of such mirror objective is “blind” (the first reflecting mirror is placed there). The laser spot was focused on  $\sim 1\mu\text{m}^2$  area of the sample surface. The PL signal from the sample was collected via the same objective, and its polarization properties tested by a set of linear polarizers and quarter-waveplates. All polarization optics were mounted in frames which enabled rotation around their optical axes. The signal was analyzed spectrally by a 0.25m **spectrograph** with a 1800 (or 1200 or 600) lines per millimeter grating. The lower resolution gratings were used only to see larger spectral range when characterizing new samples. The spectra were detected by a thermo-electrically cooled **CCD camera** (*CCD DV420-FI, Andor Technology*). To have an overview of the sample surface, we illuminated it with white light from a halogen lamp via optical fiber and placed a beam-splitter cube in the beam. This setup enabled us to see the white light reflection imaging the sample surface and the PL light indicating the laser spot position. The beam-splitter was removed for “real” measurements to avoid perturbations of the light polarization.

The setup was used to study II-VI samples, which had no structures on the surface (e.g. metallic electrodes) and could be placed directly on the objective. Such a construction ensures excellent collection efficiency, thanks to increased refractive index of the medium above the sample <sup>6</sup>. The excitation source, the PL detector, and all the optical elements were selected to work optimally for visible wavelengths (the full wavelength range of the setup was from UV to near infrared: 300 – 750nm).

**Fine structure splitting** of excitonic lines was measured by recording the spectra at different position of the linear polarizer(analyzer)in the detection path . Usually it was rotated by  $2\pi$  with a step of  $9^\circ$ . Even though the FSS is smaller than the setup resolution the splitting can be analyzed by this technique – when changing the polarization we can follow the central position of a given line which is determined with a precision generally better than its width. For analyzer positions corresponding to the pure components of the excitonic doublet there is a minimum for the linewidth and an extremum of line deviation with respect to its average position (calculated over all angles).

The spectral resolution, defined as the minimal linewidth which can be measured, was  $120\mu\text{eV}$  (<sup>7</sup>). The numerical error on the line position from a Gaussian (or Lorentzian) fit is of the order of a few  $\mu\text{eV}$ . As the accuracy of the line position

<sup>6</sup>For QDs this technique was also realized in another way by authors of Refs. [92, 93]. They used solid-immersion-lens (SIL) into a confocal micro-photoluminescence system.

<sup>7</sup>In our case the setup resolution was determined experimentally from measurements of the laser line.

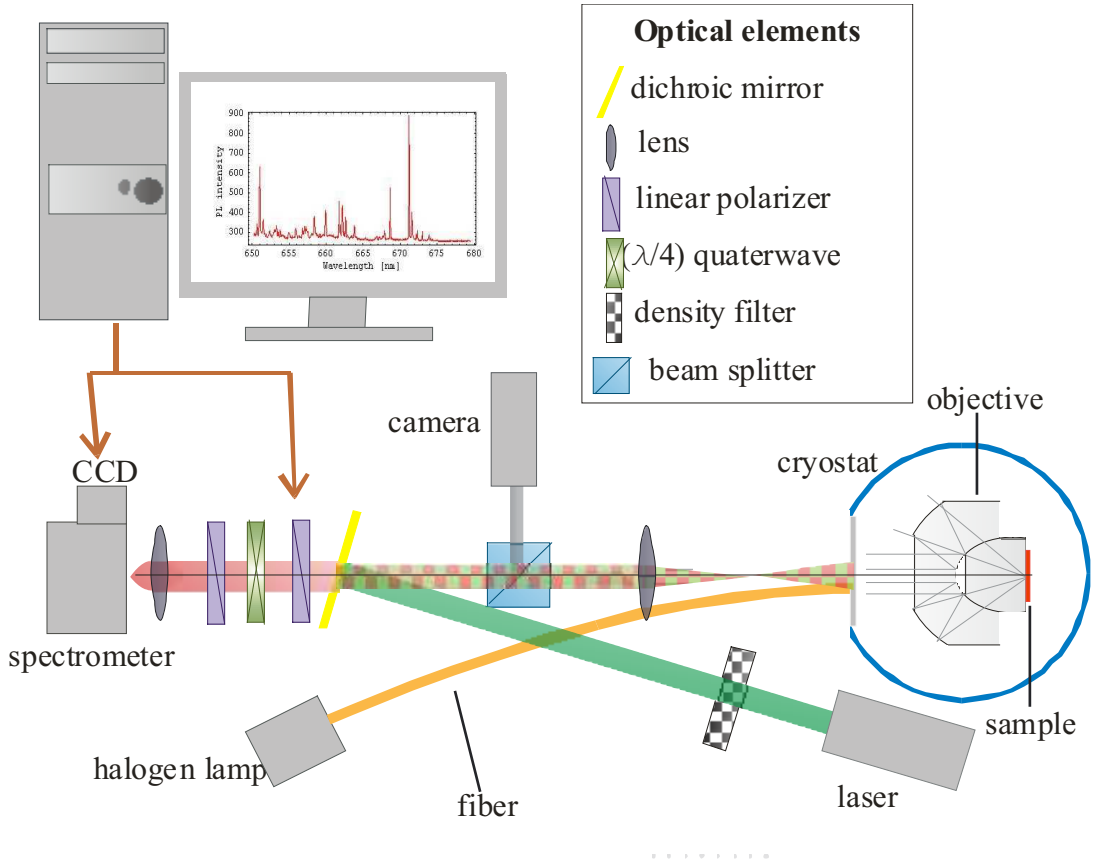


**Figure 2.13.** Scheme of experimental setup for  $\mu$ -PL measurements in magnetic field. Three beams are drawn: laser (green), luminescence (red), and white light illumination (bright gray). The legend for the optical elements is placed in the upper right corner.

measurements in this setup we took the value  $30\mu\text{eV}$ , which corresponds to the standard deviation of the line position observed when repeating measurements under the same conditions. Spectral diffusion is the most likely origin of this effect. This standard deviation was not measured for all investigated quantum dots, therefore we generally cannot plot meaningful error bars in the plots which will be shown in *Chapter 4*. Spectral wandering has a typical timescale of several minutes, thus this effect can be easily eliminated in the fine structure splitting measurements, as each spectrum takes only a few seconds. It manifests itself by a slow shift of the line in time that can be subtracted from the data.

### 2.3.2 Setup for measurements of III-V materials

In LPN, we used two setup configurations: (i) for measurements with external electric field only and in temperatures down to  $\sim 4 K$ , and (ii) for measurements in electric and magnetic fields at pumped helium temperatures. Because of the electrical bondings on the top surface of the III-V samples, a different type of microscope than that described above was required. Attaching such samples against the objective flat side of a mirror microscope would obviously destroy the fragile electrical connections.

Let us first present the first configuration of experimental setup (see Fig. 2.14). The sample glued on its ceramic holder (see Fig. 2.11) was fixed by silver paste on the cold finger of the cryostat (*Oxford Instruments*) and the macroscopic wires connected the ceramic holder with cryostat's electric pins. The liquid helium flux cryostat was fixed on the step-motor stages easily adjustable in all three directions with a precision better than  $1\mu\text{m}$ . That facilitated focusing of the laser spot on the suitable place of the electric device. Such an experimental solution permitted to conserve the same alignment of optical elements during many days of measurements. The long working distance microscope (*Mitotuyo*, magnification  $50x$ ), situated in front of the cryostat window, focused the laser beam on  $\sim (2\mu\text{m})^2$  area of the sample surface. The Titanium-Sapphire laser used for excitation covered a wide excitation range ( $840 - 980\text{nm}$ ) and the beam polarization was controlled by a set of waveplates and polarizer. A spectral filter put on the laser beam provided additional rejection of laser background. This was essential for quasi-resonant excitation. A set of density filters was used to adjust the excitation laser to the required power. The laser beam was sent into the objective after reflection from a non-polarizing beamsplitter cube (50/50). The part of the beam which passed through the cube went to the power meter (the typical power used in experiment was around  $2\text{ mW}$ , measured after the beamsplitter, when exciting below the wetting layer edge). The PL signal was collected by the objective and sent through the cube toward the spectrometer. It was first analyzed by a set of polarization waveplates and spectrally by a  $0.6\text{ m}$ -focal double monochromator (*Jobin-Yvon*) equipped with 1200 lines/mm gratings. The spectra were recorded using a liquid-nitrogen cooled CCD camera (*Princeton Instruments*). Spatial filtering of the signal was done in two ways. The metallic electrodes on the sample surface limited the excitation/collection area, and additionally with the CDD in imaging mode, one could resolve (vertically only) different luminescence lines originating from different nano-objects in the sample. In order to see the sample surface a mirror was placed in front of the monochromator (and removed for spectra recording). It sent white light from a halogen lamp and the reflection from the sample to an imaging camera. As the magnification of this system was very large, we could follow the laser spot displacement of the order of a fraction of a micron. A second web-cam standing next to the objective, imaged the whole ceramic holder and was very helpful for alignment of the setup at higher scale. In order to apply an electric field an electric source-meter (*Keithley*) was used. We used it mainly as a voltage source (from  $\text{mV}$  up to  $21\text{ V}$ ) and a current multimeter (from fractions of  $\text{nA}$  to a few  $10\text{ mA}$ 's). The working wavelength for the presented setup (optical elements

and detection) covered the range 870 – 1000 nm. All measurements reported in Chapter 3 were carried out with this experimental configuration.

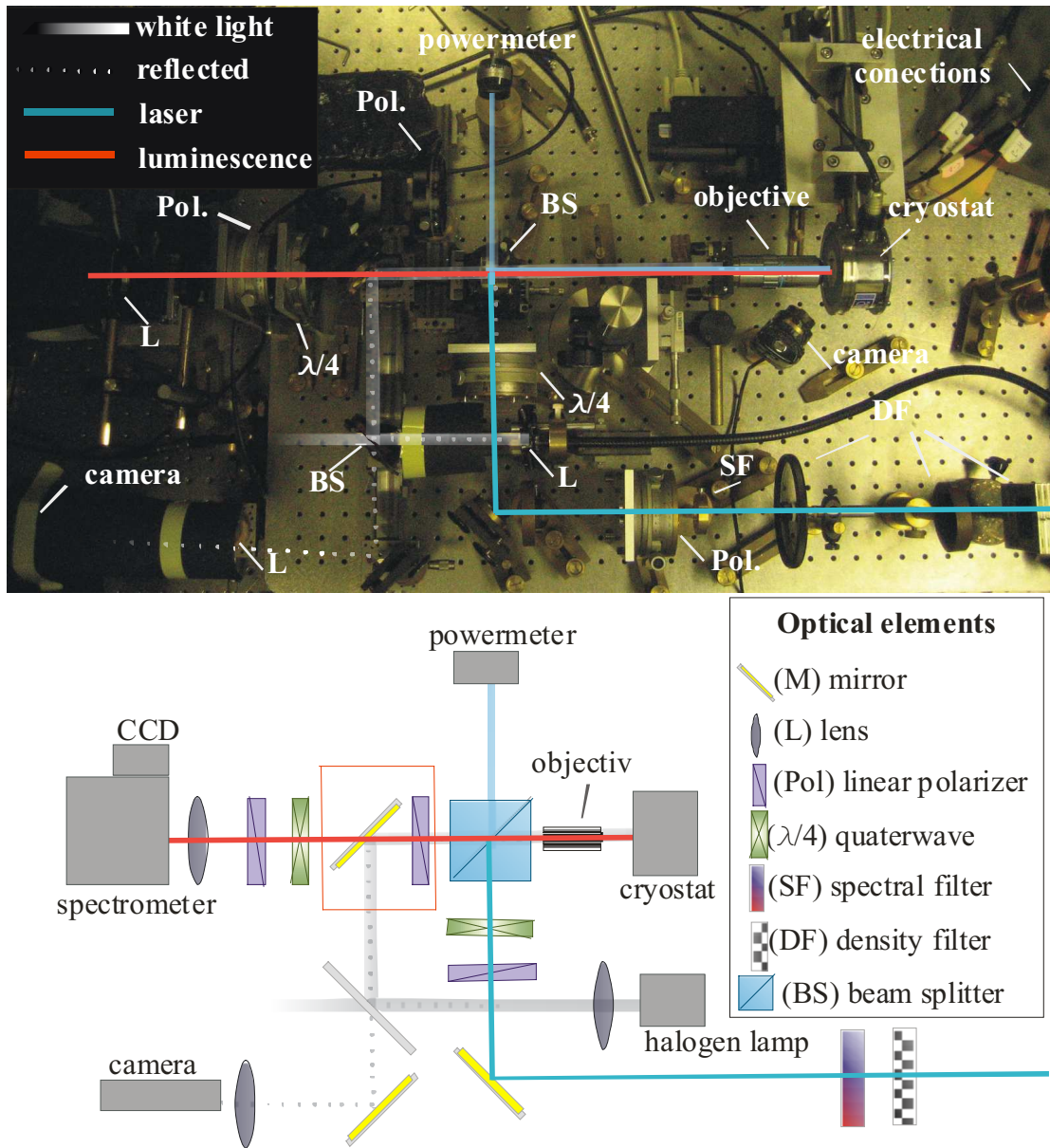


**Figure 2.14.** Scheme of experimental setup for  $\mu$ -PL measurements in electric field. Upper panel shows a photograph (*by O. Krebs*) of the setup with the most important elements marked. Additionally three beams are drawn: laser (blue), luminescence (red), and white light illumination (bright gray). Lower panel shows a scheme of the setup with the legend of optical elements. The two elements in the red square (a polarizer and a mirror) can be easily removed during experiment.

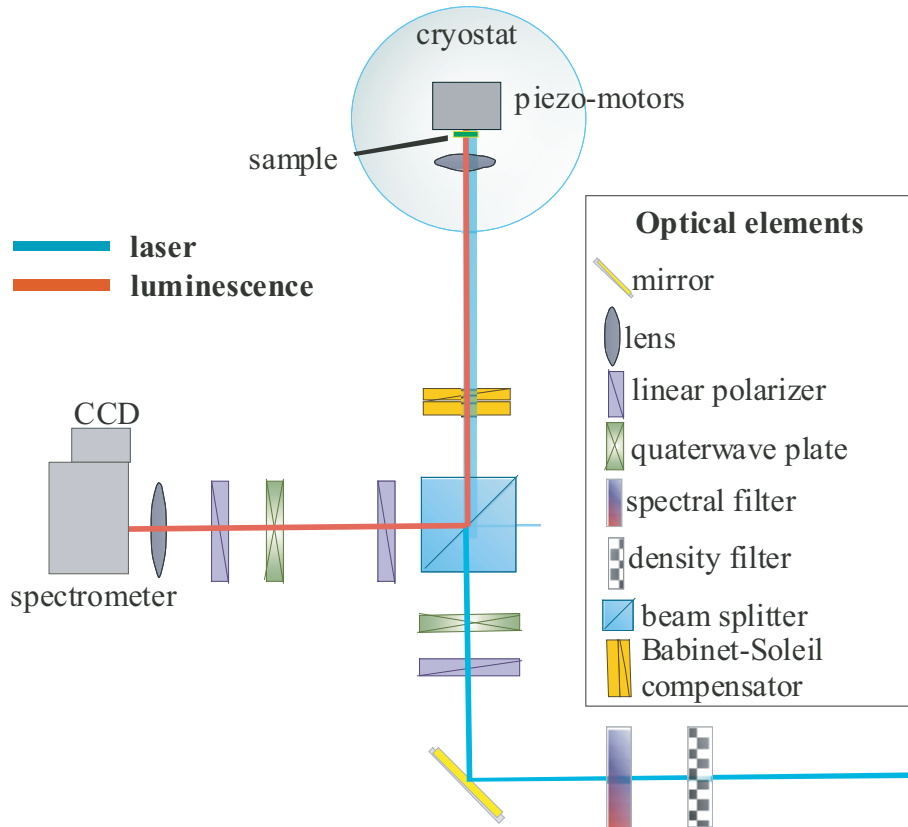


**Figure 2.15.** Scheme of experimental setup for  $\mu$ -PL measurements in electric and magnetic fields. Almost all elements are the same as in the previous configuration.

The second configuration of the setup differs mainly by the cryostat part (see Fig. 2.15). Instead of the cold finger cryostat a pumped helium cryostat with a superconducting coil was used. It was placed in on the laser beam transmitted through the cube beamsplitter, not facing the monochromator as in the previous case. The sample was mounted on a home-made nanopositioning system (with *Attocube* piezo-actuators). The piezo stages offered a precise positioning of the sample over a few millimeters in all three directions. Two stages moved the sample in focal plane in order to find the right position with respect to the metallic gates. The third piezo-motor moved a small lens (*Optoprism*, focal length  $2\text{mm}$ ) in front of the sample<sup>8</sup>. The positioning system with the sample and the lens were immersed in liquid helium. The temperatures of the measurements were at around  $1.6\text{--}1.8\text{K}$ . In order to image the sample surface a He-Ne laser beam was used. When slightly defocusing the beam one could form outside the cryostat an image of the sample part illuminated by the laser. The main optical part of the setup was the same as in the first configuration described above. For the excitation we used in this configuration the laser beam passing through the cubic beamsplitter. The precise measurements of the degree of the polarization were performed in this setup. In that aim, we added one optical element: a Babinet-Soleil compensator was placed

<sup>8</sup>The system has been designed by A. Kudelski in LPN.

behind the cubic beam splitter (see Fig. 2.15). It was used to compensate the beamsplitter birefringence, which gave a small degree of linear polarization. The Babinet-Soleil retardation was set for the wavelengths  $\sim 956\text{nm}$ , where the PL from quantum dots was studied. The usual configuration of the setup allowed us to perform measurements under different excitation conditions: both circular and linear vertical polarizations. In order to rotate linear polarization of the excitation a quarter-waveplate was added between the cube and quarter-waveplate to form a half-waveplate. The linear polarizer just behind the cube in the detection path was removed for measurements of circular polarization of the emission. It was placed in the PL beam to investigate linear polarization. The rotating polarizer was mounted in the frame fixed together with the quarter-waveplate frame. Such a solution guaranteed that the light passing through was circularly polarized. In such case the linear polarizer in front of the monochromator slit is not necessary and it was removed for measuring the degree of linear polarization. This configuration was used only for the experiments presented in *Chapter 5*.

The accuracy of FSS measurements with the above setups is limited by spectral diffusion of the lines (a few  $\mu\text{eV}$ 's). It is much better than the spectral resolution ( $\sim 25 \mu\text{eV}$  at  $1.3 \text{ eV}$ ).

**SUMMARY.** *Chapter 2* reports technical preparation for the experiments. Short survey of investigated samples and their processing to obtain electric field effect structure is presented. The relevant information regarding the experimental setup is given.



---

---

## CHAPTER 3

---

# Influence of electric field on quantum dots

### Contents

---

<b>3.1 In-plane electric field</b> . . . . .	<b>45</b>
3.1.1 PL intensity and linewidth . . . . .	47
3.1.2 Fine structure splitting vs. in-plane field . . . . .	50
<b>3.2 Vertical electric field</b> . . . . .	<b>52</b>
3.2.1 Permanent vertical dipole . . . . .	54
3.2.2 Direct Coulomb integrals . . . . .	55
3.2.3 Fine structure splitting vs. vertical field . . . . .	57
<b>3.3 Local electric field</b> . . . . .	<b>57</b>
3.3.1 Transition identification . . . . .	57
3.3.2 Fine structure vs. local field . . . . .	61
<b>3.4 Conclusion – FSS tuning</b> . . . . .	<b>63</b>

---

*"Experience without theory is blind, but theory without experience is mere intellectual play."*  
Immanuel Kant

THE QUANTUM CONFINED STARK EFFECT has been successfully investigated in the last decade to develop deeper insight into the essential physics of quantum dots [32, 85, 94]. In an electric field  $F$ , an electron-hole pair acquires a static dipole  $\alpha F$  ( $\alpha$  is the polarizability) which gives rise to the Stark shift  $-\alpha F^2$  of the corresponding exciton line. However, as we will see in this *Chapter*, this effect may be significantly reduced because of the decrease of the direct Coulomb interaction between the carriers as a result of their larger separation. Predicting quantitatively the effect of an electric field is thus not straightforward, since it modifies the single particle wave-functions which in turn changes their Coulomb interaction. Regarding the influence on the exciton fine structure splitting (FSS) we can still rely on



the expression given in *Section 1.8* where the exciton wave functions  $F_x$  and  $F_y$  may be considered as solutions of the Schrödinger equation including the direct Coulomb term. Clearly, the field influence on FSS decomposes into two terms. The first one is related to the modification of the overlap of the electron and hole wave-functions, which obviously determines the strength of the exchange interaction <sup>1</sup>. The second mechanism is related to the symmetry change of the exciton wavefunction. This can be achieved e.g. when the field changes the extension  $L_x$  of  $F_x$  while keeping constant the perpendicular one (see discussion in 1.9). The whole effect is thus not trivial – both, increase and decrease of exchange interaction can be obtained depending on the field direction. In experiments the two mechanisms interplay and the effective FSS change may be difficult to estimate <sup>2</sup>.

In order to address this issue we have studied two different configurations of field-effect structures : (i) electric field applied in the QD plane provided by biased metallic gates (or Ohmic contact) evaporated (diffused) on the sample surface or along edges of a chemically etched mesa (samples  $A_{35}^{nS}$ ,  $A_{35}^{SSsurf}$ , and  $A_{35}^{SSetch}$ ), (ii) electric field applied parallel to the QD growth axis  $z$  (“vertically”) in p- or n-Schottky diode structures (samples  $B_{35}^{nS}$  and  $B_{35}^{pS}$ ). The anisotropy change was expected to be the prominent effect in the in-plane structures, where the symmetry of the wave functions should be strongly affected by the electric field. In vertical configuration it was rather expected that change of the wave functions overlap should dominate (as indicated by the factor  $P(q)$  in Eq. 1.9).

*Sections 3.1* and *3.2* present the experimental investigations of QD FSS in the presence of in-plane electric field and vertical field respectively. In addition to these measurements carried out with a controllable field we have also examined the influence of the fluctuating electrostatic environment on quantum dots. Spectral wandering and FSS modifications of the exciton lines due to local charge fluctuation will be the topic of *Section 3.3*.

In next *Sections* the following color coding for the data points and fits will be used in the illustrations: **black** for the exciton (X), **gray** for biexciton (XX), **red** for positively charged exciton (X+), and **blue** for negatively charged exciton (X-).

---

<sup>1</sup>The FSS scales as  $1/L^3$  in Eq. 1.10 where  $L$  is the typical size of the wave function overlap.

<sup>2</sup>Reducing the FSS by a decrease of the electron-hole overlap is not very satisfying in the perspective entangled photon emission, since the optical oscillator strength of the excitonic transition becomes reduced as well.

### 3.1 In-plane electric field

Let us first discuss the electric field influence on the emission energy from different QDs. Since we developed a new technology for applying an in-plane field, we first stumbled upon the problem of estimating the actual field experienced by a given QD. The difficulties met for sample processing, as described in *Section 2.2.1*, suggest that the nominal field  $V_g/d$  where  $V_g$  is the applied voltage (in Schottky-Schottky structure) and  $d$  the distance between the gates could be far from the effective one. For this reason, most of the results will be shown as a function of the applied *bias*. Only for comparison with a theoretical model, some experimental results will be displayed as a function of the nominal electric field.

A rough estimate of the quantum confined Stark effect (QCSE) without Coulomb correction can be readily derived in the parallelepiped box model for the single particle states:

$$\Delta_{\text{QCSE}} \equiv -\alpha F^2 = -\frac{1}{32} \left( \frac{eFL^2}{\hbar} \right)^2 (m_e^* + m_h^*) \quad (3.1)$$

where  $F$  is the electric field strength,  $L$  is the length of confinement in the direction of the applied field, and  $m_{e(h)}^*$  is the effective electron (hole) mass. For a lateral QD size  $L = 20 \text{ nm}$ , this yields an in-plane polarizability  $\alpha \sim 0.1 \text{ meV} \cdot \text{cm}^2 / \text{kV}^2$  when assuming an effective transverse hole mass of  $0.1 m_0$ . Obviously, the uncertainty on the relevant QD size  $L$  with enters in Eq. 3.1 as  $L^4$  makes this estimate very approximate. For a typical field of a few  $10 \text{ kV/cm}$ 's which in principle could be applied with the structures we have fabricated, a Stark shift of a few  $\text{meV}$ 's should be observed. Experimentally (see Fig. 3.1), the typical maximum quantum confined Stark shift amounted only to a few hundreds of  $\mu\text{eV}$  (as also recently reported by another group [95]). The effective in-plane field experienced by the QD seems thus much smaller than the nominal value. This conclusion holds as long as the Coulomb correction is not included in the above theoretical estimate. If so, this effect would be the indication that the QD plane tends to remain nearly equipotential, meaning that most of the potential drop takes place in a depletion region formed below the top Schottky electrodes. This problem could be specific to the chosen technology of electrodes on the sample surface. We could indeed expect that a real planar p-i-n structure would allow a better control of in-plane electric field (at the expense of more stringent control of ohmic contact annealing). However neither in our Schottky-Schottky device on etched heterostructures, nor in similar p-i-n structures done by ion implantation by V. Stavarache *et al.*[95] (which possesses in principle the required in-plane geometry) the observed Stark shift was higher than several hundreds of  $\mu\text{eV}$ . The authors of Ref. [95] attribute it to a strong modification of the exciton binding energy (or Coulomb correction), but the effect of residual doping can not be ruled out for a distance between the electrodes of a few  $\mu\text{m}$ . As long as no complete theory of the QCSE in quantum dots is available it is not possible to confidently determine the actual applied field from the experimental stark-shift.

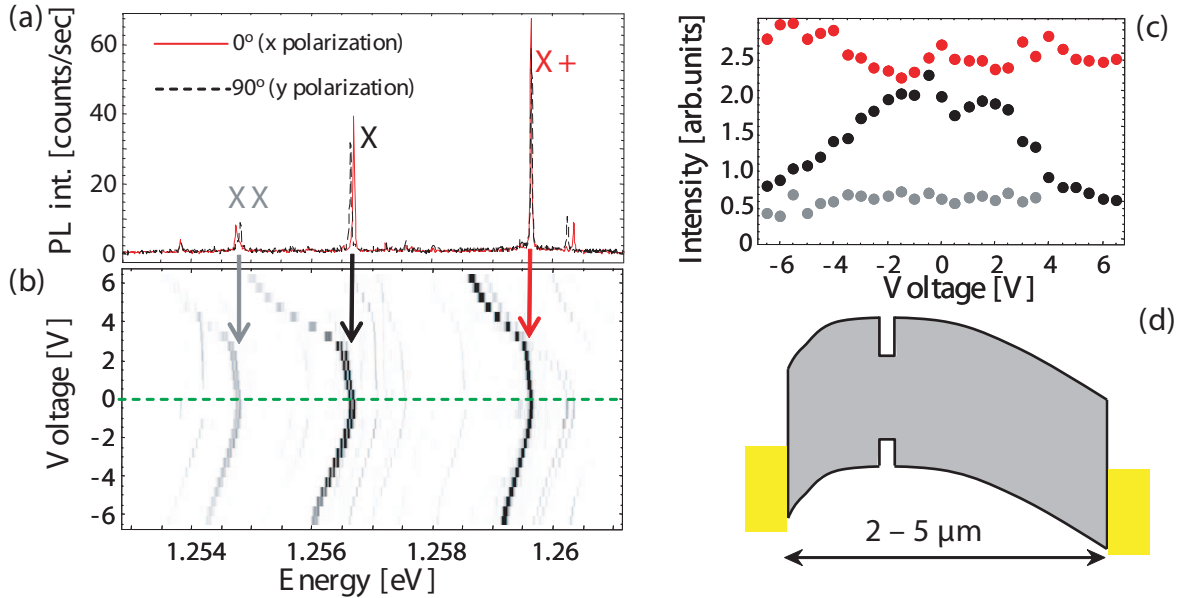


**Figure 3.1.** [Sample  $A_{35}^{SSsurf}$ ] (a) PL under quasi-resonant excitation energy ( $1.38\text{eV}$ ) at zero bias for two perpendicular polarizations (black dashed and solid red lines). Three transitions from the same QD are visible: X, XX, and X+. (b) Evolution of PL spectra in electric field (PL intensity is encoded in a gray-scale). Polarization of detection was set at  $45^\circ$  (X and XX doublets are clearly visible). (c) Intensity of X (black), XX (gray), and X+ (red) transitions obtained from Gaussian fit of the lines vs. applied voltage. (d) Scheme of the effective band curvature possibly generated under applied bias in presence of a residual doping.

The hypothesis of non-uniform field due to residual doping (see schematics in Fig. 3.1(d)) can yet be discussed further by comparing the QCSE measured for different QDs. As the laser spot size was comparable to the size of the channel between the gates, it does not provide itself the spatial resolution to probe the field homogeneity, but the spatial position of a specific QD with respect to the gates should determine its Stark shift. The part of sample investigated in Fig. 3.1 contained a rather high QD density, so that in focal point we had many of them randomly distributed. As illustrated in Figure 3.1(b), different dots in the same series of spectra do not exhibit the same field-dependence. Fluctuations in size or composition of particular QDs, which obviously affect the precise Stark shift amplitude, cannot yet explain the strong scatter of behaviors we observed. In contrast, the QCSE from a specific QD emitting photons from different excitonic complexes is almost the same. This is illustrated in Fig. 3.1. The zero-field spectrum (a) is dominated by three lines, identified as exciton (X), biexciton (XX), and positively charged trion (X+) originating from the same QD. This identification relies on several observations: (i) the FSS of the exciton mirrored by the biexciton, and (ii) the typical binding energy of positive trion and its voltage dependence. All these lines shift in a very similar way in the electric field. The weak discrepancy between them may be ascribed to the binding energy changes (depending on direct Coulomb integrals) due to the field. The comparison of different QDs sup-

ports thus the interpretation of field inhomogeneity, an effect which was actually observed in all studied in-plane devices <sup>3</sup>.

Simultaneous observation of neutral and charged transitions in the spectra implies that with in-plane devices we have no absolute control over the process of QD charging with a carrier. The emission from neutral excitonic complexes is stronger for zero field (see Fig. 3.1), while emission corresponding to positively charged exciton gains slightly in intensity with applied voltage. Following the X and XX lines in Fig. 3.1(b) one can distinguish in zero bias both linearly polarized components, but with increasing voltage the broadening of the lines progressively hinders the fine structure. These effects are now discussed in more detail in the following *Section*.

### 3.1.1 PL intensity and linewidth

To tackle the problem of PL intensity decrease with electric field we have performed measurements under different excitation energies. It was varied from around 1.36 eV to 1.42 eV, i.e. from an intra-dot (or quasi-resonant) to a non-resonant excitation regime in the 2D continuum of the QD wetting layer (WL). From the obtained results we could conclude that the in-plane component of the electric field does not vanish in the intrinsic region of the fabricated structures, even for n-Schottky devices. Indeed, the photo-carriers created in the WL are very efficiently swept by the electric field, leading to a dramatic decrease of their capture and thus of the PL intensity. This behavior is visible in Figures 3.2 ((a) and (b)) that show on a gray scale the contour-plots of PL intensity against bias and energy: the PL intensity of the lines decreases more rapidly with the bias under non-resonant excitation (a) than under quasi-resonant excitation. In parallel, the associated Stark-shift (shown in Fig. 3.2(c) for the line marked by an arrow) is less pronounced likely because of a stronger field-screening produced by the accumulation of photo-carriers on both electrodes. As a consequence of this observation, we decided to study the field influence on FSS mainly in the regime of intra-dot excitation which extends significantly the domain of useful field. Another advantage of this excitation regime is that it naturally selects a smaller number of QDs making the analysis of single lines easier.

In practice the strength of the applied field was systematically limited by the strong reduction of luminescence intensity for a characteristic nominal field of about 30 kV/cm. In addition this effect was accompanied by a strong broadening of the PL lines. These effects are illustrated in Fig. 3.3 which shows the linewidth and intensity evolution of 2 single PL lines from 2 different samples as a function of applied voltage. A very similar behavior is observed in both cases. The linewidth increases with the applied field up to 100 μeV and 50 μeV while in the same time the intensity is reduced by 80%. The field-induced escape of electrons from the ground state or from a higher state likely explains this effect. Indeed, using a

---

<sup>3</sup>This is also observed by B. D. Gerardot *et al.* [89] who have studied devices with longer intrinsic channel ( $\sim 20\mu m$ ). In their work, only the QDs near the gates exhibit QCSE, which proves that the voltage drop takes place only in the depletion region close to the gates.

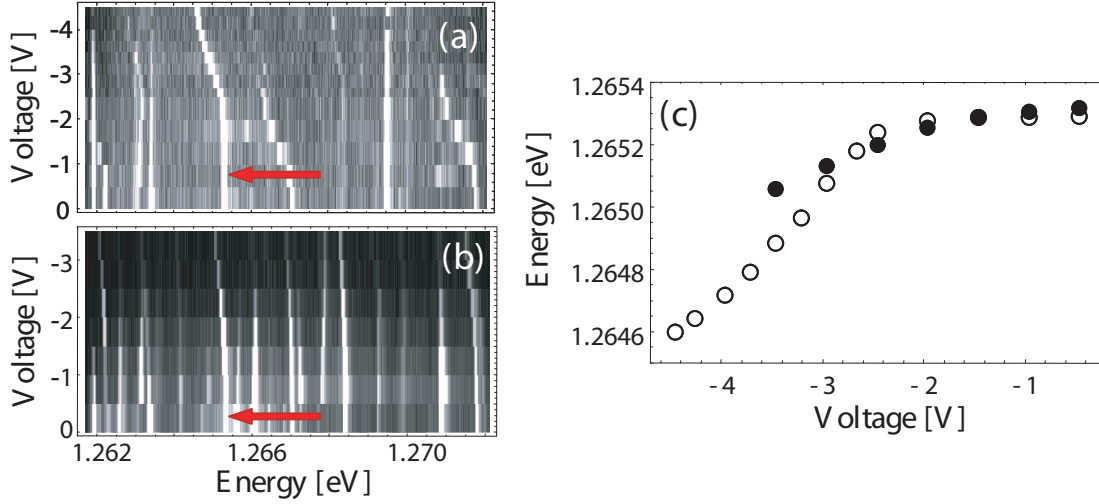


**Figure 3.2.** [Sample  $A_{35}^nS$ ] PL evolution under in-plane field for non- and quasi-resonant excitation. On the left hand side: contour-plots in a gray scale of the PL intensity as a function of the energy detection and applied bias : (a) under quasi-resonant excitation, (b) non-resonant excitation. On the right – (c) energy position of the chosen line (marked with the red arrow) against the bias under quasi-resonant (open symbols) and non-resonant (closed symbols) excitation. .

simple tunneling model developed in the WKB approximation <sup>4</sup> (see e.g. [96]) one can estimate the electron escape rate as:

$$\tau^{-1} \geq \frac{\hbar^2}{4m_e^*a} \text{Exp}\left[-\frac{4\sqrt{2m_e^*}}{3eF\hbar} V_d^{3/2}\right] \quad (3.2)$$

to which is associated a level broadening  $\Gamma$  through the Heisenberg uncertainty principle [97]:

$$\Gamma \cdot \left(\frac{1}{\tau} + \frac{1}{\tau_1}\right)^{-1} \geq \frac{\hbar}{2}. \quad (3.3)$$

where  $V_d$  is the barrier height (or ionization energy) from the electron level to the wetting layer continuum, and  $a$  the QD vertical size (geometrical potential size) as schematically represented in Fig. 3.3(c). Assuming that the loss of intensity ( $I_{PL}$ ) is mainly caused by such a carrier escape in competition either with the radiative recombination (for the electron ground state) or with the intra-dot relaxation (for an excited state), the PL intensity is given by:

$$I_{PL} \propto \frac{\tau}{\tau + \tau_1} \quad (3.4)$$

where  $\tau_1$  is the characteristic time of the competing relaxation mechanism. To de-

<sup>4</sup>Wentzel-Kramers-Brillouin approximation developed to treat semi-classically quantum mechanical problems.

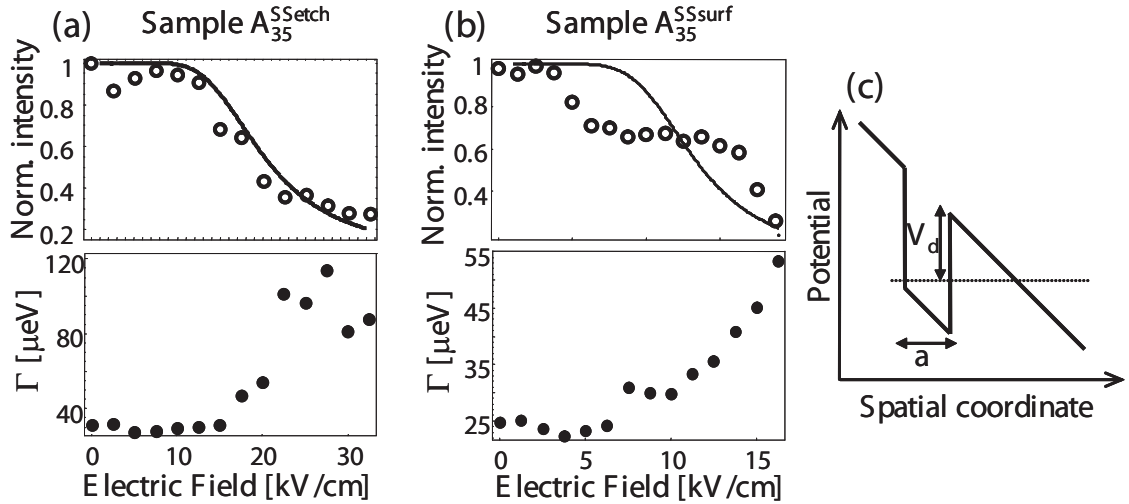


**Figure 3.3.** Linewidth ( $\Gamma$ ) and intensity (normalized to measured without applied tension) for excitonic line (points - experimental data, lines - fit according to model described in the text) vs. applied electric field : (a) for sample  $A_{35}^{SSetch}$ , and (b) for sample  $A_{35}^{SSsurf}$ . (c) the scheme of QD potential illustrating the model parameters  $V_0$  and  $a$ .

to determine which mechanism is the most likely, we tried to fit with above formula the intensity variation for both samples (see Fig. 3.3). Assuming a constant dot height  $a = 6 \text{ nm}$ , we obtained similar values of barrier height and electron escape rate,  $V_d = 30 \text{ meV}; 25 \text{ meV}$ , and  $\tau_1 = 9 \text{ ps}; 14 \text{ ps}$  (at  $F = 0$ ) for the samples  $A_{35}^{SSetch}$  and  $A_{35}^{SSsurf}$ , respectively. These values strongly suggest that the mechanism competing with PL is the tunnel escape of photo-created electrons from an excited state. To bypass this effect strictly resonant excitation should be used to measure the FSS at higher applied field, which however is not easily achievable when measuring PL. Besides, this tunneling effect does not explain the strong broadening of the PL lines observed for the ground state. We infer from this calculation that the spectral diffusion of the lines due to charge fluctuation in the QD vicinity is very probably responsible for this broadening. This is also supported by the Gaussian lineshape observed in high field in contrast to a Lorentzian lineshape expected for a homogeneous lifetime reduction [98].

### 3.1.2 Fine structure splitting vs. in-plane field

Figure 3.4 presents the evolution of the FSS with the applied voltage for an individual QD. The electric field was applied parallel to one of the eigenaxes of the QD<sup>5</sup>. The large FSS of this QD allowed the direct observation of both linearly-polarized components with the analyzer at  $45^\circ$  to the eigenaxes (Fig. 3.4(a)). When applying the in-plane electric-field, both excitonic components have slightly different Stark shift (Fig. 3.4(b)) and the FSS is then strongly reduced from  $140 \mu eV$  to  $60 \mu eV$  (see Fig. 3.4(c)). Meanwhile, the average Stark shift of the lines is relatively small about  $120 \mu eV$ . Similar results are observed for a significant number of quantum dots. It is worth to note that the studies of similar QDs in vertical field-devices did not reveal comparable change of FSS (see next *Section* for details) up to a field limit of  $50 kV/cm$  for which the reported vertical Stark shift [32] reaches  $\sim 1 meV$ . We can thus conclude that the FSS is certainly reduced in the present case *thanks* to the partly recovered symmetry of the exciton wave-function.

Although the absolute value of FSS change amounts up to  $80 \mu eV$  in Fig. 3.4, in general the reduction of the splitting to zero is difficult to achieve. One of the reasons already mentioned is the loss of PL signal accompanied by a strong linewidth broadening when the field increases. The exciton degeneracy could be achieved only for some QDs with initial small FSS – typically below  $10 \mu eV$ . Such a case is presented in Figure 3.5. There is still a significant Gaussian broadening of the line because the required field is still relatively large. Clearly, the amplitude of FSS modulation by an electric field is not determined by the sole amplitude of electric field. It depends also on the initial anisotropy strength. Like for the QCSE, this could be the consequence of field-induced Coulomb corrections, but currently no self-consistent theory is available to confirm this interpretation<sup>6</sup>.

In this *Section*, we have shown that an in-plane electric field can effectively be used to modify the fine structure splitting of excitonic levels. Though not systematically successful, this technique appeared rather promising for the control of entanglement of photons emitted in the biexciton-exciton cascade. We will discuss in *Chapter 5* a supplementary investigation performed to better assess the relevance of this technique in an “entanglement-oriented” experiment.

---

<sup>5</sup>For InAs/GaAs QDs, in almost all studied cases the direction of the PL polarization of excitonic doublet corresponds to the main crystallographic directions  $[110]$  and  $[\bar{1}10]$ . For similar QD’s obtained under different growth conditions the eigenaxes orientation of dots with  $FSS < 30 \mu eV$  may become more random [89].

<sup>6</sup>In Ref. [71] a pronounced field-induced FSS is calculated for cylindrical QD in a model where Coulomb corrections are not taken into account.

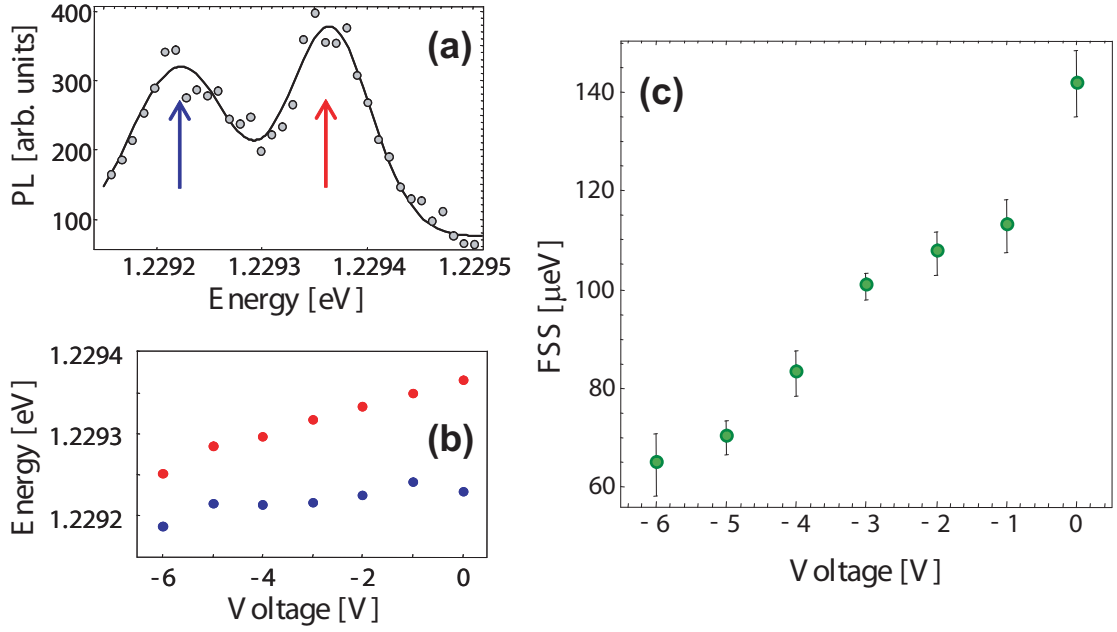


**Figure 3.4.** [Sample  $A_{35}^S$ ] (a) PL of excitonic line (polarization of detection  $45^\circ$ ) under zero bias. Blue and red arrows mark both linearly polarized components of the excitonic doublet. (b) Stark shift of two excitonic lines. (c) Fine structure splitting vs. applied voltage.

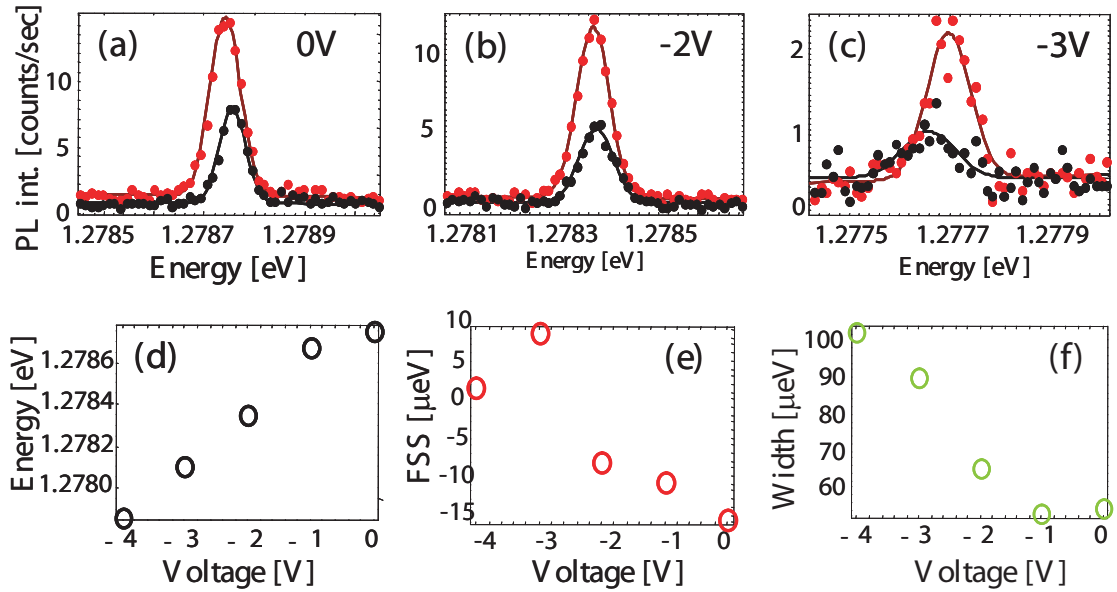


**Figure 3.5.** [Sample  $A_{35}^{Setch}$ ] (a),(b), and (c) – PL of exciton line under three different voltages : 0V, -2V, and -4V, respectively. Points – experimental data (red and black correspond to measured for two orthogonal linear polarizations), lines – Gaussian fits. (d) Stark shift of the studied line. (e) FSS vs. applied voltage. (f) Linewidth vs. applied voltage.



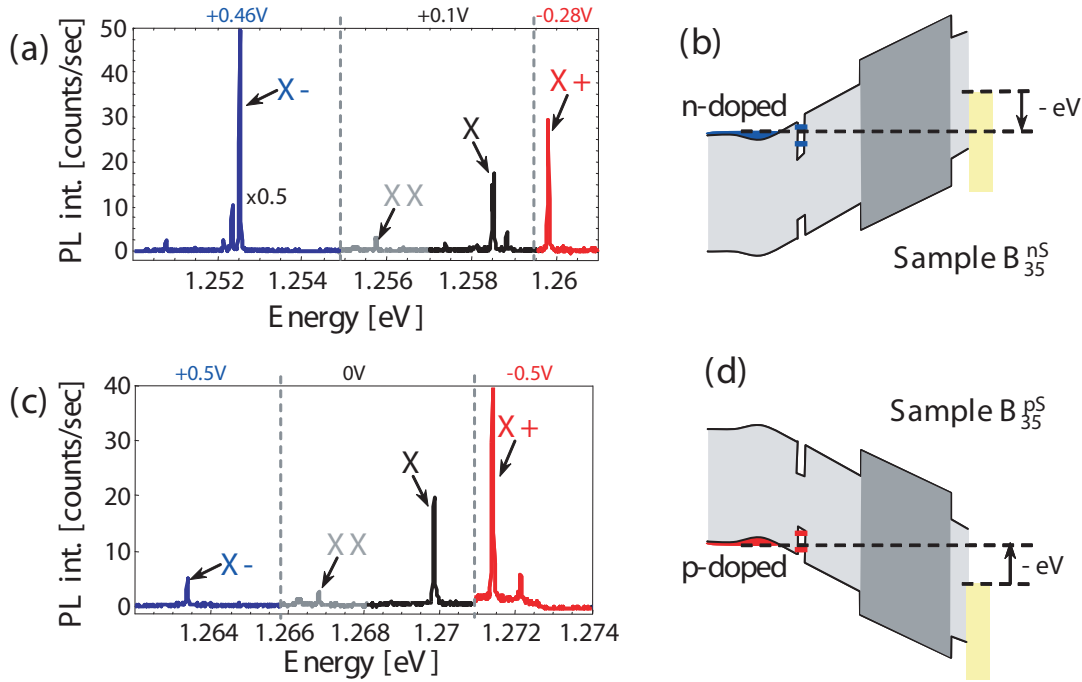


**Figure 3.6.** (a),(c) – spectra measured at three different voltages for n-doped sample  $B_{35}^{nS}$  (quasi-resonant  $1.34\text{eV}$  excitation) and p-doped sample  $B_{35}^{pS}$  (non-resonant  $1.425\text{eV}$  excitation), respectively. Strong positive voltage – blue part of the spectrum (significant intensity of X- line), zero voltage – gray and black part of the spectrum (neutral emission from X and XX), strongly negative voltage – red part of the spectrum (significant intensity of X+ line). For clarity the blue part of the spectrum in part (a) was scaled by the factor of 0.5. (b), (d) – corresponding band curvature for doped structures.

## 3.2 Vertical electric field

Vertical field-effect nanostructures have been widely developed in the last decade to provide charge tunability of individual nano-objects (see e.g. vertical gated QDs [99]). Since it was adopted for self-assembled QDs by B. T. Miller *et al.* [100], it opened a new opportunity to study in PL experiments charging process of individual QDs. Further investigations of such vertical field-effect devices [101, 85] have provided some rules to optimize the position of the QD layer to be embedded in the intrinsic region of the structure. The carriers fill a specific dot by tunnelling through the field-induced triangular barrier, whose length and height determine in cw experiments the population ratio between neutral and charged excitons [101, 85]. In principle the Coulomb blockade prevents the coexistence of different QD charge state, but under optical excitation which creates non-equilibrium carriers (e.g. one hole in the valence band of a n-Schottky structure) it modifies the effective barrier height controlling the QD charge state [84]. In PL experiments, lines corresponding to different charge states may coexist in contrast to resonant transmission experiments [57].

The general features of vertical field-effect structures are now well established and the performances of our samples turned out to be very similar to those fabri-

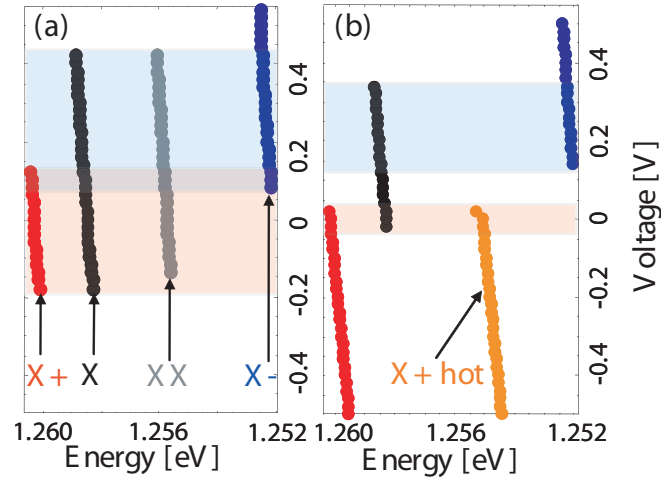


**Figure 3.7.** [Sample  $B_{35}^{nS}$ ] Stark shift of different excitonic complexes from a single QD under (a) non-resonant ( $1.42\text{eV}$ ) and (b) quasi-resonant ( $1.31\text{eV}$ ) excitation. Points – fitted energy position of the lines: X – exciton, XX – biexciton, X- – negatively charged exciton, X+ – positively charged exciton. The semitransparent areas correspond to the voltage ranges where exciton is observed simultaneously with X+ (red) and X- (blue). Note that for quasi resonant excitation an additional line was observed (its position marked with orange points), which appears exactly for the same voltage range as positive trion. Thus we assign it to hot X+.

cated in other groups. The applied electric field can be estimated quite precisely from the formula:  $F = -(V + V_S)/d$ , where  $V$  is the voltage applied between the Schottky gate and the back ohmic contact,  $V_S$  is the Schottky barrier height ( $\approx -0.8\text{V}$  for n-type,  $\approx +0.8\text{V}$  for p-type, see Ref. [86]) and  $d$  is the distance between the gates (175 nm). Contrary to previous *Section*, this nominal field agrees rather well with the quadratic evolution of the observed QCSE.

In each of the two samples investigated here (n-Schottky ( $B_{35}^{nS}$ ) and p-Schottky ( $B_{35}^{pS}$ )), we could analyze a series of well separated PL lines assigned to an exciton (X), a biexciton (XX), and charged excitons (X+ and X-) from the same quantum dot (see Fig.3.6). Since we cannot see all transitions for the same bias, like in the case of in-plane devices, the spectra in Figure 3.6 consist of three joined parts measured at different voltages. The dot charge state changes while sweeping the electric field. Let us explain it using n-Schottky structure as an example: (i) for strongly positive bias (large  $|-eV|$  value in Fig. 3.6 b) the dot is filled with electrons (from the back-gate) and X- line dominates the spectra, (ii) while decreasing the bias the neutral state of the dot becomes the most preferable (emission from X and XX appears), (iii) for strong negative bias an emission from X+ occurs <sup>7</sup>. Note

<sup>7</sup>Although the structure does not possess any hole-reservoir, with decreasing the voltage a small triangle quantum well is formed on the interface between the QD barrier and GaAlAs additional barrier. This quantum well captures holes, which can tunnel to the QD. We note that the photoluminescence from charged states is much stronger if the carriers tunnel from the back-contact (X- for n-Schottky structure and X+ for p-Schottky structure), see Fig. 3.6 (a) and (c).

that in Fig. 3.6(a,c) the energy separations between different exciton complexes do not correspond exactly to the real “binding” energies because the three displayed spectra are measured at different voltages: the corresponding QCSE yields typical spectral shifts of a few 100  $\mu\text{eV}$ 's.

Like for in-plane devices, the excitation energy plays an important role in the investigation of transitions from a single QD. The optical charging of the QDs or of its environment modifies the charging rules imposed by the tunnel coupling to the electron (or hole) reservoir. Evidently, this property depends on the parameters of the structure, in particular the barrier width between the dot layer and the doped layer. In our case this coupling can be considered rather weak and by changing excitation condition we were able to control the occupation of the reservoir and of the QD to select a specific exciton line. This is illustrated in Figure 3.7 which presents the Stark shift of different PL lines from the same QD for under non-resonant (a) or quasi-resonant (b) excitation. For negative voltage the strongest transition is related to the positively charged exciton (red points), for high positive tension – only emission from negatively charged exciton (blue points) is seen. The semitransparent red (blue) areas shadow the voltage ranges where X and X+ (X-) are simultaneously observed. For higher energy excitation the trion lines can be followed together with excitonic one for wide voltage range, while for intra-dot excitation we got a spectra evolution typical for charge tunable device – the QD state “switches” between neutral and charge state abruptly. In order to follow the exciton line on a large field range we thus privileged non resonant excitation.

### 3.2.1 Permanent vertical dipole

As it has been already discussed in *Chapter 1* a self-assembled QD made from III-V materials possesses strong vertical potential asymmetry. This results in a vertical static dipole  $p$  of the ground state of an electron-hole pair. We indeed observed a shift  $F_0$  (from  $F = 0$ ) of the maximum X transition energy deduced from the quadratic fit over the voltage range where X appears. For both structures we found a finite positive field  $F_0$  as shown in Fig. 3.8. This effect evidences the inverted carrier alignment in zero electric field (hole at the top, electron at the bottom of the dot) and thus indicates the asymmetry of the QD along the growth axis due to non-homogenous In content along the dot axis  $z$  [32]. Phenomenologically, the exciton energy Stark shift is well described by  $\Delta E_X = -\alpha(F - F_0)^2$  where  $F_0 = p/2\alpha$  reveals the permanent dipole of the electron-hole pair. The latter amounts to  $\sim 0.1\text{nm}\cdot\text{C}$  in the examined QD. It means that for  $F < F_0$  (n-Schottky sample) the hole ground state is localized above the electron ground state whereas it is localized below for  $F > F_0$  (p-Schottky sample). This X energy shift  $\Delta E_X$  actually includes both the single particle quantum confined Stark shift as well as the subsequent changes of electron-hole Coulomb interaction denoted  $J_{eh}$ . This is obviously a first order description since actually both effects must be treated simultaneously, e.g. in a configuration interaction approach.

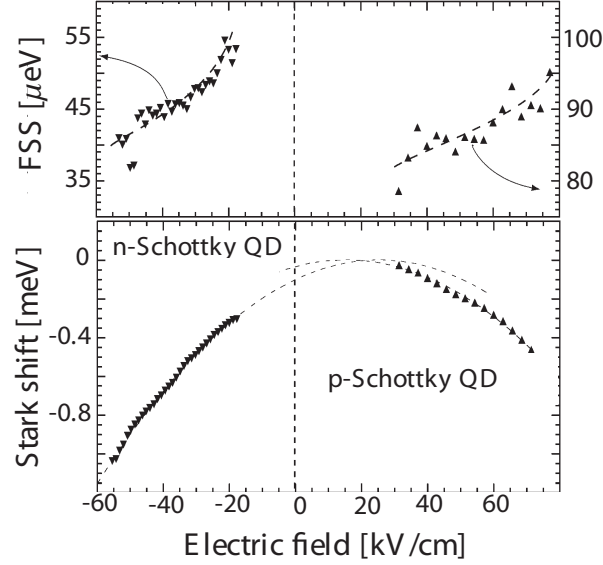


**Figure 3.8.** Exciton Stark-shift and FSS as a function of the vertical electric field for two quantum dots of n- or p-Schottky structure (samples:  $B_{35}^{nS}$  and  $B_{35}^{pS}$ ) as indicated.

### 3.2.2 Direct Coulomb integrals

The role of the Coulomb interaction in the QCSE of excitons can be further discussed by examining the evolution of the binding energies of  $X^+$ ,  $XX$ , and  $X^-$  with respect to  $X$ . To the zeroth order <sup>8</sup>, they read:

$$\begin{aligned}
 \Delta E_{X^+} &= E_{X^+} - E_X = J_{hh} - |J_{eh}| \\
 \Delta E_{X^-} &= E_{X^-} - E_X = J_{ee} - |J_{eh}| \\
 \Delta E_{XX} &= E_{XX} - E_X = J_{ee} + J_{hh} - 3|J_{eh}|
 \end{aligned} \tag{3.5}$$

Here,  $J_{ee(hh)}$  denotes the Coulomb interaction between two ground state electrons (holes). These expressions agree well with the observed energy sequence of  $X^-$ ,  $X$  and  $X^+$  since we can reasonably assume  $|J_{hh}| > |J_{eh}| > |J_{ee}|$  due to the stronger confinement of the heavy-hole ground state. The field-induced changes of trion binding energies should reflect the field-induced change of the Coulomb terms only (we neglect modification of single particle energies). As shown in Fig. 3.9 these binding energies show a monotonous dependence on electric field from  $-50 \text{ kV/cm}$  to  $80 \text{ kV/cm}$ , the main feature being a rather small relative variation ( $< 3\%$ ). This indicates that the Coulomb terms are weakly perturbed by the field. The monotonous dependence, decrease for  $J_{hh}$  (increase for  $J_{ee}$ ), is likely an other consequence of the QD vertical asymmetry. Assuming e.g. a pyramid-like shape allows indeed to explain this trend: when two identical carriers (hole or electron) are pushed by the field towards the narrow top of the QD they experience a stronger repulsion than when they are less confined in the bottom of the QD. As sketched in Fig. 3.9,

<sup>8</sup>Direct Coulomb term calculated for the single particle electron and hole wavefunctions in their ground state.

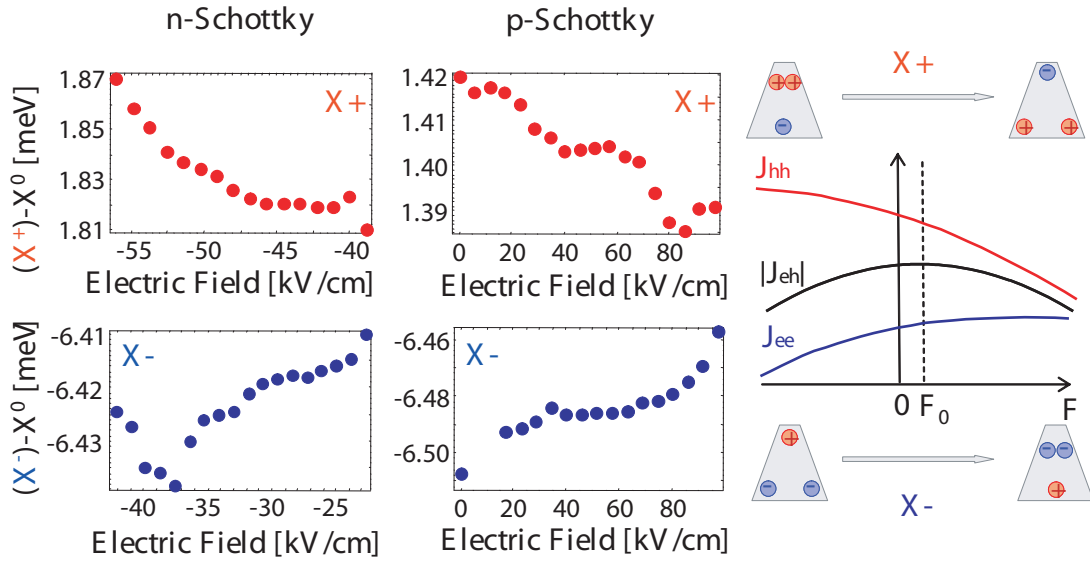


**Figure 3.9.** The measured binding energies of  $X^+$ ,  $X^-$  (relative to  $X$ ) in vertical n- and p-Schottky structures (samples:  $B_{35}^{nS}$  and  $B_{35}^{pS}$ ). On the right side – scheme of Coulomb integral variation against electric field assuming a stronger repulsion between identical carriers when they are in the top of the QD and a symmetrical electron-hole variation with respect to  $F_0$  (see text).

this leads to a monotonous dependence of the  $J_{ee(hh)}$  Coulomb terms, whereas  $J_{eh}$  has clearly a maximum when electron and hole are not separated, i.e. at  $F = F_0$ . This qualitatively explains the differences in trend for p-Schottky and n-Schottky devices (opposite field directions), and different behaviors for positively and negatively charged excitons as well. For n-Schottky diode the electron-hole overlap is further from the Stark shift maximum (assumed to be the maximum overlap because static dipole is zero), so that the permanent dipole is “bigger” and  $\Delta E_{X^+}$  varies more rapidly. For the  $X^-$  binding energy, we observed a decrease in n-Schottky sample, but an opposite trend in p-Schottky. As the behavior is the same as for  $X^+$ , this suggests that the  $J_{hh}$  integral dominates other Coulomb integrals introduced in Eq.’s 3.5. This set of equations can be used to fit the experimental data but the obtained values of Coulomb integrals (e.g.  $J_{ee} = 8.4 meV$ ) are much smaller than expected (18.9 meV in [101], 23 meV in [57]). The first order description of the binding energies is not sufficient to deduce quantitatively the contribution of the Coulomb terms in the effective QSCE.

Similar results of binding energy asymmetry for  $X^+$  in In-GaAs QDs have been reported in Ref. [94]. The authors attribute it to the difference of Stark shift maximum for excitonic complexes. In comparison with the results of Ref. [94] the values of relative binding energy changes presented in this *work* are much smaller, which is certainly due to differences in the shape and height of the QDs.

The results obtained on similar heterostructures by R. Seguin *et al.* [24] confirm the hypothesis that the gradient of In composition causes the strong vertical asymmetry of the QD. By following the Coulomb interactions for the same QD during the annealing procedure they found: (i) reduction of FSS for neutral exci-

ton, (ii) decrease of relative distance between trions and neutral exciton, (iii) the same trend for XX and X+ upon annealing.

### 3.2.3 Fine structure splitting vs. vertical field

We could follow simultaneously the FSS variation for the exciton and biexciton from the same QD over a wide voltage range. The results are shown in the upper part of Fig. 3.8. In this configuration, we should not expect a strong effect since the vertical field does not *a priori* change the QD in-plane anisotropy responsible for the FSS. Indeed, the bright exciton splitting is only weakly reduced by more than  $10 \mu\text{eV}$  for a Stark-shift of the order of  $1 \text{ meV}$  before the X emission vanishes due to the field-induced carrier escape. More surprising, the change is not symmetrical in field with respect to  $F_0$  when comparing both samples, although the isotropic electron-hole exchange is directly governed by the electron-hole overlap : in n-Schottky we observed a reduction of FSS as a function of the field, whereas for p-Schottky there is an increase. Again this asymmetry likely indicates that the anisotropy of the QD is not uniformly distributed along the growth axis. This conclusion is supported by the distribution of strain-induced piezo-electric potentials (see Fig. 1.3) which is currently considered as the leading source of anisotropy in InAs QDs [34]. When the electric field moves the single particles to the top and bottom of the QD, the effective potentials experienced by each of them acquires a clear in-plane anisotropy of  $C_{2v}$  symmetry.

Eventually, a vertical field manifests itself as a pure  $C_{2v}$  perturbation whose “sign” depends on the direction of the field. To some extent it appears thus as a natural means to possibly cancel the FSS. However, in practice we could not reach such a regime with the samples we have studied. For the data shown in Fig. 3.8, the required field for FSS cancelling (if we assume a linear dependence) would be very large (negative), and single carrier ionization takes place first. This method appears interesting only for QDs of small FSS (below  $10 \mu\text{eV}$ ). In such a case the better electrical quality of the samples brings a clear benefice.

## 3.3 Local electric field

In this *Section* we present the role of charge fluctuations in the vicinity of a quantum dot. We did not apply any macroscopic electric field, but we exploited time-dependent local electric fields, originating from charge state fluctuations of centers in the neighborhood of the quantum dot. This type of field induces sudden jumps of line position, which occurs more often for II-VI [102, 103] than for III-V [104] QDs. The results shown below were obtained on sample  $A_{26}$  containing CdTe quantum dots.

### 3.3.1 Transition identification

Before we focus on the influence of the local electric field on the fine structure let us first describe the **systematic method of identification of various emission**

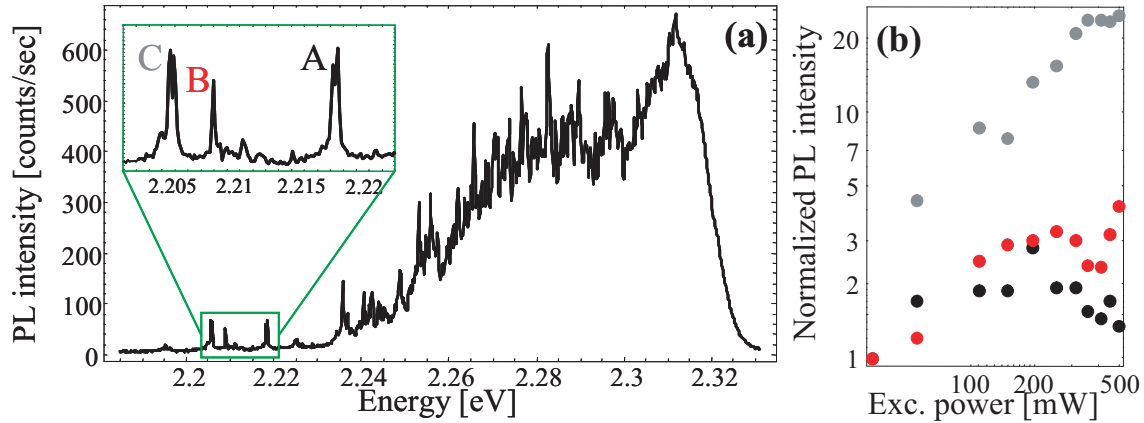


**Figure 3.10.** [Sample  $A_{26}$ ] (a)  $\mu$ -PL spectrum with a zoom of the low energy tail. Three labelled lines  $A$ ,  $B$ , and  $C$  are assigned to different excitonic complexes in the same QD. (b) Excitation power dependence of intensities for the lines  $A$ ,  $B$ , and  $C$ . The line intensities were normalized to that measured at lowest excitation power.

**lines originating from the same individual dot** [11]. It is necessary to know how to recognize different excitonic complexes in the sample which is not a charge tunable device and contains a high density of QDs. Although in the low energy tail of the QD inhomogeneous distribution a few lines can be spectrally isolated (see Fig. 3.10), we need to assign them confidently to different excitonic complexes from the same QD. Figure 3.10 shows the full spectrum with a zoom for the spectral region with individual QD lines we have focused on. The spectral positions of the three lines labelled  $A$ ,  $B$ , and  $C$  suggest their identification as exciton ( $X$ ), charged exciton ( $X^*$ ), and biexciton ( $XX$ ), respectively.

The above mentioned phenomena of synchronized spectral jumps evidence the same spatial origin of the lines. The temporal evolution of the spectrum is presented in Fig. 3.11. The discussion of the **time dependent Stark shift** should be started with a comment on the simultaneous observation of the neutral ( $A$  and  $B$ ) and charged ( $C$ ) excitonic transitions on the timescale of CCD accumulation (typically 1 s). This means that the charge state of the dot fluctuates between the neutral and charged states on a short timescale (compared to the CCD accumulation time), while the electric field fluctuations producing a significant spectral shift for all lines occur on a longer timescale. Thus the dot charge state evolution does not occur by exchanging a carrier with nearby centers responsible for the electric field fluctuations, and both effects turn out to be essentially uncorrelated. The three lines  $A$ ,  $B$ , and  $C$  change their energy position in a synchronized way, with energy shift in the same direction and of similar amplitude. It is important to note that not all of the lines changed their spectral positions during the measurement time. The local field changes only for some dots with a specific position in the host matrix (close to some charge traps).

The control of the local fluctuating field is rather limited, we tried to do it in two ways: by changing either the temperature, or the excitation power. At pumped helium temperatures the “jump effect” was rather rare, at timescale of several tens

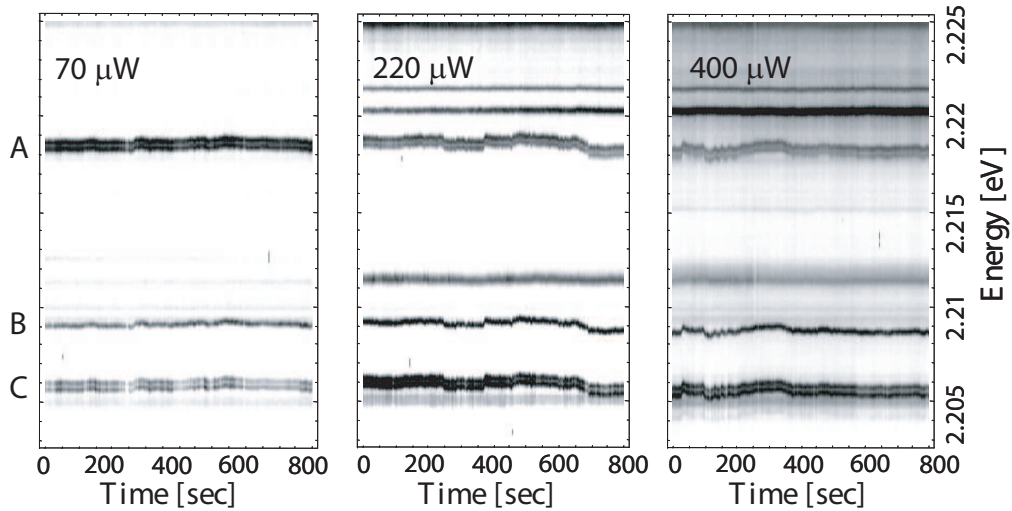


**Figure 3.11.** [Sample  $A_{26}$ ] Temporal evolution of the spectrum for three different excitation powers  $70 \mu\text{W}$ ,  $220 \mu\text{W}$ , and  $400 \mu\text{W}$ . The grayscale corresponds to PL intensity (white color – minimum of signal; black – maximum scaled as  $90 + 0.5 \cdot \text{power}$ ). Lines A, B, and C correspond to exciton, charged exciton, and biexciton, respectively.

of minutes. For the different temperatures tested, we observed that above  $10 \text{ K}$  the jump effect appears for more QDs and the timescale of the fluctuations is of the order of a few seconds. We decided to keep the temperature constant at  $20 \text{ K}$  and change the excitation power. As it is visible in Fig. 3.11 the fluctuations vary with the excitation power. With increased beam power the spectral jumps become bigger in amplitude and for the highest power used the typical time of jumps is comparable with the accumulation time. The studies of Stark effect caused by the local field do not allow us to distinguish between positively and negatively charged excitons. Besides the  $X^*$  an additional line appears close the biexcitonic transition. It corresponds to the second charged exciton of opposite sign. It is characterized usually by a weaker intensity. Taking into account possible binding energy relations we conclude that the main trion line is positively charged. According to our observations for II-VI samples the lines related with charge states never appear at higher energy than the excitonic line. It suggests that for these materials, contrary to III-V compounds (see previous *Section*), the Coulomb interaction between the holes is not a dominant term in binding energy. A second information supporting our identification comes from binding energies of complexes. The energy distances between the lines A, B, and C may suggest the above identification as done for a similar system by L. Besombes *et al.* [103]. Although from their identification one could conclude that the line  $X^*$  is most probably the  $X^+$  line (as also expected for an intentionally not doped structure, for which the most likely carrier source is the sample surface [77]), there are important evidences indicating that  $X^*$  is related with negatively charged QD state. The results obtained on sample  $A_{26}$  by J. Suffczyński *et al.* [105] show that the carrier remaining after  $X^+$  emission is an electron. Figure 3.12 contains the information about energy variation of studied excitonic complexes. The energy position of the trion and the biexciton lines, ob-



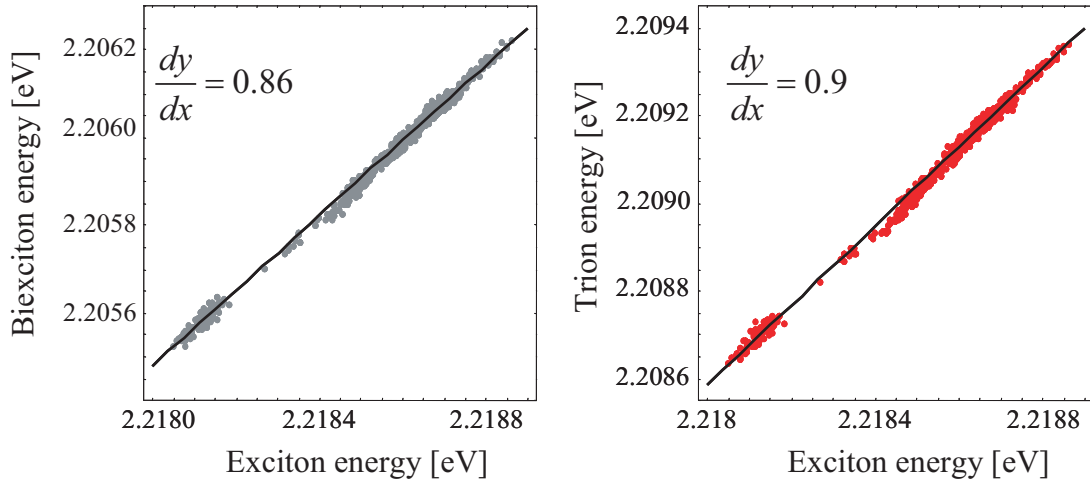


**Figure 3.12.** [Sample  $A_{26}$ ] Correlation between the energy positions of the biexciton and trion lines with neutral exciton.

tained from the spectra presented in Fig. 3.11 (measured at  $220\mu W$ ), was plotted as a function the neutral exciton energy. The perfect correlation confirms the same origin of the lines. Additionally it also shows the trend in binding energy changes. An analysis of the Stark shift indicates that the  $X^*$  and  $XX$  dissociation energies with respect to  $X$  state are lowered for both lines when the effective electric field experienced by the QD increases (see the coefficient of the linear fit are given in Fig. 3.12).

In order to check the biexcitonic character of the line  $C$  the spectra were measured as a function of the excitation power. The intensity of the line  $C$  increases superlinearly with the excitation power, while for  $A$  and  $B$  the behavior is approximately linear (see right panel of Fig. 3.10). As the biexciton creation requires two electron-hole pairs, the faster growth of  $C$  is thus a strong indication. At high excitation power the intensities of all transitions saturate. Theoretically, assuming weak excitation and purely radiative recombination, the increase of intensity with the number of photon flux should be quadratic for  $XX$  and linear for  $X$ . The relations observed in the experiment are weaker. The reason for that can be competition of other recombination mechanisms and/or excitation intensity not weak enough. This effect can be also seen on the grayscale in Fig. 3.11. The range of scale for the spectra measured at higher excitation power was scaled linearly with excitation power, but the linear scaling factor was chosen 0.7. At lower excitation power the QD neighborhood is "frozen" (no charge fluctuations) and other tests should be performed. Photoluminescence measurements in magnetic field gave us the possibility to obtain values of Zeeman splitting for individual quantum dots. Approximately the exciton effective Landé factors are the same for all transitions from the same QD <sup>9</sup>, which might be an additional proof for the same origin of the lines  $A$ ,  $B$ , and  $C$ . We have listed four verification points for the line iden-

<sup>9</sup>The determined values of the  $g$  factors for the sample  $A_{26}$  vary around  $-3.2$  with a scatter of about 18% [106], see next *Chapter 4*.

tification: synchronization in reaction to local field fluctuations, relative energy positions, excitation power dependence, and Zeeman splitting in magnetic field. A fifth point is provided by analyzing the fine structure. The charged exciton line  $B$  has no splitting [107], as expected for a trion ground state, since two particles are paired in a spin-singlet configuration. On the contrary, the lines  $A$  and  $C$  consist of two linearly polarized doublets (FSS for exciton and biexciton has the same value but opposite sign [108]). Here, the FSS is much larger than the individual linewidths, so both excitonic doublet components are clearly visible in the spectra even without polarization resolved techniques (see Fig. 3.10). We checked that the signs of FSS for  $X$  and  $XX$  are opposite and the value is approximately the same.

Eventually, let us mention that the definitive evidence for such line identification could have been achieved by measuring cross-correlation of photon counting. Such measurements were performed for sample  $A_{26}$  by J. Suffczyński *et al.* (see Ref. [54]) for another set of lines quite similar to  $A$ ,  $B$  and  $C$  and lead to the same conclusion.

### 3.3.2 Fine structure vs. local field

In the following we analyze in more detail the statistical set of measurements presented in Fig 3.11. The relative energy positions of  $X$ ,  $X^*$ , and  $XX$  were already discussed, so now we focus our attention on the relative intensities of the transitions. It can be expected that the local fluctuating potential controls (via charge trapping probability) the intensity of  $X^*$  relative to  $X$  and  $XX$  ones. The competition of the two charge states clearly manifests itself by the negative correlation between respective intensities shown in Fig. 3.13. The correlation arises not only for the relative intensities<sup>10</sup> of  $X^*$  and  $XX$  lines, but for the field magnitude as well. One can see that for the strongest field (lowest transition energy) the intensity of the charged exciton transition increases at the expense of the biexcitonic transition.

Let us now consider the relation between the local electric field and the FSS shown in Figure 3.14. This correlation is negative, i.e., an increase of the transition energy corresponds to a decrease of the FSS, in contrast with a positive correlation, observed in experiments on III-V QDs (see *Section 3.1.2*).

The experimental points in Fig. 3.14 form two distinct clouds. This suggests that two types of field fluctuations are present. One, caused by charging and discharging of the closest local center, produces electric field of a given amplitude and direction, to which correspond the jumps between the two clouds. A second type of fluctuations comes likely from charge state variations of several distant centers, giving rise to the broadening of both clouds. Assuming such a situation we can conclude that the observed correlation predominantly comes from the first type of fluctuations, i.e. from field variations oriented along a constant direction. Such a field has two effects relevant for the determination of the FSS: (i) it reduces the FSS by diminishing the electron-hole overlap, (ii) if applied along an appropriate direction it can increase the FSS by modifying the symmetry of the excitonic

<sup>10</sup>Relative intensity is defined here as normalized to the sum of  $X$ ,  $X^*$ , and  $XX$  intensities.

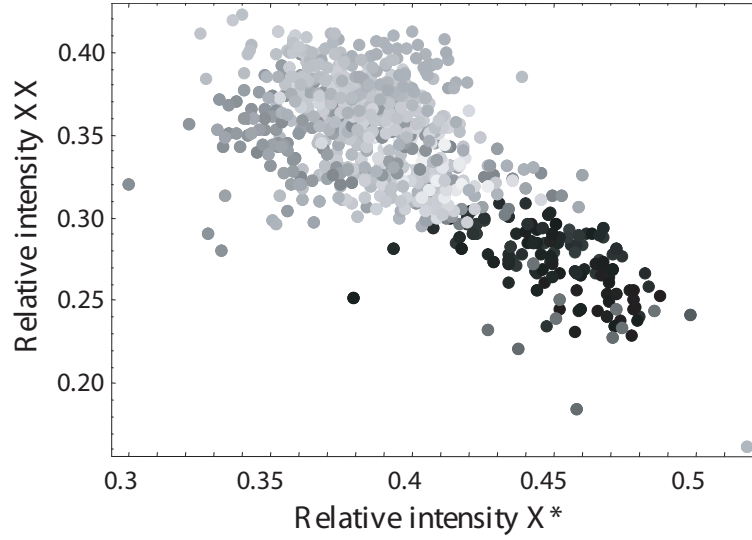


**Figure 3.13.** [Sample  $A_{26}$ ] Correlation between the intensities of the charged exciton and biexciton lines. Transition energy has been gray tone coded (dark points correspond to lower energy).

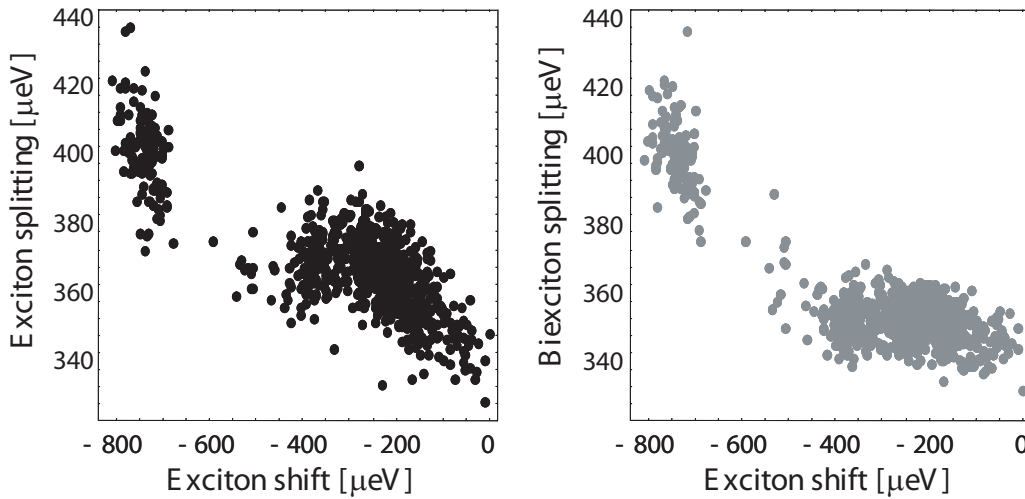


**Figure 3.14.** [Sample  $A_{26}$ ] Correlations between line position (Stark effect) and FSS for excitonic (left) and biexcitonic (right) lines.

wavefunction<sup>11</sup> [71]. The negative correlation of FSS indicates that in our case the second effect is dominant and gives rise to a stronger FSS when the electron and hole are better separated (strong Stark shift). Even if the net effect obtained here does not bring us closer to perfectly degenerate excitonic states, this result is still important because it represents an evidence for the symmetry modification mechanism of the FSS variation in electric field for CdTe/ZnTe quantum dots.

<sup>11</sup>Note that the native FSS (in absence of time-dependent fluctuations) may result from a native QD anisotropy plus a possible contribution due to some built-in electric field.

Strong modification of FSS in local fields supports the hope for bringing the FSS to zero by applying with electrodes an electric field in the appropriate direction. It shows the need for a technology development in II-VI materials, in order to produce field-effect structures, which in case of III-V materials guaranteed a control over FSS (see previous *Sections 3.1.2* and *3.2.3*).

The origin of local fields can be manifold. The features of such fields have some statistical characters, so that our interpretation of the data should be supported by a statistical test of validity. It was not discussed for the energy shift of the lines, because its relation with the Stark shift is obvious and confirmed by the perfect correlations between the energy positions of studied transitions (see Fig. 3.12). The variation of FSS as a function of the field (energy position) is not that clear, but the value of the correlation coefficient (*Corr*) coming out from the measurements turns out to be still very high ( $-0.8$ ), even when taking into account measurement errors <sup>12</sup>.

Local electric fields strongly influence the properties of the emission from a QD. This leads to the effects of (non-controlled) dot charging and modification of the exciton/biexciton FSS. These effects were rarely observed at liquid helium temperatures, at which most experiments were performed. However, the measurements with higher resolution, e.g. absorption, show that small spectral fluctuations exist even at low temperatures [58]. If the environment fluctuations influence significantly FSS of an exciton state, then even for an ideally symmetrical QD the entanglement in the biexciton-exciton cascade could be hindered.

### 3.4 Conclusion – FSS tuning

In conclusion, we have demonstrated the possibility of controlling the anisotropic exchange splitting in semiconductor quantum dots by using a small in-plane electric field. Although the absolute values of FSS changes amount up to several tens of  $\mu eV$ 's, the reduction of the splitting to zero was difficult to achieve, because of the following reasons: i) a strong reduction of luminescence intensity occurs due to the tunneling out of the carriers, ii) a strong broadening of the lines is caused by spectral wandering. The analysis of vertical dipole and binding energy changes of positively and negatively charged excitons shows in more detail the structure of carriers' alignment in the QD. Larger changes of bright exciton fine structure in the in-plane electric field compared to those observed for the vertical diode structures indicates the possible modification of excitonic wave-function symmetry, promising for future in-situ control of the photon entanglement. We have investigated additionally the influence of fluctuating electric field in the structure, which came from the charging of the traps in the QD vicinity. Such fluctuating field also induces Stark shift and changes in FSS up to several 10  $\mu eV$ 's. The reduction of

---

<sup>12</sup>Following definitions were used for correlation coefficient *Corr* between *X* and *Y* variables:  $Corr = cov(X, Y) / \sqrt{var(X) \cdot var(Y)}$ , where covariance:  $cov(X, Y) = MeanProduct(X, Y) - Mean(X) \cdot Mean(Y)$ , and variance:  $var(X) = MeanSquare(X) - Mean(X) \cdot Mean(X)$ . To include the measurement errors we used the *bootstrap method* [109].

these fluctuations is thus a prerequisite for achieving the entangled photon pairs, even though it proves that controlling the electric field works as well in CdTe/ZnTe quantum dots for a FSS control.

**SUMMARY.** *Chapter 3* presents the studies of the influence of electric field on the photoluminescence from individual quantum dots. Both field configurations, in-plane and perpendicular, are discussed. The results demonstrate the possibility of controlling FSS using a small in-plane electric field. The FSS can be tuned over a large range and in some cases through zero. From studies in charge tunable devices with vertical field configuration we obtain information about alignment of an electron and a hole inside a dot. The small change of FSS is also achieved in this geometry, which reveals the role of the vertical QD asymmetry on the FSS strength. Finally, the study of random line jumps in PL spectra of a single CdTe/ZnTe QDs reveals important field-induced reduction of the FSS.

---

---

## CHAPTER 4

---

# Influence of magnetic field on exciton fine structure

### Contents

---

<b>4.1</b>	<b>Exciton Zeeman Hamiltonian</b>	<b>67</b>
<b>4.2</b>	<b>Faraday configuration</b>	<b>68</b>
<b>4.3</b>	<b>Voigt configuration</b>	<b>71</b>
4.3.1	Theoretical model	72
4.3.2	Isotropic hole $g$ factor ( $\beta = 0$ )	74
4.3.3	Anisotropic $g$ factor ( $\beta \neq 0$ )	76
<b>4.4</b>	<b>Experimental results</b>	<b>79</b>
<b>4.5</b>	<b>Orbital effects</b>	<b>81</b>
<b>4.6</b>	<b>Conclusions - FSS manipulation</b>	<b>84</b>
<b>4.7</b>	<b>Nuclear field</b>	<b>85</b>

---

*“It doesn’t matter how beautiful your theory is, it doesn’t matter how smart you are. If it doesn’t agree with experiment, it’s wrong.”*

Richard P. Feynman

SEVERAL INTERESTING PHENOMENA regarding exciton FSS in quantum dots occur in the presence of an external magnetic field. Indeed, the latter influences efficiently the spin-degeneracy of the excitonic levels thanks to the Zeeman effect with a typical sensitivity given by the Bohr magneton  $\mu_B = 58 \mu\text{eV/T}$ . Even though the QD anisotropy is not really reduced, this may provide a mean to achieve an “accidental” exciton degeneracy, as demonstrated in 2006 by R. M. Stevenson *et al.* [55]. However, since this effect relies on the coupling between bright and dark excitons in a transverse magnetic field, it changes the branching ratio between the two paths of the biexciton cascade (see *Chapter 1*) and opens new recombination channels. Therefore this method brings in intrinsic drawbacks preventing

the generation of maximally entangled 2-photon states. Regarding symmetries, the magnetic field breaks the time inversion invariance of the Schrödinger equation. In Faraday configuration the angular momentum projection along the magnetic field direction is still a good quantum number, but the corresponding eigenstates become split. For the exciton this could be seen as the restoration of cylindrical symmetry, since the anisotropic exchange then manifests itself as a coupling between non-degenerate states. For a field applied along the QD growth axis such that  $\Delta E_{Zeeman} \gg \delta_1$ , this gives rise to the restoration of purely circularly polarized lines. Nevertheless, we still end up with only *classical* polarization correlations (in  $\sigma^+/\sigma^-$  basis) for photons emitted in biexciton cascade. Obviously, the degeneracy of the bright exciton doublet is still lifted (actually increased) by the magnetic field, and the cylindrical symmetry is not restored at all <sup>1</sup>. In fact, only a shrewd combination of the exchange and magnetic interactions is susceptible to lead to exact exciton degeneracy, as it will be shown in this *Chapter*. In particular the discussion will bring up the issue of hole Landé factor in a magnetic field perpendicular to the growth axis. If weak, it will affect the FSS only for large magnetic fields above a few Tesla's, so that the second order orbital effect produced by the magnetic field (or diamagnetic effect) should be treated on an equal footing. The latter, which amounts to an anisotropic harmonic potential may intervene as well to modify straightforwardly the FSS.

Another origin of exciton spin-splitting similar to a magnetic-field can occur under certain conditions of strong optical excitation because of the hyperfine interaction between optically oriented electrons and QD nuclei. When optically polarized, the nuclear spins generate a static magnetic-like field producing the electron spin splitting named Overhauser shift <sup>2</sup> which can reach a few tens of  $\mu eV$ . Such effects can play an important role for III-V materials (with large magnetic moments of the host material nuclei), but for CdTe/ZnTe QDs they should remain negligible.

*Chapter 4* is organized in the following way. In the main part we review the influence of the Zeeman effect produced by an external magnetic field on the properties of QDs emission. Two experimental configurations are considered: parallel (Faraday configuration) and perpendicular (Voigt configuration) to the growth direction. Each of them starts with a theoretical background, useful to see what kind of phenomena occur depending on QD parameters and magnetic field direction. Then, looking at the experimental data one can judge which approximations are appropriate to fit our observations. As it will be shown, the theoretical model provides criteria to determine if for a given QD system the FSS can be cancelled or not. The presented model used for comparison with experiments involves primarily the Zeeman interaction of excitonic states. The orbital effects are discussed at the end of the *Sections* devoted to the measurements in Voigt geometry with the analytical approach developed by M. Glazov and E. L. Ivchenko. Most of this *Chapter* spans over possible field configurations (longitudinal and transverse) and

---

<sup>1</sup>What happens is that the spatial symmetry reduction becomes to some extent “negligible” as compared to the time inversion symmetry breaking. But the latter is also a problema for photon entanglement.

<sup>2</sup>This was originally observed as a frequency *shift* of the electron spin resonance.

interactions (Zeeman, diamagnetic shift) in QDs induced only by an external magnetic field. Since the experiments were performed on CdTe/ZnTe QDs, we ignored possible nuclear effective magnetic fields in the discussion.

At the end of this *Chapter* the role of the dynamic nuclear polarization for InAs/GaAs QDs in vertical diodes will be shortly presented. The Overhauser effect measurements are the continuation of studies from *Chapter 3*. Their presentation points out to the importance of excitation conditions when measuring polarization correlations as done in *Chapter 5*.

## 4.1 Exciton Zeeman Hamiltonian

Similarly to the previously described electric field effects, the orientation of the magnetic field with respect to the investigated nanostructures plays a crucial role in symmetry considerations. Indeed, in flat biaxially strained QD's the ground state hole is basically a pure heavy-hole and therefore its response to a magnetic field is strongly anisotropic. This clearly appears when we consider the expression of the Zeeman Hamiltonian for bulk excitons (see H. W. van Kesteren *et al.* [110]):

$$\hat{H}_{Zeeman} = \mu_B \sum_{i=x,y,z} (g_e \hat{S}_i B_i - 2(\kappa \hat{J}_i B_i + q \hat{J}_i^3 B_i)) \quad (4.1)$$

where  $g_e$  is the electron Landé factor,  $q, \kappa$  are Luttinger coefficients and the  $\hat{J}_i$ 's are the angular momentum projections of the Bloch states in the  $\Gamma_8$  hole band along the crystallographic axes  $\langle 100 \rangle$ . Usually, the main term driving the hole Zeeman splitting is the linear term  $-2\mu_B \kappa \hat{\mathbf{J}} \cdot \mathbf{B}$  while the cubic term in Eq. 4.1 is considered as negligible. Since the in-plane operators  $\hat{J}_x$  and  $\hat{J}_y$  couple hole states which differ by  $|\Delta J|=1$ , an in-plane magnetic field has no direct first order effect on the ground state heavy hole, in contrast to a longitudinal field. When including in a perturbative approach the light-hole states this term contributes to the in-plane  $g$  factor at the third order only, and would be quite small because the heavy- to light-hole splitting  $\Delta_{h-l}$  is of the order of a few tens of  $10 \text{ meV}$ . Without any additional hypothesis the effective in-plane hole  $g$  factor would remain very small, which is actually not observed in experiments. Therefore we have taken into account the effect of the QD anisotropy on the valence band mixing by introducing in the hole Hamiltonian a perturbation of  $C_{2v}$  symmetry as we did in *Chapter 1* for the electron-hole pair. This term is proportional to the symmetrized product of the in-plane angular momentum components  $\{\hat{J}_{x'} \hat{J}_{y'}\}$  [38, 111] where the indexes  $x', y'$  denote axes which are rotated by  $\pi/4$  with respect to the mirror planes of the  $C_{2v}$  symmetry (the QD eigenaxes). This term introduces a direct coupling from  $J_z = \pm 3/2$  heavy-hole states to  $J_z = \mp 1/2$  light-hole states respectively. After a  $-\pi/4$  rotation to use the same referential axes as for exchange Hamiltonian (Eq. 1.4), we obtain the following Hamiltonian for the heavy-hole to light-hole



coupling:

$$\hat{H}_{C_{2v}} = \beta \left( \hat{J}_x^2 - \hat{J}_y^2 \right) \quad (4.2)$$

where  $\beta$  represents the strength of the coupling. In the above formalism the respective signs of  $\delta_1$  and  $\beta$  are not correlated although they are necessarily determined by the features of a given QD. We will see further that this sign correlation is of major importance for the control of the FSS and enlightens the concept of “inverted” FSS introduced in Ref. [6]. Actually, the coupling described by  $\hat{H}_{C_{2v}}$  contributes to the FSS through the short-range electron-hole exchange  $-\frac{4}{3}\delta_0\hat{\sigma}^e \cdot \hat{\mathbf{J}}$ , by an amount equal to  $2\beta\delta_0/\Delta_{h-l}^2$ . However, since the dominant contribution in  $\delta_1$  originates from the long-range part of the electron-hole exchange (see *Chapter 1*), this does not permit to establish the sign correlation with  $\beta$ . Experimentally the perturbation  $\hat{H}_{C_{2v}}$  leads also to dichroism of the ground state excitonic transition as reported in the past for quantum wells of  $C_{2v}$  symmetry [111] and more recently for trions in CdSe QDs [112]. It is worth mentioning that in InAs QD’s similar dichroism has been reported, but no correlation was found between the sign of the linear polarization degree (related to  $\beta$ ) and the sign of  $\delta_1$  [113].

## 4.2 Faraday configuration

In Faraday configuration the Zeeman Hamiltonian (Eq. 4.1) has a diagonal form. The eigenvalues of pure heavy-hole excitons submitted to exchange interaction (Eq. 1.4) read:

$$\begin{aligned} E_1(B_z) &= \frac{1}{2}\delta_0 + \frac{1}{2}\sqrt{\delta_1^2 + \mu_B^2(g_e + g_{h,z})^2 B_z^2} \\ E_2(B_z) &= \frac{1}{2}\delta_0 - \frac{1}{2}\sqrt{\delta_1^2 + \mu_B^2(g_e + g_{h,z})^2 B_z^2} \\ E_3(B_z) &= -\frac{1}{2}\delta_0 + \frac{1}{2}\sqrt{\delta_2^2 + \mu_B^2(g_e - g_{h,z})^2 B_z^2} \\ E_4(B_z) &= -\frac{1}{2}\delta_0 - \frac{1}{2}\sqrt{\delta_2^2 + \mu_B^2(g_e - g_{h,z})^2 B_z^2} \end{aligned} \quad (4.3)$$

where we have introduced the effective hole  $g$  factor  $g_{h,z} = 6\kappa$  obtained when the cubic in  $J$  term is neglected. No mixing between states with different absolute values of angular momentum occurs (between bright  $M = \pm 1$  and dark  $M = \pm 2$  states). The first two levels correspond to the bright states. The typical field-induced shift is shown in Fig. 4.1 (a). It is mostly linear except in the narrow field range where  $\delta_1$  dominates over the Zeeman splitting  $(g_e + g_{h,z})\mu_B B_z$ .

Figure 4.1(b) shows on a color scale PL spectra of a single QD in longitudinal magnetic field carried out in the range from  $-7$  to  $+7$  T. The detection was  $\sigma^+$  so that a single component of the bright doublet is visible. For this particular QD, the zero field FSS is not observed in such circularly-polarized plot because it was

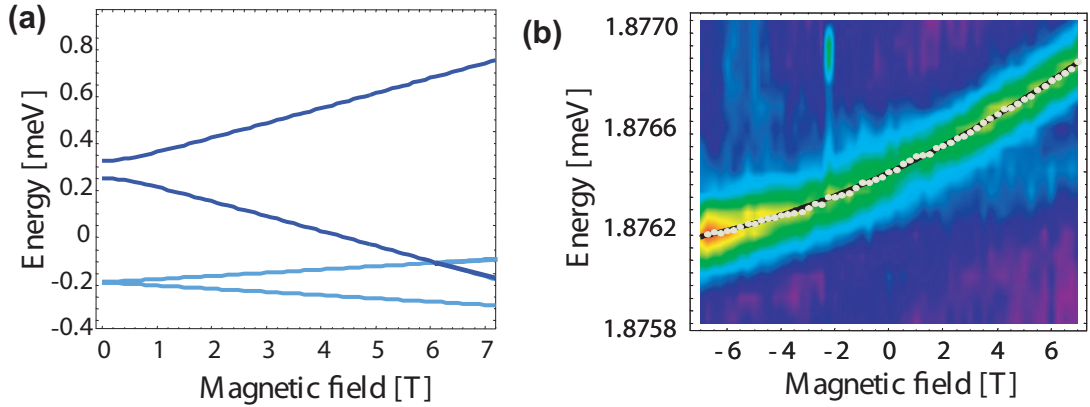


**Figure 4.1.** (a) Calculated evolution of heavy-hole excitonic levels as a function of magnetic field (relative energy scale), following parameters were used  $\delta_0 = 0.40$  meV,  $\delta_1 = 0.074$  meV,  $\delta_2 = 0.001$  meV,  $g_{eff.} = 1.71$ . Two upper levels (dark blue) correspond to the bright states and two lower levels (bright blue) to the dark states. (b) [Sample  $B_{26}$ ] Measured spectra in magnetic field, colors correspond to the PL intensity. White points – energy position of the excitonic line from Gaussian fit, black curve – quadratic polynomial fit of the energy position vs. magnetic field.

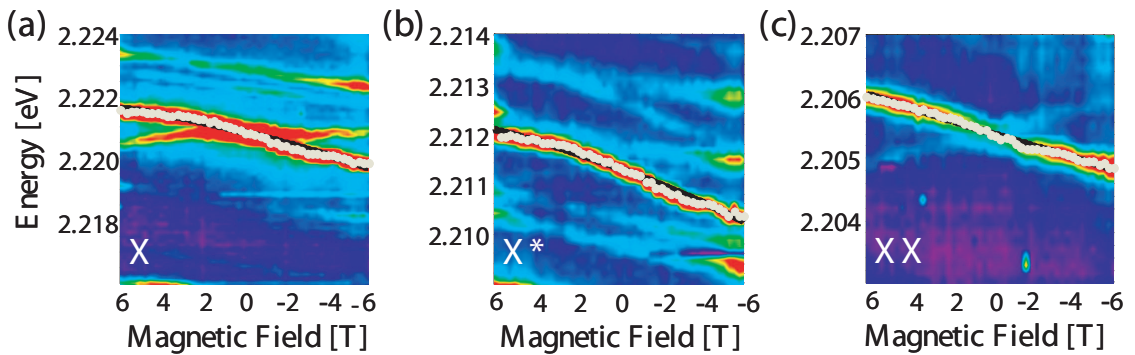


**Figure 4.2.** [Sample  $A_{26}$ ] Evolution of measured spectra in magnetic field (colors correspond to the PL intensity) for three different transitions from the same QD (see Section 3.3 in Chapter 3). White points – energy position of the excitonic line from Gaussian fit, black curve – quadratic polynomial fit of the energy position vs. magnetic field. (a) – exciton, (b) – charged exciton, and (c) – biexciton.

below our spectral resolution. In addition, if the QD symmetry is not completely broken (i.e. still close to  $C_{2v}$ ), the dark states are absent from the spectra<sup>3</sup>, then in Faraday configuration the electron and hole  $g$  factors cannot be measured separately (only the information about the sum of the  $g$  factors is accessible). Hence for longitudinal magnetic field the determination of both electron and hole  $g$  factors is possible only if the dark states appear. This can be achieved experimentally by tilting the field direction from Faraday to Voigt configuration (see e.g. Ref. [115]).

<sup>3</sup>It was shown by M. Bayer *et al.* [114], that the presence of dark states in zero magnetic field arises from a “complete” symmetry breaking.

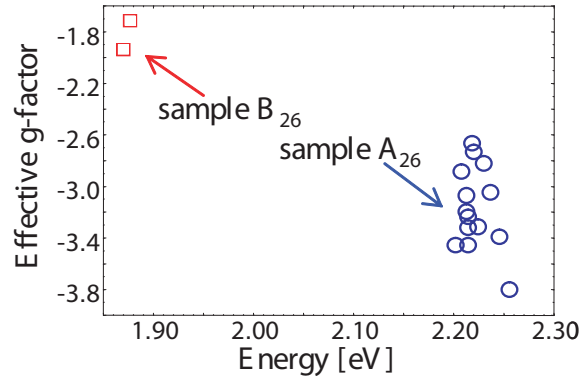


**Figure 4.3.** Effective  $g$  factors vs. transition energy for samples:  $A_{26}$  – blue circles and  $B_{26}$  – red squares.

Our experiments give us only the effective exciton Landé factor values  $g_{eff}$ , corresponding to the linear shift. A small quadratic dispersion is also visible (solid line fit in Fig. 4.1(b)). This results from the diamagnetic shift  $\propto B_z^2$  produced by the second order perturbation of the magnetic field on the electron and hole orbitals.

For sample  $A_{26}$  we performed a statistical study of the effective  $g$  factors by analyzing a few exciton lines from different QDs. The mean value amounts to  $-3.2$  with a standard deviation of about 18% [106]. We did not find any correlation between  $g$  factor and other QD parameters (like energy position – see Fig. 4.3, fine structure [106]). However in sample  $A_{26}$ , we found it systematically greater (in absolute value) than in sample  $B_{26}$  ( $g$  factors around  $-2$ ) and than CdTe/ZnTe self-assembled QDs grown in Stransky-Krastanov mode [116]. We remind that both samples differ strongly in growth method: QDs in sample  $A_{26}$  are fluctuation-type, whereas sample  $B_{26}$  contains QDs produced by amorphous Tellurium desorption [82].

Figure 4.2 displays the zoom of the three PL lines identified as X, X\*, and XX in Section 3.3. In this case the detection was set to  $\sigma^-$  so that the main lines have a negative slope as compared to Fig. 4.1(b). For X\*, there is still a single line originating from the zero field region, while for X and XX, we clearly see a second line with opposite slope which progressively vanishes when the field increases. This is the second bright exciton component linearly polarized in zero field and which is converted to a  $\sigma^+$  line by the field. There is a clear deviation from the expected symmetry  $(B_z, \sigma^+) \rightarrow (-B_z, \sigma^-)$  that we ascribe to slow drift of the set-up when measuring from  $-7 T$  to  $+7 T$ .

The difference of PL intensity for a given line between positive and negative magnetic field brings interesting information on the exciton spin lifetime. Under non-resonant excitation, the degree of circular polarization due to spin relaxation on the low energy bright state reads  $\tanh(g_{eff}\mu_B B_z/2k_B T)\tau_r/(\tau_r + \tau_s)$  where  $\tau_{r(s)}$  is the radiative (spin) lifetime of the exciton. The absence of significant circular polarization in Fig.'s 4.1 and 4.2 indicates that the exciton spin lifetime is very long as compared to the radiative lifetime. Similar results regarding the spin memory of a single resident carrier have been obtained recently by J. Suffczyński *et al.* [117]

in cross-correlation measurements between neutral and charged excitons, with a typical timescale  $\gg 10$  ns.

As briefly discussed above, the linearly polarized excitonic doublet is converted by the field into a circularly polarized one : both branches of the bright states get fully circularly polarized. It turns out that in strong magnetic field pairs of photons emitted in the  $XX-X$  cascade become correlated in orthogonal circular polarizations. From diagonalization of exchange plus Zeeman Hamiltonians the field dependent exciton eigenvectors take the following form:

$$\begin{aligned} |X_x\rangle &= \cos \lambda | + 1 \rangle + \sin \lambda | - 1 \rangle; \\ |X_y\rangle &= \cos \lambda | - 1 \rangle - \sin \lambda | + 1 \rangle; \end{aligned} \quad (4.4)$$

where the angle  $\lambda$  describes the mixing between exciton spin states  $| + 1 \rangle$  and  $| - 1 \rangle$  emitting respectively  $\sigma^+$  or  $\sigma^-$  photons. It depends on the magnetic field as follows:

$$\tan 2\lambda = \frac{\delta_1}{(g_e + 3g_{h,z})\mu_B B_z} \quad (4.5)$$

The recombination of excitons described by Eq. 4.5 leads to elliptically polarized emission, which can be characterized by circular polarization degree  $P_{circ} = \cos 2\lambda$  and/or linear polarization degree  $P_{lin} = \sin 2\lambda$ . The plot in Fig. 4.4 represents the calculation of the degree of linear polarization as a function of applied magnetic field. The experimental points were obtained for excitonic line shown in Fig. 4.1(b). Equation 4.5 shows in a simple way how magnetic field converts the exciton basis. Without magnetic field  $\tan 2\lambda = \infty$  and the exciton has equal admixture of both spin states. If Zeeman energy dominates over exchange splitting ( $(g_e + 3g_{h,z})\mu_B B_z \gg \delta_1$ ) then  $\tan 2\lambda \rightarrow 0$ , so that both excitonic components become pure spin states. In Faraday configuration strong field enables to obtain two excitonic states:  $| + 1 \rangle$  and  $| - 1 \rangle$ , however they are still separated by Zeeman interaction and this configuration is not suitable for photon entanglement.

The experiments presented here in longitudinal magnetic field configuration allowed us to determine the effective Landé factors characteristic for the studied samples  $A_{26}$  and  $B_{26}$ . The bright exciton levels are shifted very efficiently by the field but their initial splitting can only be increased, which makes the restoration of circularly polarized states of rather weak interest for the photon entanglement in biexciton cascade. In the next *Section*, we will see that the in-plane field configuration offers a more suitable configuration.

### 4.3 Voigt configuration

The in-plane configuration of magnetic field seems to be more suitable to achieve the degeneracy of the bright excitons. Experimentally the modification of

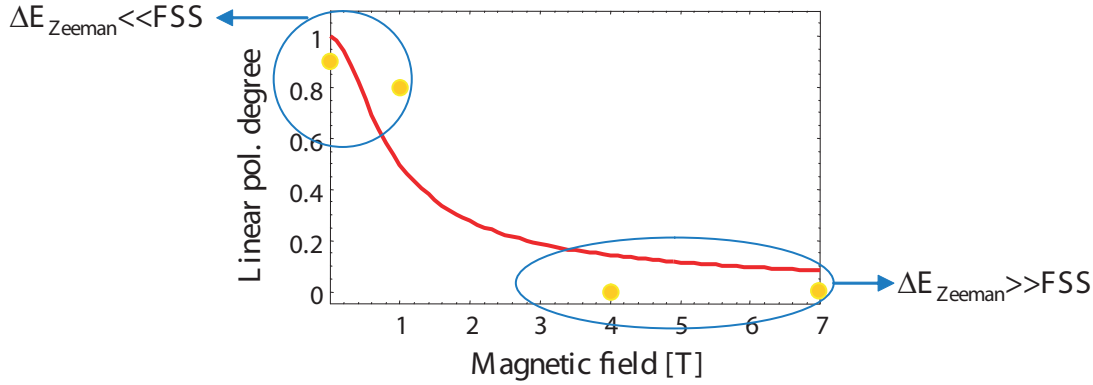


**Figure 4.4.** [Sample  $B_{26}$ ] Linear polarization degree vs. magnetic field (model parameters as in Fig. 4.1(a)). Red curve represent theoretical calculation, yellow points - experimental data for quantum dots presented in Fig. 4.1. Two blue circles mark the two field ranges: small field ( $FSS \gg$  Zeeman splitting) – high linear polarization degree, strong field ( $FSS \ll$  Zeeman splitting) – high circular polarization degree.

FSS induced by the field has been observed in different III-V heterostructures (see Refs. [114, 6, 118]). The successful restoring of exciton degeneracy was confirmed by entanglement measurements by R. M. Stevenson *et al.* [55]. These experimental data clearly evidence the influence of in-plane magnetic field on FSS, however the explanations in literature were limited to some crude approximations. The entire description involves three objects: the host crystal, the quantum dot potential and the in-plane field. Using the electric field as a perturbation (in *Chapter 3*) we stressed the role of the perturbation symmetry. The in-plane orientation of the electric field fully determined the contribution to the FSS. Analogically the angle between the QD eigenaxes and the in-plane magnetic field should play an important role. Yet for magnetic field one has to take into account additionally the QD orientation with respect to the crystal lattice due to the form of the Zeeman spin Hamiltonian for holes (Eq. 4.1). It is important to determine how both effects interplay for a given field orientation. A comprehensive illustration of the influence of in-plane magnetic field on the photoluminescence can be found in the literature for 2D low-dimensional structures like quantum wells (see e.g. [119]). For QDs usually two utmost approaches were used: the Zeeman Hamiltonian for holes was limited either to the linear in  $J$  term with some heavy- to light-hole coupling (approximation proposed by A. V. Koudinov *et al.* [112]) or to the cubic in  $J$  term (approximation proposed by R. M. Stevenson *et al.* [6] after M. Bayer *et al.* [114]). In order to better understand the experimental results both terms in the Zeeman Hamiltonian are considered in our approach.

### 4.3.1 Theoretical model

For taking into account both  $\hat{H}_{Zeeman}$  and  $\hat{H}_{C_{2v}}$  we have to introduce the angle  $\phi$  between the QD eigenaxis  $x$  and the crystallographic direction [100] in order to rotate the cubic term of  $\hat{H}_{Zeeman}$  in the QD coordinate frame (see Fig. 4.5).

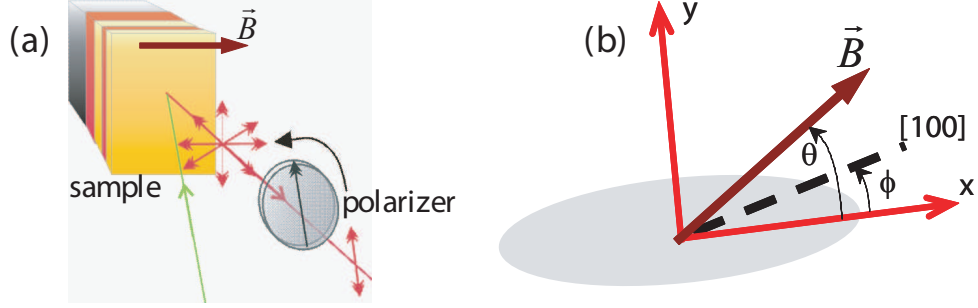


**Figure 4.5.** (a) Scheme of experimental configuration in Voigt experiment. External magnetic field was applied along one of the main crystallographic axis of the sample. A linear polarizer was rotated in the photoluminescence beam. (b) Scheme introducing two angles in the theoretical model. The angle  $\phi$  between QD eigenaxis  $x$  (marked with red arrows) and  $[100]$  crystal axis (dashed line). The angle  $\theta$  between QD eigenaxis  $x$  and field direction (brown arrow). Gray shaded area represents a QD elongated along its eigenaxis  $x$ .

In this way, we obtain the effective Zeeman Hamiltonian to the first order in  $\beta/\Delta_{h-l}$  and in the basis of electron spin and hole pseudo-spin:

$$\hat{H}_Z(\mathbf{B}_\perp) = \frac{1}{2}\mu_B \left( \sum_i g_e \hat{\sigma}_i^e B_i + \sum_{i,j} \hat{\sigma}_i^h g_{h,ij} B_j \right) \quad (4.6)$$

with the hole  $g$  factor tensor:

$$g_h = 3q \begin{pmatrix} \cos 4\phi + \rho_g & \sin 4\phi \\ -\sin 4\phi & \cos 4\phi - \rho_g \end{pmatrix} \quad (4.7)$$

where  $\rho_g = \frac{(4\kappa + 7q)\beta}{q\Delta_{h-l}}$

As it could be expected, the transverse hole  $g$  factor becomes anisotropic due to the term  $\rho_g \propto \beta$ . This was already emphasized in Ref. [112]. Of course, the parameters  $g_e$ ,  $\kappa$  and  $q$  in Eqs. 4.6, 4.7 are not the *bulk* parameters of InAs (or GaAs): in QDs the strong confinement of eigenstates considerably affects the values of these parameters as predicted [120, 121] and experimentally observed [114]. In particular the mixing allowed in  $D_{2d}$  symmetry between heavy-hole and light-hole with *envelope* wave functions of different angular momentum may explain the significant value often reported for the transverse hole  $g$  factor<sup>4</sup>. In the

<sup>4</sup>For a quantum dot with  $D_{2d}$  symmetry, the projection of the total angular momentum  $\hat{M}_z = \hat{L}_z^{envelope} + \hat{J}_z$  is a good quantum number and the hole ground states correspond to  $M_z = \pm 3/2$ . Yet, due to the coupling of heavy-hole to light-hole induced at  $\mathbf{k}_\perp \neq 0$  by a term  $\propto \hat{p}_z^2(\hat{p}_x \pm i\hat{p}_y)$  in the  $\Gamma_8$  Luttinger Hamiltonian, the QD eigenstates are not eigenstates of  $\hat{J}_z$ .

following we assume first a symmetric transverse  $g$  factor for the hole ( $\beta=0$ ) and then discuss the effect produced by the hole mixing ( $\beta \neq 0$ ) responsible for the antisymmetric part of  $g_h$ .

### 4.3.2 Isotropic hole $g$ factor ( $\beta = 0$ )

Let us first discuss the evolution of exciton energy levels as a function of the field. The eigensystem (eigenvalues and eigenvectors) can be obtained analytically only for 2 specific field orientations with respect to the QD eigenaxis, namely for  $\theta - 2\phi = (\pi/4)(1 \pm 1) [\pi]$ <sup>5</sup>. In both these cases, the isotropic<sup>6</sup> in-plane hole  $g$  factor amounts to  $3q$  and the eigenvalues for the heavy-hole excitons are:

$$\begin{aligned}
 E_1 &= \frac{1}{4}(\delta_1 \pm \delta_2) + \frac{1}{4}\sqrt{(2\delta_0 + \delta_1 \mp \delta_2)^2 + (2\mu_B(g_e \mp 3q)B)^2} \\
 E_2 &= -\frac{1}{4}(\delta_1 \pm \delta_2) + \frac{1}{4}\sqrt{(2\delta_0 - \delta_1 \pm \delta_2)^2 + (2\mu_B(g_e \pm 3q)B)^2} \\
 E_3 &= \frac{1}{4}(\delta_1 \pm \delta_2) - \frac{1}{4}\sqrt{(2\delta_0 + \delta_1 \mp \delta_2)^2 + (2\mu_B(g_e \mp 3q)B)^2} \\
 E_4 &= -\frac{1}{4}(\delta_1 \pm \delta_2) - \frac{1}{4}\sqrt{(2\delta_0 - \delta_1 \pm \delta_2)^2 + (2\mu_B(g_e \pm 3q)B)^2}
 \end{aligned} \tag{4.8}$$

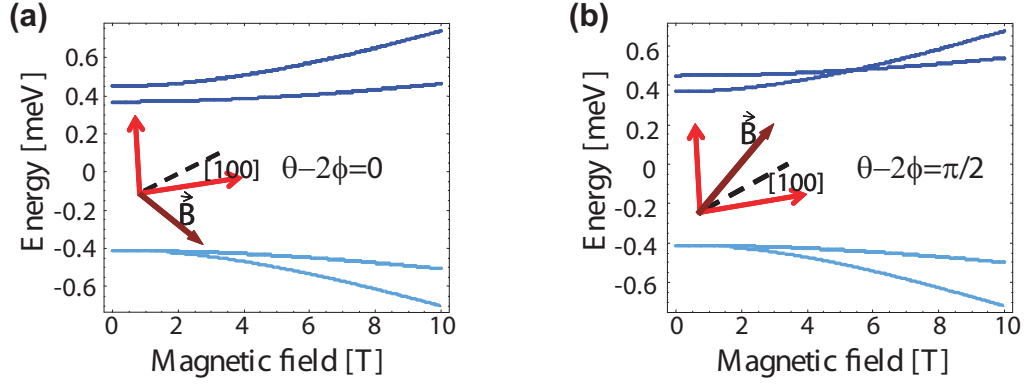
The bright exciton states correspond to the first two levels  $E_1$  and  $E_2$ . It clearly appears that depending on the field direction (given by the sign  $\pm$  in the above expression) these states will get closer to each other with the magnetic field strength  $B$ , or on the contrary move away, as illustrated in Fig. 4.6. For drawing this plot we took the QD parameters used to fit to experimental data which will be presented afterwards. Both field orientations (field applied along  $\theta = 2\phi$  direction and perpendicularly) are represented. First conclusions are following: (i) energy shift is small for the field of the order of a few Tesla due to the large splitting  $\delta_0$  (as compared to  $\delta_1$  in Faraday configuration), (ii) the splitting between “bright” and “dark” states<sup>7</sup> increases with the field, and the splitting for the “dark” states increases as well, (iii) the influence of the field on “bright” states FSS strongly depends on its in-plane direction.

Figure 4.6 illustrates only the relative energy position of the states (eigenvalues). To get a deeper insight into the mechanism leading to the possible FSS change, it is useful to rewrite the exciton Hamiltonian in the basis of linearly polarized states ( $(|+1\rangle \pm |-1\rangle)/\sqrt{2}$ ,  $(|+2\rangle \pm |-2\rangle)/\sqrt{2}$ ). In the specific case  $\phi = \pi/4$ , it takes the following form:

<sup>5</sup>For III-V QDs where generally  $\phi = \pm\pi/4$  this corresponds to field orientations parallel and perpendicular to the QD eigenaxes.

<sup>6</sup>The eigenvalues of the  $g_h$  tensor are  $3qe^{\pm i4\phi}$ . Depending on the arbitrary choice of pseudo-spin basis for the heavy-hole it might be seen as antisymmetric, but the Zeeman splitting of the heavy-hole states is constant whatever is the in-plane field orientation.

<sup>7</sup>Except for zero in-plane field the energy levels are mixed, all transitions become optically allowed. For simplicity we keep the wording “bright” for the states with  $M = \pm 1$  at zero field, and “dark” for that ones with  $M = \pm 2$ .



**Figure 4.6.** Evolution of heavy-hole excitonic levels as a function of in-plane field for two perpendicular directions of the field (a)  $\theta - 2\phi = 0$ , (b)  $\theta - 2\phi = \pi/2$ . Two upper levels (dark blue) correspond to the “bright” states and two lower levels (bright blue) to the “dark” states. Inserts show schematically the field configuration with respect to the QD axes and crystal axis [100]. The model parameters are following:  $\delta_0 = 0.82$  meV,  $\delta_1 = 0.082$  meV,  $\delta_2 = 0.001$  meV,  $g_e = 1.75$ ,  $g_h = 0.78$ . Mixing with light-holes is neglected.

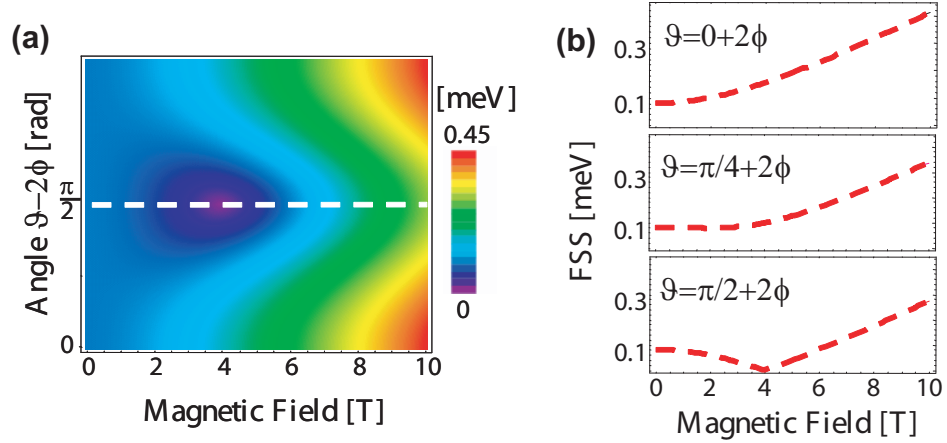


**Figure 4.7.** (a) FSS absolute value vs in-plane field direction  $\theta - 2\phi$  and magnitude encoded on a color scale. White dashed line shows the field direction for FSS cancellation. (b) Cross-sections for three directions  $\theta - 2\phi = 0, \pi/4$  and  $\pi/2$  of the field. Parameters like for Fig. 4.6

$$\mathcal{H}_{X^0} = \frac{1}{2} \begin{pmatrix} \delta_0 + \delta_1 & \delta_- \cos \theta & i\delta_+ \sin \theta & 0 \\ \delta_- \cos \theta & -\delta_0 + \delta_2 & 0 & i\delta_- \sin \theta \\ -i\delta_+ \sin \theta & 0 & -\delta_0 - \delta_2 & \delta_+ \cos \theta \\ 0 & -i\delta_- \sin \theta & \delta_+ \cos \theta & \delta_0 - \delta_1 \end{pmatrix} \quad (4.9)$$

$$\delta_+ = (g_e + 3q)\mu_B B \quad (4.10)$$

$$\delta_- = (g_e - 3q)\mu_B B \quad (4.11)$$



The field induced splitting of the bright states can be seen as a difference in coupling strength to both dark states. The coupling is indeed proportional to  $\delta_{\pm} = (g_e \pm 3q)\mu_B B$  where the sign  $\pm$  refers respectively to one of the linearly-polarized dark states. Hence, the field orientation  $\theta$  determines for a given bright state the effective coupling to the dark levels, and consequently its field-induced shift. From the matrix 4.9 it is clear that the field orientations  $\theta = 0$  and  $\theta = \pi/2$  correspond to remarkable configurations where a given bright state is coupled to a single dark state. As a result, this unbalanced coupling should give rise to a strong intensity anisotropy of the “dark” excitonic doublet, as their finite oscillator strength will arise from the mixing to bright states.

Numerical computations of the FSS evolution in the general case ( $\phi \neq \pi/4$ ) were performed with steps of 0.1 T in magnetic field and  $3.6^\circ$  in relative angle  $\theta - 2\phi$ <sup>8</sup>. Calculations presented in Fig. 4.7 (a) show that FSS cancelation is achieved for  $\theta = \pi/2 + 2\phi$  (changing the sign of  $q$  with respect to  $g_e$  shifts this angle by  $\pm\pi/2$  as it changes  $\delta_{\pm}$  to  $\delta_{\mp}$ ). A small discrepancy of the field orientation leads to a continuous rotation of the eigenaxes directions when passing near the critical point ( $B_{crit.}, \pi/2 + 2\phi$ ) of exact cancelation as shown in Fig. 4.7(b). Nevertheless, choosing correctly the field direction with respect to the QD orientation allows in principle to compensate the FSS of any QD. This point was not clearly established in the analytical treatment presented by Stevenson *et al.* [6] where only the isotropic contribution of Eq. 4.1 was considered<sup>9</sup>.

### 4.3.3 Anisotropic $g$ factor ( $\beta \neq 0$ )

Taking now into account the  $g$  factor anisotropy given by  $\rho_g$  in Eq. 4.7 may considerably change the effect produced by a transverse magnetic field on the FSS. Figure 4.8 presents calculations of the FSS evolution for two values of  $\rho_g$ . The key feature turns out to be the sign of  $\rho_g$  (determined by that of the term  $\kappa\beta$ ) with respect to  $\delta_1$ . If opposite, we find that it is still possible to reduce to zero the FSS for  $\theta - 2\phi = 0$  or  $\pi/2$ , and actually when the antisymmetric part really dominates ( $|\rho_g| \gg 1$ ) this can be achieved for any field direction. On the contrary, for  $\rho_g$  and  $\delta_1$  of same sign the critical field  $B_{crit.}$  for which cancelation could be achieved diverges when  $|\rho_g|$  approaches 1. For larger values of the anisotropy the magnetic field produces an increase of the FSS whatever its in-plane orientation  $\theta$  is, as illustrated in Fig. 4.8(b). Our analysis reveals thus that in the case of a strong anisotropy of  $g_h$  the possibility of tuning the QD FSS by a magnetic field depends essentially on the sign of  $\beta$  with respect to  $\delta_1$ . This behavior can be clarified when considering the analytical expression of the bright state energies obtained again for  $\theta - 2\phi = (\pi/4)(1 \pm 1)$  [ $\pi$ ] and neglecting the dark state exchange splitting  $\delta_2$ :

<sup>8</sup>The numerical grid for calculations was chosen arbitrary from 0 to 10 T for magnetic field and full range for angles, for both parameters the whole range was divided in 100 equal steps. Improving the resolution of the numerical grid by a factor 2 does not change much the quality of the obtained figures.

<sup>9</sup>For InAs QDs, the polarization eigenaxes are in most cases parallel to the [110] crystallographic axes leading to  $\phi = \pi/4$ . As a result  $g_h$  gets diagonal and actually is equal to the scalar factor  $3q$  when no heavy-hole light-hole coupling is included.

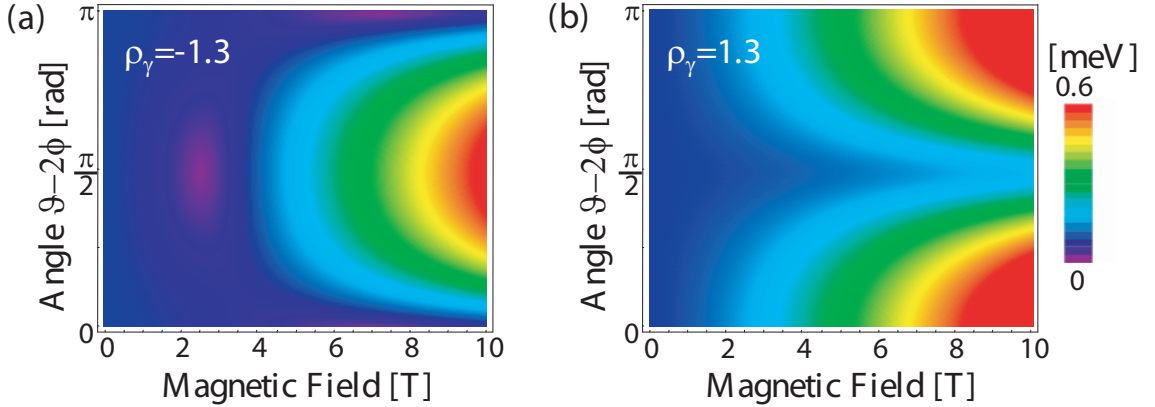


**Figure 4.8.** FSS absolute value on a color scale vs in-plane field direction  $\theta - 2\phi$  and magnitude for a strong  $g$  factor anisotropy  $\rho_g$ . Depending on its sign with respect to the initial splitting (here  $\delta_1 = 80\mu\text{eV}$ ) it produces very different behaviors : (a)  $\rho_g = -1.3$ , (b)  $\rho_g = +1.3$ . We used the same average  $g$  factor  $\bar{g}_h = 0.78$ ,  $g_e = 1.75$  and  $\delta_0 = 0.8$  meV as in Fig. 4.7.

$$\begin{aligned}
 E_1 &= \frac{1}{4} \left( \delta_1 + \sqrt{(2\delta_0 + \delta_1)^2 + [2\mu_B(g_e - 3q(\rho_g \pm 1))B]^2} \right) \\
 E_2 &= -\frac{1}{4} \left( \delta_1 + \sqrt{(2\delta_0 - \delta_1)^2 + [2\mu_B(g_e + 3q(\rho_g \pm 1))B]^2} \right)
 \end{aligned} \tag{4.12}$$

When  $|\rho_g| \gg 1$  the splitting between the levels  $E_1$  and  $E_2$  does no longer depend on the field orientation (associated to “ $\pm$ ” in above equation). The level  $E_1$  will increase faster or slower than  $E_2$  depending on the sign of  $q\rho_g$  actually with respect to  $g_e$ . Depending on the initial relative position  $\delta_1$ , canceling the FFS is achievable or not.

FSS measurements in magnetic field are not sufficient to determine whether the  $g$  factor anisotropy plays an important role or not in actual QDs. One has to perform additional tests based on other features of QD emission, like for example the sensitivity to in-plane magnetic field of PL polarization. When the anisotropy dominates ( $|\rho_g| \gg 1$ ) the principal axes of the PL polarization remain essentially parallel to their initial orientation (see Fig. 4.9), in contrast to the case  $\beta = 0$ . If mixing with light-holes is negligible then the field induced coupling of the excitons gives rise to a rotation of PL polarization (see Fig. 4.10).

If the in-plane field direction  $\theta - 2\phi$  is 0 or  $\pi/2$ , the emission polarization remains the same. When crossing the point of zero FSS the energy positions of two bright states reverse, hence for  $\pi/2$  one sees an abrupt change of polarization of higher energy component of excitonic doublet. However the main polarization axes of the emission do not change. For any other field direction the PL polarization rotates systematically with the field. The direction of PL polarization with respect to the QD principal axes are schematically presented in Fig. 4.9, precise calculations (see Fig. 4.10) reveal that above the critical field (for which FSS changes the

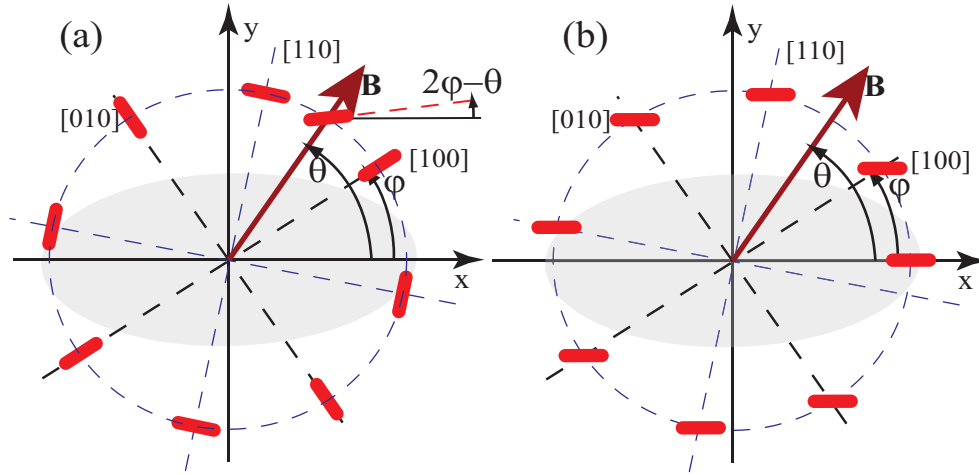


**Figure 4.9.** Schematics of the crystallographic axis configuration with respect to the QD principal axes  $x, y$ . Thick red dashes represent one of the exciton polarization eigenaxis resulting only of the field-induced splitting (namely  $\delta_1 = 0$ ) for different directions of the field  $\theta$ . (a) Effect of the cubic term (see text), (b) effect of the linear term, including heavy-hole to light-hole coupling. The grey shaded area represents a QD elongated along the polarization eigenaxis  $x$ .

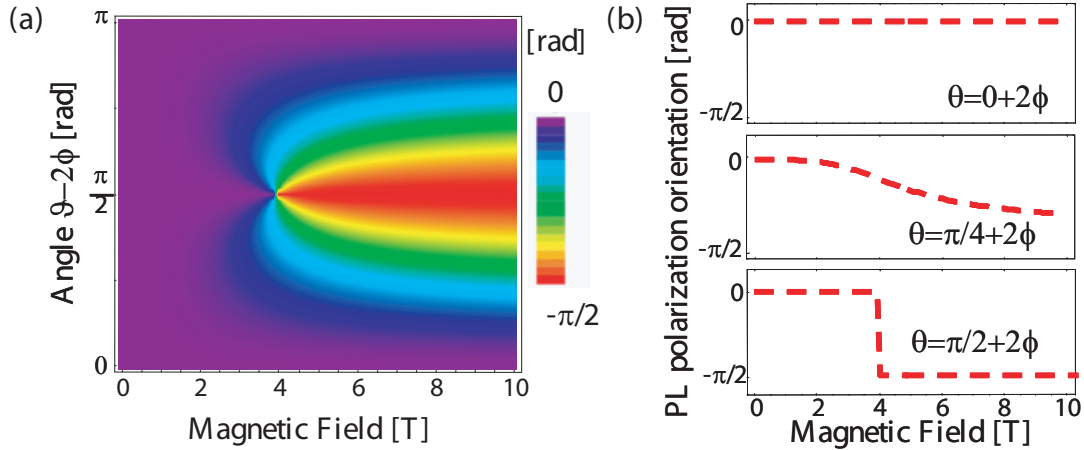


**Figure 4.10.** Rotation angle  $\Delta\theta$  of the PL polarization orientation vs in-plane magnetic field direction and magnitude. Three cross-sections for  $\theta - 2\phi = 0, \pi/4$  and  $\pi/2$  are also shown.

sign) the PL rotation can be significant.

## 4.4 Experimental results

The polarization-resolved  $\mu$ -PL spectra of a QD in Voigt configuration at various fields are shown in Fig. 4.11 for sample  $B_{26}$ . The investigated QD1 is a special case, because it is nearly oriented along  $\mathbf{B}$  ( $\theta = 18^\circ$ ). The most salient feature is a line appearing  $\sim 1$  meV below the excitonic doublet, and developing when the field is increased. This line is attributed to the dark exciton that becomes optically active due to field-induced mixing of bright and dark states [114]. Detailed analysis shows in general a blueshift of the excitonic doublet (105  $\mu$ eV at 7 T), an increase of the bright-dark exciton splitting, and in this case, an increase of FSS from 87  $\mu$ eV at  $B = 0$  to 185  $\mu$ eV at  $B = 7$  T. In all studied QDs, the observed dark state was fully linearly polarized parallel to the higher energy component of the bright excitonic doublet. In order to explain experimental observations we performed calculations in Zeeman spin interaction model described above. Bright exciton shift and splitting, as well as bright-dark splitting were fitted simultaneously. The QD1 parameters used for calculation were taken from experiment :  $\delta_0 = 0.82$  meV and  $\delta_1 = 0.082$  meV. We assumed  $\delta_2 = 0.001$  meV. We included in the model the field orientation  $\theta$  with respect to the dot main axis, which also defines  $\phi$ , as in our experiment the field was parallel to one of the cleaved edges of the sample corresponding to  $|\theta - \phi| = \pi/4$ . The only free parameters in the model are  $g$  factors. Figures 4.11 (b) and (c) show the fit realized for the bright exciton shift and dark-bright splitting. Obtained values for electron and hole  $g$  factors are  $g_e = 1.75$ ,  $g_h = 0.78$ . We can predict from the fitted  $g$  factors an intensity ratio for both dark-state component of  $\simeq 8$ , which qualitatively explains the lack of one of the dark-state components in the spectra.

The influence of the magnetic field on FSS is presented in more detail in Fig. 4.12 for QD1 and for another quantum dot (QD2) with approximately orthogonal orientation ( $\theta = 110^\circ$ ). For QD1, an increase from 87  $\mu$ eV to 185  $\mu$ eV at  $B = 7$  T is found while a decrease of about 200  $\mu$ eV is observed for QD2. This effect turns out to be quite similar to the results of measurements on InAs QDs reported in Ref. [6] where an increase (decrease) of FSS was also observed for a field parallel (orthogonal) to the orientation of the low energy component of excitonic doublet. The decrease of FSS observed for QD2 (characterized by  $\theta \approx \pi/2$ ) could also be reproduced by the model with values  $|g_e| = 1.75 \pm 0.2$  and  $|g_h| = 0.9 \pm 0.2$ . The dark states being absent from the spectra,  $\delta_0 = 1$  meV was arbitrary chosen for the latter fitting.

Finally, we have also investigated some dots with a tilted field configuration (i.e.  $\theta \approx \pi/4$  or  $\theta \approx 3\pi/4$ ). In such cases, in addition to the FSS change, the dot orientation shows a clear rotation when increasing the field. Figure 4.13 illustrates this effect for only a few selected dots, but observations were the same for the set of QDs that we have studied (about 20). As shown, the QD eigenaxes rotate systematically towards the direction of the applied field. This indicates that the in-plane magnetic field  $\mathbf{B}$  contributes to the FSS by an effective spin splitting of the bright exciton states characterized by the low (high) energy component polarized parallel (orthogonal) to the field. As shown, the reference QD eigenaxis rotates systematically towards the direction of the applied field ( $\theta + \Delta\theta \rightarrow 0$ ). This

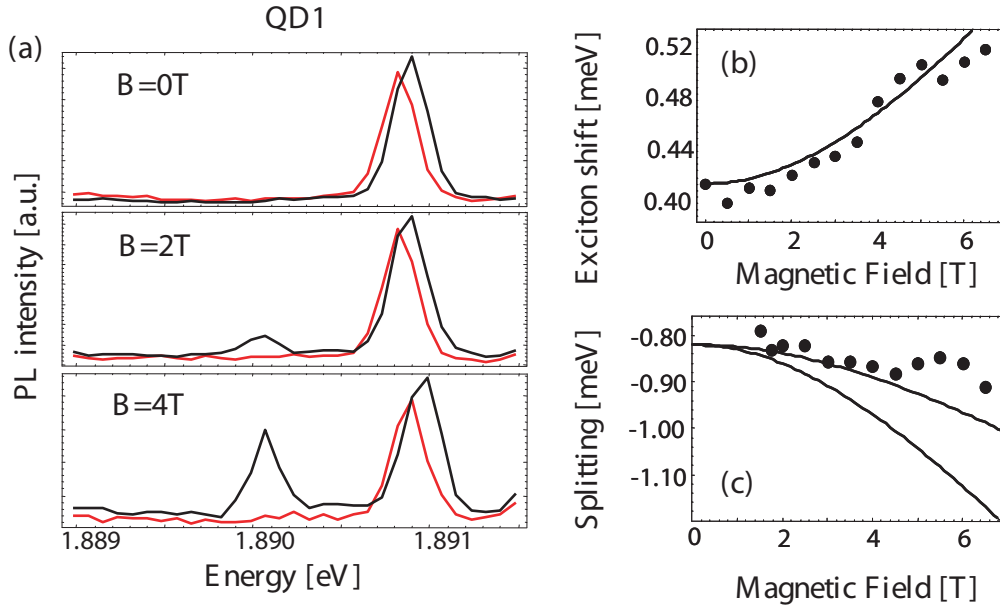


**Figure 4.11.** [Sample  $B_{26}$ ] (a) Linearly polarized excitonic doublet (red and black) for magnetic fields  $B = 0, 2,$  and  $4\text{ T}$  in a dot characterized by  $\theta = 18^\circ$ . (b) Mean energy of the bright excitonic doublet versus magnetic field and (c) splitting of bright to dark states vs magnetic field. For (b) and (c) solid lines are theoretical curves calculated with the model described in the text.

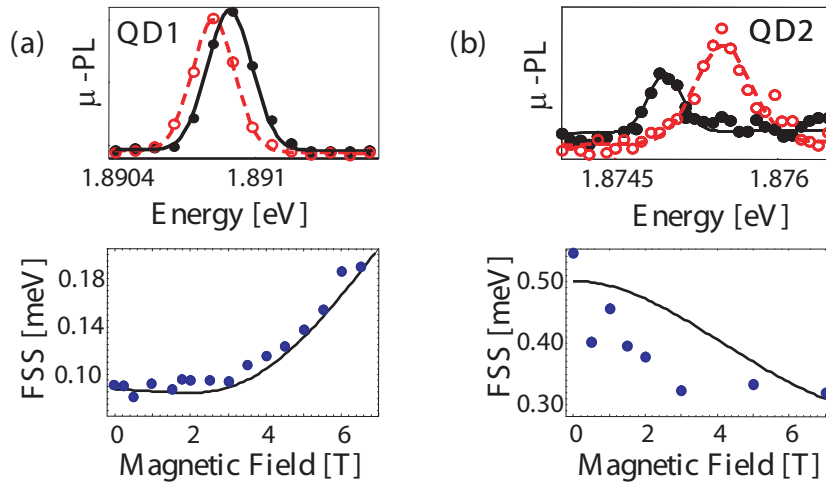


**Figure 4.12.** [Sample  $B_{26}$ ] Upper panel:  $\mu$ -PL spectra at  $B = 0\text{ T}$  for two dots QD1 and QD2 with perpendicular anisotropy orientations,  $\theta=20^\circ$  and  $\theta=110^\circ$  respectively. (open symbols and dashed line: measured at  $20^\circ$ , closed symbols and solid line: measured at  $110^\circ$ ). Lower panel: Fine structure splitting (FSS) vs in-plane magnetic field  $B$ . Solid lines are theoretical curves according to the model discussed in the last Section.

suggests that the in-plane magnetic field  $\mathbf{B}$  contributes to the FSS essentially by an additional term characterized by the low (high) energy exciton component polarized parallel (orthogonal) to the field. However, the field influence on the

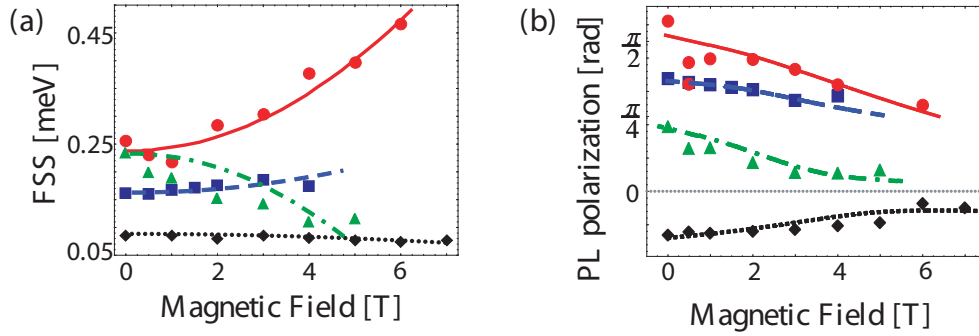


**Figure 4.13.** [Sample  $B_{26}$ ] (a) Fine structure splitting (FSS), and (b) PL polarization orientation  $\theta$  against in-plane magnetic field of four different QDs (different symbols). Lines are guide to the eyes.

FSS is not univocally determined by  $\theta$ : the QD with  $\theta \approx \pi/2$  in Fig. 4.13 (circles) exhibits an increase of FSS in contrast to QD2. This lack of strict correlation to  $\theta$  points toward a combination of different factors determining the field induced splitting.

## 4.5 Orbital effects

We can note some small discrepancies between the experiments and the model of Zeeman spin interactions, revealing insufficiency of the model. In this *Section* we examine theoretically another possible contribution to the modification of FSS splitting. The in-plane field creates an anisotropic magnetic potential, which adds to the QD confinement. To estimate the order of magnitude of this effect we used the approach proposed by M. Glazov and E. L. Ivchenko [72], which relies on the harmonic oscillator approximation to describe the QD potential. Assuming a simple form of the excitonic wavefunction one can get an analytical description of the exciton contraction with an in-plane magnetic field. The resulting orbital effect directly influences the FSS and depending on the field orientation with respect to the QD axes it should lead either to an increase or a decrease of the exciton splitting. Assuming a strong confinement along  $z$  enables us to focus on the in-plane part of the excitonic wavefunction:

$$\Psi_{exciton}(\rho_e, \rho_h) = \Psi_e(\rho_e)\Psi_h(\rho_h) \quad (4.13)$$

where  $\Psi_e$  and  $\Psi_h$  are the single particle wave-functions for an electron and a hole, respectively. In the harmonic potential provided by the QD the latter can be

represented by:

$$\Psi_e(\rho_e) = \frac{1}{\sqrt{\pi a_{e,x} a_{e,y}}} \exp\left(-\frac{x_e^2}{2a_{e,x}^2} - \frac{y_e^2}{2a_{e,y}^2}\right); \Psi_h(\rho_h) = \frac{1}{\sqrt{\pi a_{h,x} a_{h,y}}} \exp\left(-\frac{x_h^2}{2a_{h,x}^2} - \frac{y_h^2}{2a_{h,y}^2}\right) \quad (4.14)$$

The anisotropy of a QD is introduced by the parameters describing lateral size of wavefunctions ( $a_{e,x}$ ,  $a_{e,y}$  for electrons and  $a_{h,x}$ ,  $a_{h,y}$  for holes). The directions  $x$  and  $y$  correspond to the main axes of the dot.

The in-plane magnetic field manifests itself by a parabolic confinement in the plane orthogonal to  $\mathbf{B}$  over a typical magnetic length  $l_B = \sqrt{\hbar/eB}$ . The corresponding kinetic part of the Hamiltonian reads:

$$\hat{H}_{kinetic} = \frac{1}{2m_e}(\hat{p}_e^2) + \frac{1}{2m_h}(\hat{p}_h^2) + \frac{1}{2m_e} \frac{x_e^2}{l_B^4} + \frac{1}{2m_h} \frac{x_h^2}{l_B^4} - \frac{eB}{m_h} x_h p_{z,h} - \frac{eB}{m_e} x_e p_{z,e} \quad (4.15)$$

where  $\hat{p}_i$  – momentum of  $i$ th particle,  $m_i$  – effective mass of  $i$ th particle. The two last terms can be neglected as they couple to  $P$ -states far above in energy. When the magnetic confinement takes place along the direction of longer electron and hole extension, it may reduce the wave-function anisotropy, and subsequently the long-range part of the anisotropic exchange calculated by Eq. 1.8. With the wave-functions introduced here, M. Glazov and E. L. Ivchenko [72] obtained the following expression:

$$\delta_1 = \frac{1}{4\pi} \frac{3\sqrt{\pi}}{2\epsilon_0\epsilon_r} \left(\frac{e\hbar|P_{cv}|}{m_0 E_g}\right)^2 \frac{a_e^3 d_h + a_h^3 d_e}{(a_e^2 + a_h^2)^{3/2} a_e^2 a_h^2} \quad (4.16)$$

where  $a_i$  is the mean size of the wave-function for particle  $i$  and  $d_i = (a_{i,y} - a_{i,x})/2$  describes anisotropy of the corresponding wave-functions<sup>10</sup>. With this expression after some algebraic manipulation one can get the magnetic field which leads to FSS cancelling:

$$B_{canceling} = \frac{\hbar}{e} \sqrt{8 \frac{d_e/a_e^3 + d_h/a_h^3}{a_e^2 + a_h^2}} \quad (4.17)$$

This field scales like the square root of the dot anisotropy  $\xi = d_e/a_e = d_h/a_h$ <sup>11</sup>. The sign in Eq. 4.17 depends on the definition of anisotropy. If the canceling field is imaginary it means that the field is applied along the “wrong” axis of the QD.

<sup>10</sup>This expression is similar to Eq. 1.10 if we assume equal extension and anisotropy for electron and hole, namely  $a_e = a_h = 2L$  and  $d_e = d_h = 2L\xi$ . In such case, both expressions differ only by about 25% due to the different numerical pre-factor which is model-dependent.

<sup>11</sup>Assuming equal anisotropy for electron and hole wave-functions.

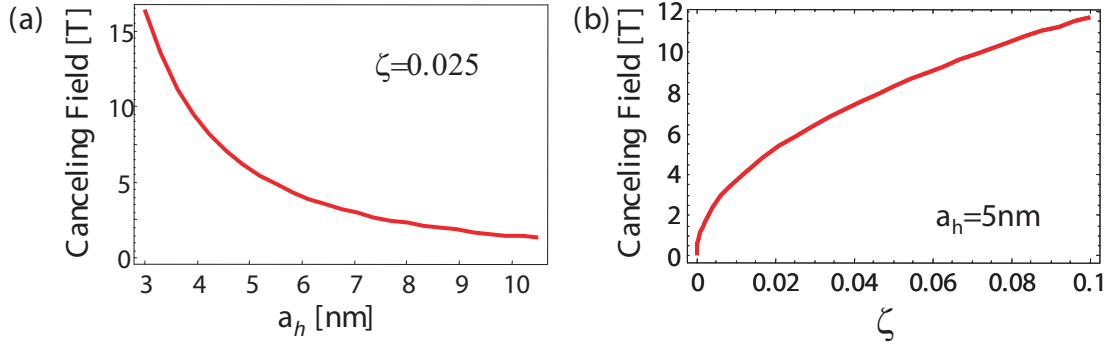


**Figure 4.14.** (a) Canceling field as a function of mean wavefunction size ( $\xi$ )=0.025. (b) Canceling field as a function of anisotropy (fixed size of the wavefunction:  $a_h = 5$ nm).

To cancel the splitting the orthogonal field direction should be used. Note that orbital effect depends only on the angle between the dot principal axes and the field direction. The field orientation with respect to the crystal lattice does not matter here. Let us emphasize that the parameters  $a$  and  $d$  refer to the wavefunction size, not to the QD potential extension. The values we took for numerical evaluations are taken from [122]. For simplicity the ratio  $a_h = 2a_e$  was fixed and only the mean size of the wave-functions or their anisotropy are varied in Fig. 4.14.

The diamagnetic contraction of the excitonic wave-function may play an important role in the case of weakly elongated QDs, since then the canceling field is of the order of a few Tesla. The orbital effect appears comparable with spin interactions. Additionally the potential created by in-plane magnetic field could also affect PL polarization. In case of the field tilted with respect to the QD principal axes a rotation of PL polarization should occur. However we can assume that in the experimental results presented above such orbital effects were negligible, because the examined QDs exhibited a rather strong anisotropy.

Experimentally there is no simple way to distinguish between the contributions of orbital and spin effects to the FSS changes. Following the PL polarization in the field, we can conclude about the role of  $g$  factor anisotropy. If the PL orientation remains the same in any field orientation then in Eq. 4.1 the term linear in  $J$  (hole angular momentum) should be considered as dominant. In such a case the QD intrinsic properties determine whether exists or not a field direction for canceling the FSS. If PL polarization rotates towards the field then the value of the splitting  $\delta_1$  decides the role of orbital effects in our descriptions. For QDs with small anisotropy it is possible to distinguish between both contributions only if the QD orientation is tilted with respect to the crystallographic axes  $\langle 100 \rangle$  and if we can experimentally vary the field direction to determine the canceling field direction.



## 4.6 Conclusion on FSS manipulation by an external magnetic field

In summary, we have shown that a magnetic field influences noticeably the fine-structure related optical properties of QDs. The longitudinal field induces Zeeman splitting which suppresses the effect of in-plane anisotropy on the exciton and leads to circular polarization of the emission. In Faraday configuration it is possible to study exciton spin lifetime and coherence which are also important requirements for photon entanglement with QDs.

However, the most important result regarding symmetry effects is that an in-plane field modifies the fine structure of the excitonic emission from CdTe/ZnTe quantum dots. The field applied along one of the main axes of the dot can either increase or decrease the splitting. Additionally a rotation of the emission polarization was systematically observed. These effects are in qualitative or rough quantitative agreement with our model based on the Zeeman spin Hamiltonian, where the effective transverse  $g$  factor for heavy holes turns out to be essentially isotropic. Further experimental investigations consisting in mapping the influence of the magnetic field as a function of its in-plane orientation should be performed to determine more quantitatively a possible  $g$  factor anisotropy due to the heavy-hole light-hole coupling. When this anisotropic contribution dominates, our analysis shows that the orientation of the field with respect to the QD principal axes does not play any role, the possibility of FSS canceling being completely determined by intrinsic properties of the QD. It was shown by Stevenson *et al.* [6] that for InAs/GaAs QDs in-plane field can tune FSS over large values ( $\sim 50\mu eV$  in  $5T$ ) and through zero. Obtained in this way the full degeneracy of the levels can be used for entangled emission [55]. As discussed in this manuscript, the  $C_{2v}$  heavy- to light-hole mixing contributes to the hole  $g$  factor by an anisotropic term which reduces or even cancels out the effect of strong dependence of the emission on the field direction. This could be the case with InAs QDs as in experiments the field-induced changes do not depend strongly on the in-plane field orientation <sup>12</sup>.

---

<sup>12</sup>Unpublished results, private communication from one author of Ref. [6].

## 4.7 Effective magnetic field: the role of nuclear spins

In this *Section*, we will discuss magnetic-like effects, which are not directly related with an external magnetic field, but appear due to the influence of the magnetic moments of the QD nuclei. In QDs, the conduction electrons with  $S$ -like Bloch functions experience a significant hyperfine interaction with the host nuclei, which affects the spin dynamics exactly as a magnetic field. Measurements of the electron spin orientation induced by optical excitation can be used to probe the consequences of this interaction. The optically oriented electrons can transfer their polarization to the nuclear spins through a hyperfine flip-flop process. Then the nuclear polarization creates an effective magnetic field which acts on the electron spin, leading to the so-called Overhauser shift, e.g. the Zeeman splitting produced by the nuclear field. Especially the polarization of trions, which contain an unpaired spin and thus have no exchange splitting, is sensitive to the nuclear field<sup>13</sup>.

The hyperfine interaction of a single electron spin ( $\hat{S}_e$ ) with  $N$  nuclear spins has following form [123]:

$$\hat{H}_{hf} = \frac{v_0}{2} \sum_j A^j |\Psi(\mathbf{r}_j)|^2 \left( \hat{I}_z^j \sigma_{e,z} + \frac{\hat{I}_+^j \sigma_{e,-} + \hat{I}_-^j \sigma_{e,+}}{2} \right) \quad (4.18)$$

where the sum goes over interacting nuclei,  $\mathbf{r}_j$  denotes the position of the  $j$ th nucleus with spin  $\hat{I}^j$ ,  $\Psi(\mathbf{r})$  is the electron envelope function,  $v_0$  is the two-atom unit cell volume, and  $A^j$  are hyperfine interaction constant on the nucleus  $j$ . This interaction can be expressed in terms of an effective magnetic hyperfine field  $\mathbf{B}_n$  such that  $\hat{H}_{hf} = g_e \mu_B \hat{S} \cdot \mathbf{B}_n$ , which reads:

$$\mathbf{B}_n = \sum_j A^j \hat{I}^j / (N g_e \mu_B) \quad (4.19)$$

The hyperfine constants  $A^j$ , the values of the host nuclear spins  $I^j$ , and the isotopic fraction of nuclei carrying a non-zero spin are larger for III-V than for II-VI compounds [87, 124, 125]. Thus InAs/GaAs quantum dots are nanostructures where these hyperfine effects are more pronounced, and only this system will be discussed here.

Without optical orientation of spins the hyperfine field is random with typical standard deviation amounting to  $\sim 30$  mT and it mostly affects spin relaxation<sup>14</sup>. In usual PL experiments, we do not observe the effect of such a small additional

<sup>13</sup>The PL polarization of negatively charged trions ( $\mathbf{X}^-$ ) is determined by the spin of the hole, while that of positively charged trion ( $\mathbf{X}^+$ ) is determined by the electron.

<sup>14</sup>The Larmor precession period amounts then to  $\sim 0.5$  ns in this field, a timescale comparable to the exciton radiative lifetime.

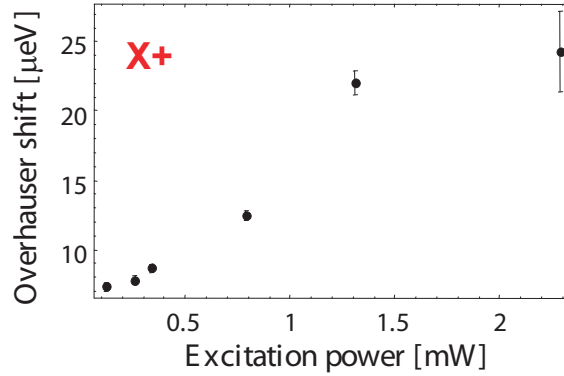


**Figure 4.15.** [Sample  $B_{35}^{nS}$ ] Overhauser shift for X+ vs. excitation power (measured in front of the objective.). Small external longitudinal magnetic field parallel to the QD growth was applied  $B_{ext} = 0.2T$ .

magnetic field. Under efficient dynamic nuclear polarization by a quasi-resonant circularly polarized excitation, one can observe the Zeeman splitting (or Overhauser shift) of individual lines due to the nuclear field  $\mathbf{B}_n$  [87]. This dynamical effect is sensitive to the excitation power (as shown for X+ in Fig. 4.15). Detailed studies of dynamical nuclear polarization in InAs QDs are developed in the PhD thesis of Benoît Eble [87] and some of his most important conclusions can be found in Ref. [126].

The emission of charged excitons is not the main topic of this *work*. So let us now focus on the consequences of Overhauser effect for neutral excitons. The hyperfine-induced splitting of X (in circular basis) can experimentally appear when there is coexistence of neutral and trion excitons over a specific range of gate voltages. In Figure 4.16 one can follow the evolution of the  $\sigma + / \sigma -$  splitting for the exciton vs. applied voltage. The splitting is zero for the voltage range for which only neutral emission is observed, as well as the corresponding circular polarization degree. When the negatively charged trion appears (see 4.16(a)) the X splitting increases up to  $20 \mu\text{eV}$  and becomes comparable with the native FSS. Additionally the polarization ratio is enhanced up to 20%. We have checked that for this exciton the FSS (measured under linear excitation) does not reach zero at any value of applied bias. Hence the observed increase of circular polarization is not due to FSS reduction, but to restoration of circularly polarized eigenstates exactly like in a longitudinal magnetic field. In *Chapter 5* we will discuss the enhancement of PL circular polarization by cancelling the FSS, in a regime of zero nuclear field.

The aim of this *Section* was to sketch the most important features of the Overhauser effect and its possible consequences on the neutral exciton FSS and polarization. We have shown that the effects related to the dynamic nuclear polarization can strongly modify the effective optical properties of an individual InAs/GaAs QD. As a result, entangled photon emission cannot occur for biexciton-exciton cascade in the presence of a nuclear polarization, whose effect is similar to a longitudinal magnetic field. Noteworthy, the nuclear field fluctuations of  $30 \text{ mT}$  always

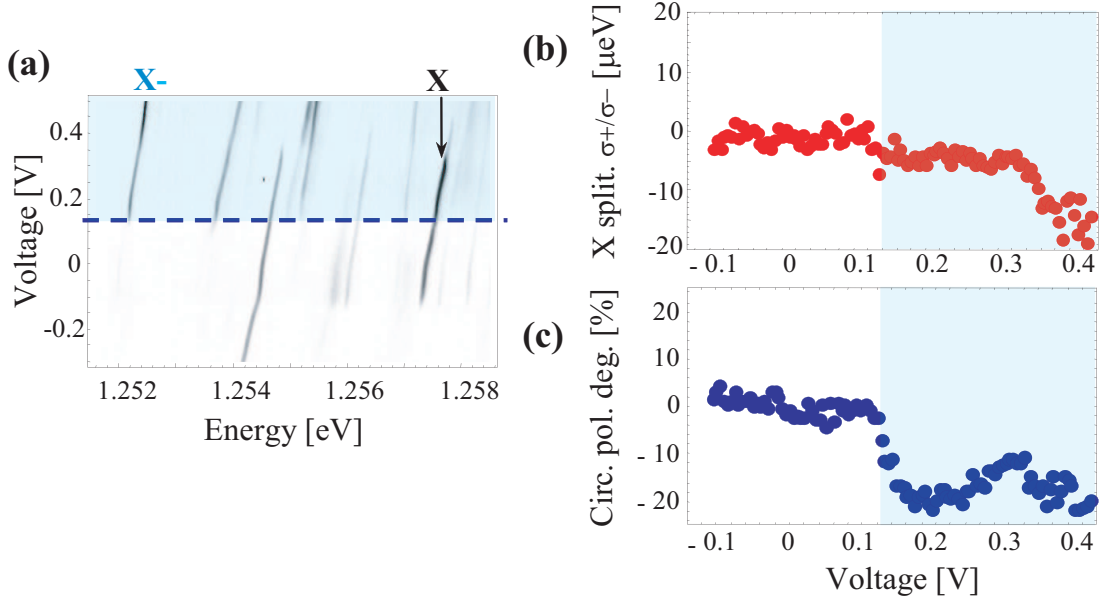


**Figure 4.16.** [Sample  $B_{35}^{nS}$ ] (a) Contour-plots in a gray scale of the PL intensity as a function of the energy detection and applied bias (white – 0counts/sec, black – 80counts/sec). The two transitions from the same QD are identified: X and X-. The excitonic line splitting measured in circular polarization  $\sigma_+/\sigma_-$  (b), and circular polarization degree (c) as a function of applied voltage (under  $\sigma_-$  excitation). The blue shaded area marks the voltage range for which the neutral and negatively charge emission exist simultaneously.

contribute to the effective splitting of the bright excitons by about  $1 \mu\text{eV}$ , which is not negligible as compared to the homogeneous linewidth. This results in an intrinsic limit for InAs QDs, which seems difficult to overcome for the generation of maximally entangled photons.

Eventually, the possible build up of nuclear field must be carefully kept in mind when looking for a “good” QD: a simple solution to avoid optically induced nuclear polarization is to use a modulated excitation (with a modulation time faster than nuclear polarization dynamics recently estimated to a few  $ms$  [127]). More generally, for checking the polarization features of a given QD under circularly-polarized excitation, it is better to not generate charged excitons at the same time as neutral excitons, since they are very efficient to polarize the nuclei.

**SUMMARY.** The influence of magnetic field on the optical properties of QDs is discussed in *Chapter 4*. To describe the experimental observations we used the model of Zeeman spin interaction, with a particular attention to the issue of hole  $g$  factor in Voigt configuration. In this respect, the role of the heavy- to light-hole mixing is clarified. It contributes to the hole  $g$  factor by an anisotropic term. We explicit the conditions to achieve FSS canceling by applying an in-plane magnetic field. The dependence of the QD principal axes on the field direction is analyzed in detail. In the last *Section*, we briefly discuss the role of the nuclear spins and of the associated Overhauser shift depending on excitation conditions.

---

---

## CHAPTER 5

---

# Toward Entanglement

### Contents

---

<b>5.1</b>	<b>Exciton spin dynamics in density matrix formalism . . . . .</b>	<b>92</b>
5.1.1	Time evolution of the exciton density matrix . . . . .	92
5.1.2	Geometrical representation of spin precession . . . . .	96
5.1.3	Polarization relaxation and conversion in cw experiments	98
<b>5.2</b>	<b>Optical orientation/alignment of exciton . . . . .</b>	<b>101</b>
5.2.1	Optical orientation in QDs with tunable FSS . . . . .	101
5.2.2	Optical orientation for different excitations . . . . .	104
<b>5.3</b>	<b>Measurements of polarization conversion . . . . .</b>	<b>107</b>
5.3.1	Circular-to-linear conversion . . . . .	107
5.3.2	Linear-to-circular conversion . . . . .	110
5.3.3	Conversion of polarization for trions . . . . .	112
<b>5.4</b>	<b>Conclusion . . . . .</b>	<b>114</b>

---

*“I would call entanglement not one but rather the characteristic trait of quantum mechanics, the one that enforces its entire departure from classical lines of thought.”*

Erwin Schrödinger

OUR ATTEMPTS TO PREPARE THE EXCITONIC STATE for emission of entangled photons naturally drove us to the study of exciton spin coherence in a quantum dot. In GaAs/AlAs superlattices it was theoretically predicted and experimentally evidenced by E. L. Ivchenko *et al.* ([128, 129]) that excitonic transitions can lead to conversion of photon polarization. This effect takes place when the quantum system has an anisotropic feature, which gives rise to the phenomenon of spin precession (or quantum beat) during the exciton lifetime. Observing this effect in semiconductors relies on the spin-dependent <sup>1</sup> optical selection rules applied to

---

<sup>1</sup>Because of large spin-orbit interaction in the valence band.

a  $\Lambda$ -type system (one ground and two excited states), which is the case for the ground excitonic transition. The empty QD state is the ground state, and the two (more or less degenerate) bright excitons are the two excited states. Under a resonant excitation of this system, we can create any superposition of these two levels determined by the light polarization. For example, choosing  $\sigma^+$  or  $\sigma^-$  excitation amounts to optical preparation of the exciton in one of the spin state  $|\pm 1\rangle$ . This optical orientation of exciton spin is preserved during the lifetime and can lead to significant effects e.g. in PL experiments if two conditions are fulfilled: i) the exciton spin relaxation between the two levels must be weak, i.e. much slower than radiative recombination, ii) the splitting  $\delta_1$  (or FSS) which determines the period of quantum beats must be lower than the QD homogeneous excitonic linewidth (in the absence of external magnetic field). The first condition is generally fulfilled in semiconductor QDs, thanks to the 3D confinement which inhibits most of the spin relaxation mechanisms acting in bulk or quantum-wells. Yet, in recent publications, I. Favero *et al.* interpreted their experimental measurements (a strong degree of PL linear polarization) by arguing that the exciton spin lifetime in QD is very short [113, 130]. This puzzling conclusion, based on rather indirect observations and some controversial assumptions, made this issue to be examined in more detail. Experimentally, there is a real difficulty to measure the spin lifetime because of the second point mentioned above, i. e. the FSS. Both effects can not be tackled independently, as it will appear more obvious in the next *Section*. In this regard, measuring the optical orientation or alignment of a single exciton, and more generally the degree of polarization conversion from an excitation basis into a detection basis brings a lot of informations on the coherent (or not) evolution of an exciton during its lifetime. It should be emphasized that such experiments really amount to determination of the possibility of entanglement in biexciton-exciton cascade from a given QD, like direct measurements of polarization correlation in the bi-exciton cascade. In particular, measuring the degree of circular polarization under optical orientation conditions probes the strength of the FSS and its effective change (for entanglement) when applying an external perturbation to tune it through zero. This investigation of optical pumping in quantum dots will be discussed in *Section 5.2*. The studies of exciton spin coherence via measurements of the polarization conversion will be presented in *Section 5.3*. First *Section 5.1* will briefly sketch the density matrix formalism applied to an exciton state, to be used to interpret the experimental observations.

In order to study the effects of optically induced orientation of excitons it was first crucial to optimize the process of resonant excitation. As strictly resonant excitation and PL measurements are rather incompatible, we took advantage of the quasi-resonant  $1LO$ -phonon-assisted excitation, which has proven to be very efficient in the case of quantum wells [128, 129]. For the sample  $B_{35}^{nS}$  it was found previously by S. Laurent *et al.* [84] that a strong resonance in the excitation spectrum of a QD ensemble occurs at  $35meV$  above the ground state transition, i.e. between the GaAs  $LO$ - and  $TO$ -phonon features. This  $1LO$ -phonon-assisted excitation was thus chosen, as already performed by G. V. Astahov *et al.*[131] to establish polarization conversion in an ensemble of CdSe/ZnSe QDs. Such a quasi-resonant excitation should provide an efficient transfer of light polarization into

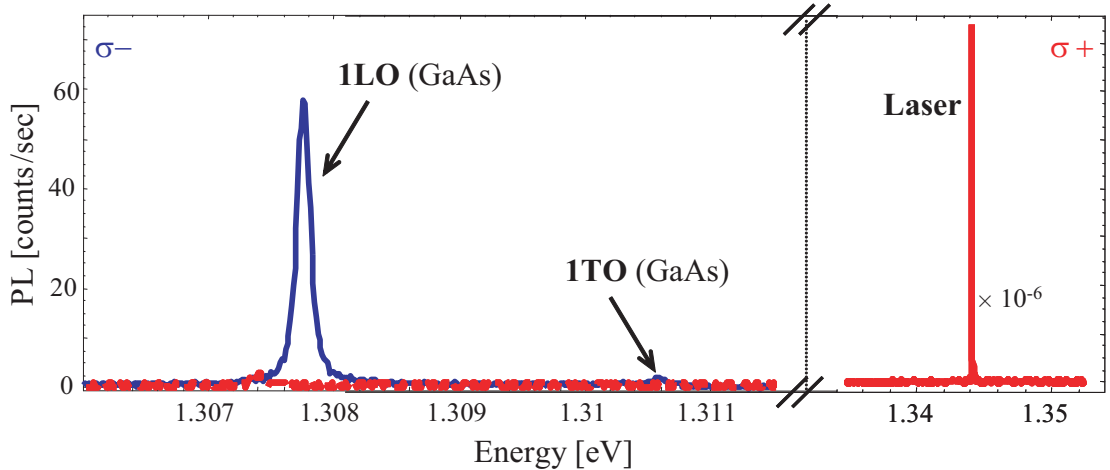


**Figure 5.1.** [Sample  $B_{35}^{nS}$ ] Raman scattering of the laser line in the GaAs barrier. The excitation (right part) laser beam was circularly  $\sigma+$  polarized, whereas in the detection both polarization were checked:  $\sigma+$  (red curve) and  $\sigma-$  (blue curve). The spectrum was recorded under strong negative bias  $-1V$  in order to suppress PL from QDs.

exciton spin polarization. This is a rather reasonable assumption since electron-phonon interaction is spin-independent. The spin polarization can be transferred in turn to the polarization of emitted light, if the exciton spin is conserved during the phonon emission. As we will see in next *Sections*, a strong degree of exciton polarization could be achieved under polarized pump proving that this condition is fulfilled in experiments.

First, to clearly identify Raman diffusion of the laser line from the barrier material, PL spectra were recorded with a strong electric field applied to the structure to get rid of all PL signal from QDs. The symmetry of the Raman second-rank tensors in zinc-blende crystals (see e.g. [132]) determines the selection rules of this diffusion mechanism: the GaAs  $LO$ - and  $TO$ -phonon features appear in cross-circular polarizations of the excitation and the detection (see Fig. 5.1). They are present at around  $36meV$  ( $1LO$ ) and  $34meV$  ( $1TO$ ) below the laser line<sup>2</sup>. While shifting the laser line to lower energy, both phonon lines move down and photoluminescence of QDs resonantly selected in the laser spot also follows the changes in excitation. Besides, these Raman replicas of the laser line have a rather weak intensity, and thus do not interfere much with the PL lines of single QD. If necessary, the spectra can still be “cleaned” by subtracting a spectrum taken at a gate voltage  $V_g = -1$  V. Actually, this quasi-resonant excitation of QD excitons probably involves  $LO$ -phonon from an InGaAs alloy and thus occurs at a different energy than the GaAs phonon line.

Let us mention here a few additional experimental details. The experiments of optical pumping and polarization conversion presented further were performed on an in-plane electric gate structure (sample  $A_{35}^{SSetch}$ ) and on a vertical field effect

<sup>2</sup>For light propagating along [001] no Raman diffusion associated to TO mode is expected along the same direction, but experimentally the finite aperture of the laser excitation beam (N.A.~0.6) likely enables this observation.



structure (sample  $B_{35}^{nS}$ ) through the semitransparent part of a Schottky gate. We indeed noticed that the measurements of polarization via micrometer size holes in a solid mask were sometimes perturbed for some dots (e.g. under strong resonant excitation, no significant circular polarization for negatively charged excitons could be achieved). One of the most probable reason for that was ascribed to the depolarization of light propagating close to the edges of the holes in the shadow mask. For the structure  $B_{35}^{nS}$  neutral excitonic emission was measured under fixed applied voltage (at  $+0.2V$ ), for which formation of charged excitons is forbidden. This rules out any effect related with dynamic nuclear polarization of the QD, as for example described in last *Section* of *Chapter 4*. For studies of polarization conversion, the experimental setup of polarization-resolved measurement was improved to reduce polarization anisotropy of the beam-splitter (as described in *Section 2.3*), which can reveal dramatic when measuring conversion effects.

## 5.1 Exciton spin dynamics in density matrix formalism

### 5.1.1 Time evolution of the exciton density matrix

The density matrix formalism is an intelligible way to rewrite the Schrödinger equation describing the temporal evolution of a quantum system, to better focus on its measurable quantities. In this *work*, it will be applied to the exciton two-level system. Instead of deriving the exciton wavefunction  $\Psi_{exc.}(t)$  from the time-dependent Schrödinger equation, one can equivalently solve the Liouville equation for the density operator  $\hat{\rho}$ <sup>3</sup>:

$$\frac{d\hat{\rho}}{dt} = -\frac{i}{\hbar}[\hat{H}, \hat{\rho}] \quad (5.1)$$

where  $\hat{H}$  is the Hamiltonian of the system. The density operator is defined as  $\hat{\rho} = \sum_i p_i |\Psi_i\rangle\langle\Psi_i|$ , where the sum runs over a set of pure quantum states  $|\Psi_i\rangle$ 's and the  $p_i$ 's are the probabilities to find the system in the associated state. This operator is particularly suitable to describe a quantum system prepared in an uncertain state, or a statistical collection of identical quantum systems prepared in a pure (or uncertain) state. In a specific basis of states, this operator takes the form of an Hermitian matrix with diagonal elements  $\rho_{ii}$  which are *positive* and correspond to the occupation probabilities (or population) of the states  $|i\rangle$ , whereas the off-diagonal elements  $\rho_{ij}$  are the “coherences” between basis states  $|i\rangle$  and  $|j\rangle$ . In an eigenstate basis of  $\hat{H}$ , the non-zero coherences (if any) between non-

---

<sup>3</sup>Originally the density matrix formalism was introduced by John von Neumann and its description can be found in his “Mathematische Grundlagen der Quantenmechanik” (“Mathematical Foundations of Quantum Mechanics”). This formalism is commonly used in optics for solving optical Bloch equations, thus reader can find more detailed evaluations of the formulas in any textbook devoted to quantum optics.

degenerate states will oscillate under the driving force of  $\hat{H}$  giving rise to quantum beats.

Yet, frequently an actual quantum system described by  $\hat{\rho}$  is not closed. Its evolution involves interactions with an environment which is not possible or useless to include in a larger quantum system. To describe such an open system, the density matrix formalism is generally supplemented by terms which describe phenomenologically relaxation, annihilation or creation. In the case of the two-level QD excitons which are photo-created, recombine optically and submitted to possible spin relaxation, the evolution equation of  $\hat{\rho}$  takes thus the following form:

$$\frac{d\hat{\rho}}{dt} = -\frac{i}{\hbar}[\hat{H}, \hat{\rho}] + \left(\frac{\partial\hat{\rho}}{\partial t}\right)_{rec} + \left(\frac{\partial\hat{\rho}}{\partial t}\right)_{s.r.} + \left(\frac{\partial\hat{\rho}}{\partial t}\right)_{cr.} \quad (5.2)$$

The first of the terms, which represents the change in the density matrix due to exciton recombination reads in our case:

$$\left(\frac{\partial\hat{\rho}}{\partial t}\right)_{rec} = -\frac{\hat{\rho}}{\tau_r} \quad (5.3)$$

where the decay time  $\tau_r$  corresponds essentially to the exciton radiative lifetime. Note that when restricting our quantum system to the two-level bright excitons, we do not describe the possible optical coherence between exciton and the “empty quantum dot” state. This is absolutely not a limit of our model because here we are interested only in the polarization properties of emitted photons which are fully determined by the bright states population and their coherence. The coupling with light is not used here to control coherently or probe the absolute population of QDs but “only” the exciton polarization state. For this reason, the possible transfer of population between dark and bright states is also of very weak importance. Its impact on population and coherence can be to some extent included in the effective recombination time  $\tau_r$  and spin relaxation time  $\tau_s$ . The third term of Eq. 5.2 which describes how the internal coherence relaxes without changing the total population reads thus:

$$\left(\frac{\partial\hat{\rho}}{\partial t}\right)_{s.r.} = -\frac{\hat{\rho} - \hat{\rho}_{Th.}}{\tau_s} \quad (5.4)$$

where  $\hat{\rho}_{Th.}$  is the density matrix corresponding to thermal equilibrium within the excitonic subspace. It corresponds to the Boltzmann distribution in a finite temperature  $\Theta$  over the different exciton eigenstates:

$$\hat{\rho}_{Th.} = n_X \frac{\exp(-\hat{H}/k_B\Theta)}{Tr\left(\exp(-\hat{H}/k_B\Theta)\right)} \quad (5.5)$$

where  $n_X$  describes total population of the exciton states. It should be yet noted that for an open system in a non-stationary regime the total population given by  $Tr(\hat{\rho})$  is not constant. Then  $n_X$  takes into account this temporal evolution, e.g. in the form of an exponential decay  $\exp(-t/\tau_r)$  to describe the evolution following a

pulsed excitation.

Equation 5.4 results from the assumption that there is no pure dephasing in the system, i.e. in any unitary basis of the 2-level excitons the coherence relaxation and transfer of populations between the two levels occurs at the same rate  $\tau_s^{-1}$  <sup>(4)</sup>. Physically, this amounts to assume that the mechanisms of spin relaxation have a spherical symmetry <sup>5</sup>. Eventually, Eq. 5.4 means that due to spin relaxation the system irretrievably relaxes toward the thermodynamical state  $\hat{\rho}_{Th}$ .

The last term in Eq. 5.2 which represents the creation rate of excitons must be chosen to reproduce as well as possible the experimental conditions to be simulated. For example, it could be a Dirac function  $\rho_0\delta(t - t_0)$  to analyze quantum beats following a pulsed excitation. In our conditions of cw excitation it will be represented by a constant density matrix which ensures that the derivative of  $\hat{\rho}(t)$  is the zero matrix (stationary regime).

### QD Hamiltonian, optical selection rules and PL intensity

The exciton spin dynamics can be strongly affected by an external field. As seen in *Chapter 4*, a field applied perpendicularly to the QD growth axis can modify the exciton splitting  $\delta_1$ . Yet, this effect relies on a coupling between bright and dark states. As a result, treating this configuration in the density matrix would require to include the dark states in our quantum system making not possible the analytical solving of Eq. 5.2. In contrast, a longitudinal magnetic field  $B_z$  strongly influences the bright exciton spin dynamics thanks to the Zeeman effect without any coupling to external states. As we will see below, it besides enables to address the issue of exciton spin coherence in polarization conversion experiments in the particular case of large splitting  $\delta_1$  with respect to the homogeneous linewidth  $\hbar/\tau_r$ . We will thus consider in the following an exciton Hamiltonian containing two terms:

$$\hat{H} = \hat{H}_{exchange} + \hat{H}_{Zeeman}$$

It is convenient to rewrite the exchange Hamiltonian for bright excitons as an effective magnetic field orthogonal to the quantization axis of the 2 states  $|\pm 1\rangle$  considered as a pseudo-spin 1/2 <sup>(6)</sup>. The QD Hamiltonian takes thus the simple form:

$$\hat{H} = -\frac{\hbar}{2}\Omega_{ex}(\hat{\sigma}_x \cos 2\alpha_0 + \hat{\sigma}_y \sin 2\alpha_0) + \frac{\hbar}{2}\Omega_z\sigma_z \quad (5.6)$$

where  $\hbar\Omega_{ex} = |\delta_1|$ ,  $\hbar\Omega_z = (3g_h - g_e)\mu_B B_z$ ,  $\alpha_0$  is the angle of the QD low energy eigenaxis in the referential of the laboratory, and  $\sigma_x$ ,  $\sigma_y$ ,  $\sigma_z$  are the Pauli matrices.

<sup>4</sup>This gives rise to the well-known relation  $T_2 = 2T_1$  in the high temperature limit.

<sup>5</sup>By describing these mechanisms by an effective time-dependent perturbation  $\hat{H}_1(t)$  the latter would be invariant by any unitary transformation of the 2-level basis.

<sup>6</sup>One has to keep in mind that it is only a mathematical trick enabling for some simplifications in the description and it has nothing to do with real physical magnetic field. Using this form of exchange Hamiltonian we followed E. L. Ivchenko [133].

Once the density matrix is known, the PL intensity emitted in a specific polarization  $\vec{\varepsilon}$  can be calculated by the formula [134]:

$$\mathcal{I}_{PL}(\vec{\varepsilon}) = \text{Tr}(\hat{\rho} \hat{a}_{\vec{\varepsilon}} \hat{a}_{\vec{\varepsilon}}^\dagger) \quad (5.7)$$

where the trace is taken over the 2-level states of our system, whereas the operators of exciton creation  $\hat{a}_{\vec{\varepsilon}}^\dagger$  and exciton annihilation  $\hat{a}_{\vec{\varepsilon}}$  couple the bright states  $|\pm 1\rangle$  to the empty quantum dots state  $|0\rangle$ . The optical selection rules expressed in term of these operator read:

$$\begin{aligned} \hat{a}_{\vec{\varepsilon}}^\dagger |0\rangle &= \vec{\varepsilon} \cdot (\vec{P}_{+1} | + 1\rangle + \vec{P}_{-1} | - 1\rangle) \\ \hat{a}_{\vec{\varepsilon}}^\dagger | + 1\rangle &= 0 \\ \hat{a}_{\vec{\varepsilon}}^\dagger | - 1\rangle &= 0 \end{aligned} \quad (5.8)$$

where  $\vec{P}_{\pm 1}$  is the electric dipole of the exciton state  $|\pm 1\rangle$ . In order to better describe some details of our experimental results presented further, it turns out useful to consider that the excitonic states involve actually a ‘‘heavy-light’’ mixed hole due to the QD  $C_{2v}$  symmetry. The two bright excitons are no longer eigenstates of angular momentum operator but one can still denote them by  $|\pm 1\rangle$ . The mixing between the heavy and light hole components is described by a complex number  $\beta e^{-2i\psi}$  which gives rise to the following expression for the actual bright excitons:

$$\begin{aligned} | + 1\rangle &= \sqrt{1 - \beta^2} | - \frac{1}{2}, + \frac{3}{2}\rangle + \beta e^{-2i\psi} | - \frac{1}{2}, - \frac{1}{2}\rangle \\ | - 1\rangle &= \sqrt{1 - \beta^2} | + \frac{1}{2}, - \frac{3}{2}\rangle + \beta e^{2i\psi} | + \frac{1}{2}, + \frac{1}{2}\rangle \end{aligned} \quad (5.9)$$

where the complex phase  $\psi$  of the mixing determines in real space the eigenaxis angle of the oscillator strength, and  $\beta$  the level of heavy-light mixing reflects its degree of linear polarization<sup>7, 8</sup>. Taking into account this effect, the dipolar vectors introduced above read:

$$\vec{P}_{+1} = \begin{pmatrix} \frac{\sqrt{1-\beta^2}}{\sqrt{2}} - \frac{\beta e^{-2i\psi}}{\sqrt{6}} \\ i \frac{\sqrt{1-\beta^2}}{\sqrt{2}} + i \frac{\beta e^{-2i\psi}}{\sqrt{6}} \\ -\sqrt{\frac{2}{3}} \beta e^{-2i\psi} \end{pmatrix} \quad \vec{P}_{-1} = \begin{pmatrix} -\frac{\sqrt{1-\beta^2}}{\sqrt{2}} + \frac{\beta e^{2i\psi}}{\sqrt{6}} \\ i \frac{\sqrt{1-\beta^2}}{\sqrt{2}} + i \frac{\beta e^{2i\psi}}{\sqrt{6}} \\ -\sqrt{\frac{2}{3}} \beta e^{2i\psi} \end{pmatrix} \quad (5.10)$$

Finally, the formalism of the density matrix offers a powerful framework to analyze quantitatively the exciton coherence that can be produced in a resonant excitation experiment. Yet, before solving Eq. 5.2 in some particular cases and discuss our

<sup>7</sup>We could reasonably expect that  $\psi = \alpha_0$ , but in the most general case the multiple causes of symmetry reduction may lead to different orientations.

<sup>8</sup>Note that the mixing with the light holes described here is introduced in slightly different way than in *Chapter 4*. Here we operate with the wavefunctions, whereas in previous *Chapter* we used matrix elements. Thus the parameter  $\beta$  does not mean the same in both cases.

experimental results, we can give a geometrical representation of the exciton spin dynamics based on the analogy to the Larmor precession in a magnetic field of a classical magnetic moment  $\vec{S}$  whose components are given by  $S_i = Tr(\hat{\rho}\sigma_i)$ .

### 5.1.2 Geometrical representation of spin precession

The geometrical representation by a classical magnetization vector  $\vec{S}$  helps to guess more intuitively exciton spin dynamics and to interpret the analytical solutions. To depict the precession of the effective magnetization  $\vec{S}$ , we will use the Poincaré's sphere representation. A point on this sphere represents a pure quantum state, while a vector of length inferior to the sphere radius represents a statistical mixture of states (or an uncertain state). The relation between the polarization of the emitted light and  $\vec{S}$  deduces straightforwardly from Eq.'s 5.7-5.10. If we consider pure heavy-hole exciton states (i.e.  $\beta = 0$ ), the  $\sigma^\pm$  polarization corresponds to the point of coordinates  $\pm\vec{u}_z$  (the north and south poles), as illustrated in Figure 5.2 (a). The equator plane represents the linear polarization states. If we choose the  $x$  axis for the Pauli matrices such that  $\alpha_0 = 0$ , then the symmetrical points defined by  $\vec{u}_x$  and  $-\vec{u}_x$  correspond to the linear polarization states along both QD eigenaxes in real space. Another specific points are  $\pm\vec{u}_y$  which correspond in real space to the  $45^\circ$  linear polarization states with respect to the QD eigenaxes. The two in-plane axes  $x$  and  $y$  of the Poincaré's sphere define thus two interesting polarization bases which will be also named "QD-basis" and " $45^\circ$ -basis", respectively. Similarly, the north and south poles are related to "circular-basis". The very interesting feature of this representation is that the projection of  $\vec{S}$  on one of these axes gives the degree of polarization measured in the corresponding basis. In experiments which are not time-resolved, we need further to average this projection during the dynamical evolution of  $\vec{S}$ . When neglecting the spin relaxation ( $\tau_s \gg \tau_r$ ), the latter deduces straightforwardly from Eq. 5.2 and simply reads:

$$\frac{\partial \vec{S}}{\partial t} = \vec{\Omega} \times \vec{S} - \frac{\vec{S} - \vec{S}_0}{\tau_r} \quad (5.11)$$

where  $\vec{S}_0$  is the initial magnetization vector (an analog of  $\hat{\rho}_0$  in density matrix formalism), and  $\vec{\Omega} = (\Omega_{ex}, 0, \Omega_z)$  acts as an effective magnetic field (we still assume  $\alpha_0 = 0$ ). The first term in righthand side of Eq. 5.11 illustrates the precession of  $\vec{S}$  about this field at a Larmor pulsation  $\Omega = \sqrt{\Omega_{ex}^2 + \Omega_z^2}$ , while the second term represents the damping/source mechanism. Without external field, the precession vector  $\vec{\Omega}$  is non-zero because of the electron-hole exchange and lies in the equatorial plane. When a magnetic field is applied the precession vector  $\vec{\Omega}$  gets out of this plane. Noteworthily, its strength and sign strongly influence the projection of  $\langle \vec{S}(t) \rangle_t$  on the  $x$ -axis, i.e. the degree of linear polarization in the QD-basis (see Fig. 5.2). In particular, it considerably increases the conversion of linear polarization from the  $45^\circ$ -basis or circular basis (determined by  $\vec{S}_0$ ) with an odd symmetry: changing the sign of the field is equivalent with changing the sign of  $\vec{S}_0$ .

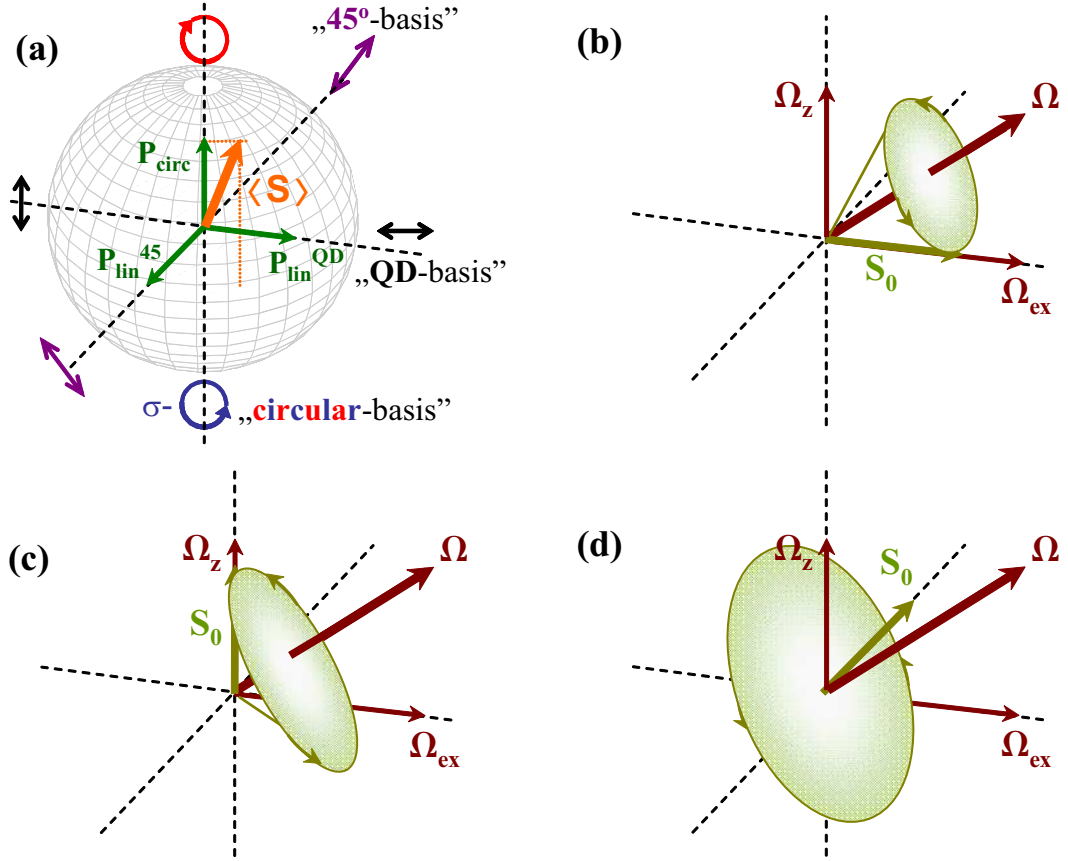


**Figure 5.2.** Scheme of the Poincaré's sphere (a): the three bases are marked, namely "QD-basis", "45°"-basis", and circular-basis. Examples illustrating spin precession in magnetic field for three cases: (b) initial spin vector parallel to one of the direction in QD-basis, (c)  $\vec{S}_0$  along one of circular-basis direction, and (d)  $\vec{S}_0$  parallel to one of 45°-basis direction. Spin relaxation is neglected.

The description presented above is very general. Let us now consider a few simple cases defined by an initial  $\vec{S}_0$  which may have been created by a ps-pulse at  $t = 0$ , in the regime  $\nu \gg 1$  (neglecting spin relaxation):

- $\vec{S}_0 = \vec{u}_x$

Figure 5.2 (b) illustrates the situation when the initial spin vector  $\vec{S}_0$  is parallel to the effective magnetic field, namely to one of the directions in "QD-basis". The spin vector precesses around the total field (sum of effective exchange field and external magnetic field). In this simple geometrical representation it becomes obvious that under such conditions a non-zero projection on the  $\vec{u}_z$  axis reveals in experiment as a degree of circular polarization. Hence linearly polarized excitation can convert into circularly polarized emission (**linear-to-circular polarization conversion**).

- $\vec{S}_0 = \vec{u}_z$

If the initial spin vector is parallel to external magnetic field (along  $\vec{u}_z$ ) (see Fig. 5.2 (c)) then one gets analogical situation to the previous case – under circularly polarized light the emission occur in linear polarization (**circular-to-linear polarization conversion**).

- $\vec{S}_0 = \vec{u}_y$

**No conversion** effect occurs when the precession vector  $\vec{\Omega}$  is perpendicular to  $\vec{S}_0$  as its average obviously vanishes. This occurs when the initial spin vector is parallel to  $\vec{u}_y$  whatever the strength of the magnetic field is.

Classical description of spin  $\vec{S}$  precession allows to predict phenomenon of polarization conversion. Additionally if we consider only two-level excitonic system, the simple geometrical representation brings together polarization of the excitation light and spin properties of excitonic state. This model was extensively used by other authors used to describe the conversion effect in quantum wells [128, 129] and QD ensemble [131]. Nevertheless we prefer to use density matrix formalism to describe spin coherence in quantum dots. More naturally one can include there the interaction with environment and some other features of QDs, like e.g. heavy-to-light hole mixing. Thus it offers more precise calculations of the conversion.

### 5.1.3 Polarization relaxation and conversion in cw experiments

As seen in the previous *Section*, the time evolution of the exciton spin  $\vec{S}$  can be translated in terms of optical alignment and polarization of the photoluminescence. In this *Section*, we will solve Eq. 5.2 in case of cw excitation and in presence of an external longitudinal magnetic field. For such a stationary problem, which is formally characterized by  $d\hat{\rho}/dt = 0$ , the creation term in Eq. 5.2 has the form of normalized<sup>9</sup>  $\rho_0/\tau_r$ , where  $\rho_0$  is the density matrix determined by the excitation intensity, optical selection rules, and the polarization chosen for the excitation. In stationary regime the solutions of Eq. 5.2 are analytical. Yet, only for pure heavy-hole excitons ( $\beta = 0$ ), we could express the degree of PL polarization in formulas of reasonable size. First, it turns out useful to define some new reduced parameters as follows:

$$\begin{aligned}
 T &= (\tau_r^{-1} + \tau_s^{-1})^{-1} && \text{Exciton spin effective lifetime.} \\
 \nu &= \Omega T && \text{Typical precession angle during spin lifetime.} \\
 \eta &= T/\tau_r = \tau_s/(\tau_s + \tau_r) && \text{Spin conservation parameter.} \\
 \gamma &= \Omega_z/\Omega && \text{Relative strength of applied magnetic field.}
 \end{aligned}
 \tag{5.12}$$

---

<sup>9</sup>normalized to  $n_X$ .

Obviously the model developed above is valid for any polarization of excitation and detection, but in the following we will restrict ourselves to three specific configurations:

**(i) Optical orientation/alignment of exciton spin**

In this configuration, the degree of PL polarization is measured in the same basis as the excitation. The wording “orientation” is generally used for the circular basis, whereas the term “alignment” better fits to the QD-basis [38]. Such a simple configuration enables first to check the efficiency of the quasi-resonant phonon-assisted excitation scheme as well as possible spin relaxation.

Considering that the generated exciton polarization is oriented at angle  $\alpha$  and amounts to  $P_{lin}^0$ , we find that the linear polarization measured in PL is:

$$P_{lin}(\theta) = \eta P_{lin}^0 \frac{1 + (1 - \gamma^2)\nu^2 \cos^2 \theta}{1 + \nu^2} + \cos \theta \sqrt{1 - \gamma^2} (\eta - 1) \tanh \left( \frac{\hbar\Omega}{2k_B\Theta} \right) \quad (5.13)$$

where  $\theta = 2(\alpha - \alpha_0)$  is twice the angle between the optical alignment axis defined by  $\alpha$  and the QD eigenaxis defined by  $\alpha_0$ . Similarly, for an initial polarization  $P_{circ}^0$ , the measured circular polarization signal reads:

$$P_{circ} = \eta P_{circ}^0 \frac{1 + \gamma^2\nu^2}{1 + \nu^2} + \gamma(\eta - 1) \tanh \left( \frac{\hbar\Omega}{2k_B\Theta} \right) \quad (5.14)$$

In zero magnetic field ( $\gamma = 0$ ), this provides a simple and direct estimate on the value of FSS and on its possible dependence against e.g. an electric field. This will be shown experimentally in the next *Section*.

**(ii) Conversion from linear polarization to circular polarization**

Here we consider an excitation linearly polarized at an angle  $\alpha$  and we assume that it yields an effective initial polarization  $P_{lin}^0$ . The initial density matrix reads:

$$\hat{\rho}_0 = \frac{1}{2} \begin{pmatrix} 1 & -P_{lin}^0 e^{-2i\alpha} \\ -P_{lin}^0 e^{2i\alpha} & 1 \end{pmatrix} \quad (5.15)$$

and the degree of circular polarization which results from the averaged precession of exciton spin reads:

$$P_{l2c}(\theta) = -\sqrt{1 - \gamma^2} \left[ \frac{\eta\nu}{1 + \nu^2} (\gamma\nu \cos \theta + \sin \theta) P_{lin}^0 + \gamma(\eta - 1) \tanh \left( \frac{\hbar\Omega}{2k_B\Theta} \right) \right] \quad (5.16)$$

where  $\theta = 2(\alpha - \alpha_0)$ .



### (iii) Conversion from circular polarization to linear polarization

Similarly, for a circularly polarized excitation producing the effective initial exciton polarization  $P_{circ}^0$ , the source density matrix is given by:

$$\hat{\rho}_0 = \frac{1}{2} \begin{pmatrix} 1 + P_{circ}^0 & 0 \\ 0 & 1 - P_{circ}^0 \end{pmatrix} \quad (5.17)$$

The resulting linear polarization of photoluminescence measured in a basis specified by the angle  $\alpha$  reads:

$$P_{c2l}(\theta) = \sqrt{1 - \gamma^2} \left[ \frac{\eta\nu}{1 + \nu^2} (-\gamma\nu \cos \theta + \sin \theta) P_{circ}^0 + (\eta - 1) \cos \theta \tanh \left( \frac{\hbar\Omega}{2k_B\Theta} \right) \right] \quad (5.18)$$

where again  $\theta = 2(\alpha - \alpha_0)$ . As it could be expected, in both cases, the polarization conversion depends only on the relative angle between the chosen basis of linear polarization (for excitation or detection) and the QD-basis<sup>10</sup>.

In zero magnetic field ( $\gamma = 0$ ), these expressions are identical to formulas obtained by G. V. Astakhov *et al.* [131] who used the equivalent formalism of classical magnetic moment  $\vec{S}$ . In Eq.'s 5.16 and 5.18, we can easily identify the different causes of spin precession discussed above with the geometrical representation. Here are a few general comments:

1. If there is no QD FSS, then  $\gamma = 1$  (or indefinite in zero field) and no conversion effect occurs. In other words the exciton spin is essentially conserved, apart from possible spin relaxation, whatever the excitation polarization is.
2. If the spin lifetime is very short as compared to  $\tau_r$  (i.e.  $\eta \rightarrow 0$ ), again no real conversion occurs. The PL polarization is determined by the polarization of the QD eigenstates onto which the system thermalizes. Besides, the magnetic field influences the linear or circular polarization by changing these eigenstates. More specifically, the linear polarization given by Eq. 5.18 goes monotonously to zero when  $B_z$  increases (i.e.  $\gamma \rightarrow 1$ ) at a rate which depends on the temperature  $\Theta$ , while the circular polarization given by Eq. 5.16 increases, also depending on  $\Theta$ .
3. In zero magnetic field ( $\gamma = 0$ ), and neglecting now the spin relaxation ( $\eta = 1$ ), Eq's. 5.18 and 5.16 show that the maximum of polarization conversion is achieved for  $\theta = \pi/2$ , i.e. for an angle  $\alpha = \alpha_0 + \pi/4$  corresponding to the "45°-basis". Obviously, the larger  $\nu$  the weaker the conversion effect, as we expect due to averaging over an increasing number of quantum beats.
4. Eventually, the magnetic field contributes also to the degree of polarization conversion, yet in an orthogonal basis, i.e. when the linear polarization exci-

---

<sup>10</sup>Note that in previous *Chapter 4* we did not need to introduce a phase for the orientation of QD anisotropy  $\alpha_0$ , because all calculations were done in "QD-basis".

tation (or detection) corresponds to the QD-basis. In this case the maximum conversion ratio cannot exceed 50% (see Eq's. 5.16 and 5.18).

## 5.2 Measurements of optical orientation/alignment of excitonic state

### 5.2.1 Optical orientation vs. fine structure splitting (FSS)

First, we present results of polarization-resolved micro-photoluminescence measurements performed on single InAs/GaAs quantum dots under quasi-resonant excitation at about  $2LO$  phonons above the excitonic transition. The original idea of this experiment was to check whether the exciton spin degeneracy can be measured via optical orientation effects. The principle is shown schematically in Fig. 5.3. For simplicity let us restrict ourselves to a circular excitation. Under such a quasi-resonant excitation one cannot obtain a strongly circularly polarized PL signal from a significantly anisotropic QD (see part b) of Fig. 5.3) since the QD eigenstates are linearly polarized. Either circular-to-linear conversion, or spin relaxation occurs. These effects may give rise to a significant degree of linear polarization either in the  $45^\circ$ -basis, or in the QD-basis, whereas the circular polarization remains rather small. Yet, when tuning the fine structure splitting by e.g. an electric field, one may gradually reach the situation of exact exciton degeneracy (see Fig. 5.3(a)). In such a case, the initial exciton circular polarization should be conserved during the exciton lifetime (neglecting possible spin relaxation). As a result, measuring the PL circular polarization provides a very sensitive probe of the excitonic system in the perspective of entangled photon emission.

The sample  $A_{35}^{SSetch}$  with in-plane electrical gates (see *Chapter 3*) was used for the experiment. We found a specific QD with a small FSS, that moreover could be tuned through zero (see Fig. 5.4(a)). The level degeneracy was first measured by linearly-polarized detection along the two linearly polarized components of the excitonic doublet (under excitation linearly polarized at  $45^\circ$ ). Under quasi-resonant pumping of the exciton level with  $\sigma^+$  light, we observed a clear enhancement of the degree of circular polarization for the same applied voltage of zero crossing (see Fig. 5.4(b)). The degree of PL polarization depending on the excitation is theoretically given by Eq. 5.14. In cw experiments one measures the effective lifetime  $T = (\tau_r^{-1} + \tau_s^{-1})^{-1}$  of the exciton polarization. When neglecting exciton thermalization during the exciton lifetime (here  $\delta_1/k_B T < 0.01$  and  $\tau_s > \tau_r$ ), the time-averaged degree of PL circular polarization is theoretically given by [129]:

$$P_{circ} = \frac{\eta P_{circ}^0}{1 + (\delta_1 \eta \tau_r / \hbar)^2} \quad (5.19)$$

where  $\eta = \tau_s / (\tau_s + \tau_r)$  and  $P_{circ}^0$  is the effective initial circular-polarization determined by the laser polarization, but possibly reduced during the secondary emission of LO-phonons.

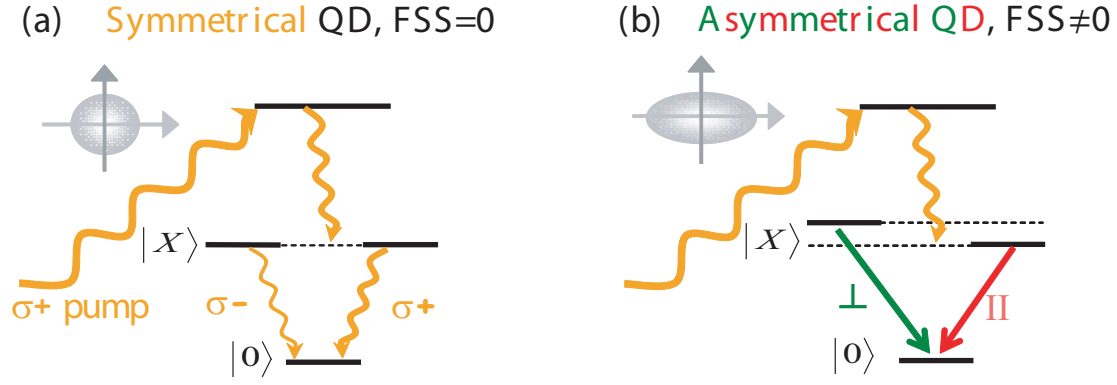


**Figure 5.3.** Idea how to test the spin degeneracy of the excitonic states. Under fixed circularly polarized pump we probe the polarization of the emission while tuning the splitting through zero. It is sufficient to measure the circular polarization degree, which should be zero in case of big splitting (part b)) and enhanced if FSS= 0 (part a)).

Let us notice a direct correspondence of this formula to the well-known Hanle effect [135, 136], with  $\delta_1$  playing the role of the Zeeman splitting in the transverse magnetic field. By tuning  $\delta_1$  with an electric field and monitoring the PL circular polarization we are thus able to detect the restoration of the exciton degeneracy with the precision corresponding to the homogeneous linewidth  $\hbar/T$ . This accuracy is precisely that required for applicability of quantum dot to emission of entangled photon pairs. Like in Hanle experiments, by fitting with Eq. 5.19 the polarization dependence on  $\delta_1$  one can determine the effective exciton polarization lifetime which is masked by inhomogeneous broadening and spectral resolution in  $\mu$ -PL spectroscopy.

Under quasi-resonant pumping of the exciton level with  $\sigma^+$  light, we observed a clear enhancement of the degree of circular polarization for the applied voltage corresponding to zero crossing, with a maximum value of about 70%. Remarkably, the circular polarization resonance plotted as a function of fine structure splitting ( $\delta_1$ ) can be fitted with the Lorentzian function in Eq. 5.19 as shown in Fig. 5.3. Note we limited ourselves to the range of bias for which neither the line intensity nor the linewidth are dramatically affected by the electric field. This guarantees that only the splitting  $\delta_1$  experiences appreciable variations while other parameters in Eq. 5.19 remain essentially constant. Within our model, two parameters are determined from the fit: the maximum polarization degree  $\eta P_{circ}^0 = 0.66 \pm 0.05$  and the resonance FWHM  $2\hbar/\eta\tau_r = 3.6 \pm 0.3 \mu\text{eV}$ . Neglecting any polarization loss in the two phonon quasi-resonant excitation ( $P_{circ}^0 = 1$ ) would lead to estimates of  $\tau_r = 0.6$  ns and  $\tau_s = 0.97$  ns. The  $\tau_r$  value reasonably compares with data available from time-resolved measurements [56, 84] or transmission spectroscopy on similar QDs [58]. The value of  $\tau_s$  may actually be larger if other broadening mechanisms are taken into account, e.g. the effective exciton lifetime may be reduced due to the in-plane electric field and possible charge fluctuations in the vicinity of the QD. As an improvement of the measurement presented here, using an excitation at 1LO phonon above the exciton ground state should increase the initial polarization

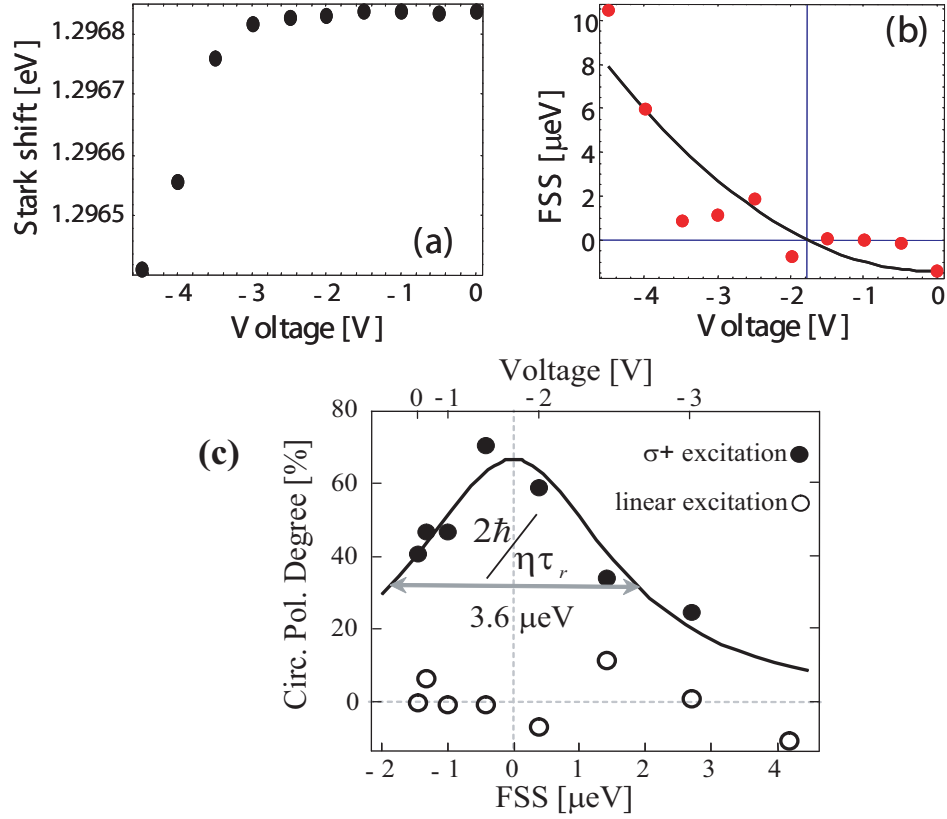


**Figure 5.4.** [Sample  $A_{35}^{S5etch}$ ] (a) Stark shift induced by in-plane electric field. (b) FSS vs. applied bias (measured as a difference in the excitonic line position for two orthogonal linear polarization of detection) under linear  $45^\circ$  excitation. (c) Circular polarization degree vs. voltage (upper axis) and FSS (lower axis) measured under circular  $\sigma+$  and linear  $45^\circ$  excitation, closed and opened symbols respectively.

state close to 100%, enabling the absolute determination of both lifetimes <sup>11</sup>.

This method for probing the strength of FSS and its effective change via optical orientation experiment in a field effect structure seems very promising as a preliminary test for entanglement possibility of two photons in biexciton-exciton cascade. Its clear advantage is that it measures how much the exciton spin (the intermediate state in a biexciton cascade) is effectively conserved, including both the effect of non-zero FSS and possible decoherence. Another factor to consider when checking the entanglement is the time of measurements. To record a reliable photon statistics under pulsed excitation one needs hours, and to conclude about the entanglement one has to perform measurements in few different basis. By using the method proposed above one can determine the potential of a specific QD for polarization entanglement in much less than one hour.

<sup>11</sup>This study which actually was rather preliminary, revealed the importance of careful laser filtering and single QD selection. In the results presented in the next *Section* we overcame this problem and used 1 LO phonon excitation.

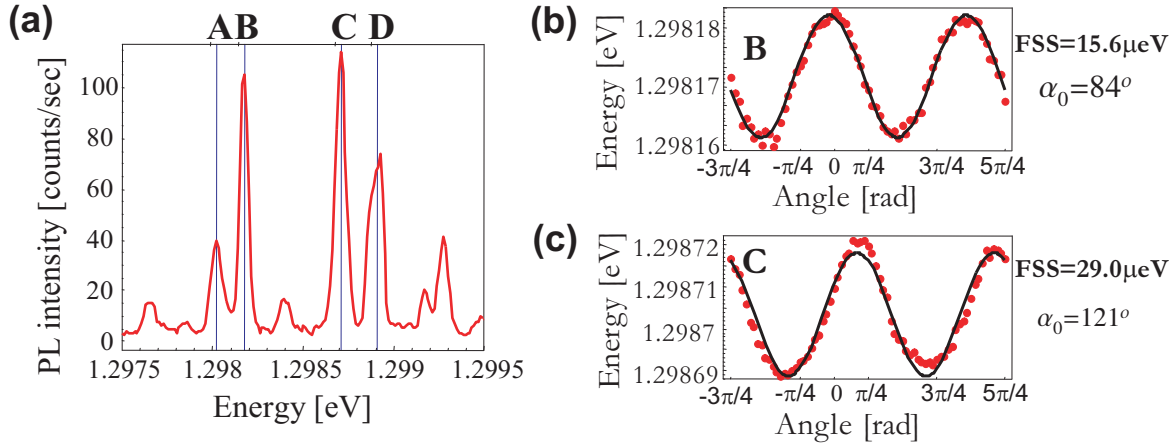


**Figure 5.5.** [Sample  $B_{35}^{nS}$ ] (a) PL spectra of individual quantum dots under quasi-resonantly (1LO-Phonon assisted) excitation. Four excitons from different QDs are labeled A, B, C, and D. (b) and (c) Evolution of energy position of the excitonic lines B and C as a function of the linear analyzer rotation angle. Points – central line energy from Gaussian fit, solid line – cosine fit with constant offset, from which FSS and orientation of the QD eigenaxis ( $\alpha_0$ ) deduce.

## 5.2.2 Optical orientation for different excitation polarizations

In order to improve conditions of resonant excitation we have investigated QDs excited at about  $1LO$  above their ground state emission. These studies have been carried out for the vertical electric field sample  $B_{35}^{nS}$  with the  $\mu$ -PL set-up dedicated to magneto-optics studies described in *Chapter 2*. With such a sample the FFS is only weakly modified by the gate voltage, as compared to in-plane field structures<sup>12</sup>. However, the applied bias enables to control the charge state of QDs which is of major importance for studying optical orientation and polarization conversion effects. Basically, we used a fixed bias of  $+0.2 V$  which corresponds to the center of the neutral exciton plateau as explained in *Chapter 2*.

Figure 5.5 (a) shows the PL spectrum of a few QDs that we have selected for the conversion experiments. We chose this set of lines after moving with  $1 \mu\text{m}$ -step the sample in the focal plane of the set-up (excitation and excitation energy being fixed) until we find lines of high brightness<sup>13</sup>, sufficiently separated in spectral domain and in obvious resonance with the laser excitation. In this *Section*, we will focus more specifically on the excitons denoted B and C which are well representative of the investigated physics. Actually, in the series of measurements performed at this position almost 10 lines could be analyzed and exhibited similar behaviors. The right-hand side of Fig. 5.5 reports the energy position of lines B and C as a function of the rotation angle  $\alpha$  of the linear analyzer. From this preliminary

<sup>12</sup>We yet observed in some cases an increase of circular polarization when tuning the voltage, which could be associated to the reduction of the splitting down to  $\sim 2\mu\text{eV}$ , but with no clear resonance as reported above.

<sup>13</sup>According to our own standards – 100 counts per second.

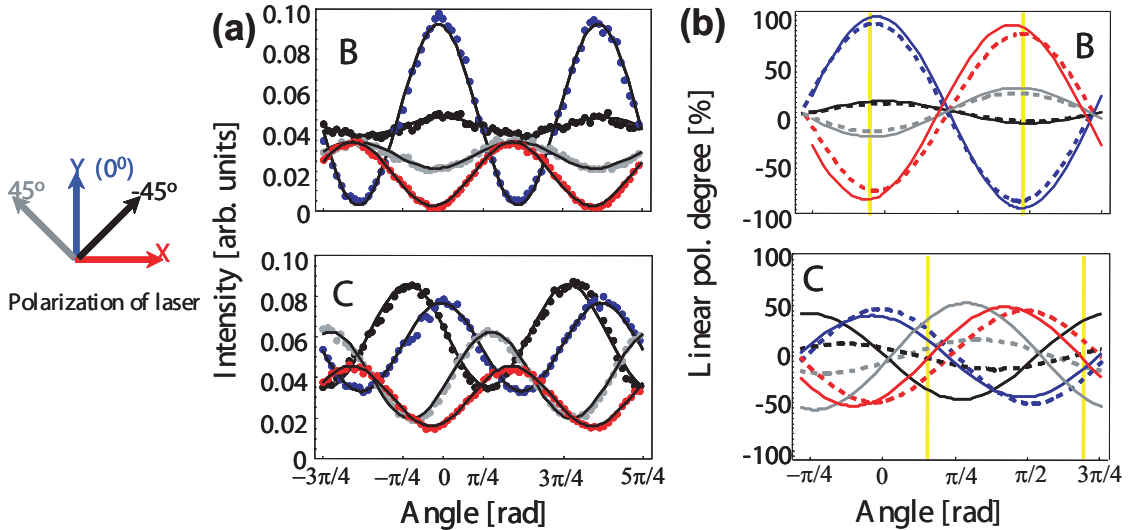


**Figure 5.6.** [Sample  $B_{35}^nS$ ] Left – scheme of the excitation polarizations: blue (Y) – vertical polarization, red (X) – horizontal polarization, black –  $45^\circ$ , gray –  $-45^\circ$ . (a) Intensity evolution for excitons  $B, C$  (upper, and lower part of the graph) as a function of the detection angle. Points – experimental data, solid lines – cosine fits with constant offset. Four colors correspond to four different excitations. (b) Calculated from part (a) linear polarization degree for excitons  $B, C$  as a function of the angle basis. Dashed lines presents theoretical calculations described in the text. Yellow lines mark the “QD-basis”.

measurement we can extract both parameters which characterize the anisotropy of these QDs, i.e. the FSS (around  $15\mu\text{eV}$  for exciton  $B$  and  $30\mu\text{eV}$  for exciton  $C$ ) and the orientation of their eigenaxes  $\alpha_0$  defined with respect to one of the cleaving planes of the sample. QD- $B$  is nearly oriented along that plane, while QD- $C$  is strongly tilted by around  $30^\circ$ .

In Fig. 5.6 the studies of optical alignment for excitons  $B$  and  $C$  are presented. Four different linear polarizations of the excitation were used successively as illustrated on the left-hand side – horizontal ( $X$ ),  $-45^\circ$ , vertical ( $Y$ ), and  $+45^\circ$  in the referential of the laboratory<sup>14</sup>. These specific directions, which were chosen before the precise determination of QD eigenaxes shown in Fig. 5.5, correspond almost to the directions of the QD-basis or  $45^\circ$ -basis for QD- $B$ , but turn out to be significantly tilted for QD- $C$ . The PL intensity measured as a function of the linear analyzer angle is shown in Fig. 5.6(a). It presents strong oscillations evidencing a large degree of optical alignment, while the averaged PL intensity depends also on the excitation polarization, indicating a possible dichroism. However, as the latter could be due to a slight displacement of the laser spot when changing excitation polarization,<sup>15</sup> we will focus on the polarization degree measured at a

<sup>14</sup>The sample was mounted with cleaved edges approximately parallel to vertical and horizontal directions within a precision better than  $5^\circ$ .

<sup>15</sup>In experiments, we did not check the full symmetry of this effect by rotating by  $\pi$  the linear polarizer. Yet, as this effective degree of linear polarization is not constant for all the lines in the same PL spectra, its interpretation in terms of QD dichroism is quite

fixed polarization, defined by  $(I_\alpha - I_{\alpha+\pi/2})/(I_\alpha + I_{\alpha+\pi/2})$  and shown on the right-hand side of Fig. 5.6<sup>16</sup>. Obviously, excitons *B* and *C* exhibit different behaviors. For QD-*B*, a very efficient optical alignment characterized by a degree of linear polarization over 80% is achieved for excitation polarization *X* and *Y*, i.e. almost parallel to the QD eigenaxes, while for polarizations at  $\pm 45^\circ$ , the amplitude is much smaller. This effect is perfectly well reproduced by Eq. 5.13 (dashed lines in Fig. 5.6(b)) by taking into account the small misalignment ( $6^\circ$ ) of the excitation polarization with respect to the QD eigenaxes, which yields the non-zero effect for  $\pm 45^\circ$  polarizations, and a finite heavy-light hole mixing ( $\beta = 0.04$ ) to explain the small difference in amplitude between *X* and *Y* polarizations<sup>17</sup>. The important result drawn out from this measurement is the long spin lifetime of the exciton spin as compared to  $\tau_s$ , which clearly contradicts the conclusion of Ref. [130]. Theoretically, this result only proves that there is no spin relaxation between both eigenstates of the system. The conversion measurements discussed further will enable us to assess whether this conclusion holds also for the exciton coherence.

For exciton *C*, all excitation polarizations are significantly off the QD eigenaxes. For this reason, the efficiency of optical alignment turns out to be strongly reduced, even though it still amounts to  $\sim 40\%$ , and depends only weakly on the specific excitation polarization. This effect is well explained by our model. However, the shift of the alignment maxima is definitely more surprising: to the first order, these maxima should correspond to the QD eigenaxes which determine the effective magnetic field  $\vec{\Omega}$  about which the exciton spin precesses whatever its initial spin orientation. Here, it clearly follows the angular orientation of excitation polarization. The only way to reproduce this effect within our model requires to assume a relatively short exciton lifetime in order to simulate a small number of spin precessions ( $\nu \sim 1$ )<sup>18</sup>. We do not have a direct evidence for such a reduced lifetime, but we observed a clear increase of exciton *C* linewidth ( $\sim 60 \mu\text{eV}$ ) as compared to other lines ( $\sim 35 \mu\text{eV}$ ) which supports this conclusion: if we ascribe the difference of  $\sim 25 \mu\text{eV}$  to a lifetime reduction it gives us an upper value for  $\tau_r$  of  $\sim 25 \text{ ps}$  (<sup>19</sup>). The quasi-resonant nature of the excitation could explain this unusual property, if e.g. stimulated emission takes place. With such a parameter, the theoretical model provides a good agreement with the measurements (see dashed lines in Fig. 5.6(b) bottom). Nevertheless, this assumption is not very satisfying.

---

plausible.

<sup>16</sup> $I_\alpha$  is the PL intensity at detection angle  $\alpha$ , actually determined from the cosine fit shown in Fig. 5.6.

<sup>17</sup>A “good probe” of light-hole admixture is linear polarization degree under non-resonant excitation. In our situation it was not possible to perform such a test. We worked with high QD-density part of the sample and under non-resonant excitation too many lines (other excitons and excitonic complexes) appeared in the spectra.

<sup>18</sup>A shorter spin lifetime could also reduce the effective number of spin precessions, but it would also drastically reduce the degree of optical alignment.

<sup>19</sup>We remind that our optical set-up provides an ultimate spectral resolution of  $\sim 25 \mu\text{eV}$  and that some spectral diffusion which depends on specific excitation condition, also contributes to the experimental linewidth.

We will see in the next *Section* that Exciton  $C$  has a rather “pathological” behavior which can not be fully described by our model.

Finally, all our measurements of individual QDs (not only  $B$  and  $C$ ) under quasi-resonant excitation have revealed a large degree of optical alignment which evidences that exciton spin relaxation is essentially suppressed at the timescale of the exciton recombination. In the next *Section*, we will see that this conclusion can be extended to the coherence of excitonic polarization states.

### 5.3 Measurements of polarization conversion: a test for excitonic spin coherence

We have investigated the phenomenon of polarization conversion on the same set of excitonic lines presented above for both configurations discussed theoretically in *Section 5.1*. The degree of linear (circular) polarization was studied under circular (linear) polarization of excitation. From the model, we expect emission from states with a specific electric-dipole moment different from the photo-created one. Additionally, a longitudinal magnetic field was applied to the structure in the range  $-0.5 \rightarrow +0.5$  T in order to evidence the competition between exchange and magnetic fields. This also enables to rule out any possible artifacts due the optical set-up as the magnetic field dependence has a very specific symmetry.

#### 5.3.1 Conversion of circular-to-linear polarization of the emission from a single QD

As long as the exciton spin relaxation is negligible, Eq. 5.18 shows that the linear polarization depends linearly on the initial circular polarization  $P_{circ}^0$ . In particular, it must change sign when the  $\sigma^+$  excitation is changed to  $\sigma^-$ . This prediction has been verified in a small magnetic field ( $\sim 30$  mT) which enables to enhance the degree of conversion, because for most of the excitons we have studied the precession angle  $\nu = \Omega T$  is generally much larger than 1. Under this condition the conversion can be measured in the QD-basis (a term  $\propto B_z \nu^2 / (1 + \nu^2)$ ). The results are presented in the upper part of Fig. 5.7 for excitons  $B$  and  $C$ . In both cases, we clearly observe a change of sign between  $\sigma^+$  and  $\sigma^-$  excitation. As expected the conversion is maximum in the QD-basis (vertical dashed lines) for exciton  $B$ , whereas for exciton  $C$  there is a significant shift of the maximum conversion with respect to its eigenaxes. This again reveals that exciton  $C$  has a specific behavior characterized by  $\nu \sim 1$ . In a weak magnetic field there is a competition between conversion into the QD-basis versus the  $45^\circ$ -basis (see Eq. 5.18). When increasing the magnetic field the maximum of conversion will progressively move to the QD-basis. Eventually, the comparison between  $\sigma^+$  and  $\sigma^-$  excitation reveals also an asymmetry in the absolute value of the linear polarization which is not predicted by Eq. 5.18. We will see further that this effect can be ascribed to the heavy-light hole mixing neglected in Eq. 5.18.

For measuring the circular-to-linear polarization conversion as a function of a longitudinal magnetic field, we have recorded a series of 399 PL spectra. The field



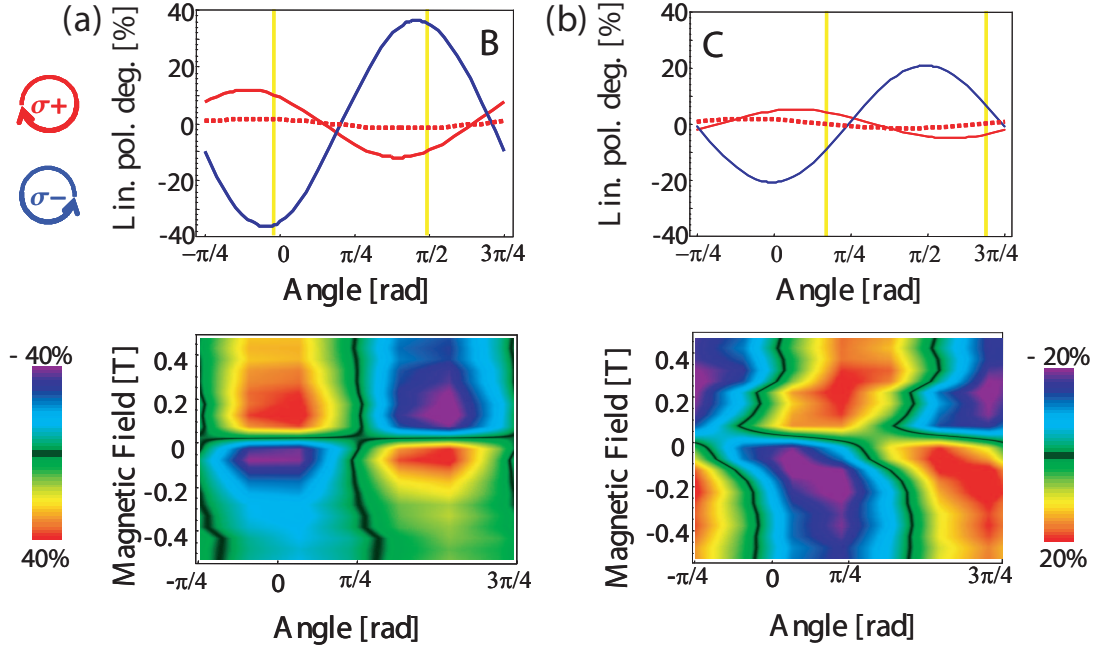


**Figure 5.7.** [Sample  $B_{35}^{nS}$ ] Upper part: linear polarization degree vs. detection angle under circular excitation  $\sigma+$  (red) and  $\sigma-$  (blue) for excitons  $B$  – part (a) and  $C$  – part (b). Solid lines: measurements at small magnetic field  $+0.028T$ , dotted line – measurements at zero field. Yellow lines mark the “QD-basis”. Below: evolution of linear polarization degree (encoded in a color scale) in longitudinal magnetic field for excitons  $B$  and  $C$ , respectively.

was varied from  $-0.5 T$  to  $+0.5 T$  with a step of  $50 mT$ , and the linear analyzer from  $-90^\circ$  to  $+90^\circ$  with a step of  $10^\circ$ , while the excitation polarization was kept unchanged ( $\sigma^+$ ). The results are presented in the lower part of Fig. 5.7 with shows 2D interpolated density plots of the degree of circular polarization as a function of the magnetic field and of the basis angle.

For exciton  $B$  (lower part of Fig. 5.7 a), this measurement confirms the observation in a weak magnetic field (upper part). The level of conversion from circular to linear polarization reaches a maximum in the QD-basis for all the fields. It exhibits a change of sign between positive and negative fields (as expected from Eq. 5.18) which definitely guarantees that the measured linear polarization is not an artefact of the optical set-up. Besides, the absolute value depends on the sign of the magnetic field which is obviously equivalent to the difference between  $\sigma^+$  and  $\sigma^-$  excitation at weak magnetic field (upper part of Fig. 5.7 a). A probable explanation of this effect relies on a non-zero heavy- to light-hole mixing described by the parameter  $\beta$  which was introduced in the effective optical selection rules of the bright exciton (see eq. 5.10). For  $\beta \ll 1$ , we found that its first order contribution to  $P_{c2l}(\theta)$  reads:

$$-\frac{2}{\sqrt{3}}\beta \cos 2(\alpha + \psi) \quad (5.20)$$

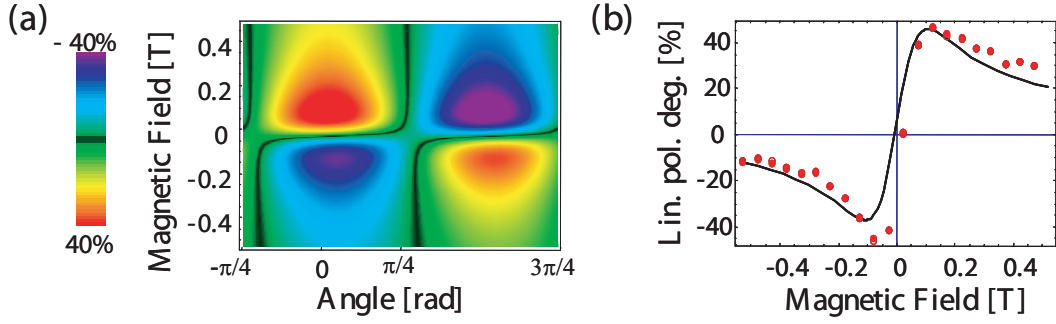


**Figure 5.8.** Left: Simulation of linear polarization degree vs detection angle under circular excitation for Exciton  $B$ . Right: Cross-section in the QD-basis showing the asymmetrical conversion due to the heavy- to light-hole mixing. Experimental data at  $\sim \pm 5^\circ$  off the QD-basis (red open and closed circles) and theory (solid line). Model parameters are:  $\delta_1 = 15.6 \mu\text{eV}$ , exciton effective  $g$ -factor  $g_X = 2.5$ , initial polarization  $P_{circ}^0 = 0.9$ , radiative lifetime  $\tau_r = 0.85$  ns, spin lifetime  $\tau_s = 10$  ns, HH-LH mixing  $\beta = 0.04$  and phase  $\psi = 10^\circ$ . Corresponding reduced parameters are following:  $\eta = 0.92$ ,  $\nu(B = 0) = 1.84$ , and  $\gamma \in [0, 4.65]$ .

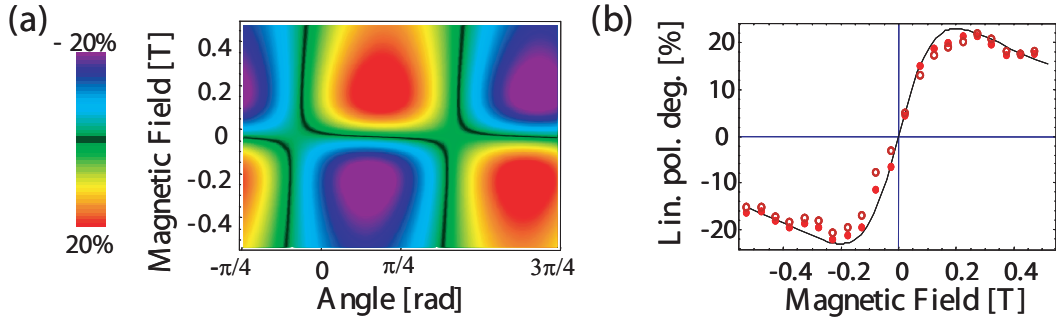


**Figure 5.9.** Left: Simulation of linear polarization degree vs detection angle under circular excitation for Exciton  $C$ . Right: Cross-section in the QD-basis showing the asymmetrical conversion due to the heavy- to light-hole mixing. Experimental data at  $\sim \pm 5^\circ$  off the QD-basis (red open and closed circles) and theory (solid line). Model parameters are:  $\delta_1 = 29 \mu\text{eV}$ , exciton effective  $g$ -factor  $g_X = 2.5$ , initial polarization  $P_{circ}^0 = 0.5$ , radiative lifetime  $\tau_r = 0.85$  ns, spin lifetime  $\tau_s = 10$  ns, HH-LH mixing  $\beta = 0.03$  and phase  $\psi = -50^\circ$ . Corresponding reduced parameters are following:  $\eta = 0.92$ ,  $\nu(B = 0) = 3.43$ , and  $\gamma \in [0, 2.5]$ .

where  $\psi$  is the complex phase of the mixing which determines in real space the axes for the maximum ( $\pi/2 - \psi$ ) and minimum ( $-\psi$ ) of the exciton oscillator strength in linear polarization. This term which is independent on magnetic field and initial exciton polarization results from the symmetry reduction of the QD. In consequence, we could expect it to possess the same eigenaxes as the electron-hole exchange term (i.e.  $\psi = -\alpha_0 \in [\pi/2]$ ), but if the actual symmetry is very far from  $C_{2v}$ , these terms may reveal uncorrelated<sup>20</sup>. By taking into account a heavy- to

<sup>20</sup>See Y. Léger *et al.*, Phys. Rev. B, to be published.

light-hole mixing parameter  $\beta = 0.04$  with associated eigenaxes slightly tilted from the QD ones ( $\psi = +10^\circ$ ) we could reproduce fairly well the field dependence of  $P_{c2l}$  for exciton  $B$ . The theoretical simulation is presented in Fig. 5.8. Note that the non-zero value of  $\psi$  enables us to reproduce the deviation from  $\pi/4$  of the zero crossing polarization at negative fields (black line in Fig. 5.7 a). The agreement obtained with our model of exciton spin dynamics enables to draw the main conclusion of these experiments: the very high degree of conversion obtained here, close to the maximum theoretical value of 50% (see Eq's. 5.16 and 5.18), proves the long-living coherence of the bright exciton spin (i.e. of any linear superposition of excitons  $|\pm 1\rangle$ ) during its radiative lifetime.

For exciton  $C$ , the field-induced evolution of polarization conversion appears dramatically different (see Fig. 5.7). The rotation of conversion basis is now more pronounced, and even exceeds the value of  $45^\circ$  corresponding to the passage from  $45^\circ$ - to QD-basis as predicted by Eq. 5.18. Choosing the angle  $\psi$  of the HH-LH mixing at  $\sim 45^\circ$  (with respect to the QD eigenaxes) enhances this effect as illustrated in Fig. 5.9. Simultaneously, it produces now a rather weak asymmetry between positive and negative fields. This result is obvious when considering Eq. 5.20 which shows how the angle  $\psi$  determines the basis into which the HH-LH mixing appears. However, our model turns out to be clearly insufficient to fully explain the field evolution measured for exciton  $C$ . In addition, slow spin relaxation and precess with respect to the exciton lifetime considered previously in *Section 5.2.2* to explain the large optical alignment for any linear polarizations is no longer valid. Even though some features of exciton  $C$  are qualitatively understood within our model, a more complete theory is certainly necessary. The latter would certainly require an extended basis, to e.g. better take into account the mixing between heavy and light holes and to possibly include the role of the dark excitonic states in an anomalous QD <sup>21</sup>. Other possible explanation of the "pathological" behavior of exciton  $C$  relies on taking into account experimental technique. One cannot be sure that this exciton is excited as resonantly as for example exciton  $B$ .

The recent results of polarization conversion published by G. V. Astakhov *et al.* [131] did not show such a complexity. This is obviously because they performed measurements on an ensemble of CdTe QDs, where averaging over a huge number of excitons (and possibly charged excitons) masks the richness of the exciton spin physics in QDs. In particular they could achieve only a small degree of optical orientation/alignment (around 3%), even though they concluded that the degree of conversion could reach 50%.

### 5.3.2 Conversion of linear-to-circular polarization from a single QD

In the previous *Section*, we have shown that the coherent exciton spin dynamics leads to the conversion of circular polarization to a linear polarization, an effect which is actually enhanced by applying a longitudinal magnetic field. This is not an obvious effect, even though we have in mind that the QD eigenstates

<sup>21</sup>When eigenaxes are not the same for exchange term and HH-LH term.

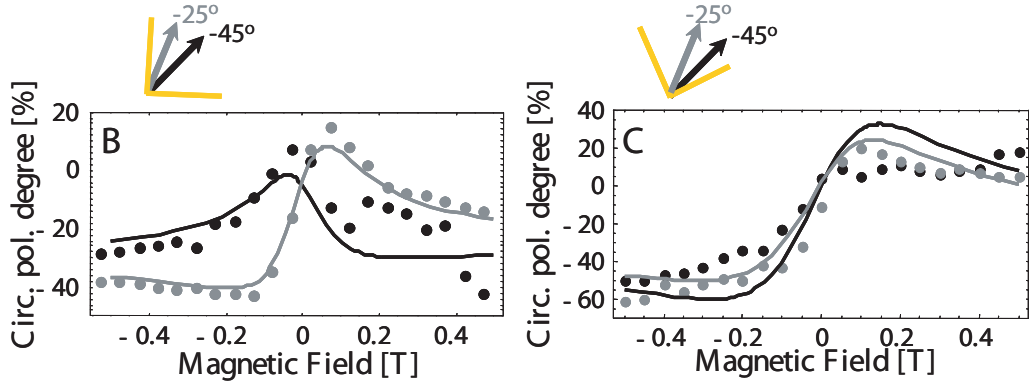


**Figure 5.10.** [Sample  $B_{35}^n$ ] Circular polarization degree vs. longitudinal magnetic field for excitons  $B$  (left) and  $C$  (right), measurements under two linear excitations:  $-45^\circ$  (black points) and  $-25^\circ$  (gray points). Lines – theoretical calculations described in the text. Above scheme of the direction of the excitation (corresponding black and gray arrows) with respect to the QD eigenaxes.

are linearly polarized: the conversion in the QD-basis first increases, while the QD eigenstates get progressively circularly polarized. In this *Section*, we will examine the counterpart of this effect, i.e. the conversion from linearly polarized excitation to a circularly polarized emission and its dependence on a longitudinal magnetic field. Again, the observed effect will contradict the naive intuition that a magnetic field leads irremediably to a circular polarization to satisfy the optical selection rules of the QD ground eigenstate. The expected conversion of polarization has a maximum in a finite magnetic field and then decreases to zero when the field gets higher.

Theoretically, Eq.'s 5.16 and 5.18 are very similar. Both effects depend on the same physical parameters and therefore should manifest themselves with the same efficiency. However, to evidence experimentally the conversion to circular polarization, we did not use a set-up enabling to rotate the excitation polarization step by step. For simplicity<sup>22</sup>, we only chose two specific angles, given by  $\alpha = -45^\circ$  and  $\alpha = -25^\circ$ , while the detection was performed alternatively in both  $\sigma^\pm$  polarizations. Besides, the excitation polarizations were not defined very precisely, because we simply used a second quarter-wave plate with axes parallel to those of the quarter-wave plate already installed, in order to form a half-wave plate. We could check that with this system the excitation was strongly linearly polarized but we did not pay much attention to its remaining circular polarization. The latter was actually quite significant as it appeared when the measurements were analyzed<sup>23</sup>. Figure 5.10 which reports the magnetic field dependence of the circular polarization

<sup>22</sup>Installing a second motor on the excitation path would have required too much time, with the risk to lose the position of the QD's  $B$  and  $C$ .

<sup>23</sup>We remind that a pure polarization state of light is in general elliptical with the property that  $P_{lin}^2 + P_{circ}^2 = 1$  where  $P_{lin}$  is the degree of linear polarization measured with respect to the ellipse eigenaxes, and  $P_{circ}$  the degree of circular polarization. For example,  $P_{lin}=0.99$  is still compatible with  $P_{circ}=0.14\dots$

for excitons  $B$  and  $C$ , shows that the average circular polarization is significantly shifted to negative values. This observation which is not expected from Eq. 5.16 can be interpreted when we take into account a finite circular polarization  $P_{circ}^0$  of the excitation beam. Actually it simply adds a term to Eq. 5.16 which reads:

$$\frac{1 + \gamma^2 \nu^2}{1 + \nu^2} \eta P_{circ}^0 \quad (5.21)$$

For excitons  $B$  and  $C$  we have seen that  $\nu \gg 1$ , therefore this term does not appear in zero magnetic field ( $\gamma = 0$ ): the initial spin component associated to  $P_{circ}^0$  precesses many times about the in-plane exchange magnetic field  $\vec{\Omega}_{ex}$  and then averages to zero. When a magnetic field  $B_z$  is applied ( $\gamma \neq 0$ ), it gives rise to a shift of the circular polarization toward the initial polarization  $P_{circ}^0$ , *independently* on the sign of  $B_z$ . In our experiments, this corrective term turns out to be of the same order of magnitude as the conversion term from the linear polarization, and therefore modifies strongly the field dependence expected from Eq. 5.16. In Fig. 5.10 we could fit fairly well the measurements with the same parameters used in previous *Section* by assuming effective excitation polarizations  $P_{lin}^0=0.95$  and  $P_{circ}^0=-0.3$ . In contrast to the conversion into linear polarization discussed in the previous *Section* we can remark that the heavy- to light-hole mixing plays a minor role here. It is rather intuitive that such a mixing may not privilege the PL signal in  $\sigma^+$  with respect to  $\sigma^-$  or vice versa. This intuition is confirmed by our analytical model which yields that the effect of HH-LH mixing consists in a reduction of circular polarization by a factor  $(1 - 4/3\beta^2)$  only, which besides can be neglected here because  $\beta^2 \ll 1$ .

As a conclusion, this series of measurements agrees also very well with the picture of an exciton spin *coherently* precessing during its radiative lifetime about the total effective magnetic field  $\vec{\Omega}$ .

### 5.3.3 Conversion of polarization for trions in a single QD

With the same sample we could investigate similarly optical alignment and polarization conversion for negative trions ( $X^-$ ) by setting the gate voltage to  $\sim +0.5$  V. Like an exciton, a trion is a 2-level system that can be described by a 1/2 pseudo-spin, which for  $X^-$  corresponds to the two hole states of angular momentum  $j_z = \pm 3/2$  (in  $D_{2d}$  symmetry). In principle, any superposition of these two states can be created, and its coherence could be studied in cw PL experiments. However, the trions differ from the excitons by two crucial features:

- In zero magnetic field, there is no fine structure splitting between the two levels.
- In a longitudinal magnetic field, the trion states are coupled by light to different singly charged QD states. For this reason, they do not form a  $\Lambda$ -like system and the coherent superpositions of trion states can neither be photo-created, nor evidenced in PL emission.

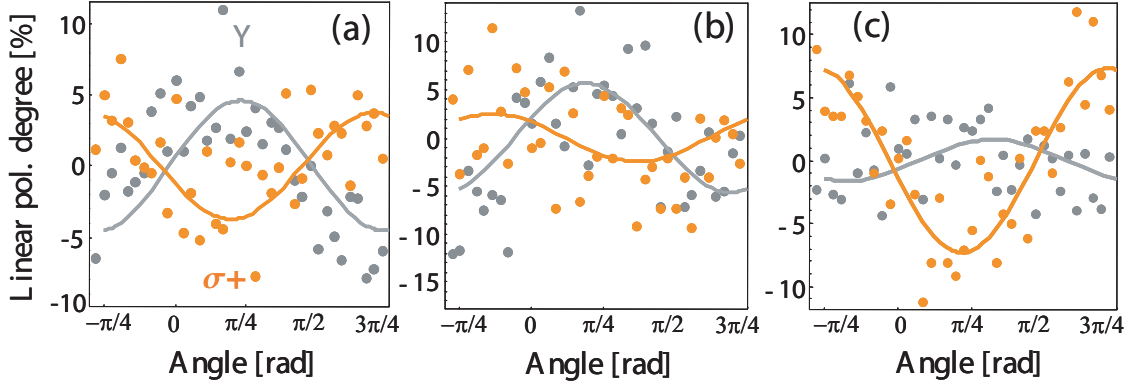


**Figure 5.11.** [Sample  $B_{35}^{nS}$ ] Linear polarization degree vs. basis angle for three negatively charged trions (a), (b), and (c). Two different polarizations of excitation were used – linear vertical (gray) and circular  $\sigma+$  (orange).

Taking into account these features, we found that the circular polarization of trion PL, which is actually given by the same equations 5.16 and 5.21, reduces to <sup>24</sup>:

$$P_{circ}^{X^-} = (1 - 4\beta^2/3) \left[ \eta P_{circ}^0 + (1 - \eta) \tanh \left( \frac{\hbar\Omega}{2k_B\Theta} \right) \right] \quad (5.22)$$

whereas the degree of linear polarization does no longer depend on the initial trion polarization (linear or circular) and simply reads:

$$P_{lin}^{X^-} = -\frac{2\beta}{\sqrt{3}} \sqrt{1 - \beta^2} \cos \theta \quad (5.23)$$

Here  $\theta = 2(\alpha + \psi)$ , with  $\alpha$  the angle of the reference basis used for measuring the linear polarization, and  $\psi$  the complex phase of the HH-LH mixing introduced in the previous *Section*. From these equations, it clearly appears that the optical orientation of trions is possible only under circularly polarized excitation. Such experiments were performed in the recent years by S. Laurent *et al.* [84] and B. Eble *et al.* [126] proving the long spin relaxation of  $X^-$  trions <sup>25</sup>. Eventually, the main interest of trions regarding our own experiments on exciton coherence is to evidence by Eq. 5.23 the role played by the heavy- to light-hole mixing. In practice, we did not measure the same QD's ( $A$ ,  $B$ ,  $C$ ,...) in the regime of trion formation <sup>26</sup>. Therefore we can only examine the general trend assuming that the

<sup>24</sup>Without exchange term we have  $\gamma = 1$ .

<sup>25</sup>In this case, only the diagonal spin relaxation time is investigated, since all off-diagonal terms in the trion density matrix are zero. In a tilted magnetic field, optical alignment of trions could be partially achieved, and subsequently the coherence time of trion spin could be addressed.

<sup>26</sup>The study of trions was done as a preliminar test of the set-up, before we focused on neutral excitons with more interesting features. Besides, since the density of QDs

HH-LH mixing  $\beta$  amounts typically to  $\sim 0.1$ .

For the measurements of linear polarization shown in Fig. 5.11 of three different trion lines, a residual magnetic field of  $\sim 30$  mT along the optical axis was applied and two excitation polarizations ( $\sigma^+$  and linear polarization  $\alpha = 0^\circ$ ) were used. In both cases, only a small effect of the order of a few % is measured, which confirms the absence of strong optical alignment and polarization conversion for trions. Since a trion in its ground state contains two same carriers forming a singlet, no exchange splitting is expected and the only anisotropy axis is related with heavy-to-light hole mixing. However, in spite of the weak signal to noise ratio of these measurements, it seems that this small degree of linear polarization has eigenaxes which depend on the excitation polarization in contrast to the prediction of polarization conversion for trions (maximum for  $\alpha = -\psi$ ). To elucidate this effect, we should certainly develop a more complete theory including e.g. the possible coherence of electron spin states due to the hyperfine interaction with nuclear spins. The latter was indeed invoked to explain the electron spin cooling achieved under strictly resonant excitation of  $X^-$  [137]. Before, a systematic study of polarization conversion for trions should be carried out to confirm this surprising shift of eigenaxes as a function of excitation polarization.

## 5.4 Conclusion

The original results presented in this last *Chapter* mostly answered to the question of exciton spin coherence in a quantum dot, which is one of the crucial requirements for a QD-based source of entangled photons. Besides, we have seen that the technique of optical orientation/alignment offers an efficient way to determine whether a specific quantum dot fulfills both requirements of exciton spin degeneracy and long coherence time. In summary:

- Optical orientation combined with electric field induced FSS tuning under quasi-resonant excitation was successfully used to probe the spin degeneracy of the excitonic levels. Such experiments are very promising to test the preparation of the excitonic states for entangled emission. Indeed, there is a correspondence between this method and the exciton-biexciton polarization correlation measurements usually performed to prove the entanglement. With the latter method, measurements of all polarization configurations in different basis takes much time and if additionally entanglement depends on a tunable parameter (FSS) it may cost up to a few days for a single QD. Therefore the presented method offers the possibility to quickly verify if the emission from a specific QD can lead to entanglement. Remarkably, when the FSS can be tuned to zero, we can extract from this relatively simple measurement the natural linewidth of the QD ground state transition.

---

was not very low and the binding energy of trions may vary by a few hundred meV's from dot to dot, it would have been difficult to establish reliably a correlation between exciton and trion lines.

- The investigation of PL polarization conversion revealed the importance of the light-hole admixture to the hole ground states. This feature is strongly supported by the good qualitative agreement between a whole series of experimental results (conversion for different excitation polarizations as a function of magnetic field) and a theoretical model describing the coherent evolution of exciton spin in the total effective magnetic field with optical selection rules including the HH-LH mixing. From the agreement with this model we can conclude firmly that the exciton spin experiences neither significant relaxation nor pure dephasing during the exciton radiative lifetime.

**SUMMARY.** *Chapter 5* described the phenomenon of spin precession in the exciton two-level system. Under quasi-resonant excitation the optical alignment of excitons was achieved in the polarization basis corresponding to the QD eigenstates, whereas conversion of polarization was observed in the general case with an efficiency close to the theoretical maximum. Most of the experimental results could be interpreted using the density matrix formalism to describe the exciton spin and its evolution in a longitudinal magnetic field. These measurements are a direct evidence of the long spin coherence time in a quantum dot.





---

## CHAPTER 6

---

# Conclusions

*"On ne connaît que les choses qu'on apprivoise"*  
Antoine de Saint-Exupéry , "Le petit Prince"

THIS THESIS presents experimental results and theoretical modeling of the spin phenomena in semiconductor quantum dots. We focused on the studies of the spin-splitting of excitonic states, their sensitivity to external fields, and effects related to the spin precession in this two-level system. We have shown that by applying an external perturbation of a specific symmetry, we can modify optical properties of self-assembled quantum dots in a controllable way. A reliable technique enabling such a control over features of emitted photons from nanostructures remains highly demanded to envisage future applications in quantum-information processing. We have tested two kind of external fields, namely an electric field applied parallel to one of the in-plane symmetry axis of the QD, and an in-plane magnetic field. We presented results showing how these perturbations influence optical transitions from individual quantum dots.

Our spectroscopic studies in the presence of external electric field revealed that exchange interaction between an electron and a hole, which form an exciton, can be strongly modified if we have "a tool" to symmetrize the wavefunctions. Intuitively the Coulombic character of this interaction suggests that it should be affected by an electric field. By applying in-plane electric field it was possible to tune the exciton splitting and even cancel it. Although the modification of the exciton splitting in electric field is always accompanied by the intensity reduction and the spectral broadening of the lines, this technique is powerful and may produce an enhancement of the QD symmetry, which can be evidenced in optical pumping experiments. Studies of the spin coherence phenomena brings together Stark modulation technique and strong resonant excitation. It allowed us to determine the excitonic lifetime and spin relaxation time in two-levels of excitonic optically active states.

The control over spin degeneracy of the excitonic states in a QD can be achieved not only by manipulating the symmetry of electron and hole wavefunctions. Another possibility is to mix those states with different ones. If the strength of coupling is not the same for both excitonic states, then the energy shift induced by the perturbation can reduce or increase the initial splitting between them. In-plane

magnetic field acts in this way: it modifies the transition energies and depending on the direction and magnitude can tune the fine structure splitting thanks to the mixing between the excitonic states of different angular momenta. The description using Zeeman Hamiltonian reveals that not only the direction of the field with respect to the QD principal axes does play a crucial role — additionally crystal lattice direction should be taken into account and in case of strong mixing with light-holes the possibility of splitting canceling is completely determined by intrinsic properties of the QD.

Innovative techniques of nanostructure fabrication, like e.g. producing field-effect structures, should be a driving force for optoelectronics. New technologies should satisfy the requirements of sophisticated applications in new electronics. Future experiments should focus on time-resolved studies of QDs under external perturbations in order to highlight the conditions for coherent control of spins inside a QD.

---

# Bibliography

- [1] R. J. Young, R. M. Stevenson, P. Atkinson, K. Cooper, D. A. Ritchie, and A. J. Shields. "Improved fidelity of triggered entangled photons from single quantum dots". *New J. Phys.*, 8:29, 2006.
- [2] N. Akopian, N. H. Lindner, E. Poem, Y. Berlatzky, J. Avron, D. Gershoni, B. D. Gerardot, and P. M. Petroff. "Entangled photon pairs from semiconductor quantum dots". *Phys. Rev. Lett.*, 96:130501, 2006.
- [3] R. J. Young, R. M. Stevenson, A. J. Shields, P. Atkinson, K. Cooper, D. A. Ritchie, K. M. Groom, A. I. Tartakovskii, and M. S. Skolnick. "Inversion of exciton level splitting in quantum dots". *Phys. Rev. B*, 72:113305, 2005.
- [4] A. I. Tartakovskii, M. N. Makhonin, I. R. Sellers, J. Cahill, A. D. Andreev, D. M. Whittaker, J-P. R. Wells, A. M. Fox, D. J. Mowbray, M. S. Skolnick, K. M. Groom, M. J. Steer, H. Y. Liu, and M. Hopkinson. "Effect of thermal annealing and strain engineering on the fine structure of quantum dot excitons". *Phys. Rev. B*, 70:193303, 2004.
- [5] S. Seidl, M. Kroner, A. Högele, K. Karrai, R. Warburton, A. Badolato, and P. M. Petroff. "Effect of uniaxial stress on excitons in a self-assembled quantum dot". *Appl. Phys. Lett.*, 88:203113, 2006.
- [6] R. M. Stevenson, R. J. Young, P. See, D. G. Gevaux, K. Cooper, P. Atkinson, I. Farrer, D. A. Ritchie, and A. J. Shields. "Magnetic-field-induced reduction of the exciton polarization splitting in InAs quantum dots". *Phys. Rev. B*, 73:033306, 2006.
- [7] K. Kowalik, O. Krebs, A. Lemaître, S. Laurent, P. Senellart, J. A. Gaj, and P. Voisin. "Influence of an in-plane electric field on exciton fine structure in InAs-GaAs self-assembled quantum dots". *Appl. Phys. Lett.*, 86:041907, 2005.
- [8] K. Kowalik, O. Krebs, A. Golnik, J. Suffczyński, P. Wojnar, J. Kossut, J. A. Gaj, and P. Voisin. "Manipulating the exciton fine structure of single CdTe/ZnTe quantum dots by an in-plane magnetic field". *Phys. Rev. B*, 75:195340, 2007.
- [9] K. Kowalik, O. Krebs, P. Senellart, A. Lemaître, B. Eble, A. Kudelski, J. Gaj, and P. Voisin. "Stark spectroscopy of Coulomb interactions in individual InAs/GaAs self-assembled quantum dots". *Phys. Stat. Sol. (c)*, 3:3890, 2006.

- [10] K. Kowalik, A. Kudelski, A. Golnik, J. Suffczyński, O. Krebs, P. Voisin, G. Karczewski, J. Kossut, and J. A. Gaj. "Influence of electric field on fine structure of exciton complexes in CdTe/ZnTe self-assembled quantum dot". *Phys. Stat. Sol. (c)*, 3:865, 2006.
- [11] A. Kudelski, K. Kowalik, A. Golnik, G. Karczewski, J. Kossut, and J. A. Gaj. "Spatially correlated 0D exciton states in CdTe/ZnTe semiconductor system". *J. Lumin.*, 112:127, 2005.
- [12] J. E. Lilienfield, Method and apparatus for controlling electric currents, US Patent 1,745,175, application filed October 8, 1926, granted January 18, 1930 (first known patent describing a MESFET or metal/semiconductor FET), and J. E. Lilienfield, Device for controlling electric current, US Patent 1,900,018 application filed March 28, 1928, patented March 7, 1933 (first known patent describing a depletion mode MOSFET), (1928).
- [13] W. Shockley and J. Bardeen and W. Brattain, US Patent 02569347 (1951).
- [14] B. Schumacher. "Quantum coding". *Phys. Rev. A*, 51:2738, 1995.
- [15] K. Gödel. "Über formal unentscheidbare Sätze der Principia und verwandter Systeme". *Monatsch. Math. Phys.*, 38:173, 1930.
- [16] A. M. Turing. "On computable numbers, with an application to the Entscheidungsproblem". *Proc. London Math. Soc.*, 42,43:230,544, 1936.
- [17] A. Church. "A note on the Entscheidungsproblem". *J. Symb. Logic*, 1:40,101, 1936.
- [18] A. Einstein, B. Podolsky, and N. Rosen. "Can quantum-mechanical description of physical reality be considered complete?". *Phys. Rev.*, 47:777, 1935.
- [19] J. S. Bell. "On the Einstein-Poldolsky-Rosen paradox". *Physics*, 1:195, 1964.
- [20] C. H. Bennett, G. Brassard, S. Briedbart, and S. Wiesner. "Quantum cryptography, or unforgeable subway tokens". In *Advances in Cryptology: Proceedings of Crypto '82*, page 267, New York, 1982. Plenum.
- [21] C. H. Bennett and G. Bassard. "The dawn of a new era for quantum cryptography: the experimental prototype is working!". *Sigact News*, 20:78, 1989.
- [22] P. Michler, A. Kiraz, C. Becher, W. V. Schoenfeld, P. M. Petro, Lidong Zhang, E. Hu, and A. Imamoglu. "A quantum dot single-photon turnstile device". *Science*, 290:2282, 2000.
- [23] id Quantique SA, Geneva, Switzerland. See <http://www.idquantique.com>.
- [24] R. Seguin, A. Schliwa, T. D. Germann, S. Rodt, K. Pötschke, A. Strittmatter, U. W. Pohl, D. Bimberg, M. Winkelnkemper, T. Hammerschmidt, and P. Kratzer. "Control of fine-structure splitting and excitonic binding energies in selected individual InAs/GaAs quantum dots". *Appl. Phys. Lett.*, 89:263109, 2006.

- [25] A. Rastelli, A. Ulhaq, Ch. Deneke, L. Wang, M. Benyoucef, E. Coric, W. Winter, S. Mendach, F. Horton, F. Cavallo, T. Merdzhanova, S. Kiravittaya, and O. G. Schmidt. "Fabrication and characterization of microdisk resonators with In(Ga)As/GaAs quantum dots". *Phys. Stat. Solidi (c)*, 3:3641, 2006.
- [26] T. Yamauchi, Y. Matsuba, L. Bolotov, M. Tabuchi, and A. Nakamura. "Correlation between the gap energy and size of single InAs quantum dots on GaAs (100) studied by scanning tunneling spectroscopy". *Appl. Phys. Lett.*, 77:4368, 2000.
- [27] P. Offermans, P. M. Koenraad, J. H. Wolteraand, K. Pierz, M. Roy, and P. A. Maksym. "Formation of InAs quantum dots and wetting layers in GaAs and AlAs analyzed by cross-sectional scanning tunneling microscopy". *Physica E*, 26:236, 2005.
- [28] F. Glas, G. Patriarche, L. Largeau, and A. Lemaitre. "Determination of the local concentrations of Mn interstitials and antisite defects in GaMnAs". *Phys. Rev. Lett.*, 93:086107, 2004.
- [29] A. Lemaître, G. Patriarche, and F. Glas. "Composition profiling of InAs/GaAs quantum dots". *Appl. Phys. Lett.*, 85:3717, 2004.
- [30] P. M. Koenraad, D. M. Bruls, J. H. Davies, S. P. A. Gill, Fei Long, M. Hopkinson, M. Skolnick, and J. H. Wolter. "Composition profiling at the atomic scale in III-V nanostructures by cross-sectional STM". *Physica E*, 17:526, 2003.
- [31] D. M. Bruls, J. W. A. M. Vugs, P. M. Koenraad, H. W. M. Salemink, J. H. Wolter, M. Hopkinson, M. S. Skolnick, Fei Long, and S. P. A. Gill. "Determination of the shape and indium distribution of low-growth-rate InAs quantum dots by cross-sectional scanning tunneling microscopy". *Appl. Phys. Lett.*, 81:1709, 2002.
- [32] P. W. Fry, I. E. Itskevich, D. J. Mowbray, M. S. Skolnick, J. J. Finley, J. A. Barker, E. P. O'Reilly, L. R. Wilson, I. A. Larkin, P. A. Maksym, M. Hopkinson, M. Al-Khafaji, J. P. R. David, A. G. Cullis, G. Hill, and J. C. Clark. "Inverted electron-hole alignment in InAs-GaAs self-assembled quantum dots". *Phys. Rev. Lett.*, 84:733, 2000.
- [33] A. Vasanelli, R. Ferreira, and G. Bastard. "Continuous absorption background and decoherence in quantum dots". *Phys. Rev. Lett.*, 89:216804, 2002.
- [34] G. Bester and A. Zunger. "Cylindrically shaped zinc-blende semiconductor quantum dots do not have cylindrical symmetry: Atomistic symmetry, atomic relaxation, and piezoelectric effects". *Phys. Rev. B*, 71:045318, 2005.

- [35] M. Grundmann, O. Stier, and D. Bimberg. "InAs/GaAs quantum dots: strain distribution, optical phonons, and electronic structure". *Phys. Rev. B*, 52:11969, 1995.
- [36] G. L. Bir and G. E. Pikus. "Symetria i odkształcenia w półprzewodnikach" ("Symmetry and Strain-induced Effects in Semiconductors"). PWN, Warszawa, 1977.
- [37] G. Bester, S. Nair, and A. Zunger. "Pseudopotential calculation of the excitonic fine structure of million-atom self-assembled  $\text{In}_{1-x}\text{Ga}_x\text{As}$ -GaAs quantum dots". *Phys. Rev. B*, 67:161306, 2003.
- [38] E. I. Ivchenko and G. E. Pikus. "Superlattices and Other Heterostructures, Symmetry and Optical Phenomena". Springer-Verlag, Berlin, 1995.
- [39] D. Gammon, E. S. Snow, B. V. Shanabrook, D. S. Katzer, and D. Park. "Homogenous linewidths in the optical spectrum of a single gallium arsenide quantum dot". *Science*, 273:87, 1996.
- [40] R. Seguin, A. Schliwa, S. Rodt, K. Pötschke, U. W. Pohl, and D. Bimberg. "Size-dependent fine-structure splitting in self-organized InAs-GaAs quantum dots". *Phys. Rev. Lett.*, 95:257402, 2005.
- [41] M. Ediger, K. Karrai, A. Badolato, P. M. Petroff, , and R. J. Warburton. "Controlled charging of the same single quantum dot from +6e to -8e: emission, shell filling and configuration interactions". *Phys. Stat. Solidi (c)*, 3:3806, 2006.
- [42] L. He, G. Bester, and A. Zunger. "Electronic phase diagrams of carriers in self-assembled quantum dots: Violation of Hund's rule and the Aufbau principle for holes". *Phys. Rev. Lett.*, 95:246804, 2005.
- [43] B. Urbaszek, R. J. Warburton, K. Karrai, B. D. Gerardot, P. M. Petroff, and J. M. Garcia. "Fine structure of highly charged excitons in semiconductor quantum dots". *Phys. Rev. Lett.*, 90:247403, 2003.
- [44] F. De Martini, G. Di Giuseppe, and M. Marracco. "Single-mode generation of quantum photon states by excited single molecules in a microcavity trap". *Phys. Rev. Lett.*, 76:900, 1996.
- [45] R. Brouri, A. Beveratos, J.-P. Poizat, and P. Grangier. "Photon antibunching in the fluorescence of individual color centers in diamond". *Optics Lett.*, 25:1294, 2000.
- [46] J. Kim, O. Benson, H. Kan, and Y. Yamamoto. "A single-photon turnstile device". *Nature*, 397:500, 1999.
- [47] E. Moreau, I. Robert, J. M. Gerard, I. Abram, L. Manin, and V. Thierry-Mieg. "Single-mode solid-state single photon source based on isolated quantum dots in pillar microcavities". *Appl. Phys. Lett.*, 79:2865, 2001.

- [48] O. Benson, C. Santori, M. Pelton, and Y. Yamamoto. "Regulated and entangled photons from a single quantum dot". *Phys. Rev. Lett.*, 84:513, 2000.
- [49] A. G. White, D. F. V. James, P. H. Eberhard, and P. G. Kwiat. "Nonmaximally entangled states: Production, characterization, and utilization". *Phys. Rev. Lett.*, 83:3103, 1999.
- [50] O. Krebs and P. Voisin. "Giant optical anisotropy of semiconductor heterostructures with no common atom and the quantum-confined Pockels effect". *Phys. Rev. Lett.*, 77:1829, 1996.
- [51] E. L. Ivchenko, A. Yu. Kaminski, and U. Rössler. "Heavy-light hole mixing at zinc-blende (001) interfaces under normal incidence". *Phys. Rev. B*, 54:5852, 1996.
- [52] R. Hanbury Brown and R. Q. Twiss. "Correlation between photons in two coherent beams of light". *Nature*, 177:27, 1956.
- [53] M. Kroutvar, Y. Ducommun, D. Heiss, M. Bichler, D. Schuh, G. Abstreiter, and J. J. Finley. "Optically programmable electron spin memory using semiconductor quantum dots". *Nature*, 432:81, 2004.
- [54] J. Suffczyński, T. Kazimierczuk, M. Goryca, B. Piechal, A. Trajnerowicz, K. Kowalik, P. Kossacki, A. Golnik, K. P. Korona, M. Nawrocki, J. A. Gaj, and G. Karczewski. "Excitation mechanisms of individual CdTe/ZnTe quantum dots studied by photon correlation spectroscopy". *Phys. Rev. B*, 74:085319, 2006.
- [55] R. M. Stevenson, R. J. Young, P. Atkinson, K. Cooper, D. A. Ritchie, and A. J. Shields. "A semiconductor source of triggered entangled photon pairs". *Nature*, 439:179, 2006.
- [56] J. M. Smith, P. A. Dalgarno, R. J. Warburton, A. O. Govorov, K. Karrai, B. D. Gerardot, and P. M. Petroff. "Voltage control of the spin dynamics of an exciton in a semiconductor quantum dot". *Phys. Rev. Lett.*, 94:197402, 2005.
- [57] S. Seidl, M. Kroner, P. A. Dalgarno, A. Högele, J. M. Smith, M. Ediger, B. D. Gerardot, J. M. Garcia, P. M. Petroff, K. Karrai, and R. J. Warburton. "Absorption and photoluminescence spectroscopy on a single self-assembled charge-tunable quantum dot". *Phys. Rev. B*, 72:195339, 2005.
- [58] A. Högele, S. Seidl, M. Kroner, K. Karrai, R. J. Warburton, B. D. Gerardot, and P. M. Petroff. "Voltage-controlled optics of a quantum dot". *Phys. Rev. Lett.*, 93:217401, 2004.
- [59] C. Kammerer, C. Voisin, G. Cassabois, C. Delalande, Ph. Roussignol, F. Klopff, J. P. Reithmaier, A. Forchel, and J. M. Gerard. "Line narrowing in single semiconductor quantum dots: Toward the control of environment effects". *Phys. Rev. B*, 66:041306, 2002.



- [60] E. Moreau, I. Robert, L. Manin, V. Thierry-Mieg, J. M. Gerard, and I. Abram. "Quantum cascade of photons in semiconductor quantum dots". *Phys. Rev. Lett.*, 87:183601, 2001.
- [61] J. M. Gerard, B. Sermage, B. Gayral, B. Legrand, E. Costard, and V. Thierry-Mieg. "Enhanced spontaneous emission by quantum boxes in a monolithic optical microcavity". *Phys. Rev. Lett.*, 81:1110, 1998.
- [62] T. Yoshie, A. Scherer, J. Hendrickson, G. Khitrova, H. M. Gibbs, G. Rupper, C. Ell, O. B. Shchekin, and D. G. Deppe. "Vacuum Rabi splitting with a single quantum dot in a photonic crystal nanocavity". *Nature*, 432:200, 2004.
- [63] A. Badolato, K. Hennessy, M. Atatüre, J. Dreiser, E. Hu, P. M. Petroff, and A. Imamoglu. "Deterministic coupling of single quantum dots to single nanocavity modes". *Science*, 308:1158, 2005.
- [64] K. Hennessy, A. Badolato, M. Wigner, D. Grace, M. Atatüre, S. Gulde, S. Fält, E. L. Hu, and A. Imamoglu. "Quantum nature of a strongly coupled single quantum dot-cavity system". *Nature*, 445:896, 2007.
- [65] J. P. Reithmaier, G. Sęk, A. Löffler, C. Hofmann, S. Kuhn, S. Reitzenstein, L. V. Keldysh, V. D. Kulakovskii, T. L. Reinecke, and A. Forchel. "Strong coupling in a single quantum dot–semiconductor microcavity system". *Nature*, 432:197, 2004.
- [66] E. Peter, P. Senellart, D. Martrou, A. Lemaître, J. Hours, J. M. Gérard, and J. Bloch. "Exciton-photon strong-coupling regime for a single quantum dot embedded in a microcavity". *Phys. Rev. Lett.*, 95:067401, 2005.
- [67] G. E. Pikus and G. L. Bir. "Exchange interaction in excitons in semiconductors". *Sov. Phys. JETP*, 33:108, 1971.
- [68] G. E. Pikus and G. L. Bir. *Sov. Phys. JETP*, 35:174, 1972.
- [69] E. L. Ivchenko. "Fine structure of excitonic levels in semiconductor nanostructures". *Phys. Stat. Sol. (a)*, 164:487, 1997.
- [70] S. V. Gupalov, E. L. Ivchenko, and A. V. Kavokin. "Fine structure of localized exciton levels in quantum wells". *Sov. Phys. JETP*, 86:388, 1998.
- [71] A. Jankovic. "Etats électroniques des boîtes quantiques de semiconducteur: rôle de l'environnement et couplage dépendant du spin". PhD thesis, Université Paris VI, Paris, 2004.
- [72] M. M. Glazov, E. L. Ivchenko, O. Krebs, K. Kowalik, and P. Voisin. "Diamagnetic contribution to the effect of in-plane magnetic field on a quantum dot exciton fine structure". *to be published*, 2007.

- [73] A. Golnik, P. Kossacki, K. Kowalik, W. Maślana, J. A. Gaj, M. Kutrowski, and T. Wojtowicz. "Microphotoluminescence study of local temperature fluctuations in n-type (Cd,Mn)Te quantum well". *Solid. State Comm.*, 131:283, 2004.
- [74] K. Kowalik, A. Kudelski, J. A. Gaj, T. Wojtowicz, O. Krebs, and P. Voisin. "In-plane optical anisotropy of parabolic and half-parabolic  $\text{Cd}_{1-x}\text{Mn}_x\text{Te}$  quantum wells". *Solid. State Comm.*, 126:467, 2003.
- [75] I. N. Stranski and L. Krastanov. "Theory of orientation separation of ionic crystals". *Akad. Wiss. Lit. Wien, Math.-Natur. Kl. Iib*, 797:146, 1938.
- [76] J. Eymery, B. Daudin, D. Brun-Le Cunff, N. Boudet, and S. Tatarenko. "Anisotropic relaxation during the first stages of the growth of Zn Te/(001)Cd Te strained layers studied by reflection high energy electron diffraction". *Appl. Phys. Lett.*, 66:25, 1995.
- [77] W. Maslana, P. Kossacki, M. Bertolini, H. Boukari, D. Ferrand, S. Tatarenko, J. Cibert, and J. A. Gaj. "p-type doping of II–VI heterostructures from surface states: Application to ferromagnetic  $\text{Cd}_{1-x}\text{Mn}_x\text{Te}$  quantum wells". *Appl. Phys. Lett.*, 82:1875, 2003.
- [78] Y. Merle d'Aubigné, A. Wasiela, H. Mariette, and T. Dietl. "Polariton effects in multiple-quantum-well structures of  $\text{CdTe}/\text{Cd}_{1-x}\text{Zn}_x\text{Te}$ ". *Phys. Rev. B*, 54:14003, 1996.
- [79] S. Maćkowski. "Optical Properties of CdTe-based Self-Assembled Quantum Dots". PhD thesis, Warsaw University, Warsaw, 2001.
- [80] H. Mariette, L. Marsal, L. Besombes, F. Tinjod, B. Gilles, K. Kheng, and J. L. Rouvière. "Nanostructures formation and optical properties of II–VI semiconductor compounds". *Journ. of Crystal Growth*, 237:227, 2002.
- [81] G. Karczewski, S. Maćkowski, M. Kutrowski, T. Wojtowicz, and J. Kossut. "Photoluminescence study of  $\text{CdTe}/\text{ZnTe}$  self-assembled quantum dots". *Appl. Phys. Lett.*, 74:3011, 1999.
- [82] F. Tinjod, B. Gilles, S. Moehl, K. Kheng, and H. Mariette. "II–VI quantum dot formation induced by surface energy change of a strained layer". *Appl. Phys. Lett.*, 82:4340, 2003.
- [83] F. Tinjod, S. Moehl, K. Kheng, B. Gilles, and H. Mariette. "CdTe/ $\text{Zn}_{1-x}\text{Mg}_x$  self-assembled quantum dots: Towards room temperature emission". *J. Appl. Phys.*, 95:102, 2004.
- [84] S. Laurent, B. Eble, O. Krebs, A. Lemaître, B. Urbaszek, X. Marie, T. Amand, and P. Voisin. "Electrical control of hole spin relaxation in charge tunable InAs-GaAs quantum dots". *Phys. Rev. Lett.*, 94:147401, 2005.

- [85] J. J. Finley, P. W. Fry, A. D. Ashmore, A. Lemaître, A. I. Tartakovskii, R. Oulton, D. J. Mowbray, M. S. Skolnick, M. Hopkinson, P. D. Buckle, and P. A. Maksym. "Observation of multicharged excitons and biexcitons in a single InGaAs quantum dot". *Phys. Rev. B*, 63:161305 R, 2001.
- [86] S. Laurent. "*Orientation optique et relaxation du spin du trion dans les boîtes quantiques d'InAs/ GaAs*". PhD thesis, Université Paris VI, Paris, 2004.
- [87] B. Eble. "*Interaction hyperfine dans les boîtes quantiques d'InAs/GaAs sous pompage optique orienté*". PhD thesis, Université Paris VI, Paris, 2006.
- [88] B. Alén, F. Bickel, K. Karrai, R. J. Warburton, and P. M. Petroff. "Stark-shift modulation absorption spectroscopy of single quantum dots". *Appl. Phys. Lett.*, 83:2235, 2003.
- [89] B. D. Gerardot, D. Granados, S. Seidl, P. A. Dalgarno, R. J. Warburton, J. M. Garcia, K. Kowalik, O. Krebs, K. Karrai, A. Badolato, and P. M. Petroff. "Manipulating exciton fine-structure in quantum dots with a lateral electric field". *Appl. Phys. Lett.*, 90:041101, 2007.
- [90] J. Jasny, J. Sepiol, T. Irngartinger, M. Traber, A. Renn, and U. P. Wild. "Fluorescence microscopy in superfluid helium: Single molecule imaging". *Rev. Sci. Instrum.*, 67:1425, 1996.
- [91] A. Kudelski. "*Optical anisotropy of semiconductor heterostructures*". PhD thesis, Warsaw University, Warsaw, 2004.
- [92] B. Dal Don, H. Zhao, S. Moehl, C. Ziegler, and H. Kalt. "Solid-immersion-lens-enhanced nanophotoluminescence for spectroscopy of quantum dot systems". *Phys. Stat. Solidi (c)*, 4:1237, 2003.
- [93] B. D. Gerardot, S. Seidl, P. A. Dalgarno, R. J. Warburton, M. Kroner, K. Karrai, A. Badolato, and P. M. Petroff. "Contrast in transmission spectroscopy of a single quantum dot". *Appl. Phys. Lett.*, 90:221106, 2007.
- [94] J. J. Finley, M. Sabathil, P. Vogl, G. Abstreiter, R. Oulton, A. I. Tartakovskii, D. J. Mowbray, M. S. Skolnick, S. L. Liew, A. G. Cullis, and M. Hopkinson. "Quantum-confined Stark shifts of charged exciton complexes in quantum dots". *Phys. Rev. B*, 70:201308 R, 2004.
- [95] V. Stavarache, D. Reuter, A. D. Wieck, M. Schwab, D. R. Yakovlev, R. Oulton, and M. Bayer. "Control of quantum dot excitons by lateral electric fields". *Appl. Phys. Lett.*, 89:123105, 2006.
- [96] W. Heller, U. Bockelmann, and G. Abstreiter. "Electric-field effects on excitons in quantum dots". *Phys. Rev. B*, 57:6270, 1998.
- [97] W. Heisenberg. "Über den anschaulichen Inhalt der quantentheoretischen Kinematik und Mechanik". *Zeitschrift für Physik*, 43:172, 1927.

- [98] I. Favero, A. Berthelot, G. Cassabois, C. Voisin, C. Delalande, Ph. Rousignol, R. Ferreira, and J. M. Gérard. "Temperature dependence of the zero-phonon linewidth in quantum dots: An effect of the fluctuating environment". *Phys. Rev. B*, 75:073308, 2007.
- [99] S. Tarucha, D. G. Austing, T. Honda, R. J. van der Hage, and L. P. Kouwenhoven. "Shell filling and spin effects in a few electron quantum dot". *Phys. Rev. Lett.*, 77:3613, 1996.
- [100] B. T. Miller, W. Hansen, S. Manus, R. J. Luyken, A. Lorke, J. P. Kotthaus, S. Huant, G. Medeiros-Ribeiro, and P. M. Petroff. "Few-electron ground states of charge-tunable self-assembled quantum dots". *Phys. Rev. B*, 56:6764, 1997.
- [101] R. J. Warburton, B. T. Miller, C. S. Dürr, C. Bödefeld, K. Karrai, J. P. Kotthaus, G. Medeiros-Ribeiro, P. M. Petroff, and S. Huant. "Coulomb interactions in small charge-tunable quantum dots: A simple model". *Phys. Rev. B*, 58:16221, 1998.
- [102] V. Türk, S. Rodt, O. Stier, R. Heitz, R. Engelhardt, U. W. Pohl, D. Bimberg, and R. Steingrüber. "Effect of random field fluctuations on excitonic transitions of individual CdSe quantum dots". *Phys. Rev. B*, 61:9944, 2000.
- [103] L. Besombes, K. Kheng, L. Marsal, and H. Mariette. "Few-particle effects in single CdTe quantum dots". *Phys. Rev. B*, 65:121314, 2002.
- [104] S. Rodt, A. Schliwa, K. Pötschke, F. Guffarth, and D. Bimberg. "Correlation of structural and few-particle properties of self-organized InAs/GaAs quantum dots". *Phys. Rev. B*, 71:155325, 2005.
- [105] J. Suffczyński, K. Kowalik, A. Trajnerowicz, T. Kazimierczuk, M. Goryca, P. Kossacki, A. Golnik, M. Nawrocki, J. A. Gaj, and G. Karczewski. "Polarization dependent correlations of single photons from CdTe/ZnTe quantum dots". In *PROC. 27TH Int. Conf. Phys. Semicond.*, page 1089, Vien, 2007. AIP Conf. Proc. 893.
- [106] K. Kowalik, A. Kudelski, A. Golnik, J. A. Gaj, G. Karczewski, and J. Kossut. "Characterization of self-assembled CdTe/ZnTe quantum dots". *Acta Phys. Pol. A*, 103:539, 2003.
- [107] B. Patton, W. Langbein, and U. Woggon. "Trion, biexciton, and exciton dynamics in single self-assembled CdSe quantum dots". *Phys. Rev. B*, 68:125316, 2003.
- [108] L. Besombes, K. Kheng, and D. Martrou. "Exciton and biexciton fine structure in single elongated islands grown on a vicinal surface". *Phys. Rev. Lett.*, 85:425, 2000.
- [109] A. C. Davison and D. V. Hinkley. "Bootstrap methods and their application". Cambridge University Press, 1997.

- [110] H. W. van Kesteren, E. C. Cosman, W. A. J. A. van der Poel, and C. T. Foxon. "Fine structure of excitons in type-II GaAs/AlAs quantum ". *Phys. Rev. B*, 40:5283, 1990.
- [111] A. A. Toropov, E. L. Ivchenko, O. Krebs, S. Cortez, P. Voisin, and J. L. Gentner. "Excitonic contributions to the quantum-confined Pockels effect". *Phys. Rev. B*, 63:35302, 2000.
- [112] A. V. Koudinov, I. A. Akimov, Yu. G. Kusrayev, and F. Henneberger. "Optical and magnetic anisotropies of the hole states in Stranski-Krastanov quantum dots". *Phys. Rev. B*, 70:241305(R), 2004.
- [113] I. Favero, G. Cassabois, A. Jankovic, R. Ferreira, D. Darson, C. Voisin, C. Delalande, Ph. Roussignol, A. Badolato, P. M. Petroff, and J. M. Gérard. "Giant optical anisotropy in a single InAs quantum dot in a very dilute quantum-dot ensemble". *Appl. Phys. Lett.*, 86:041904, 2005.
- [114] M. Bayer, G. Ortner, O. Stern, A. Kuther, A. A. Gorbunov, A. Forchel, P. Hawrylak, S. Fafard, K. Hinzer, T. L. Reinecke, S. N. Walck, J. P. Reithmaier, F. Klopff, and F. Schäfer. "Fine structure of neutral and charged excitons in self-assembled In(Ga)As/ (Al)GaAs quantum dots". *Phys. Rev. B*, 65:195315, 2002.
- [115] Y. Léger, L. Besombes, L. Maingault, and H. Mariette. "Valence band mixing in charged self-assembled quantum dots". *Phys. Stat. Solidi (c)*, 3:3895, 2006.
- [116] L. Besombes, L. Marsal, K. Kheng, T. Charvolin, Le Si Dang, A. Wasiela, and H. Mariette. "Fine structure of the exciton in a single asymmetric CdTe quantum dot". *J. Cryst. Growth*, 214:742, 2000.
- [117] J. Suffczyński, K. Kowalik, A. Trajnerowicz, M. Goryca, T. Kazimierzczuk, P. Kossacki, A. Golnik, M. Nawrocki, J. A. Gaj, and G. Karczewski. "Polarization correlated emission from an anisotropic CdTe/ZnTe quantum dot". *to be published*, 2007.
- [118] T. Mukumoto, R. Kaji, H. Sasakura, S. Adachi, H. Kumano, S. Muto, and I. Suemune. "Overhauser shift in photoluminescence of excitons with fine structure from a single self-assembled InAlAs quantum dot". *Phys. Stat. Solidi (c)*, 3:4372, 2006.
- [119] Y. G. Semenov and S. M. Ryabchenko. "Effects of photoluminescence polarization in semiconductor quantum wells subjected to an in-plane magnetic field". *Phys. Rev. B*, 68:045322, 2003.
- [120] A. A. Kiselev, E. L. Ivchenko, and U. Rössler. "Electron g factor in one- and zero-dimensional semiconductor nanostructures". *Phys. Rev. B*, 58:16353, 1998.

- [121] B. Patton, W. Langbein, and U. Woggon. "Landé g factors and orbital momentum quenching in semiconductor quantum dots". *Phys. Rev. Lett.*, 68:125316, 2003.
- [122] M. M. Glazov, E. L. Ivchenko, L. Besombes, Y. Léger, L. Maingault, and H. Mariette. "Fine structure of exciton excited levels in a quantum dot with a magnetic ion". *Phys. Rev. B*, 75:205313, 2007.
- [123] D. Gammon, Al. L. Efros, T. A. Kennedy, M. Rosen, D. S. Katzer, D. Park, S. W. Brown, V. L. Korenev, and I. A. Merkulov. "Electron and nuclear spin interactions in the optical spectra of single GaAs quantum dots". *Phys. Rev. Lett.*, 86:5176, 2001.
- [124] D. Paget, G. Lampel, B. Sapoval, and V. I. Safarov. "Low field electron-nuclear field coupling in GaAs under optical pumping conditions". *Phys. Rev. B*, 15:5780, 1977.
- [125] I. A. Akimov, D. H. Feng, and F. Henneberger. "Electron spin dynamics in a self-assembled semiconductor quantum dot: The limit of low magnetic fields". *Phys. Rev. Lett.*, 97:056602, 2006.
- [126] B. Eble, O. Krebs, A. Lemaître, K. Kowalik, A. Kudelski, P. Voisin, B. Urbaszek, X. Marie, and T. Amand. "Dynamic nuclear polarization of a single charge-tunable InAs/GaAs quantum dot". *Phys. Rev. B*, 74:081306, 2006.
- [127] P. Maletinsky, A. Badolato, and A. Imamoglu. "Dynamics of quantum dot nuclear spin polarization controlled by a single electron", 2007.
- [128] E. L. Ivchenko, V. P. Kochereshko, A. Yu. Naumov, I. N. Uraltsev, and P. Lavallard. "Magnetic-field-effects on photoluminescence polarization in type II GaAs/AlAs superlattices". *Superlattices and Microstr.*, 10:497, 1991.
- [129] R. I. Dzhioev, H. M. Gibbs, E. L. Ivchenko, G. Khitrova, V. L. Korenev, M. N. Tkachuk, and B. P. Zakharchenya. "Determination of interface by observation of linear-to-circular polarization conversion under optical orientation of excitons in type-II GaAs/AlAs superlattices". *Phys. Rev. B*, 56:13405, 1997.
- [130] I. Favero, G. Cassabois, C. Voisin, C. Delalande, Ph. Roussignol, R. Ferreira, C. Couteau, J.-P. Poizat, and J. M. Gérard. "Fast exciton spin relaxation in single quantum dots". *Phys. Rev. B*, 71:233304, 2005.
- [131] G. V. Astakhov, T. Kiessling, A. V. Platonov, T. Slobodskyy, S. Mahapatra, W. Ossau, G. Schmidt, K. Brunner, and L. W. Molenkamp. "Circular-to-linear and linear-to-circular conversion of optical polarization by semiconductor quantum dots". *Phys. Rev. Lett.*, 96:027402, 2006.
- [132] P. Y. Yu and M. Cardona. "Fundamental of semiconductors". Springer, Berlin Heidelberg New York, 2005.

- 
- [133] E. I. Ivchenko. *"Optical spectroscopy of semiconductor nanostructures"*. Alpha Science, Harrow, 2005.
- [134] Claude Cohen-Tannoudji. *"Photons and Atoms: Introduction to Quantum Electrodynamics"*. Wiley-Interscience, 1989.
- [135] W. Hanle. Über magnetische beeinflussung der polarisation der resonanzfluoreszenz. *Z. Phys.*, 30:93, 1924.
- [136] F. Meier and B. Zakharchenya. *Optical Orientation*, volume 8 of *Modern Problem in Condensed Matter Sciences*. North-Holland, Amsterdam, 1984.
- [137] M. Atatüre, J. Dreiser, A. Badolato, A. Högele, K. Karrai, and A. Imamoglu. "Quantum-dot spin-state preparation with near-unity fidelity". *Science*, 28:551, 2006.

---

# List of publications

## ARTICLES PUBLISHED IN JOURNALS

1. "In-plane optical anisotropy of parabolic and half-parabolic  $Cd_{1-x}Mn_xTe$  quantum wells" (**K. Kowalik**, A. Kudelski, J. A. Gaj, T. Wojtowicz, O. Krebs, P. Voisin, Solid State Comm. **126**, (2003) 467).
2. "Characterization of self-assembled CdTe/ZnTe quantum dots" (**K. Kowalik**, A. Kudelski, A. Golnik, J. A. Gaj, G. Karczewski, J. Kossut, Acta Phys. Pol. A. **103**, (2003) 539).
3. "Magnetic field controlled in-plane optical anisotropy in parabolic (Cd, Mn, Mg)Te quantum wells" (A. Kudelski, **K. Kowalik**, J. Kasprzak, A. Golnik, J. A. Gaj, T. Wojtowicz, G. Cywiński, Phys. Stat. Solidi (c) **1**, (2004) 965).
4. "Localization of neutral and charge excitons in (Cd,Mn)Te quantum well a microphotoluminescence study" (J. A. Gaj, A. Golnik, P. Kossacki, **K. Kowalik**, W. Maślana, M. Kutrowski, T. Wojtowicz, Phys. Stat. Solidi (c) **1**, (2004) 831).
5. "Microphotoluminescence study of local temperature fluctuations in n-type (Cd,Mn)Te quantum well" (A. Golnik, P. Kossacki, **K. Kowalik**, W. Maślana, J. A. Gaj, M. Kutrowski, T. Wojtowicz, Solid State Comm. **131**, (2004) 283).
6. "Influence of electric field on anisotropic exchange splitting in quantum dots systems" (**K. Kowalik**, O. Krebs, A. Kudelski, A. Golnik, A. Lemaître, P. Senellart, G. Karczewski, J. Kossut, J. Gaj, P. Voisin, Acta Phys. Pol. A. **106**, (2004) 177).
7. "Spatially correlated 0D exciton states in CdTe/ZnTe semiconductor system" (A. Kudelski, **K. Kowalik**, A. Golnik, G. Karczewski, J. Kossut, J. A. Gaj, Journ. Lumin. **112**, (2005) 127).
8. "Influence of an in-plane electric field on exciton fine structure in InAs-GaAs self-assembled quantum dots" (**K. Kowalik**, O. Krebs, A. Lemaître, S. Laurent, P. Senellart, J. A. Gaj, P. Voisin, Appl. Phys. Lett. **86**, (2005) 041907). Chosen for January 31, 2005 issue, Virtual Journal of Nanoscale Science and Technology.



9. "Influence of an electric field on fine structure of exciton complexes in CdTe/ZnTe self-assembled quantum dots" (**K. Kowalik**, A. Kudelski, J. Suffczyński, O. Krebs, P. Voisin, G. Karczewski, J. Kossut, J. A. Gaj, Phys. Stat. Sol. (c) **3**, (2006) 853).
10. "Determination of the number of Mn ions inside CdMnTe self assembled quantum dots" (P. Wojnar, J. Suffczyński, **K. Kowalik**, A. Golnik, G. Karczewski, J. Kossut, Phys. Stat. Sol. (c) **3**, (2006) 865).
11. "Optical probing of spin-dependent interactions in II-VI semiconductor structures" (J. A. Gaj, J. Cibert, D. Ferrand, A. Golnik, M. Goryca, G. Karczewski, P. Kossacki, J. Kossut, **K. Kowalik**, O. Krebs, A. Kudelski, M. Kutrowski, A. Lemaître, W. Maślana, M. Nawrocki, W. Pacuski, P. Płochocka, S. Tatarenko, P. Voisin, T. Wojtowicz, Phys. Stat. Sol. (b) **243**, (2006) 906).
12. "Spin dynamics and hyperfine interaction in InAs semiconductor quantum dots" (B. Eble, P.-F. Braun, O. Krebs, L. Lombez, X. Marie, T. Amand, D. Lagarde, P. Renucci, P. Voisin, A. Lemaître, **K. Kowalik**, A. Kudelski, Phys. Stat. Sol. (b) **243**, (2006) 2266).
13. "Dynamical nuclear polarization of a single charge-tunable InAs/GaAs quantum dot" (B. Eble, O. Krebs, A. Lemaître, **K. Kowalik**, A. Kudelski, P. Voisin, B. Urbaszek, X. Marie, T. Amand, Phys. Rev. B **74** (2006) 081306).
14. "Excitation mechanisms of individual CdTe/ZnTe quantum dots studied by photon correlation spectroscopy" (J. Suffczyński, T. Kazimierzczuk, M. Goryca, B. Piechal, A. Trajnerowicz, **K. Kowalik**, P. Kossacki, A. Golnik, K. Korona, M. Nawrocki, J. A. Gaj, G. Karczewski, Phys. Rev. B **74** (2006) 085319). Chosen for September 11, 2006 issue of Virtual Journal of Nanoscale Science and Technology, and to September 2006 issue of Virtual Journal of Ultrafast Science.
15. "Strong linear polarization induced by a longitudinal magnetic field in II-VI semimagnetic semiconductor layers" (A. Kudelski, J. Kasprzak, **K. Kowalik**, A. Golnik, J. A. Gaj, G. Cywiński, O. Krebs, G. Patriarche, P. Voisin, Phys. Rev. B **74** (2006) 073308).
16. "Single photon correlation measurements in a study of excitation process of individual CdTe/ZnTe quantum dots" (J. Suffczyński, T. Kazimierzczuk, M. Goryca, A. Trajnerowicz, **K. Kowalik**, P. Kossacki, A. Golnik, M. Nawrocki, J. A. Gaj, G. Karczewski, Phys. Stat. Sol. (c) **3**, (2006), 3802).
17. "Stark spectroscopy of Coulomb interaction in individual InAs/GaAs self-assembled quantum dots" (**K. Kowalik**, O. Krebs, P. Senellart, A. Lemaître, B. Eble, A. Kudelski, J. Gaj, P. Voisin, Phys. Stat. Sol. (c) **3**, (2006), 3890).
18. "Charge-controlled nuclear polarization of a single InAs/GaAs quantum dot under optical pumping" (B. Eble, O. Krebs, A. Lemaître, **K. Kowalik**, A. Kudelski, B. Urbaszek, T. Amand, X. Marie, P. Voisin, Phys. Stat. Sol. (c) **3**, (2006), 3752).

19. "Role of hyperfine interaction on electron spin optical orientation in charge-controlled InAs-GaAs single quantum dots" (B. Eble, O. Krebs, A. Lemaître, B. Urbaszek, **K. Kowalik**, A. Kudelski, X. Marie, T. Amand, P. Voisin, Phys. Stat. Sol. (a) 204, (2007), 202).
20. "Manipulating exciton fine-structure in quantum dots with a lateral electric field" (B. D. Gerardot, D. Granados, S. Seidl, P. A. Dalgarno, R. J. Warburton, J. M. Garcia, **K. Kowalik**, O. Kres, K. Karrai, A. Badolato, P. M. Petroff, Appl. Phys. Lett. 90, (2007), 041101).
21. "Semiconductor heterostructures for spintronics and quantum information" (J. A. Gaj, J. Cibert, A. Golnik, M. Goryca, E. Janik, T. Kazimierzuk, Ł. Kłopotowski, P. Kossacki, J. Kossut, **K. Kowalik**, O. Krebs, A. Lemaître, S. Maćkowski, W. Maślana, M. Nawrocki, P. Płochocka, B. Piechal, P. Senellart, J. Suffczyński, S. Tatarenko, A. Trajnerowicz, P. Voisin, C. R. Physique 8, (2007), 243).
22. "Microluminescence from  $Cd_{1-x}Mn_xTe$  magnetic quantum dots containing only a few Mn ions" (P. Wojnar, J. Suffczyński, **K. Kowalik**, A. Golnik, G. Karczewski, J. Kossut, Phys. Rev. B 75, (2007), 155301).
23. "Manipulating the exciton fine structure of single CdTe/ZnTe quantum dots by an in-plane magnetic field" (**K. Kowalik**, O. Krebs, A. Golnik, J. Suffczyński, P. Wojnar, J. Kossut, J. A. Gaj, P. Voisin, Physical Review B 75, (2007), 195340). Chosen for June 11, 2007 issue of Virtual Journal of Nanoscale Science Technology.

## ACCEPTED ARTICLES

1. "Diamagnetic contribution to the effect of in-plane magnetic field on a quantum-dot exciton fine structure" to appear in Physical Review B (M. M. Glazov, E. L. Ivchenko, O. Krebs, **K. Kowalik**, P. Voisin).
2. "Monitoring electrically-driven cancellation of exciton fine structure in a semiconductor quantum dot by optical orientation" to appear in Applied Physics Letters (**K. Kowalik**, O. Krebs, A. Lemaître, B. Eble, A. Kudelski, P. Voisin, S. Seidl, J. A. Gaj).

## ARTICLES PUBLISHED IN PROCEEDINGS

1. "Control of the anisotropic exchange splitting of individual InAs/GaAs quantum dots with an in-plane electric field" (**K. Kowalik**, O. Krebs, A. Lemaître, P. Senellart, J. Gaj, P. Voisin, AIP Conf. Proc. 772 (2005), 717).

2. *"Spin-dependent dynamics of individual CdTe/ZnTe quantum dot states studied by correlation spectroscopy"* (J. Suffczyński, T. Kazimierzuk, M. Goryca, B. Piechal, A. Trajnerowicz, **K. Kowalik**, P. Kossacki, A. Golnik, K. Korona, M. Nawrocki, J. Gaj, G. Karczewski, Proc. of SPIE The International Society for Optical Engineering (2007), 647101).
3. *"Polarization Dependent Correlations of Single Photons from CdTe/ZnTe Quantum Dots"* (J. Suffczyński, **K. Kowalik**, A. Trajnerowicz, T. Kazimierzuk, M. Goryca, P. Kossacki, A. Golnik, M. Nawrocki, J. A. Gaj, G. Karczewski, AIP Conf. Proc. 893 (2007), 1089).
4. *"Self-quenching of hyperfine-induced electron spin relaxation in InAs/GaAs quantum dots due to dynamic nuclear polarization"* (B. Eble, O. Krebs, A. Lemaître, **K. Kowalik**, A. Kudelski, P. Voisin, AIP Conf. Proc. 893 (2007), 1341).
5. *"Dynamic nuclear polarization of a single InAs/GaAs quantum dot : positive versus negative trions"* (B. Eble, O. Krebs, A. Lemaître, **K. Kowalik**, A. Kudelski, B. Urbaszek, T. Amand, X. Marie, P. Voisin, AIP Conf. Proc. 893 (2007), 1345).